Damage-induced signalling mechanisms in the neonatal rat cochlea

Manuela Lahne

A thesis submitted for the Degree of Doctor of Philosophy

Department of Physiology

and

UCL Ear Institute

University College London

August 2007

ProQuest LLC
789 East Eisenhower Parkway
P.O. Box 1346
Ann Arbor, MI 48106-1346

Declaration

I, Manuela Lahne, confirm that the work presented in this thesis is my own. Where information has been derived from other sources, I confirm that this has been indicated in the thesis.

Abstract

Sound overstimulation and exposure to ototoxic drugs damage cochlear hair cells (HCs) and cause their death. The surrounding support cells maintain an epithelial barrier and the appropriate physiological environment for surviving HCs during pathological conditions. Coordination of this homeostatic process requires cellular signalling. However, the signalling events that are activated during damage in the mammalian cochlea, are poorly understood.

Neonatal rat cochlear explants were subjected to mechanical damage or exposed to neomycin – an ototoxin. Mechanical damage triggered the immediate propagation of an intercellular wave of increased intracellular Ca^{2+} from the lesion site into distinct cochlear regions. The properties of the Ca^{2+} wave and the source of Ca^{2+} required were specific to the cochlear region. IP_3-mediated release from intracellular stores and influx of extracellular Ca^{2+} contribute differentially to the rise in intracellular Ca^{2+}. The release of extracellular ATP is crucial for the propagation of the damage-induced Ca^{2+} wave. Gap junctions or connexin hemichannels also contribute to its formation.

A subsequent damage-induced signalling event is the transient phosphorylation of ERK1/2 that arises within minutes of the insult occurring in support cells specifically. Similarly to the formation of the Ca^{2+} wave, release of extracellular ATP and gap junctions are critical for ERK1/2 activation. UTP-induced activation of ERK1/2 reveals the involvement of P2Y receptors. In addition, a requirement for the influx of extracellular Ca^{2+} also suggests a role for ion channels – potentially P2X receptors. $P2X_{2,3,4}$ and $P2Y_{2,4,11}$ receptors were expressed in cochlear explants with $P2X_2$ and $P2Y_2$ being exclusive to support cells. Damage-induced currents were recorded from Deiters' cells in a syncytium during mechanical damage of the cochlea.

Finally, when HCs were specifically targeted using neomycin, ERK1/2 activation occurred in support cells surrounding pyknotic HC nuclei. Inhibition of ERK1/2 delayed HC death.

Acknowledgements

I would like to thank, first and foremost my supervisor Dr. Jonathan Gale for his guidance and support throughout my PhD.

I would also like to thank labmembers and friends Zoé Mann and Jonathan Bird for their help regarding science matters and their support and friendship especially over the past few months. Coffee and wine breaks were crucial to re-gain perspectives and energy.

My thanks are also directed to the members of the Centre for Auditory Research for their scientific contributions throughout my PhD and for their continued attempts (often unsuccessful) to drag me away from my "24/7 seat" to one of the local venues.

I am grateful that I had the opportunity to obtain a Bogue Research fellowship to undertake one of my PhD projects in the labs of Drs. Dwight Bergles and Elisabeth Glowatzki at Johns-Hopkins Medical School. I would like to thank Dwight, Elisabeth and their labmembers for their scientific advice and stimulating discussions. Major thanks goes to Nic for initial help with experiments and company during those long nights of patch-clamping associated quite often with a sprint for the last bus.

I would like to thank my friends in the UK, Germany and US for their encouragement, and for making me laugh again during these tense times.

Finally, I would like to extend a huge thanks to my family, especially to my parents for their relentless encouragement, patience and help to keep things in perspective.

This thesis is dedicated to Elfriede Hotop.

Table of Contents

List of Figures

List of Tables

Abbreviations

ACh	Acetylcholine
ACSF	Artificial cerebro-spinal fluids
ADP	Adenosine diphosphate
AMP	Adenosine monophosphate
ATP	Adenosine triphosphate
BAPTA-AM	1,2-bis-(o-Aminophenoxy)-ethane-N, N, N', N'-tetraacetic acid tetraacetotoxy-Methyl ester
BDNF	Brain-derived neurotrophic factor
CaBPs	Calmodulin-like calcium-binding proteins
cADPR	Cyclic-ADP-ribose
cAMP	Cyclic adenosine-monophosphate
CBX	Carbenoxolone
cGMP	Cyclic guanosine-monophosphate
CREB	cAMP response element binding-protein
DAG	Diacylglycerol
DAPI	Diamidinophenolindole
DAPK	Death-associated protein kinase
DMEM/F12	Modified Eagle's medium supplemented with F12
DMSO	Dimethylsulfoxide
EGF	Epithelial growth factor
EGTA	Ethylene glycol-bis(β-aminoethyl ether)-N,N,N',N',-tetraacetic acid
ERK1/2	Extracellularly Regulated Kinases 1 and 2

FBS	Fetal bovine serum
GTP	Guanosine triphosphate
HB-HBSS	Hepes-buffered Hank's balanced salt solution
HC	Hair cell
I_{damage}	Damage-induced current
I_{fast}	Fast ATP-induced current
IHCs	Inner hair cells
I_{norm}	Normalised current
IP_3	Inositol-3-phosphate
IP_3R1-3	IP_3 receptors 1 - 3
IS	Inner sulcus
I_{slow}	Slow ATP-induced current
JNK	c-Jun-N-terminal kinase
M199	Medium 199
MAPK	Mitogen activated protein kinase
MAPKK	Mitogen activated protein kinase kinase
MAPKKK	Mitogen activated protein kinase kinase kinase
MEK1/2	Mitogen activated protein kinase/ERK1/2 kinase kinases
NAADP	Nicotinic acid dinucleotide phosphate
NGF	Neuronal growth factor
NO	Nitric oxide
NTPD	Ecto-nucleoside Triphosphate Diphosphohydrolase
OHCs	Outer hair cells
OS	Outer sulcus
P1	Postnatal day 1 old

P3	Postnatal day 3 old
PAR-1	Proteinase activated receptor-1
PARP	poly(ADP-ribose) polymerase
PBS	Phosphate buffered saline
PFA	Paraformaldehyde
PI-3 kinase	Phosphoinositol-3 kinase
PKA	Protein kinase A
PKC	Protein kinase C
PLA_2	Phospholipase A_2
PLC	Phospholipase C
PMCA	Plasma-membrane Ca^{2+} ATPase
PPADS	Pyridoxal phosphate-6-azo(benzene-2,4-disulfonic
PTS	Permanent threshold shift
R_0	Baseline ratio levels
ROI	Region of interest
ROS	Reactive oxygen species
RSK-1	Ribosomal S6 kinase
R_{sync}	Syncytial resistance
RyR1-3	Ryanodine receptors 1 - 3
S.E.M.	Standard error of mean
SERCA	Sarcoplasmic/endoplasmic reticulum Ca^{2+} ATPases
trpC	Transient receptor potential channel C
UDP	Uridine diphosphate
UTP	Uridine triphosphate

1. Introduction

1.1 Hearing loss and deafness

In the UK, 9 million people are affected by deafness or hearing deficits and 55 % of people over the age of 60 are hearing impaired[1]. Beside inherited forms of deafness, sound overexposure, treatment with drugs with ototoxic side effects and ageing are the most common causes of hearing impairment. Modern-life risk factors especially for the younger generation are frequent overexposure to loud music in night clubs, at concerts and due to the overuse of headphones with personal music devices. Thus it is likely that people will experience hearing deficits at an even earlier age and the percentage of hearing impaired people will almost certainly rise throughout the coming decades. Hearing loss results most commonly from damage or death of the sensory hair cells (HC) – the sound converting receptors in the cochlea. This introduction will describe the structure and function of the ear and its hearing organ, the cochlea. Subsequently, the cellular and molecular signalling processes that occur during drug and noise-induced hearing loss will be described.

1.1.1 Structure and function of the ear

The ear is the entity that enables us to hear and balance and is subdivided into the outer, middle and inner ear. The outer ear comprises the pinna and ear canal that funnel sound waves onto the tympanic membrane, the interface between the outer and middle ear. The tympanic membrane is connected to the malleus – one of three ossicles in the middle ear cavity. The malleus links via the incus to the stapes that attaches to the oval window of the cochlea. The cochlea is the hearing organ and together with the organs of balance forms the inner ear. The balance organs are comprised of three ampullae of the semicircular canals and two otolith organs, the utriculus and sacculus. The function of all of these organs is based on the presence of the mechano-transducing cells – the HCs. Here the focus will be directed towards the structure and function of the cochlea only, as this is the subject of this thesis.

[1] information obtained from www.deafnessresearch.org.uk

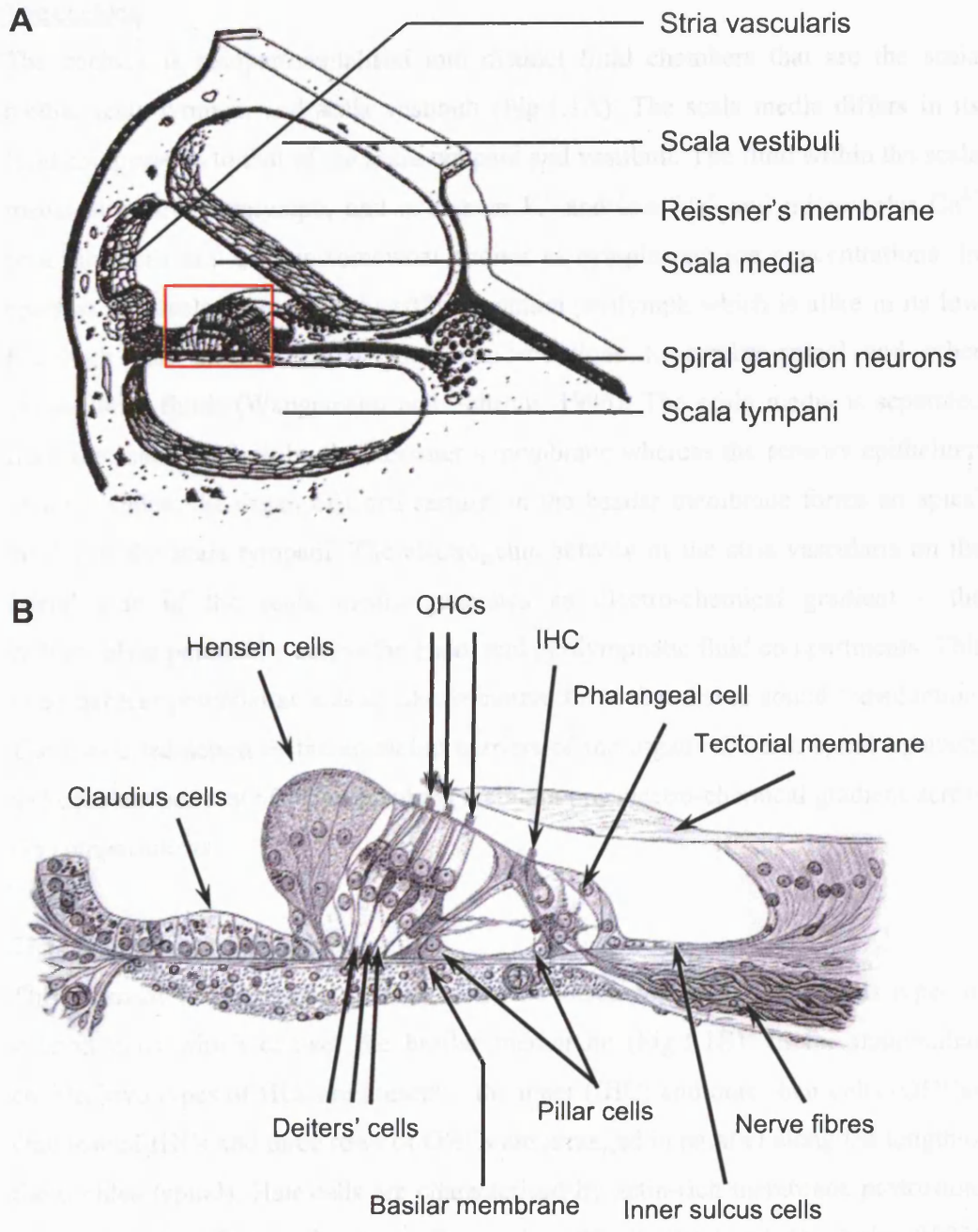

Fig 1.1 Cross section of the cochlea

A) Schematic of the cochlear compartments. Fig modified from (Pickles, 1988). Red square demarks the organ of Corti.

B) Structure of the organ of Corti. The schematic shows the different cell types of the organ of Corti and was modified after Retzius, 1884. Images throughout this PhD thesis are presented in a similar orientation along the x-axis as x-y (view on top of the epithelium) and x-z views.

The cochlea

The cochlea is compartmentalised into distinct fluid chambers that are the scala media, scala tympani and scala vestibuli (Fig 1.1A). The scala media differs in its fluid composition to that of the scala tympani and vestibuli. The fluid within the scala media is called endolymph, and is rich in K^+ and low Na^+ and micromolar Ca^{2+} concentrations and is thus somewhat similar to cytoplasmic ion concentrations. In contrast, the scala tympani and vestibuli contain perilymph which is alike in its low K^+, high Na^+ and millimolar Ca^{2+} concentrations to cerebro-spinal and other extracellular fluids (Wangemann and Schacht, 1996). The scala media is separated from the scala vestibuli by the Reissner's membrane whereas the sensory epithelium of the cochlea, the organ of Corti resting on the basilar membrane forms an apical border of the scala tympani. The electrogenic activity of the stria vascularis on the lateral side of the scala media generates an electro-chemical gradient – the endocochlear potential – across the endo- and perilymphatic fluid compartments. This endocochlear potential acts as an electromotive force that drives sound transduction. The concerted action of the epithelial barriers of the organ of Corti, spiral ligament and constant activity of stria vascularis maintain this electro-chemical gradient across the compartments.

The organ of Corti and hair cells

The organ of Corti consists of the mechano-transducing HCs and various types of support cells which contact the basilar membrane (Fig 1.1B). In the mammalian cochlea two types of HCs are present – the inner (IHC) and outer hair cells (OHCs). One row of IHCs and three rows of OHCs are arranged in parallel along the length of the cochlea (spiral). Hair cells are characterised by actin-rich membrane protrusions at their apical surfaces – the stereocilia (reviewed in Raphael and Altschuler, 2003). These are organised in a staircase-like manner forming a stereocilial 'hair bundle'. Stereocilia (in the staircase) are joined towards their apical ends by small filaments known as 'tip links' (Pickles et al., 1984). The hair bundles of the entire hair cell population are orientated in a specific direction, with their tallest stereocilia being most lateral.

At the basal poles of HCs, contacts are established with neurons. 90-95 % of afferent type I spiral ganglion neurons synapse onto IHCs and send information of the

transduced sound to the cochlear nucleus. Efferent fibres do not innervate IHCs directly but instead synapse onto their afferent neuronal dendrites. In contrast, OHCs have minimal afferent innervation and are characterised by the active motor-processes they exhibit which are thought to amplify and sharpen the sound-induced movements of the basilar membrane to enhance the input to IHCs. The OHCs are innervated by type II spiral ganglion neurons but also have efferent innervation where fibres synapse directly onto the OHC body.

The organ of Corti and support cells

Different subtypes of support cells are found in the organ of Corti. The support cells that surround the IHCs are the phalangeal and border cells whereas those of the OHCs are the Deiters' cells. The cell bodies including the nuclei of the aforementioned support cells are situated beneath HCs and they extend phalangeal processes to the surface of the epithelium, the reticular lamina where they interdigitate with HCs. Tight junctions join the apical aspects of support cells and HCs to form the epithelial barrier that is essential for maintenance of the fluid compositions of the endo- and perilymph. Consequently the apical aspects of HCs and support cells are exposed to endolymph whereas their basolateral sites are bathed in perilymph. Inner and outer pillar cells, another type of support cell, form the tunnel of Corti that separates the IHC from the OHC region. In addition to forming epithelial barriers, support cells, as their name suggests, give structural support to the organ and are also thought to be involved in maintaining the ion homeostasis through K^+ recycling (Boettger et al., 2002). Gap junctions that are formed between neighbouring support cells are suggested to partake in K^+ recycling. Connexins are the units that assemble to connexon hemichannels which form gap junctions when two opposing hemichannels meet. Two connexin subtypes are specific to cochlear function and these are connexin 26 and 30. Cochlear support cells have also been shown to remove neurotransmitters such as glutamate (Glowatzki et al., 2006). In the latter case, removal of excess glutamate will help to terminate signalling between HCs and neurons and to re-establish the appropriate environment of HCs for subsequent sound stimuli.

Sound transduction

Sound waves enter the ear via the pinna and ear canal and are channelled onto the tympanic membrane which consequently vibrates. A force is thereby transmitted onto

the middle ear ossicles resulting in their displacement and consequently that of the oval window of the cochlea. This then drives movement of the basilar membrane which results in the displacement of IHC hair stereocilia, stretching of the tip-links and opening of the mechano-transduction channel to drive a receptor potential. Movements of the basilar membrane will also result in transduction in OHCs. Depolarisation and hyperpolarisation of OHCs triggers contraction and lengthening of these cells, respectively and this is thought to contribute to cochlear amplification (reviewed in Pickles, 1988; Holley, 1996). Some aspects of the processes occurring during transduction are discussed in section 1.2 with focus on the role of Ca^{2+}.

1.1.2 Hair cell epithelia and damage

The cochlear is tonotopically arranged to encode high frequency sounds in the base and low frequencies towards the apex. Following exposure to sound of a particular frequency only hair cells in a specific region are activated and transduce the sound at any given frequency. Consequently, in the majority of cases sound overstimulation results in hearing deficits according to the environmental sound frequencies. Depending on the magnitude and duration of the insult temporary or permanent threshold shifts (PTS) can occur. PTS is most commonly a result of hair cell death (Wang et al., 2002b; Nicotera et al., 2003; Wang et al., 2003a). More severe damage can result in the rupture of the epithelium (Wang et al., 2002b).

Aminoglycoside antibiotics such as neomycin and gentamicin to only name a few, or neoplastic drugs including cisplatin also cause HC death. Until recently it was thought that the mode of entry of aminoglycosides was through receptor-mediated endocytosis (Hashino and Shero, 1995; Hashino et al., 1997). More recently evidence for the entry of aminoglycosides into HCs through the mechano-transduction channels has been provided (Gale et al., 2001; Marcotti et al., 2005). Once inside the cell they mediate the generation of free radicals including reactive oxygen species (ROS, Hirose et al., 1997; Hirose et al., 1999) that are then thought to trigger hair cell death through apoptosis and/or necrosis (Forge and Li, 2000; Pirvola et al., 2000; Jiang et al., 2006). ROS are also implicated in cell death following noise-overexposure. In support of this, treatment with free radical scavengers has been shown to reduce the degree of damage following exposure both to aminoglycosides

and noise (Garetz et al., 1994; Ohinata et al., 2003). Stress-induced cellular signalling triggered by aminoglycosides or noise results in the activation of c-Jun-N-terminal kinases (JNK, see 1.4.4) and caspases in HCs. In the mammalian cochlea the activation of several caspases has been demonstrated following noise damage (Nicotera et al., 2003; Jiang et al., 2006). However, evidence is lacking for a role for caspases during aminoglycoside induced HC death in the mammalian cochlea (Jiang et al., 2006) whereas their activation has been demonstrated in the avian hearing organ (Cheng et al., 2003; Mangiardi et al., 2004). Functional studies investigating the potency of caspase-inhibitors as protective tools are only reported for cisplatin-induced toxicity in the mammalian cochlea. The degree of cell death was reduced, when caspase activation was inhibited during cisplatin-exposure (Wang et al., 2004). Similar results are also demonstrated for the action of aminoglycosides in chick and mouse utricles (Cunningham et al., 2002; Matsui et al., 2002; Cunningham et al., 2004; Matsui et al., 2004). Other signals such as release of cytochrome c or apoptosis inducing factor have been investigated as markers for HC death (Nicotera et al., 2003; Mangiardi et al., 2004; Matsui et al., 2004; Han et al., 2006).

1.1.3 Repair of damaged hair cell epithelia

When HCs are damaged or die the surrounding support cells must close the resulting wound to preserve the physiological environment for surviving hair cells (Forge, 1985; Raphael and Altschuler, 1991; Leonova and Raphael, 1997; Forge and Li, 2000). Moreover, support cells have also been suggested to actively participate in the removal of dying/dead hair cells (Li et al., 1995; Gale et al., 2002; Abrashkin et al., 2006). Recently, it has been shown that support cells engage in an actin purse string mechanism that requires Rho kinase function to mediate the closure of large puncture wounds in neonatal mammalian utricles *in vitro*. This mechanism could not be effected in adult utricles; the underlying mechanisms are currently unknown (Meyers and Corwin, 2007). However, in the adult utricles formation of lamellapodia was still observed that could potentially give rise to a slower mechanism for re-establishing the epithelial barrier.

In the mammalian cochlea, if hair cells are lost, an epithelial scar is formed by support cells but the area is not repopulated with new hair cells (Forge, 1985; Chardin

and Romand, 1995; Kelley et al., 1995). However, there is evidence that a small number of new hair bundles are formed after hair cell damage by gentamicin or neomycin treatment in utricles both *in vivo* and *in vitro*. Both proliferation of progenitors and the transformation of support cells give rise to the newly generated cells (Forge et al., 1993; Warchol et al., 1993; Rubel et al., 1995; Forge et al., 1998). In contrast, a robust proliferative response is observed in avian hair cell epithelia following an insult that results in the repopulation of the epithelium with hair cells (Corwin and Cotanche, 1988; Ryals and Rubel, 1988). The cells that are stimulated to divide and generate new hair cells are the surrounding support cells (Warchol and Corwin, 1996). In avian utricular epithelial sheet cultures, when serum-withdrawal is used as the insult, phosphoinositol-3 kinase (PI-3 kinase) and extracellularly regulated kinases 1 and 2 (ERK1/2) were found to be critical signalling events upstream of the subsequent proliferation (Witte et al., 2001). In a similar study, mammalian utricular epithelial sheet cultures induced to proliferate by recombinant human glial growth factor 2, did so in a PI-3 kinase- and ERK1/2-dependent manner (Montcouquiol and Corwin, 2001). It is not known whether these signalling cascades are activated following aminoglycoside or noise damage in HC epithelia or whether they are critical for a robust regenerative response.

Cell-cell interactive signalling events between damaged HCs and their surrounding support cells likely trigger the wound closure that has been observed in order to maintain an adequate physiological environment for surviving hair cells. Very little is known about the signalling cascades that initiate and regulate the wound repair program by support cells. Therefore, some of the mechanisms implicated in damage-induced signalling in other systems will be discussed in the following sections in the context of their physiological function and their role during pathophysiological events. Information will be given, where appropriate about the knowledge of these processes in HC epithelia.

1.2 Ca^{2+} function and dysfunction

Ca^{2+} is a second messenger that regulates many cellular processes including metabolism, proliferation, differentiation and cell death. A variety of agonists including neurotransmitters such as glutamate and acetylcholine as well as growth

factors like epithelial growth factor (EGF) elicit intracellular Ca^{2+} signals. The signalling events and their function are cell type specific. Thus in the subsequent section aspects of Ca^{2+} signalling and handling will be discussed in the light of cochlear function. This will be followed by a summary of Ca^{2+} dysregulation during damage, toxicity and cell death.

1.2.1 Ca^{2+} homeostasis and function in the cochlea

The transduction of sound into neural cues is established at the interface of HCs and afferent neurons. The processes that accomplish mechano-transduction in HCs are regulated by Ca^{2+} at numerous stages. When stereocilia are displaced during exposure to sound mechano-electrical transduction channels open and facilitate the entry of K^+ and Ca^{2+} into the stereocilia and depolarisation of HCs. If the channels remain open, then adaptation and closure of the channels occurs enabled by the influx of Ca^{2+}. In addition, sound-induced depolarisation of HCs leads to the opening of voltage-gated Ca^{2+} channels – specifically $Ca_v1.3$ channels. The influx of extracellular Ca^{2+} through these channels mediates vesicular release of glutamate which acts as the neurotransmitter at the afferent synapse. HCs also express Ca^{2+} activated K^+ channels – the BK channels that establish efflux of K^+ and thus are part of the regulatory unit that maintains the K^+ homeostasis. Another Ca^{2+} activated K^+ channel – the SK channel is known to be expressed by mature OHCs. The release of acetylcholine (ACh) from efferent neurons projecting onto basal aspects of OHCs results in influx of Ca^{2+} into OHCs via nicotinic ACh receptors and subsequently causes the activation of SK channels. The subsequent K^+ efflux results in hyperpolarisation of OHCs and is thought to be a protective mechanism (reviewed in Housley et al., 2006; reviewed in Mammano et al., 2007).

Mediators of Ca^{2+} signalling events

The previous section illustrated that Ca^{2+} is crucial at various stages of sound transduction and to HC homeostasis. Up to this point extracellular Ca^{2+} was the primary source for the increase in intracellular Ca^{2+}. However, Ca^{2+} signalling events can also be established through the release of Ca^{2+} from intracellular stores. Several mechanisms are known to trigger the release of Ca^{2+} from intracellular stores in other cellular systems. These include the generation of inositol-3-phosphate (IP_3) or cyclic-

ADP-ribose (cADPR) that act on IP_3 or ryanodine receptors at the endoplasmic reticulum, respectively and facilitate Ca^{2+} release (reviewed in (Berridge et al., 2003). More recently, nicotinic acid dinucleotide phosphate (NAADP) was also shown to evoke intracellular Ca^{2+} release. The NAADP receptor has not yet been identified, but it has been suggested that it acts on lysosomes to mediate Ca^{2+} release (Churchill et al., 2002; Yamasaki et al., 2004). The choice of the intracellular elicitor of Ca^{2+} events and thus the compartment is determined by the agonist (Yamasaki et al., 2004).

Both IP_3 and ryanodine receptor expression and function have been studied in the cochlea. RT-PCR of microdissected pooled rat OHCs and Deiters' cell samples revealed the expression of the IP_3 receptor subtypes IP_3R1 to IP_3R3 (Lioudyno et al., 2004). The presence of IP_3 receptors in HCs has been confirmed with an immunocytochemical approach in adult guinea pigs (Mammano et al., 1999). Moreover, adenosine triphosphate- (ATP)-induced Ca^{2+} signals in HCs were reduced when IP_3 generation or binding to its receptors were compromised. IP_3 dependent signalling has also been described in cochlear support cells including Deiters', Hensen and Claudius cells (Mammano et al., 1999; Lagostena et al., 2001; Lagostena and Mammano, 2001; Gale et al., 2004). Expression of ryanodine receptor subtypes RyR1 and RyR3 but not RyR2 was observed in pooled microdissected samples of rat OHCs and Deiters' cells using RT-PCR (Lioudyno et al., 2004). Immunohistochemical studies revealed the localisation of RyR in OHCs, IHCs and various support cell subtypes including Deiters' and phalangeal cells. Moreover, ryanodine receptors were also detected in neurons (Grant et al., 2006; Morton-Jones et al., 2006). In contrast to the study by Lioudyno et al. (2004), an antibody against the RyR2 subtype revealed its expression in rat HCs, Deiters' and phalangeal cells (Morton-Jones et al., 2006). Functional studies also support the presence of ryanodine receptors. In IHCs, the depolarisation-induced rise of intracellular Ca^{2+} at the basal pole of the cell was significantly reduced in the presence of an inhibitory ryanodine concentration. The depolarisation-induced increase in Ca^{2+} levels was abolished in 0 Ca^{2+}, suggesting that ryanodine receptors were activated by the influx of extracellular Ca^{2+} providing an example for Ca^{2+} induced Ca^{2+} release in the mammalian cochlea (Kennedy and Meech, 2002). Moreover, the ACh-evoked activation of SK channels in OHCs is also modulated by ryanodine (Lioudyno et al.,

2004). In contrast to IP_3 and ryanodine receptors, at present there is no evidence that Ca^{2+} release in the cochlea is attributed to the action of NAADP. Taken together, both IP_3 and ryanodine receptor-mediated Ca^{2+} release mechanisms are employed in the mammalian cochlea. However, an understanding of their function during physiological processes is still quite limited.

Regulation of cytoplasmic Ca^{2+} concentrations

The concentration of cytoplasmic Ca^{2+} has to be tightly regulated in order to maintain the function of HCs and preserve their capacity to transduce sounds. As a result there have been a number of investigations into the mechanisms that regulate Ca^{2+} homeostasis in HCs. In contrast, Ca^{2+} signalling and regulation in the surrounding support cells are less well established.

In HCs, a major Ca^{2+} efflux pathway occurrs via the plasma-membrane Ca^{2+} ATPases 1-3 (PMCA1-3) (Dumont et al., 2001). PMCA4 was not observed in cochlear cells (Dumont et al., 2001). HCs are characterised by high expression of the PMCA2 at the tip of the stereocilia which coincides with increased efflux compared to the baso-lateral aspects of HCs (Yamoah et al., 1998; Dumont et al., 2001). The deafwaddler mouse exhibits a mutation in the gene for PMCA2 that results in hearing and balance impairment (Street et al., 1998). Recently, this mutant gene and a newly identified mutation in the human gene were assessed for their Ca^{2+} removal properties when transfected into CHO cells. Both mutants showed similar peak Ca^{2+} responses to the wildtype PMCA when challenged with the P2 receptor agonist ATP. The recovery to baseline Ca^{2+} levels was compromised in both mutants, however the deafwaddler mutant was affected to a greater extent (Ficarella et al., 2007). Beside the PMCAs other mechanisms can facilitate the removal of intracellular Ca^{2+}. These mechanisms include the uptake of Ca^{2+} by mitochondria or into the endoplasmic reticulum through SERCA pumps (Rizzuto et al., ; Boitier et al., 1999). In addition the extrusion of Ca^{2+} has also been demonstrated to occur through the action of the Na^{+}-Ca^{2+} exchanger (reviewed in Ishida and Paul, 2005). In IHCs, in addition to PMCAs, mitochondria and the endoplasmic reticulum have been demonstrated to partially regulate the uptake of Ca^{2+}. However, the Na^{+}-Ca^{2+} exchanger did not contribute to the removal of Ca^{2+} following a depolarisation-induced rise in cytoplasmic Ca^{2+} levels (Kennedy, 2002).

Ca^{2+} must not only be removed following signalling events, but depleted intracellular stores must also be replenished in order to facilitate subsequent events. The common transient receptor potential (trpC) channel has been suggested to fulfil this task. TrpC3 was recently found to be expressed in guinea pig and rat cochleae; specifically in IHCs and OHCs. Store-operated Ca^{2+} entry occurred when the extracellular solution was switched from Ca^{2+}-free to 1.5 mM Ca^{2+} (Raybould et al., 2007) demonstrating that these mechanisms are engaged in HCs. It has not been investigated whether similar mechanisms act in cochlear support cells.

Ca^{2+} binding proteins and their function in hair cells

The homeostasis and the function of HCs are also preserved and even modulated through the action of various Ca^{2+} binding proteins. A gradient of Ca^{2+} buffering proteins has been observed along the length of the turtle cochlea when adaptation of the mechano-electrical transduction current was compared in HCs at different cochlear locations (Ricci et al., 1998). Recently, the calmodulin-like calcium-binding proteins (CaBPs) have been suggested to modulate $Ca_v1.3$ channels (Yang et al., 2006). These channels show strong Ca^{2+}-dependent inhibition when expressed in a heterologous expression system. However, currents mediated in HCs by these channels do not exhibit this feature. Co-expression of $Ca_v1.3$ channels and CaBP1 or CaBP4 in HEK294 cells abolished the Ca^{2+}-dependent inhibition, suggesting that HCs might utilise this mechanism (Yang et al., 2006). This hypothesis is supported by immuno-localisation studies. CaBP1 was found to be expressed in Deiters' and pillar cells as well as in the region of the cuticular plate of OHCs in the adult rat cochlea. CaBP4 was also observed localising to OHCs, IHCs, Deiters' and pillar cells at P9. In contrast, at P28 the immuno-labelling was restricted to IHCs only (Yang et al., 2006). Other Ca^{2+} binding proteins such as calbindin, calretinin, α-parvalbumin and oncomodulin (β-parvalbumin) were detected in HCs of the mammalian cochlea (Sakaguchi et al., 1998; Yang et al., 2004a; Hackney et al., 2005). Deiters' and outer pillar cells also express α-parvalbumin during the first postnatal days (Sakaguchi et al., 1998; Yang et al., 2004a; Hackney et al., 2005) and these cells are also characterised by the abundance of the Ca^{2+} binding protein S-100 (Pack and Slepecky, 1995). It is not known whether particular Ca^{2+} binding proteins perform specific roles within support cells.

1.2.2 The role of Ca^{2+} during damage and cell death

Ca^{2+} homeostasis during toxic events

Ca^{2+} has been implicated as a regulator in the execution of cell death in various cell types including neurons (reviewed in Bano and Nicotera, 2007; reviewed in Hara and Snyder, 2007). Dysregulation of Ca^{2+} concentrations resulting in raised Ca^{2+} levels in the cytoplasm or mitochondria but also those that cause low Ca^{2+} concentrations in the ER, lead to cellular death. Increased intracellular Ca^{2+} levels were found in cells of the chick hearing organ – the basilar papilla – within 30 min of exposure to gentamicin (Hirose et al., 1999). A different study observed a similar rise in intracellular Ca^{2+} levels in response to 1 mM neomycin in cells of chick utricular epithelial cultures (Matsui et al., 2004). In addition, a substantially larger Ca^{2+} response that lasted between 30 to 120 min was recorded after ~ 4 hrs of exposure to neomycin (Matsui et al., 2004). These studies did not directly address whether Ca^{2+} is the messenger that initiates the death signalling cascades in HCs. However, HC death was not prevented in gentamicin treated organ of Corti explants from guinea pigs that were pre-incubated with the Ca^{2+} chelator Quin-2 AM (Dehne et al., 2002). The simplest explanation is that Ca^{2+} is not involved in apoptosis; however, the cells might not be protected for a number of reasons: i) the Ca^{2+} homeostasis of cells in the presence of a Ca^{2+} chelator is certainly impaired and ii) the Ca^{2+} buffering capacity by Quin-2 may have been overloaded. In the ear, increased intracellular Ca^{2+} levels have not been directly linked to the mechanisms that underlie HC death. In other cellular systems, proteases such as caspases and calpains are activated and facilitate breakdown of proteins during cell death. Both caspases and calpains have been implicated during aminoglycoside and cisplatin induced HC death (Ding et al., 2002; Cunningham et al., 2004; Matsui et al., 2004; Wang et al., 2004). These proteases have been shown to cleave the PMCA and Na^{+}-Ca^{2+} exchanger during excitotoxic events in neurons resulting in dysfunction of these elements crucial for maintenance of intracellular Ca^{2+} homeostasis (Schwab et al., 2002; Bano et al., 2005). Consequently, cells experience elevated Ca^{2+} concentrations and undergo cell death. Increased Ca^{2+} also acts on various other enzymes including protein phosphatases such as calcineurin. Pharmacological studies implicate a role for calcineurin during noise-induced hearing loss (Minami et al., 2004). Calcineurin is a phosphatase that among other roles mediates dephosphorylation of BAD – a pro-apoptotic member of

the Bcl family. Dephosphorylation enables BAD to translocate from the cytoplasm to mitochondria where it promotes apoptosis (Wang et al., 1999). These are only a small number of examples from the vast network of Ca^{2+} dependent processes occurring during cell death and more continue to be added.

Mechanical stimulation and Ca^{2+} waves

Beside chemical damage, mechanical stimulation has also been shown to elicit a rise in intracellular Ca^{2+} that travels as an intercellular Ca^{2+} wave through cell layers in various cell culture models, including airway epithelial and glial cells (Sanderson et al., 1990; Charles et al., 1991). Ca^{2+} waves have also been described to propagate between glial cells in retinal organ preparations (Newman and Zahs, 1997; Newman, 2001). The mechanically stimulated rise in intracellular Ca^{2+} was found to be initiated by the generation of IP_3 and the subsequent release of Ca^{2+} from intracellular stores, whereas extracellular Ca^{2+} was not required for Ca^{2+} wave propagation (Sanderson et al., 1990; Charles et al., 1991; Hansen et al., 1995; Newman and Zahs, 1997; Venance et al., 1997; Sung et al., 2003). Initially the mechanically evoked wave propagation was compared to that induced by exogenous application of ATP and was shown to be similar (Hansen et al., 1993). Subsequently, treatment with P2 receptor antagonists or the ATP degrading enzyme apyrase revealed that release of extracellular ATP triggers the formation of intercellular Ca^{2+} waves. Measurements of ATP released following mechanical stimulation showed that ATP-induced P2 receptor activation caused the release of ATP (Newman, 2001). The role of gap junctions in the propagation of Ca^{2+} waves is controversial. Ca^{2+} waves in HepG liver cell monolayers and between glial cells in the retina were not reduced in the presence of uncoupling agents (Newman, 2001; Sung et al., 2003). The latter study rather found an increase in the area covered by the Ca^{2+} wave in the presence of the uncoupling agent octanol (Newman, 2001). In contrast, gap junctions were suggested to participate in mechanically induced Ca^{2+} wave propagation across airway epithelial and astrocyte cell monolayers (Sanderson et al., 1990; Venance et al., 1997). In HeLa cells that express connexin 43, a Ca^{2+} wave propagated to nearby cells in the presence of apyrase following mechanical stimulation, whereas it was restricted to the stimulated cell only in control Hela cells (Paemeleire et al., 2000). This indicates that gap junctions participate in the propagation of Ca^{2+} waves, when connexin 43 is expressed. Moreover, connexins the proteins that form gap junctions have been

suggested to function as hemichannels that facilitate the release of ATP during Ca^{2+} wave propagation (Stout et al., 2002; Pearson et al., 2005).

In mammalian cochlear explants it has been shown that damaging a single HC triggered a rise in cytoplasmic Ca^{2+} that propagated initially to neighbouring cells and subsequently to cells up to 160 µm from the lesion site in form of an intercellular Ca^{2+} wave (Gale et al., 2004). The Ca^{2+} wave was suggested to be generated by release of extracellular ATP as a result of the IP_3 dependent increase in Ca^{2+} levels (Gale et al., 2004). The study focused on the propagation of the Ca^{2+} wave into the region composed of Claudius' and Hensen's cells. However, it is still unknown whether the damage-induced Ca^{2+} wave also triggers changes in Ca^{2+} levels in the HC and IS cell region (IS) of cochlear explants. Moreover, the exact nature of P2 receptors that elicit the damage-induced Ca^{2+} wave propagation is not known. P2 receptor expression and function in the mammalian cochlea will be discussed in chapter 1.3. The signalling mechanisms downstream of the damage-induced Ca^{2+} wave are also not determined yet. A potential candidate signalling cascade is the mitogen activated protein kinase (MAPK), specifically the ERK signalling cascade which is introduced in chapter 1.4.

1.3 P2 receptors

1.3.1 P2 receptors – general

The first evidence that signalling of ATP sensitive receptors – P2 receptors – might play a role in the mammalian cochlea arose from patch-clamp and Ca^{2+} imaging experiments. ATP-induced inward currents were recorded from isolated hair and support cells, including Hensen and Deiters' cells of the guinea pig cochlea. The currents were observed to coincide with intracellular Ca^{2+} changes (Ashmore and Ohmori, 1990; Nakagawa et al., 1990). ATP acts on a class of receptors called P2 receptors that are subdivided into ionotropic P2X and metabotropic P2Y receptors. The P2X subfamily consists of seven members that are the $P2X_1$ to $P2X_7$ receptors. Similarly various P2Y receptor subtypes are known and include $P2Y_1$, $P2Y_2$, $P2Y_4$, $P2Y_6$ and $P2Y_{11}$ to $P2Y_{14}$ (reviewed in King and Townsend-Nicholson, 2003). The

receptor families and their subtypes exhibit distinct features which will be discussed briefly in the following paragraphs.

P2X receptors

The members of the P2X receptor family are non-selective cation channels that are almost exclusively activated by ATP. The only receptor which represents a special case is the $P2X_3$ receptor subtype which is in addition to ATP also activated by uridine triphosphate (UTP) and to a lesser extent by adenosine triphosphate (ADP) (Liu et al., 2001; Greenwood et al., 2007). The P2 receptor subtypes exhibit variable sensitivity to agonists and the timecourse of desensitisation also differs. The receptors that are more sensitive to ATP are $P2X_1$ and $P2X_3$ receptors. These are also the rapidly desensitising receptors, whereas $P2X_2$ and $P2X_4$ desensitise more slowly (Bianchi et al., 1999). $P2X_2$, $P2X_4$ and $P2X_7$ are also characterised by their potential to allow passage of dyes during prolonged receptor stimulation (Surprenant et al., 1996; Khakh et al., 1999a; Meyers et al., 2003). Proposed mechanisms are: i) dilation of the P2X pore or ii) coupling to a different channel. Recently it has been shown that the $P2X_7$ receptor recruits pannexins – a protein with similar characteristics to connexins. The interaction with pannexins facilitates the dye entry during prolonged ATP exposure (Pelegrin and Surprenant, 2006).

In addition to homomeric P2X receptors, heteromer formation has been described. $P2X_{2/3}$, $P2X_{4/6}$, $P2X_{1/5}$ and $P2X_{2/6}$ are known to form heteromeric channels (Le et al., 1998; Le et al., 1999; King et al., 2000; Liu et al., 2001). Co-expression of P2X receptors renders agonist and antagonist specificity as well as the timecourse of desensitisation. *In vivo* several P2X receptors are simultaneously expressed resulting in a potential diversity of P2 receptor interactions and thus in an increased regulatory complexity of signalling processes. Knowledge is quite limited in regard to the interactions occurring between co-expressed P2X receptors *in vivo*.

P2Y receptors

The P2Y receptor subtypes couple to heterotrimeric guanine-nucleotide binding proteins (G-proteins). G-protein coupled receptors are characterised by seven transmembrane domains that are linked by three intracellular and three extracellular loops. The P2Y receptor subtypes exhibit different sensitivities to nucleotides. $P2Y_1$,

$P2Y_{12}$ and $P2Y_{13}$ receptors are activated by the adenosine-based nucleotides ADP and ATP but not by UTP or uridine diphosphate (UDP). In contrast $P2Y_2$, $P2Y_4$ and $P2Y_{11}$ receptors are sensitive to ATP and UTP whereas their diphosphates are not sufficient to mediate signalling events through these receptors (Nicholas et al., 1996; van der Weyden et al., 2000; White et al., 2003; Wildman et al., 2003). UDP acts in addition to UTP and ADP on the rat $P2Y_6$ receptor (Nicholas et al., 1996). The $P2Y_{14}$ receptor is subtype that is not activated by any of the common nucleotides mentioned above but by the UDP derivative UDP-glucose. The $P2Y_1$, $P2Y_2$, $P2Y_4$, $P2Y_6$ and $P2Y_{11}$ receptor subtypes couple to G_q proteins that interact with the PLC signalling axis resulting in the release of $Ca^{2+}$from intracellular stores. $P2Y_2$, $P2Y_4$, $P2Y_6$ and $P2Y_{11}$ also interact with other G-proteins to facilitate the activation of other signalling pathways. $P2Y_{12}$ to $P2Y_{14}$ receptors mediate the formation of cAMP through interaction of G_i proteins with adenocyclases (reviewed in King and Townsend-Nicholson, 2003; reviewed in von Kugelgen, 2006).

Brief overview of P2 receptor antagonists

P2X and P2Y receptor mediated signalling events can be partially distinguished on the basis of the agonist profiles of P2Y receptors. Antagonists are not very specific and act on various P2X and P2Y receptors. Commonly used broad spectrum antagonists are PPADS and suramin. A selective P2X receptor antagonist is TNP-ATP that only acts on P2Y receptors at millimolar concentrations (Virginio et al., 1998; Wildman et al., 2003). The various P2X receptors are differentially sensitive. $P2X_1$, $P2X_3$ and $P2X_{2/3}$ receptors are inhibited by TNP-ATP in the nanomolar range whereas higher doses in the micromolar range are required to antagonize $P2X_2$, $P2X_4$ and $P2X_7$ receptor activation (Virginio et al., 1998). Brilliant BlueG is a selective antagonist when used at nM concentrations at the $P2X_7$ receptor, but other P2X receptors are also sensitive at higher concentrations (Jiang et al., 2000). The potencies of the antagonists were determined using heterologous expression systems. In native tissue, co-expression of receptors occurs and this has been shown to alter pharmacological profiles (Le et al., 1998; Liu et al., 2001; Gallagher and Salter, 2003). Therefore, the half maximal effective concentration (EC_{50}) may not be applicable to complex tissues.

ATP has been implicated in physiological and pathological events in various organs including the brain and the ear. The functions of P2 receptors are diverse and cover proliferation, survival, differentiation and, during pathological conditions, also cell death (Neary et al., 2003; Arthur et al., 2005; Pearson et al., 2005; Arthur et al., 2006). A number of studies have been carried out to characterise P2 receptor expression in the cochlea and to determine their function. In the subsequent sections the current knowledge of the expression pattern of P2 receptors in the cochlea will be summarised according to their subclasses. This will be followed by a discussion about their modulation and function.

1.3.2 P2 receptor expression in the cochlea

P2X receptor expression in the cochlea

The expression patterns of P2X receptors in the mammalian cochlea are better characterised than that of P2Y receptors. Although at present, data are not available for all of the known P2X receptor subtypes. The results of various immunocytochemical studies are summarised in Table 1.1a-c. $P2X_1$ to $P2X_3$, and $P2X_7$ receptors have been characterised in the mammalian cochlea at various stages during development. Immunocytochemical localisation of $P2X_1$ receptors revealed its presence in spiral ganglion neurons of the rat cochlea between embryonic day 16 (E16) and postnatal day 6 (P6) whereas $P2X_1$ mRNA was only observed at P0 in these cells. Earlier timepoints were not studied using RT-PCR (Nikolic et al., 2001; Greenwood et al., 2007). In contrast, $P2X_1$ was expressed in isolated OHCs of adult guinea pigs (Szucs et al., 2004). $P2X_2$ receptors are the most studied P2 receptors in the cochlea and expression is observed in stereocilial bundles of HCs, in Deiters', border, Hensen, Claudius cells and spiral ganglion neurons (Housley et al., 1999; Xiang et al., 1999; Jarlebark et al., 2000; Jarlebark et al., 2002; Szucs et al., 2004). Furthermore, the existence of three splice variants $P2X_{2\text{-}1}$, $P2X_{2\text{-}2}$ and $P2X_{2\text{-}3}$ has been suggested (Brandle et al., 1997; Chen et al., 2000; Greenwood et al., 2007). These splice variants differ in their desensitisation rate as shown using oocytes or HEK293 expression systems. $P2X_{2\text{-}3}$ is distinguished from the other splice variants by its decreased sensitivity to ATP. However, these studies did not test whether co-expression of these splice variants affect their pharmacological profile as shown for other P2X receptors (Brandle et al., 1997; Chen et al., 2000; Greenwood et al., 2007).

Another type of $P2X_3$ receptors is expressed in HCs and spiral ganglion neurons during early development from E18 to P6 depending on the cochlear region. HCs in the basal region discontinue $P2X_3$ expression earlier than those of the more apical regions (Huang et al., 2005). Co-expression of the $P2X_3$ receptor subtype and the $P2X_{2\text{-}3}$ splice variant in *Xenopus* oocytes rendered the pharmacological characteristics of both receptors to a phenotype that more closely represents that of spiral ganglion neurons (Greenwood et al., 2007). In contrast to the developmental downregulation of $P2X_3$ receptors, $P2X_7$ expression is initiated and increases during postnatal development. $P2X_7$ receptors are present in IHCs and OHCs from P0-P6 and are maintained in IHCs into adulthood. Deiters' and phalangeal cells commence expression at P6, whereas spiral ganglion neurons show immunoreactivity as early as E18 (Nikolic et al., 2003). The $P2X_4$, $P2X_5$ and $P2X_6$ receptors have only been studied in spiral ganglion neurons where expression was observed using both an immunocytochemical approach and RT-PCR. The $P2X_5$ receptor mRNA expression was abolished after onset of hearing measured at P14, whereas $P2X_4$ and $P2X_6$ receptors were maintained (Xiang et al., 1999; Greenwood et al., 2007). $P2X_4$ receptor expression was additionally demonstrated in isolated OHCs cells (Szucs et al., 2004). Functional expression of P2X receptors has been demonstrated for HCs, Hensen, Deiters' cells and spiral ganglion neurons. ATP-mediated inward currents have been recorded in these cells assessed using the patch-clamp techniques (Ashmore and Ohmori, 1990; Nakagawa et al., 1990; Chen and Bobbin, 1998; Housley et al., 1999; Mammano et al., 1999; Lagostena et al., 2001; Lagostena and Mammano, 2001; Greenwood et al., 2007).

P2Y receptor expression:

The expression profile of P2Y receptors is poorly characterised in the mammalian cochlea. A study using RT PCR revealed the presence of $P2Y_1$, $P2Y_2$, $P2Y_4$ and $P2Y_6$ in P2 rat cochleae (Gale et al., 2004). The stria vascularis was removed before RNA isolation and thus did not contribute to the results. The expression of the $P2Y_2$ receptor was confirmed by immunocytochemical labelling of cochlear explants. $P2Y_2$ was observed in Hensen cells and stereocilia of IHCs (Table 1.2). In Claudius-like cells and along the HC region the labelling was fainter. The cell types in the HC region that contribute to the labelling were not identified (Gale et al., 2004). $P2Y_1$, $P2Y_2$ and $P2Y_4$ were observed in isolated OHCs of guinea pig cochleae. $P2Y_1$ was

Table1.1a: Immunocytochemical localisation of P2X receptor expression in the mammalian cochlea. ap = apical, bs = basal, gp = adult guinea pig, n.p.d = not possible to determine, n.t. = not tested.

Receptor	IHC	OHC	Deiters' cells	Phalangeal cells	Pillar cells	Hensen cells	Claudius cells	Spiral ganglion	Species	Antibody Source	Reference
P2X1	-	-	-	-	-	-	-	E16-P6 adult: n.t	rat	Alomone	Nikolic et al., 2001
	n.t.	n.t.	n.t.	n.t.	n.t.	n.t.	n.t.	+	rat	In Lab	Xiang et al., 1999
	n.t.	+	n.t.	n.t.	n.t.	n.t.	n.t.	n.t.	gp	Alomone	Szucs et al., 2004
P2X2	n.t.	n.t.	n.t.	n.t.	n.t.	n.t.	n.t.	+	rat	In Lab	Xiang et al., 1999
	Stereo-cilia	Stereo-cilia	+	n.p.d.	n.p.d.	n.p.d.	n.p.d.	+	gp	In Lab	Housley et al., 1999
	-	Stereo-cilia	+	But border cell	-	+	+	+	rat	In Lab	Jarlebark et al., 2000

Table1.1b: Immunocytochemical localisation of P2X receptor expression in the mammalian cochlea. ap = apical, bs = basal, gp = adult guinea pig, n.p.d = not possible to determine, n.t. = not tested.

Receptor	IHC	OHC	Deiters' cells	Phalangeal cells	Pillar cells	Hensen cells	Claudius cells	Spiral ganglion	Species	Antibody Source	Reference
$P2X_2$	-	Stereocilia	+	+	-	+	+	+	mouse	In Lab	Jaerlebark et al., 2002
	n.t.	+	n.t.	n.t.	n.t.	n.t.	n.t.	n.t.	gp	Alomone	Szucs et al., 2004
$P2X_3$	n.t.	n.t.	n.t.	n.t.	n.t.	n.t.	n.t.	+	rat	In Lab	Xiang et al., 1999
	E18 – P0/P3 bs/ap	E18 – P0/P6 bs/ap	-	-	-	-	-	E18-P6 tested	mouse	Neuromics, USA	Huang et al., 2005
$P2X_4$	n.t.	n.t.	n.t.	n.t.	n.t.	n.t.	n.t.	+	rat	In Lab	Xiang et al., 1999
	n.t.	+	n.t.	n.t.	n.t.	n.t.	n.t.	n.t.	gp	Alomone	Szucs et al., 2004
$P2X_5$	n.t.	n.t.	n.t.	n.t.	n.t.	n.t.	n.t.	+	rat	In Lab	Xiang et al., 1999

Table1.1c: Immunocytochemical localisation of P2X receptor expression in the mammalian cochlea. a.n.p.d. = adult not possible to determine, ap = apical, bs = basal, gp = adult guinea pig, n.p.d = not possible to determine, n.t. = not tested.

Receptor	IHC	OHC	Deiters' cells	Phalangeal cells	Pillar cells	Hensen cells	Claudius cells	Spiral ganglion	Species	Antibody Source	Reference
$P2X_6$	n.t.	n.t.	n.t.	n.t.	n.t.	n.t.	n.t.	+	rat	In Lab	Xiang et al., 1999
$P2X_7$	P0-adult	P0-P6 adult: negative	P6-adult	P2-adult	P6-adult	P6 faint a.n.p.d	P6 faint a.n.p.d	E18-adult	rat	Alomone	Nikolic et al, 2003
	n.t.	+	n.t.	n.t.	n.t.	n.t.	n.t.	n.t.	gp	Alomone	Szucs et al., 2004

Table 1.2: P2Y receptor expression in the mammalian cochlea. The $P2Y_{6, 11, 12, 13, and 14}$ which are not listed in the table have not been investigated. cc = cochlear culture, gp = adult guinea pig, n.p.d = not possible to determine, n.t. = not tested.

Receptor	IHC	OHC	Deiters' cells	Phalangeal cells	Pillar cells	Hensen cells	Claudius cells	Spiral ganglion	Species	Antibody Source	Reference
P2Y1	n.t.	+	n.t.	n.t.	n.t.	n.t.	n.t.	n.t.	gp	Alomone	Szucs et al., 2004
P2Y2	Stereocilia P3	-	n.p.d.	n.p.d.	n.p.d.	+	n.p.d.	-	rat cc	Alomone	Gale et al., 2004
	n.t.	+	n.t.	n.t.	n.t.	n.t.	n.t.	n.t.	gp	Alomone	Szucs et al., 2004
P2Y4	n.t.		n.t.	n.t.	n.t.	n.t.	n.t.	n.t.	gp	Alomone	Szucs et al., 2004
	-	-	+	-	-	+	n.p.d	n.t.	gp	Alomone	Parker et al., 2003

distributed homogenously in OHCs whereas $P2Y_2$ localised to more apical aspects and $P2Y_4$ towards the basal end of OHCs (Szucs et al., 2004). In contrast, a study examining $P2Y_4$ receptor expression in cryosections of guinea pig cochleae demonstrated labelling in Deiters' cells but not HCs (Parker et al., 2003).

The application of agonists such as UTP and UDP that predominantly act on P2Y receptors supports the expression of these receptors in Hensen and Claudius-like cells (Gale et al., 2004; Piazza et al., 2007). Furthermore, in Hensen cells from the guinea pig ATP induced two inward currents – a fast current that coincided with influx of extracellular Ca^{2+} and a slower one that was IP_3-dependent (Lagostena et al., 2001). In Deiters' cells ATP only elicited a fast current (Lagostena and Mammano, 2001). ATP-induced Ca^{2+} changes were observed in Deiters' cells. Ca^{2+} release from intracellular stores was suggested as the source; however, this was not directly tested (Dulon et al., 1993; Lagostena and Mammano, 2001). Intracellular Ca^{2+} changes in HCs resulting from exogenous application of ATP occurred in an IP_3-dependent manner suggesting a role for P2Y receptors (Mammano et al., 1999). In contrast, application of UTP did not elicit currents in isolated guinea pig OHCs and IHCs, which however does not exclude P2Y receptor function in HCs (Housley et al., 1999). These receptors might not couple to ion channels and thus measurements of agonist-induced Ca^{2+} changes are a more reliable technique to determine their presence and function. Further immunohistochemical and functional studies at different stages during development are necessary to identify the impact of P2Y receptors on cochlear development and function.

1.3.3 Modulation of P2 receptor responses in cochlear cells

P2 receptors are modulated by various external factors and physiological stimuli. P2X receptor responses are dependent on extracellular Ca^{2+}, Zn^{2+}, Cu^{2+}, and H^+ concentrations (Evans et al., 1996; King et al., 1997; Ding and Sachs, 1999, 2000; Kanjhan et al., 2003). The presence of divalent cations such as Ca^{2+} or Zn^{2+} in the extracellular space interferes with P2 receptor function and decreases resultant currents. Alkaline pH also inhibits P2X receptors whereas acidification results in the potentiation of P2 receptor currents in HCs and Deiters' cells (Kanjhan et al., 2003). Beside the modulation by environmental factors P2 receptor-mediated events are also

regulated by neurotransmitters as well as intracellular signalling cascades. ACh, the neurotransmitter released by efferent neurons, has been shown to reduce the ATP-induced rise in intracellular Ca^{2+} in OHCs (Ashmore and Ohmori, 1990; Wikstrom et al., 1998). Intracellular cascades that have been demonstrated to affect P2 receptors in cochlear cells are the cyclic guanosine monophosphate (cGMP)-protein kinase G (PKG) and cyclic adenosine monophosphate (cAMP)-protein kinase A (PKA) signalling axis. ATP has been observed to stimulate the production of nitric oxide in IHCs and OHCs that subsequently regulates the simultaneously occurring intracellular Ca^{2+} events. Although, the effect which nitric oxide exerts, differs according to the type of HC. In IHCs nitric oxide decreases the ATP-induced elevated Ca^{2+} levels whereas it provokes the opposite effect in OHCs (Shen et al., 2005; Shen et al., 2006). In addition the cAMP analogue 8-Br-cAMP or other agents that induce the generation of cAMP decrease P2X mediated currents in isolated Deiters' cells (Chen and Bobbin, 1998). Taken together P2 receptors are modulated at various levels presenting a basis for controlling physiological events.

The expression of ectonucleotidases – the enzymes that hydrolyse ATP – offers a yet additional mechanism to control P2 receptor mediated signalling cascades. The ecto-nucleotidase triphosphate diphosphohydrolases (NTPD) 1, 2 and 3 have been reported to be expressed in the rat cochlea (Vlajkovic et al., 2002a, b). This implies that a physiological function is attributed to controlled P2 receptor signalling in the cochlea.

1.3.4 P2 receptor function in the cochlea

P2 receptor function and hearing

P2X receptors are proposed to modulate sound transduction on the basis of their expression in sensory HCs and their afferent neurons (Housley et al., 1999). *In vivo* experiments give some indication that ATP can play a modulatory role in the mammalian cochlea. Enhanced electrically-evoked otoacoustic emissions measured when ATP was applied to the scala media, provide evidence that ATP can affect OHC activity (Kirk and Yates, 1998). Furthermore, ATP injected into the scala media reduced the endocochlear potential that was restored to baseline levels in the presence of PPADS (Thorne et al., 2004). It has been suggested that a shunt current is the

mechanism underlying altered endocochlear resistance resulting in decreased HC sensitivity to sounds. This shunt is however not mediated by HCs as their loss did not affect the ATP-induced changes of the endocochlear potential (Thorne et al., 2004). Thus the change in endocochlear potential is predominantly carried by other cochlear cells that express P2 receptors. Application of the purinergic agonist ATP-γ-S to the scala tympani resulted in a transient threshold shift of the compound action potential and the frequency tuning curves of single neurons (Sueta et al., 2003). At present, the cellular mechanisms underlying these threshold shifts are unidentified. Taken together P2 receptor function has been implicated in sound transduction but knowledge of its specific action is quite limited.

P2 receptors during development

The transient expression of $P2X_1$, $P2X_3$ and $P2X_5$ receptors implicates a role during development. A recent study addressed the question whether the transient expression of $P2X_3$ receptors in spiral ganglion neurons during early postnatal days is related to neuronal development. Spiral ganglion neurons cultured in the presence of brain-derived neurotrophic factor (BDNF) and the purinergic agonist ATPγS exhibited fewer and shorter neurites than those grown in BDNF alone (Greenwood et al., 2007). This suggests that P2 receptors might be involved in pruning of neurons and thereby establishing the correct number of contacts with HCs. During retinal development P2 receptors have also been shown to regulate mitosis (Pearson et al., 2005). Knowledge of the function of P2 receptors during development of the mammalian cochlea is very limited.

P2 receptors signal damage

Noise overexposure has been shown to result in the accumulation of ATP in endolymphatic and perilymphatic spaces (Munoz et al., 2001). This is accompanied by the upregulation of $P2X_2$ receptors (Wang et al., 2003b). These data suggest that ATP plays a role under pathological conditions in the cochlea. Recently, *in vitro* experiments demonstrated that damage of single HCs leads to the release of extracellular ATP that triggers the propagation of an intercellular Ca^{2+} wave. Thus ATP is a molecule that signals the impaired integrity of damaged HCs to their neighbouring cells. At present, the P2 receptor subtypes that facilitate the damage-

induced propagation of the Ca^{2+} wave are not identified. It is established that IP_3 generation and thus P2Y receptors contribute to the Ca^{2+} wave formation (Gale et al., 2004; Piazza et al., 2007). Knowledge is also lacking about the downstream targets of increased intracellular Ca^{2+} and their subsequent signalling events during damage.

1.4 ERK1/2

1.4.1 Mitogen activated protein kinases – an overview

Cellular processes are tightly regulated and among other protein kinases, the family of MAPKs are highly responsive to external stimuli. The MAPK family comprises several subclasses – ERK 1 to 5 and 8, JNK 1-3 and p38 kinases α, β, γ and δ. A wide range of receptors, including those for EGF, neuronal growth factor (NGF), glutamate and purinergic agonists are coupled to the MAPK signalling cascade (Cowley et al., 1994; Traverse et al., 1994; Neary et al., 1999; Yang et al., 2004c). The presence or absence of agonists is sensed and can result in the activation or deactivation of MAPKs initiating distinct cellular programs. The activation or deactivation of one of these members can positively or negatively influence other members of the MAPK family; for example ERK1 and 2 activation concurrently negatively regulates the activity of JNK, or vice versa JNK activation results in deactivation of ERK1/2 (Xia et al., 1995; Lavoie et al., 1996). Thus the equilibrium between activated and deactivated states of these kinases at a certain point in time can determine the cellular responses and fate.

The different MAPKs are similarly activated by a MAPK signalling cascade that involves the hierarchical phosphorylation of several intermediate kinases (Fig 1.2). Receptor activation initiates the phosphorylation of the MAPK kinase kinase (MAPKKK) followed by the MAPK kinase that then phosphorylates and activates the MAPK. The kinase cascades differ between MAPK subclasses. For example, ERK 1 and 2 (ERK1/2) activation is accomplished by one of the following MAPKKKs: A-Raf, B-Raf or c-Raf (also called Raf-1). One of these kinases phosphorylates MEK1 or 2 (MEK1/2), the MAPKKs for ERK1/2. The ERK1/2 signalling cascade has been associated with tumour growth and invasion. Mutations

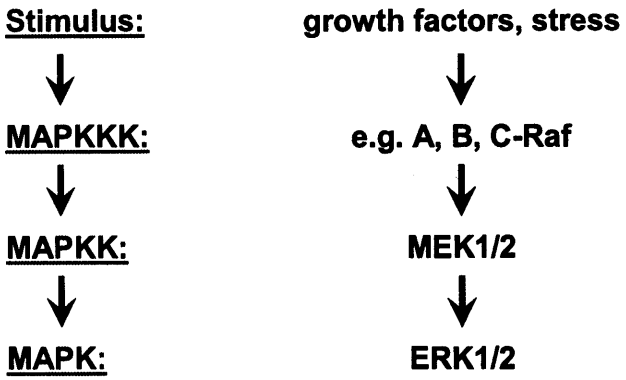

Fig 1.2 MAPK activation cascade
Left panel: hierarchical activation of MAPKs by the MAPK signalling cascade and
Right panel: ERK1/2 activation as an example.

in B-RAF or its upstream activator the small G-protein Ras were found to continuously activate ERK1/2 and thereby induce proliferation and tumour succession (reviewed in Dhillon et al., 2007).

Originally distinct functions were associated with the different MAPK subclasses. ERK1/2 activation was thought to be crucial for cellular survival, proliferation, tumour formation as well as differentiation, whereas JNKs and p38 kinases where thought to respond exclusively to cellular stress and to mediate signalling towards cell death. Hence JNKs were formerly called stress activated protein kinases (SAPK). More recently it has emerged that the functions of these kinases cannot be separated in such a clear-cut fashion. JNKs might be the death mediating kinases in one cellular system and yet in another they promote cell survival whereas the role in promoting cell death is been taken by ERK1/2. In order to accomplish their functions MAPKs either phosphorylate targets in the cytoplasm or are transferred to the nucleus where they affect gene transcription.

In the subsequent section the focus will be specifically turned to the activation of ERK1/2 and in particular its function during damage.

1.4.2 ERK1/2 – activation

ERK1/2 activation can be modulated via several signalling pathways upstream of MAPKKKs. Extracellular stimuli activate receptors that couple to heterotrimeric G-proteins. Inhibition of the pertussis-toxin sensitive subunit G_i reduces ERK1/2 activation (Soltoff et al., 1998; Neary et al., 1999; Neary et al., 2003). G-proteins can activate various enzymes including PLC or adenylyl cyclases that can result in the activation of ERK1/2 (Vossler et al., 1997; Corbit et al., 2000; Werry et al., 2005). Conversely, adenylyl cyclases that generate cAMP that subsequently activates PKA, are also reported to counteract ERK1/2 activation (Cook and McCormick, 1993; Stork and Schmitt, 2002). Another signalling event leading to ERK1/2 activation is the PLC mediated generation of IP_3 and diacylglycerol (DAG) that act on protein kinase C (PKC). DAG is a direct effector at PKC, whereas IP_3 mediates its actions in an indirect manner via the release of Ca^{2+} (Schonwasser et al., 1998; Corbit et al., 2000; Goldsmith and Dhanasekaran, 2007). Choline-specific PLC has also been suggested to result in the activation of ERK1/2 (Neary et al., 1999). In addition to G-protein coupled receptors, phosphotyrosine kinases can activate ERK1/2 via GTPases such as Ras. These activate Raf's – the MAPKKK's and thus link, together with their adaptor proteins, phophotyrosine kinase receptors to the ERK1/2 signalling cascade (Marshall, 1995). These are only a few examples of the vast number of intracellular effectors of ERK1/2 activation. The entire network of molecules involved in signalling towards ERK1/2 cannot be discussed in full detail in the scope of this introduction (for further information see Werry et al., 2005). Instead, as damage of hair cell epithelia has been shown to result in elevated Ca^{2+} levels (Hirose et al., 1999; Gale et al., 2004; Matsui et al., 2004) the focus here will be specifically turned towards the regulation of ERK1/2 by Ca^{2+}.

ERK activation/deactivation in a Ca^{2+}-dependent manner

The phosphorylation of ERK1/2 has been shown to depend on Ca^{2+} (Neary et al., 2003; Paul et al., 2003; Kupzig et al., 2005) but it can also occur independently (Cook et al., 1997; Yang et al., 2004c). The cell type and the extracellular stimuli determine the necessity for Ca^{2+} to activate ERK1/2. The activation of ERK1/2 in striatal neurons stimulated by 50 μM NMDA occurs in a Ca^{2+}-dependent manner, whereas the sub-threshold concentration of NMDA (1 μM, N-methyl-D-aspartic acid)

together with the metabotropic glutamate receptors (mGluR) agonist DHPG (3 μM, S-3,5-Dihydroxyphenylglycine) result in ERK1/2 activation independently of Ca^{2+} (Yang et al., 2004c). Ca^{2+} can act through different mechanisms that include the activation of a calmodulin dependent kinase (Schmitt et al., 2004) or of Ras-GRF (guanosine nucleotide releasing factors, (Farnsworth et al., 1995).

Three classes of phosphatases regulate the dephosphorylation and thus the deactivation of ERK1/2: i) dual specificity phosphatases, ii) serine/threonine phosphatases and iii) tyrosine phosphatases (reviewed in Raman et al., 2007). In some cells Ca^{2+} is required for the deactivation of ERK1/2. Mitogen activated protein kinase phosphatase (MKP) is newly synthesised upon activation of ERK1/2. The absence of Ca^{2+} during the induction of MKP expression results in the failure to dephosphorylate ERK1/2 and thereby ERK1/2 activation sustained (Cook et al., 1997). Another specific neuronal phosphatase STEP (striatal enriched protein tyrosine phosphatase) that deactivates ERK1/2 requires Ca^{2+} in order to be dephosphorylated and switched to its active conformation (Paul et al., 2003). In addition to the dephosphorylation of ERK1/2, the inactivation of the upstream signalling cascade leads also to the abrogation of ERK1/2 signalling. CAPRI, a Ca^{2+}-dependent Ras-GTPase activating protein induces Ras to hydrolyse the bound GTP and thereby Ras is transferred into its inactive form that is not sufficient to activate ERK1/2 (Lockyer et al., 2001).

1.4.3 ERK1/2 activation during damage and cell death

Many processes/steps during and following injury or oxidative stress are regulated by one or several members of the MAPK family. The members most studied during cytotoxic events are JNKs, p38 kinases and ERK1/2 and all of them have been implicated in stress-induced signalling. As discussed above the functions of these kinases are diverse and differ depending on cell types. Oxidative stress is a key player during HC damage and death following noise exposure and ototoxic insults. Therefore, the function of damage- or oxidative stress-induced activation of ERK1/2 will be discussed in more detail.

Acute damage such as mechanical strain was observed to activate ERK1/2 immediately within minutes following the insult (Neary et al., 2003; Matsubayashi et al., 2004). This activation has been shown to be mediated by damage-induced release of ATP. Chemical mediators including H_2O_2 and cisplatin can induce a delayed onset of ERK1/2 activation several hours after the initial exposure dependent on their concentration and mode of action (Wang et al., 2000). The function and targets of activated ERK1/2 during stress signalling are not only diverse but also opposing. In one cellular system activated ERK1/2 is critical for cell survival, whereas in another it promotes cell death (Xia et al., 1995; Nowak, 2002; Sperandio et al., 2004; Subramaniam et al., 2004; Chen et al., 2005; Arthur et al., 2006). Adding a further level of complexity, in a lung carcinoma cell line (A549) the type of toxic stimulus determines whether ERK1/2 promote cell survival or cell death. Cisplatin, a drug that is also ototoxic induces ERK1/2 mediated cell death in A549 lung carcinoma cells, whereas during oxidative stress following exposure to H_2O_2 or doxorubicin ERK1/2 act as survival factors (Wang et al., 2000). The downstream signalling events of activated ERK1/2 that lead to the execution of either survival or cell death are only beginning to be unravelled and some are discussed in more detail below. Subsequently, the function of ERK1/2 in re-establishing the integrity of damaged cell monolayers or organs will be outlined.

ERK1/2 – damage and survival signalling

Survival signalling was originally considered to be one of the main functions of ERK1/2 during pathological events. Xia et al. (1995) provided the first evidence that ERK1/2 activation resulting from overexpression of the MAP kinase kinase MKK can oppose apoptosis in PC-12 cells induced by withdrawal of neuronal growth factor (NGF). Subsequently, further research confirmed a role of activated ERK1/2 in survival signalling.

The potential mechanisms that ERK1/2 exploit to sustain the survival status can be divided into two wider categories – one is the phosphorylation of pro- and anti-apoptotic cytoplasmic targets and the second is the positive or negative regulation of transcription factors that are anti- and pro-apoptotic, respectively. ERK1/2 have been described to interact with pro-apoptotic proteins that are located in the cytoplasm. It has been suggested that activated ERK1/2 can phosphorylate

caspase-9 at threonine residue 125 and that this modulation inhibits caspase-9's ability to auto-cleave and thereby activate itself. Thus the proteolytic activation of caspase-3 and the execution of the death signalling cascade are discontinued (Allan et al., 2003). This mechanism could potentially also sense trophic factor withdrawal leading to reduced ERK1/2 activation including decreased phosphorylation of caspase-9 that then permits the initiation of the apoptotic signalling cascade.

Another mechanism that has been proposed to be crucial for cellular survival is the ERK1/2 induced phosphorylation of BAD, a pro-apoptotic member of the Bcl-2 family (Bonni et al., 1999). The dephosphorylated form of BAD binds to mitochondrial Bcl-2 proteins to trigger apoptosis, but upon phosphorylation BAD dissociates resulting in survival. Moreover, XAIP, a member of the apoptosis inhibiting protein family (AIP) that interacts with caspases and thereby maintains them in their inactive form, has also been shown to be regulated by ERK1/2 (Gardai et al., 2004). Whether ERK1/2 activation resulted in the stabilisation of XAIP or in sustained expression was not investigated.

Activated ERK1/2 not only modulate cytoplasmic target proteins, but also alter gene expression profiles through the regulation of transcription factors, thereby influencing cell survival. Phosphorylation of the transcription factor CREB (cAMP response element binding-protein) mediated by activated ERK1/2 can lead to the expression of survival genes such as Bcl-2 (Bonni et al., 1999; Wang et al., 2006a). Moreover, ERK1 has been shown to positively regulate Nrf-2-induced gene expression in C10 murine alveolar type II-like epithelial cell line during hyperoxia (Papaiahgari et al., 2004). Nrf-2 is a transcription factor that regulates the expression of genes such as glutathione-S-transferase, γ-glutamylcysteine synthetase and heme oxygenase-1 that maintain the redox-balance of cells exposed to oxidative stress (Chan et al., 2001; Braun et al., 2002). To summarise: the activation of ERK1/2 together with the action of another survival kinase the PI-3 kinase could result in a concerted response in order to preserve cellular function and survival during damaging stimuli. The exact mechanisms that are employed downstream of ERK1/2 activation to facilitate survival and those that integrate survival and death signalling events remain to be determined.

ERK1/2 activation promotes cell death

The tumour suppressor p53 is crucial for cell survival. Activation of p53 by oxidative stress can either lead to cell cycle arrest or apoptosis. One of the downstream events of activated ERK1/2 is the activation and upregulation of p53 that subsequently initiates cleavage of procaspase-3 (Wang et al., 2000; Li et al., 2005). Activated ERK1/2 are demonstrated in a different report to exert their action on phospholipase A_2 (PLA_2) that produces arachidonic acid which in turn favours the release of mitochondrial cytochrome c, the activation of caspase-3 and its downstream target poly(ADP-ribose) polymerase (PARP) (Kim et al., 2003). Arachidonic acid was observed to bind to the NADPH-oxidase (Pessach et al., 2001) resulting in the formation of ROS, that could then trigger the execution of apoptosis. Moreover, ROS formation was also observed when aminoglycosides that are ototoxic, were exposed to arachidonic acid and NADH in a cell free non-enzymatic system (Sha and Schacht, 1999). ROS have also been shown to induce ERK1/2 activation. Thus ERK1/2 induced ROS generation could result in a feedback loop that maintains ERK1/2 in an activated state. ROS scavengers or overexpression of the copper/zinc superoxide dismutase 1 are sufficient to inhibit ERK1/2 activation and attenuate cell death (Wang et al., 2000; Noshita et al., 2001). ERK1/2 activation by ROS could be accomplished directly through manipulation of the ERK1/2 activating cascade. However, recent data suggest that oxidative stress results in the inactivation of the ERK1/2 deactivating phosphatases and thereby indirectly increases ERK1/2 activation (Levinthal and Defranco, 2005). Hence, ERK1/2 activation by ROS could be a result of the action of two potential mechanisms i) modulation of the ERK1/2 activating cascade or ii) impairment of the function of the ERK1/2 deactivating phosphatases. These mechanisms could act independently but also mutually.

Calpains are calcium-dependent intracellular cysteine proteases that have also been implicated in the execution of cell death in response to oxidative stress. Knock-down of the regulatory subunit of calpain that is encoded by the gene capn4 has been observed to attenuate cell death induced by UV-irradiation or other mediators of oxidative stress (Tan et al., 2006). Cleavage of caspases and the release of mitochondrial cytochrome-c are involved in calpain-mediated apoptosis. As calpains can be directly targeted and activated by ERK1/2 (Glading et al., 2004; Tan et al.,

2006), it is possible that this is an additional mechanism by which ERK1/2 might promote cell death.

The death-associated protein kinase (DAPK) has been implicated in triggering cleavage of caspase-3 and its substrate PARP but also in the activation and upregulation of the transcription factor p53 and thereby to induce apoptosis. The activation of DAPK requires the phosphorylation of its death domain by activated ERK1/2 (Wang et al., 2002a; Chen et al., 2005; Stevens et al., 2007). Conversely, exposure to phorbol ester PMA or EGF reduced DAPK-induced apoptosis in an ERK1/2 dependent manner. In that study ribosomal S6 kinase 1 (RSK-1), one of the downstream targets of ERK1/2, was shown to phosphorylate DAPK at its calmodulin-binding domain resulting in the attenuation of apoptosis (Anjum et al., 2005). The phosphorylation sites described in those reports differ suggesting that activated ERK1/2 could have a dual role. DAPK also functions as an ERK1/2 binding protein and thereby sequesters ERK1/2 in the cytoplasm disabling its performance in the nucleus (Chen et al., 2005). Similarly, the retention of activated ERK1/2 by DAPK could interfere with the phosphorylation of RSK-1. Thus DAPK cannot be phosphorylated at its calmodulin-binding domain resulting in its release to exert its pro-apoptotic effect. Thus, cell fate is potentially determined according to the balance of phosphorylation between the two sites.

To summarise, ERK1/2 acts on a variety of targets through which it exerts its pro-apoptotic effect. The actions of ERK1/2 during cell death and the mechanisms of how single downstream events interact in the signalling network continue to be unravelled.

ERK1/2 – a role in wound repair

Damage repair is crucial to the continued survival and function of tissues and organs. Repair can be accomplished as a result of migratory wound closure which can be followed by proliferation to replace damaged or dead cells. Cells neighbouring the damaged area gain migratory competence due to the action of MAPKs including ERK1/2, that are activated following the damaging insult. Both, pharmacological inhibition of ERK1/2 activation and expression of dominant-negative mutants of ERK1 or ERK2 reduces the capacity to close wounds (Matsubayashi et al., 2004; Providence and Higgins, 2004). A proliferative response subsequent to damage and

wound closure often requires the dedifferentiation of cells. Schwann cells can be driven to dedifferentiate in a Raf-1/MEK1/2 dependent fashion. However, these cells were not able to re-enter the cell cycle and proliferate (Harrisingh et al., 2004). Following brain injury, the activation of the protease-activated receptor-1 (PAR-1) contributes to astrogliosis, measured by an increase in the number of astrocytes positive for glial fibrillary acidic protein. Exposure of astrocytes *in vitro* or in the striatum to a PAR-1 agonist promotes proliferation that requires the activation of ERK1/2 (Nicole et al., 2005). In order to initiate cell cycle entry, activated ERK1/2 control the transcriptional upregulation of proliferative effectors such cyclin D1 and the downregulation of antiproliferative gene products including JunD, Gadd45α (growth arrest and DNA damage-inducible 45α) and Sox6 (SRY box containing gene 6, (Lavoie et al., 1996; Harrisingh et al., 2004; Yamamoto et al., 2006). Taken together this indicates that ERK1/2 can play crucial roles at various stages during wound repair that depending on the types of cell and organs.

1.4.4 MAPKs and the inner ear

In the inner ear knowledge about the functions of the various MAPKs is quite limited. The focus of research has mainly been upon the role of JNKs, which have been shown to be activated in HCs during exposure to aminoglycosides and following acoustic overstimulation (Pirvola et al., 2000; Ylikoski et al., 2002; Wang et al., 2003a; Matsui et al., 2004; Sugahara et al., 2006; Wang et al., 2006b). During both noise damage and aminoglycoside-induced ototoxicity inhibition of JNK activation preserves the function of HCs (Pirvola et al., 2000; Wang et al., 2003a; Matsui et al., 2004; Wang et al., 2006b). In contrast, cisplatin-induced hearing loss was not prevented using the JNK inhibitor D-JNKI-1 (Wang et al., 2004). The role of another MAPK member – the p38 kinase – during HC damage is controversial. In rat cochlear explants p38 kinases have been suggested to promote HC death during exposure to gentamicin (Wei et al., 2005), whereas in murine utricles HCs die independently of p38 kinases (Sugahara et al., 2006). Activated ERK1/2 has been shown to be a pro-survival signal in HCs (Battaglia et al., 2003). Moreover, proliferation in chick utricular epithelial sheet cultures stimulated by serum occurred partially in an ERK1/2 dependent manner (Witte et al., 2001). Exposure of rat utricular epithelial cultures to recombinant human glial growth factor 2 triggered cells of this epithelium

to also proliferate. The ERK1/2 pathway is one of a number of signalling cascades engaged to facilitate that proliferative response (Montcouquiol and Corwin, 2001). With respect to damage signalling, studies using immortalised HC lines implicate a role for ERK1/2 during gentamicin- and cisplatin-induced toxicity (Kalinec et al., 2005; Previati et al., 2007; So et al., 2007). However, the study by Previati et al. (2007) showed that application of the ERK inhibitor PD 98059 resulted in reduced cell death in the presence of cisplatin, whereas, using Western blot analysis activated ERK1/2 were only reduced in the presence of PD 98059 at 16 hrs but not at 10 hrs or 24 hrs of cisplatin exposure. So et al. (2007) demonstrated that ERK1/2 inhibitors reduced the release of pro-inflammatory cytokines during cisplatin-induced cell death. However, these results have to be taken with caution as immortalised HC lines do not express all features of functional HCs and therefore the signalling events activated by ototoxic drugs are likely to differ. In cochlear explants treated with gentamicin HC death was enhanced when ERK1/2 activation was inhibited (Battaglia et al., 2003) suggesting that ERK1/2 are key players in HC survival. Despite these investigations it has not been determined whether ERK1/2 are activated in HC epithelia following damage of HCs.

1.5 Aims

Cell to cell communication and in particular that between hair and support cells must occur during traumatic events in order to trigger wound repair, re-establishment of the physiological environment for surviving cells and in some cases a proliferative response. As outlined in this introduction such signalling mechanisms are only poorly understood. An intercellular Ca^{2+} wave has been described to travel in an ATP-dependent manner into the outer sulcus (OS) region as a result of hair cell damage (Gale et al., 2004). The aim of this thesis was to investigate, whether damage also triggers changes in intracellular Ca^{2+} levels in the HC and inner sulcus regions and to further the understanding of the mechanisms underlying the Ca^{2+} wave formation. This included investigations to the source of Ca^{2+} and the propagation mechanisms; in particular the roles of ATP and gap junctions were examined as these have been shown to be crucial in other cellular systems. The function of the Ca^{2+} wave described by Gale et al. (2004) has not been studied.

One of the signalling cascades that is not only activated by Ca^{2+} but also reported to mediate wound closure, is the ERK1/2 signalling cascade (Matsubayashi et al., 2004; Kupzig et al., 2005). Therefore, it was tested in this thesis whether i) mechanical damage also triggers the activation of ERK1/2 and ii) whether the same mechanisms that underlie the formation of the damage-induced Ca^{2+} wave result in activation of ERK1/2. Hair cells presented with toxic stimuli such as aminoglycosides or neoplastic drugs become damaged and die. Therefore, the question was raised whether ERK1/2 play a role during such toxic events.

ATP has been shown to be increased in the endolymph following hair cell damage and has been suggested as a damage signalling molecule (Munoz et al., 2001; Gale et al., 2004). However, the exact nature of the P2 receptors activated during damage is currently not known. In this thesis, pharmacological, immunohistochemical and electrophysiological approaches were used to further this knowledge.

2. Material and Methods

2.1 Chemicals and solutions

2.1.1 Materials

Fluorescent-labelled substances were obtained from Molecular probes and all chemicals were from Sigma unless otherwise specified.

U0126, U0124 and BAPTA-AM (1,2-bis-(o-Aminnophenoxy)-ethane-N, N, N', N'-tetraacetic acid tetraacetotoxy-Methyl ester) were obtained from Cell signalling. U73122, Raf kinase inhibitor I and U0126 were obtained from Calbiochem and PPADS (Pyridoxal phosphate-6-azo(benzene-2,4-disulfonic) acid) from Tocris.

The sources of primary antibodies are given in Table 2.6.

2.1.2 External and internal solutions

External solutions

The constituents of external solutions used are given in Table 2.1. The pH of hepes-buffered Hank's balanced salt solution (HB-HBSS) was adjusted to 7.4 and those of ACSF (artificial cerebrospinal fluid) and patch ringer were 7.3. In a subset of experiments 1 mM Ca^{2+} in HB-HBSS was replaced with 1 mM Mg^{2+} and additionally chelated with 1 mM EGTA (ethylene glycol-bis(β-aminoethyl ether)-N,N,N',N',-tetraacetic acid). The conditions in which this external solution was used will be referred to as 0 Ca^{2+} throughout this thesis.

Internal patch solution

Constituents of the internal patch solution used are given in Table 2.2. In some experiments ATP and GTP were omitted. The pH was adjusted to 7.30 with KOH and osmolarity to 290 mOsm by diluting the solution. Aliquots were stored at -20 °C.

Table 2.1: Composition of external solutions.

substance	Molecular weight [g/mol]	Concentration [mM]		
		HB-HBSS	ACSF	Patch ringer
NaCl	58.44	137	119	119
KCl	74.56	5.37	2.5	2.5
$MgCl_2x6\ H_2O$	203.3	1	1.3	1.3
$CaCl_2$ x 2 H_2O	147.02	1	2.5	2.5
NaH_2PO_4 x H_2O	137.99	0.65	1	1
$NaHCO_3$	84.01	-	26.2	-
KH_2PO_4	136.9	0.44	-	-
Hepes	238.30	10	-	20
Glucose	180.16	5.5	11	11

Table 2.2 Composition of internal patch solution.

Substance	Molecular weight [g/mol]	Concentration [mM]
Methanesulfonate	96.1	131.1
EGTA (KOH)	380.4	0.2
Hepes	238.3	20
$MgCl_2$	203.3	1
Na-ATP	551.1	2
Na-GTP	523.2	0.2

2.1.3 Stock solutions of drugs

All stock solutions were prepared and stored at -20 °C in aliquots to avoid freeze-thawing unless otherwise specified. U0126, U0124, cRAF1 inhibitor 1, U73122, and carbenoxolone (CBX) were dissolved in dimethylsulfoxide (DMSO) to make a 1000x stock except for CBX. CBX was prepared as a 50 mM stock in DMSO

and then further diluted in 18 MΩ nanopure water to give a 5 mM stock solution. The final concentration used was 75 µM. Octanol was dissolved to a final concentration of 1 mM in ACSF that was supplemented with 1:1400 DMSO (10 mM). BAPTA-AM was dissolved in 10 % pluronic in DMSO to obtain a 1000x stock. PPADS and suramin were dissolved in 18 MΩ nanopure water to obtain a 50 mM or a 1000x stock, respectively. Lyophilised apyrase mixed with potassium succinate salts were reconstituted at 400 U/ml in MilliQ water. Neomycin was dissolved in Dulbecco's Modified Eagle's medium with F12 (DMEM/F12, Gibco). Neomycin, suramin, CBX and octanol were prepared on the day of the experiment.

2.2 Isolation and culture of cochlear explants

Cochleae were isolated from neonatal Sprague Dawley rats between P1 and P3. In detail, rats were sacrificed by rapid cervical dislocation according to schedule 1 procedure and then decapitated. The head was sterilized in 70 % ethanol for 5 – 10 min in order to avoid bacterial contamination during the isolation procedure. The head was cut along the midline and separated into two halves. Following removal of the brain, connective tissue and surrounding bone, the cochlear bullae were transferred into Medium 199 (M199, Gibco, UK) supplemented with penicillin and fungizone (10 U/ml; 25 ng/ml). In order to access the cochlea, the bulla was opened and freed from the surrounding cartilage. The stria vascularis and Reissner's membrane were removed and the cochlea cut into its basal to apical turns. For most of the experiments, unless otherwise indicated, only basal and middle turns were cultured. The cochlea turns were transferred onto MatTek® dishes (USA) that had been coated with Celltak® (BD Biosciences, UK). For coating, Celltak® was diluted in 0.1 mM $NaHCO_3$ to a concentration of 73 µg/ml and 30 µl was spread across the coverslip of the MatTek® dish. The dishes were incubated at room temperature for at least 1 hr. Prior to plating the cochlear coils Celltak® was removed and the dishes were rinsed four times in Dulbecco's Modified Eagle's medium with F12 (DMEM/F12, Gibco, UK) that was supplemented with 5 % fetal bovine serum (FBS, Gibco, UK). Cochlear turns were cultured in DMEM/F12 containing 5 % FBS at 37 °C in a 5 % CO_2/95 % air atmosphere. Cochlear explants were used after one day *in vitro* for all experiments except for the patch clamp studies.

2.2.2 Isolation of cochlear explants without culture

The isolation procedure of cochlear coils designated for patch clamp experiments differed only in two aspects: i) isolation was carried out in ACSF (see 2.1) saturated with 95 % O_2/5 % CO_2 and ii) isolated cochlear coils were used on the same day. Cochleae were cut into basal and middle turns and held down using a platinum harp.

2.3 Damage paradigms

2.3.1 Cochlear damage models

Several models have been employed to study cochlear pathology. These include in vivo studies in mature animals or in vitro studies, using either postnatal explants or immortalised cochlear cell lines (OC-2, HEI-OC1) (Richardson and Russell, 1991; Wang et al., 2002b; Nicotera et al., 2003; Wang et al., 2003a; So et al., 2007). In vivo models are advantageous as mature animals are used to investigate both toxic and traumatic events. However, studies of dynamic signalling processes especially of short-lasting events are very difficult to undertake in vivo. Postnatal cochlear explants offer the possibility to examine such processes while the structure of the organ of Corti is maintained. At present explants are only possible to culture during the early postnatal period. However, the onset of hearing in rats occurs at around P12 (Geal-Dor et al., 1993; Freeman et al., 1999). There are many developmental changes still occurring in cochlear cells during the first postnatal weeks. These include e.g. changes in the expression patterns of ion channels/ currents in hair cells and of connexins in support cells to only name a few (Jagger and Forge, 2006; reviewed in Housley et al., 2006).

In this PhD thesis in order to study dynamic signalling events occurring during damage of the mammalian cochlea, postnatal cochlear explants were chosen as the model. Culture of these explants allows cells to recover from the traumatic isolation procedure. In addition, cochlear explant cultures offer the opportunity to study processes over several days.

2.3.2 Laser damage

Laser damage was used to investigate the time course and mechanism of damage-induced activation of ERK1/2. The lesions were induced using a Micropoint system (Photonic Instruments Inc., USA). Briefly, the technique is based on a nitrogen laser (Laser Science Inc.) emitting energy of a wavelength at 337 nm (70 kW peak output, 70 ns). UV-light is transmitted via a fibre optic into a dye cell containing Coumarin. The dye cell is crucial to re-establish coherence of the beam that is lost during the transmission along the fibre optic. The dye emits a 440 nm beam onto steering mirrors that are used to align and focus the beam through the lens onto the specimen. The intensity of the emitted light and thus the size of the lesions were adjusted with a graded neutral density attenuator plate.

In detail, the laser beam was focused through a 40x 1.3 N.A. Zeiss Fluar objective (oil immersion) onto the specimen. The cochlear culture was placed so that a 2nd row OHC was centred in the path of the laser beam. Damage was introduced while focusing from the apical surface of the cochlear coil to its basal aspect. Several pulses were sufficient to induce a lesion once the focal plane of the laser beam was reached.

2.3.3 Needle damage

In order to image a larger area of the cochlear cultures a 20x 0.75 Zeiss Fluar objective was used The laser ablation technique was not effective with lower magnification/N.A. lenses. Therefore mechanical trauma was implemented using a microneedle. The tip of the microneedle was positioned 15 µm above the focal plane of the hair bundle of the second row of OHCs. Damage was induced by lowering the microneedle ~60 µm using the remote controlled piezoelectric manipulator (Burleigh) where it was held for two seconds and returned to its original position above the tissue. For the majority of experiments the microneedle was positioned in the centre of the field of view.

The needle damage technique was also applied in experiments investigating damage-induced currents. For these experiments the microneedle was placed 94 µm above a cell situated five cells away from the patch-clamped Deiters' cell (same row, Fig 5.1A). This technique was chosen to avoid disruption of the seal between the

electrode and the patched cell. The microneedle was lowered by 110 µm to induce the first lesion and after two seconds it was placed back to its original position. The procedure was repeated at the site of the first lesion 30 min later but the second time the microneedle was lowered 125 µm.

2.3.4 Neomycin-induced HC damage

Neomycin was used as a damage paradigm to investigate ERK1/2 signalling when HCs were targeted specifically. Neomycin (1 mM with 1:1000 DMSO vehicle) with the addition of 10 µM U0126 (in DMSO) or its inactive analogue U0124 (10 µM, in DMSO) was applied to cochlear cultures. To assess whether U0126 alone was HC toxic it was applied to cochlear cultures in the absence of neomycin. Test solutions were placed at 37 °C (5 % CO_2) for 20 min prior to use. Cochlear cultures were washed four times in test solution before incubating them at 37 °C in a 5 % CO_2/95 % air atmosphere for 8 or 24 hrs (Fig 2.1). In some experiments cultures were exposed to neomycin for 8 hrs after which they were switched into DMEM/F12 containing vehicle control, U0126 or U0124 without neomycin for further 16 hrs (Fig 2.1). Culture media were changed at 4, 8 and 20 hrs to avoid breakdown of test substances. Following the mentioned incubation paradigms cultures were fixed (fixation details see 2.7.1) and immunocytochemically labelled for activated ERK1/2, chromatin and filamentous actin following the various incubation times (see 2.7.2).

2.4 Local application of nucleotides

The responsiveness of cochlear cells to different purine nucleotides was assessed using i) voltage clamp studies, ii) Ca^{2+} imaging and iii) activation of ERK1/2. Nucleotides were prepared as 100 mM stock solutions in 18 MΩ nanopure water and were diluted to their final concentrations in HB-HBSS for Ca^{2+} imaging and for ERK1/2 activation experiments. Solutions were applied locally by a micropipette picospritzer (puff application). In order to avoid blockage of micropipettes the

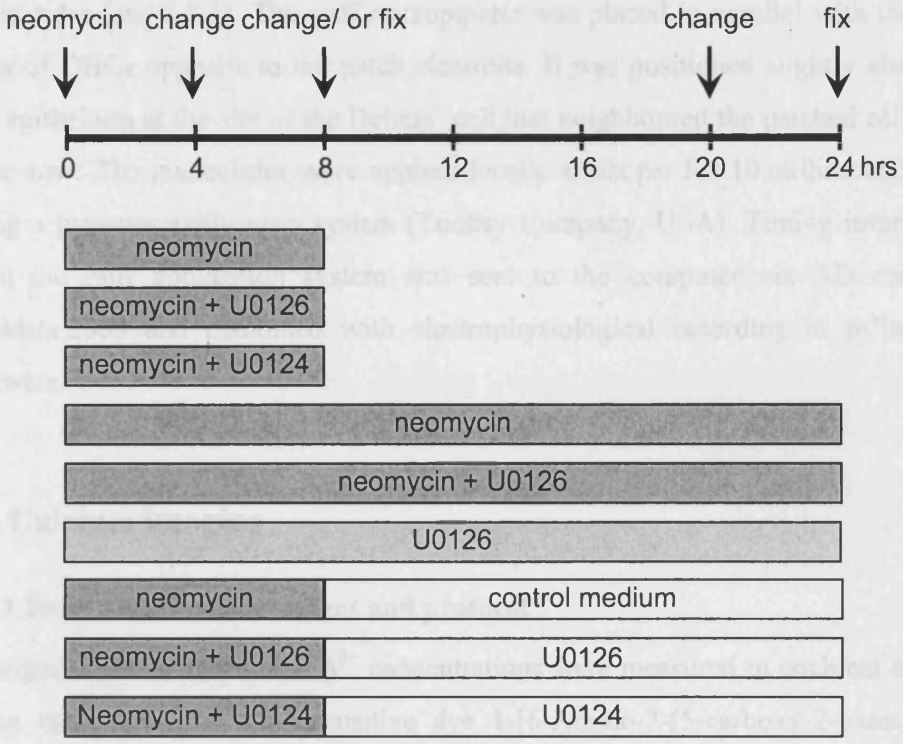

Fig 2.1 Overview of experimental set up.

Most upper panel indicates the time scale of the experiment. 'Change' indicates the time point of renewal of test medium and 'fix' that of fixation. Below are the different conditions tested.

nucleotide solution was sterile filtered and then filled into micropipettes (2 µm tip diameter) that were pulled using a two step electrode puller (Narashige, Japan).

The micropipette was placed 2 µm above the focal plane of the 1st row of OHCs but positioned above the outgrowing Claudius-like cells approximately 20 µm from the edge of 3rd row OHCs. Nucleotides were locally applied with a pressure of six psi which did not activate mechanically-induced Ca^{2+} signals. 100 µM ATP and UTP were applied for 10 s, whereas 100 µM ADP, UDP and AMP were applied for 20 s. The onset of nucleotide application was noted.

In patch clamp experiments the nucleotides were diluted in patch ringer (Table 2.1). Micropipettes prepared for patch clamp experiments were also used to puff apply

nucleotides (see 2.8.1). The puff micropipette was placed in parallel with the three rows of OHCs opposite to the patch electrode. It was positioned slightly above the HC epithelium at the site of the Deiters' cell that neighboured the patched cell in the same row. The nucleotides were applied locally at six psi for 10 milliseconds (ms) using a pressure application system (Toohey Company, USA). Timing information from the puff application system was sent to the computer via AD converter Digidata 2000 and combined with electrophysiological recording in pClamp 9.2 software.

2.5 Calcium imaging

2.5.1 Fura-2 Ca^{2+} measurement and protocol

Changes in the cytoplasmic Ca^{2+} concentrations were measured in cochlear cultures using the ratiometric Ca^{2+} sensitive dye 1-[6-Amino-2-(5-carboxy-2-oxazolyl)-5-benzofuranyloxy]-2-(2-amino-5-methylphenoxy)ethane-N,N,N',N'-tetraacetic acid (Fura-2). Fura-2-AM, which has an acetotoxy methyl group attached to make it cell permeable, was dissolved in 10 % pluronic in DMSO to a 3 mM stock solution. Cultures were loaded with 3 µM Fura-2-AM in DMEM/F12 for 40 to 50 min at 37 °C in a 5% CO_2/95 % air atmosphere, washed four times in HB-HBSS and then placed at 25 °C for 20 min to allow esterases to cleave the AM groups. Experiments were carried out at room temperature (20 – 23 °C) in HB-HBSS.

Fura-2 was alternatively excited at 340 nm and 380 nm using a monochromator (Kinetic Imaging Ltd.). Epifluorescent light was passed through a 505 nm dichroic mirror and a 510 nm long pass filter and images were captured on a 12-bit cooled CCD 1280 x 1024 pixel sensicam camera (PCO, Germany). AQM/IQ software (Kinetic Imaging Ltd./Andor Imaging Inc) controlled the specimen illumination and image capture. Routinely, the protocol comprised of 200 frames of 256 x 300 pixel images (4x4 pixel binning) and both channels were exposed for 500 ms. Needle damage was induced after collecting baseline data for approximately 20 s. Puff application of nucleotides was also initiated after a similar baseline recording. The time of damage and nucleotide application were noted.

In most cases the cochlear coils were large enough to perform at least three lesions. The distance between lesions was at least 300 µm. The first damage stimulus was always carried out in HB-HBSS containing the vehicle that the drugs were dissolved in. The second and third damage stimuli were induced following a 30 min incubation period in HB-HBSS supplemented with the drug or its vehicle except for BAPTA-AM which was pre-applied for 90 min. An interval of approximately 5 to 7 min separated the second and third damage stimuli as re-positioning and re-focussing of the microneedle was required. Similarly, nucleotides were applied at two spatially separated sites (at least 500 µm) along the cochlear turn. The cultures were fixed 5 min after the last insult or puff application (see 2.7.1) and a subset was included into the ERK1/2 study.

2.5.2 Analysis of Ca^{2+} measurements

The 340/380 ratios (R) are proportional to the cytoplasmic Ca^{2+} concentrations and the changes in the ratio (ΔR) reflect changes in cytoplasmic Ca^{2+} levels $[Ca^{2+}]_c$. 340 and 380 intensity levels were determined using Metamorph software (Molecular Devices Inc.) and exported into Microsoft Excel, where baseline levels were subtracted (F340: 108; F380: 135 grey levels, range from 0 to 4095 grey levels) and ΔRs were calculated:

$$R = \frac{F340 - baseline_{340}}{F380 - baseline_{380}}$$

$$\Delta R = R - R_0$$

Regions of interest

In order to assess the formation of the Ca^{2+} wave the analysis was subdivided according to the distinct regions of cochlear cultures that are the OS, the HC and the IS. In the OS region regions of interests (ROIs, 20 x 20 µm) were positioned at 45 ° angle to the HC rows in both directions from the lesion site at the following distances: 42-70 µm, 98-126 µm, 154-182 µm and 210-238 µm (Fig 4.2 A). ROIs

were positioned at 40-60 μm, 80-100 μm and 120-140 μm to both sites from the lesion site longitudinally along the rows of HCs (Fig 4.2C). In the IS region ROIs were placed at 60-80 μm, 100-120 μm and 140-160 μm horizontally from the lesion site (Fig 4.1E). The data were extracted and calculated as described above. If there were more than one ROI at the same distance the intensities were averaged.

In a subset of experiments the microneedle was placed at the top of the image allowing 20 x 20 μm ROIs to be positioned from 30 μm up to 270 μm from the lesion site along the HC rows. The ROIs for the IS and OS regions were kept as described above with the exception that Ca^{2+} levels were determined in only one diagonal array of ROIs in the OS region.

Determination of maximum changes in cytoplasmic Ca^{2+}

Peak Ca^{2+} changes were determined using Microsoft Excel for comparison between control and drug treatment. The two consecutive lesions in the presence of the drug were pooled together as were the initial control lesions and the 2/3 lesions performed in a small number of all control experiments. This method was verified on the basis that no differences in peak Ca^{2+} changes were observed between the two consecutive lesions in drug treated cultures. In the case of 0 Ca^{2+} for the OS region the peak Ca^{2+} changes of the 2nd lesion in 0 Ca^{2+} was reduced compared to the 1st; most likely as a result of depletion of Ca^{2+} stores. Therefore, only the 1st lesion was included in the comparison. Statistical analysis was carried out using unpaired, two-tailed Student's *t*-tests. In addition, the apyrase + CBX and U73122 + 0 Ca^{2+} data sets were subjected to ANOVA.

Changes in resting cytoplasmic calcium concentration (R_0 values)

To check whether drugs affected baseline Ca^{2+} concentration the Fura-2 ratios at time zero (R_0) were determined for each ROI in the distinct cochlear region. Measurements of R_0 were taken before and after drug exposure for comparison with controls (Tables 2.3 – 2.5). R_0 values were significantly increased in the presence of U73122 in the OS but not the HC or IS regions. Suramin increased R_0 values in all regions whereas 0 Ca^{2+} reduced R_0 in the HC region only.

Table 2.3: R0 values in the OS and IS region. *P < 0.05, *t*-Test

	OS region				IS region		
Distance from lesion [µm]	**42-70**	**98-126**	**154-182**	**210-238**	**60-80**	**100-120**	**140-160**
Control: 0 Ca^{2+}/ U73122/PPADS	0.54 ± 0.011	0.50 ± 0.011	0.48 ± 0.008	0.49 ± 0.011	0.50 ± 0.012	0.47 ± 0.018	0.44 ± 0.036
0 Ca^{2}	0.50 ± 0.022	0.48 ± 0.022	0.47 ± 0.021	0.42 ± 0.007*	0.46 ± 0.011*	0.43 ± 0.019	0.38 ± 0.022
U73122	0.68 ± 0.009*	0.64 ± 0.019*	0.64 ± 0.023*	0.61 ± 0.024*	0.49 ± 0.014	0.45 ± 0.016	0.44 ± 0.075
0 Ca^{2+} + U73122	0.64 ± 0.017*	0.60 ± 0.026*	0.57 ± 0.016*	0.52 ± 0.015	0.50 ± 0.005	0.45 ± 0.006	0.39 ± 0.006
control APY+CBX	1.18 ± 0.057	1.18 ± 0.067	1.16 ± 0.037	1.34 ± 0.122	1.10 ± 0.056	1.11 ± 0.045	1.18 ± 0.043
APY	1.13 ± 0.046	1.17 ± 0.045	1.17 ± 0.041	1.16 ± 0.087	1.18 ± 0.042	1.2 ± 0.034	1.24 ± 0.026
APY+CBX	1.15 ± 0.052	1.14 ± 0.049	1.13 ± 0.059	1.20 ± 0.069	1.29 ± 0.038	1.23 ± 0.036	1.15 ± 0.052
CBX	1.2 ± 0.062	1.17 ± 0.051	1.15 ± 0.067	1.5 ± 0.164	1.31 ± 0.043*	1.26 ± 0.039*	1.22 ± 0.051
control suramin	0.96 ± 0.015	0.89 ± 0.019	0.80 ± 0.014	0.79 ± 0.011	0.86 ± 0.023	0.88 ± 0.014	1.01 ± 0.017
suramin	1.02 ± 0.019	0.94 ± 0.027*	0.85 ± 0.016*	0.90 ± 0.025*	0.92 ± 0.009*	0.96 ± 0.015*	1.06 ± 0.018*
PPADS	0.52 ± 0.018	0.47 ± 0.026	0.47 ± 0.023	0.40 ± 0.019	0.51 ± 0.01	0.50 ± 0.01	0.50 ± 0.008

Table 2.4: R0 values in HC region for the data set investigating the source of Ca^{2+}. *P < 0.05, *t*-Test

Distance from lesion [µm]	30-50	50-70	70-90	90-110	110-130	130-150	150-170	170-190	190-210	210-230	230-250	250-270
Control: 0 Ca^{2+}/U73122 /PPADS	0.56 ± 0.009	0.55 ± 0.009	0.56 ± 0.007	0.55 ± 0.009	0.55 ± 0.007	0.56 ± 0.008	0.55 ± 0.01	0.57 ± 0.007	0.58 ± 0.04	0.58 ± 0.004	0.57 ± 0.006	0.56 ± 0.006
0 Ca^{2}	0.49 ± 0.009*	0.50 ± 0.01*	0.51 ± 0.008*	0.50 ± 0.013*	0.50 ± 0.012*	0.51 ± 0.016*	0.51 ± 0.017*	0.52 ± 0.011*	0.54 ± 0.012*	0.55 ± 0.013*	0.55 ± 0.013	0.54 ± 0.009*
U73122	0.56 ± 0.008	0.55 ± 0.008	0.55 ± 0.004	0.56 ± 0.009	0.56 ± 0.011	0.58 ± 0.016	0.59 ± 0.023	0.58 ± 0.007	0.58 ± 0.006	0.59 ± 0.01	0.60 ± 0.004*	0.58 ± 0.005
0 Ca^{2} + U73122	0.54 ± 0.016	0.52 ± 0.015*	0.52 ± 0.007*	0.53 ± 0.009	0.54 ± 0.009	0.53 ± 0.015*	0.55 ± 0.018	0.54 ± 0.005*	0.56 ± 0.002*	0.54 ± 0.01*	0.53 ± 0.008*	0.53 ± 0.005*

Table 2.5: R0 values in the HC region. *P < 0.05, *t*-Test

	HC region		
Distance from lesion [µm]	**40-60**	**80-100**	**120-140**
Control	1.25 ± 0.037	1.29 ±0.045	1.36 ± 0.045
APY	1.26 ± 0.05	1.32 ± 0.043	1.29 ± 0.055
APY + CBX	1.15 ± 0.052	1.14 ± 0.049	1.13 ± 0.059
CBX	1.34 ± 0.048	1.44 ± 0.064*	1.48 ± 0.05
Control suramin	0.94 ± 0.023	0.92 ± 0.031	0.92 ± 0.015
Suramin	1.01 ± 0.024	1.0 ± 0.037	1.01 ± 0.05*
PPADS	0.53 ± 0.008	0.52 ± 0.013	0.50 ± 0.020

All other treatments did not significantly affect baseline or resting calcium concentrations.

Measurement of Ca^{2+} wave velocity

The velocities of the damage-induced Ca^{2+} waves were determined along the HC region using data obtained when the needle was positioned at the top of the image in order to have the maximum length of the organ in the image. The differential ratio (δR) signal was derived from mean ratio values by calculating ratio derivative, where $\delta R = R_t - R_{t+1}$. δR_{max} reliably represented the onset of the calcium signal and so for each ROI the time to δR_{max} was calculated for each ROI. ROIs were placed at different distances from the damage site and that distance was plotted as a function of the time to δR_{max}. The data were fit with a linear regression in Microsoft Excel ($y = mx + c$) where the slope was equal to dx/dt or the wave velocity. This method was used to determine the velocity of the slow wave between ROIs at 50 – 70 µm to up to 150 – 170 µm. As a result of the velocity of the fast Ca^{2+} wave and image-acquisition settings there was a limited number of time points available for

curve fitting. Therefore, in this case an "instantaneous" velocity was calculated using dx/dt for one ROI using time zero (t_0) for the onset of the stimulus and time to ΔR_{max}.

Purinergic agonists

In this case, when purinergic nucleotides ATP, UTP, ADP and UDP were applied with a micropipette the same ROI template was used to analyse changes in ΔR as described for the microneedle damage. Peak ΔRs were determined and then averaged for all the ROIs in the distinct cochlear regions to give one single value for each region.

2.5.3 Data presentation

Fura-2 ratio images presented in this thesis are of two types, either time series ΔR images that are averages of two consecutive images or in the case of drug applications, averages of 15 frames of ΔR images were made from the start of damage, equivalent to approximately 20 s of imaging. The latter images provide not only an average of Ca^{2+} concentrations over 20 s but also indicate the extent of spread of the Ca^{2+} signal.

2.6 ERK1/2 activation

Damage-induced ERK1/2 activation was studied with an immunocytochemical approach using an antibody against the dually phosphorylated form of ERK1/2 (pERK, see 2.7.2). In order to study the spatio-temporal aspects of ERK1/2 activation cultures were subjected to laser damage and fixed for immunocytochemistry at the following time points: 1, 2, 5, 10, 20, 30 and 60 min post damage. Basal, middle and apical turns were included in this study.

To study the mechanism of damage-induced ERK1/2 activation only basal and middle turn cochlear cultures were used. Comparisons were performed between control and drug-treated cultures fixed 5 min and in some cases also 10 min after the damage. The cultures were pre-incubated with drugs for 30 min and maintained in

their presence throughout the experiment except for BAPTA-AM, which was pre-incubated for 90 min instead.

2.7 Immunocytochemistry

2.7.1 Fixation

Paraformaldehyde (PFA) was used as an agent to crosslink cellular components such protein structures of cells. A commercially available stock of 16 % PFA (Agar Scientific, USA) was diluted in 0.1 M phosphate buffered saline (PBS) to 4 % PFA. Cochlear cultures were incubated at room temperature with 4 % PFA that had been kept at 4 °C. Following an incubation of 30 - 60 min in 4 % PFA cultures were washed three times for 15 min in 0.1 M PBS. After the final wash they were changed into 0.1 M PBS supplemented with 0.05 % (w/v) NaN_3 in order to prevent bacterial contamination and stored at 4 °C until they were used for immunocytochemical investigations.

Cultures used to study P2 receptor expression were fixed after one day *in vitro*. Fixation time points of cochlear cultures included in the ERK1/2 study were discussed earlier (see chapter 2.3.3 and 2.6).

2.7.2 Immuno-labelling

After fixation cultures were incubated in blocking solution to reduce non-specific binding of antibodies. Triton-X100 (0.1 %) was included to the blocking solution to permeabilise lipid membranes and to permit access of antibodies to their intracellular antigen. When using the monoclonal anti-pERK antibody, specimens were incubated in blocking solution containing 10 % goat serum and 0.1 % Triton-X100 in 0.1 M PBS for one hr at room temperature while agitating. Goat serum was substituted by horse serum when P2 receptor antibodies were used. Primary and secondary antibodies were diluted in blocking solution according to the experiment and primary antibody dilutions are summarized in Table 2.6. Following overnight incubation in primary antibody at 4 °C specimens were washed three times for at least 15 min in 0.1 M PBS. Alexa Fluor-488 goat anti-mouse or goat anti-rabbit

Table 2.6: Overview of primary antibodies and their dilutions

Antibody (Ab)	Supplier	Species		Ab stock concentration	Dilution	Peptide dilution
anti $P2Y_2$	Alomone labs	rabbit	polyclonal	0.8 µg/µl	1:100, 1:500	1 µg/ 1µg Ab
anti $P2Y_4$	Alomone labs	rabbit	polyclonal	0.8 µg/µl	1:100, 1:500	1 µg/ 1µg Ab
anti $P2Y_{11}$	Alomone labs	rabbit	polyclonal	0.8 µg/µl	1:100, 1:500	1 µg/ 1µg Ab
anti $P2X_2$	Alomone labs	rabbit	polyclonal	0.8 µg/µl	1:100, 1:500	1 µg/ 1µg Ab
anti $P2X_3$	Alomone labs	rabbit	polyclonal	0.8 µg/µl	1:100, 1:500	1 µg/ 1µg Ab
anti $P2X_4$	Alomone labs	rabbit	polyclonal	0.8 µg/µl	1:100, 1:500	1 µg/ 1µg Ab
anti pERK1/2	Sigma	mouse	monoclonal	-	1:1000	-

secondary antibodies were diluted 1:1000 for pERK and 1:500 for P2 receptor antibodies, respectively. In order to avoid photo bleaching cultures were kept in the dark throughout the subsequent procedures. Cultures were incubated in secondary antibody for two hrs at room temperature and then washed in 0.1 M PBS as described above. Routinely, cultures were counter stained with the DNA intercalating dye diamidinophenolindole (DAPI, 1 µM) for 1 hr in PBS at room temperature. In some cases, specimens were also labelled with the actin binding toxin phalloidin conjugated to Alexa-546 or -633 (1:200). If both counter stains were used they were applied together for one hr at room temperature and then washed as described earlier.

In order to check whether the secondary antibodies adhere non-specifically to cochlear cells the primary antibody was omitted and cultures were treated as described above. Anti-P2 receptor antibodies were pre-adsorbed by incubation for

30 min at room temperature with the specific peptides they were raised against concentrations: see Table 2.6). Immunocytochemical labelling was carried out as described above using the antibody-antigen mix instead of the primary antibody.

2.7.4 Confocal imaging

Images of immunolabelled specimens were acquired using a Zeiss LSM510 confocal microscope. The confocal head was attached to the side-port of an inverted microscope (Zeiss Axiovert 200M). The following laser lines were used: 405 diode (DAPI excitation); the argon-krypton 488 nm line (Alexa-488), the helium-neon 543 or 633 nm lines (Alexa-546 and Alexa-633 respectively). The images were acquired using the following lenses: Plan-Apochromat/20x/0.75 dry lens, Plan-Neofluar/40x/1.3 or Plan-Apochromat 63x/ 1.4 oil lenses

Z-stack images were acquired through the thickness of the sensory region of the epithelium. For comparative studies the acquisition settings of the Zeiss LSM510 were kept the same for cultures that were labelled simultaneously i.e. in the same labelling batches. Between batches of specimens the settings were kept as close as possible.

2.7.5 Image analysis

ERK1/2 activation

To quantify the spread of damage-induced ERK1/2 activation along the OHC and IHC region a line scan analysis was performed using Metamorph software. Line widths of 30 (= 38 μm) and 20 pixels (= 25 μm) were applied for the OHC and IHC regions, respectively. Line scan intensity data were exported into Microsoft Excel and then an average intensity and standard deviation was determined from 20 pixels along the line in two non-responding region. Then this average background value plus 10 times the standard deviation was used to set a threshold for the data. Pixels above the threshold value after subtraction were > 0 and these were considered to be positive (sites of activation). At the edges of the activation regions the signals dropped close below 0 for a few pixels and then rose above the threshold again at greater distances. In order to treat all images equally the following rules were

applied: pixels below background (negative pixels) were included when three or less were followed by any number of pixels above background (positive pixels; see Table 2.7). If between 3 and 12 negative pixels were recorded, then there needed to be at least > 6 positive pixels for those negative regions to be included. If a run of 12 negative pixels was observed (~2 cell widths) then this was considered the end of the spread and any further positive pixels were not included. The distance in μm was determined as the length between the first positive pixel at the lesion site and the last positive pixel that met the criteria described above. For the OHC region the extent of ERK1/2 activation was measured on both sides of the lesion and averaged. The spread along the IHC region was continuous (not separated by a lesion site), as the lesion was induced in the OHC region. Thus in order to make a comparison between the IHC and OHC regions, the distance measure was divided by two. Data were statistically evaluated using Students *t*-test and where necessary using one-way ANOVA.

Table 2.7: Rules that describe the handling of negative pixels for measuring activated ERK1/2 spread.

No. of neg. pixels	Rules (included, if...)
≤ 3	any number of positive pixel follow
4 - 12	6 connected positive pixels follow
> 12	not included

Neomycin-induced hair cell pyknosis

In this thesis the pyknotic nature of the nucleus is used as a measure of hair cell death. The number of pyknotic and healthy nuclei were determined using DAPI-labelled confocal z-stack images throughout the thickness of the cochlear epithelium. Nuclei with condensed morphology and increased intensity were counted as pyknotic. The pyknotic nuclei count also included nuclei of extruded cells.

Signal noise of images was reduced by subjecting them to x-y pixel averaging and then averaging of two adjacent z-plane images (running average) using Lucida

imaging software (Andor, UK). DAPI-labelled nuclei were binned pyknotic and morphologically healthy appearing nuclei for the IHC and OHC regions in 460 x 230 μm images. In the OHC region morphologically healthy appearing nuclei were estimated from 1st row counts. Two to three 460 x 230 μm regions were imaged per cochlear culture and averaged to obtain one value. Data are expressed as pyknotic or total number of nuclei, comprised of healthy and pyknotic, per 100 μm. Two-tailed Student's *t*-tests were used to evaluate statistical significances between groups.

2.7.6 Image presentation

Lucida, Zeiss LSM 5 (Zeiss, UK) and Adobe Photoshop were used to produce images for data presentation.

Averages of confocal z-stack images were prepared using Lucida (Andor, UK). For comparative studies the depth of the z-stack was kept the same. Zeiss LSM 5 was used to prepare 3-D reconstructions and x-z projections. Five consecutive x-z projections were averaged for P2 receptor presentation using Lucida software. Images presented in this thesis were assembled in Adobe Photoshop.

2.8 Patch clamp

2.8.1 Electrode preparation

Glass capillaries without filaments (WPI, USA) were cleaned with 100 % ethanol. Electrodes were pulled using a two step electrode puller (Narashige, Japan). Puller settings were chosen to obtain electrode resistances between 3.0 and 4.0 MΩ. Electrodes were front and back filled with filtered internal solution (Table 2.2). When recordings of purinergic agonist-induced currents were made, ATP and GTP were omitted from the internal solution. In all other cases the internal contained ATP and GTP as it was found that they improved the stability of recordings.

2.8.3 Protocol

Acutely isolated cochlear turns (see 2.2) were continuously perfused with ACSF (Table 2.1) which was saturated with 95%O_2/5%CO_2. Recordings were made at room temperature from Deiters' cells that were maintained in their support cell syncytium unless otherwise stated. Cochlear turns were visualised with an upright microscope (Axioskop 2 FS, Zeiss) using a 40x Achroplan water-immersion objective lens and differential interference contrast optics. Currents were measured using a Multiclamp 700A amplifier and digitised using Digidata 2000 analogue to digital interface (Molecular Devices Inc, USA).

2.8.4 Seal formation

Positive pressure was applied to the electrode during micromanipulation to the level of the stereocilial bundles of hair cells using an automatic manipulator (Siskiyou Inc, USA). When the electrode entered the buffer the offset current due to slight differences between the electrode and bath potentials was adjusted to zero. Under visual control the electrode was positioned between stereocilial hair bundles and simultaneously lowered and brought forward to break through the reticular lamina at cell-cell junctions. Once in the epithelium the electrode was lowered to the level of Deiters' cell nuclei. When an indent in the cell membrane due to the positive pipette pressure was observed, the pressure was released and slight suction applied to form a tight Giga-ohm seal. Whole-cell recordings were obtained by breaking into the cell using negative pressure. Seal formation was assessed using the Clampex 9.2 (Molecular Devices Inc, USA) seal test option (10 mV steps). After forming a Giga-Ohm seal the capacitative transients were minimised using digital controls.

2.8.5 Whole cell recording protocols

Lesion protocol

In order to record damage-induced currents recordings of whole-cell or whole-syncytium currents were made for ~20 min from Deiters' cells held at -90 mV prior to stimulation. Gap free recordings of 5 min lengths were made intercalated with a

10 mV voltage step protocol to control for access and syncytial resistance (R_{sync}). At ~23 min a lesion was induced and recorded and this was followed by a further 30 min of recording at which point a second lesion was made at the same site. In a subset of experiments 150 μM PPADS was applied 10 min before the second lesion was induced. Recordings were filtered at 1 khz and sampled at a frequency of 50 khz.

Puff protocol

The nucleotides ATP, ADP, UTP and UDP were puff applied to cochlear cultures as described earlier (see 2.4). Again, ionic currents were recorded from Deiters' cells that were coupled to the support cell syncytium and held at -90 mV.

In a subset of experiments Deiters' cells were subjected to octanol (1 mM) to record from single Deiters' cells. When cells had been uncoupled, then voltage clamp protocols could be applied. The current-voltage relationship (I-V) of nucleotide-activated currents were determined for spontaneously or octanol uncoupled Deiters' cells by applying voltage-commands in a range from -100 mV to +60 mV in 40 mV increments. The voltage was stepped and 0.2 s afterwards the puff was automatically applied for 10 ms. In the same Deiters' cell the voltage-activated currents were recorded in the absence of ATP application. Recordings were filtered at 1 khz and sampled at a frequency of 50 khz.

2.8.6 Analysis

Data analysis was performed using Clampfit 9.2 (Molecular Devices Inc, USA) and Microsoft Excel. For presentation purposes the current traces were prepared in Origin (Origin Lab Corp, USA).

Determination of syncytial Resistance (R_{sync})

The syncytial resistance (R_{sync}) is an estimate of the number of cells in the syncytium. R_{sync} was estimated using a 10 mV voltage-step-protocol. The change in the steady-state current resulting from the voltage step was measured and R_{sync} was determined using Ohms Law. The pre-lesion R_{sync} was compared to the post-lesion R_{sync} following the 5 min recording. R_{sync} was also determined before nucleotide applications.

Determination of peak current and charge

The peak current was determined manually for damage-induced currents by placing the cursor over that point in the recording. The amount of charge moved during the onset and decline of the current was quantified using a specific Clampfit 9.2 function that measures the area between two cursors placed at the onset and at the point where the current had recovered to baseline. To assess the effect of PPADS the peak current and charge transferred were analysed for the second lesion in recordings made from control and PPADS-exposed cochlear turns. It was found that R_{sync} was different between control and PPADS data sets and thus consequently the magnitudes of currents would be expected to differ. In order to normalise for the differences it was assumed that the peak current and R_{sync} relationship is approximately linear. Thus the values obtained for the peak current and charge transferred were divided by the conductance G_{sync} ($I_{norm} = I / G_{sync}$) and the resulting values were subjected to statistical analysis using Student's *t*-test.

For the nucleotide-induced currents the peak current and total charge transferred were determined as described above except that specific Clampfit 9.2 functions were applied to obtain the peak currents in this case. Based on the biphasic response of the ATP-induced current, the peak currents were determined for the initial 500 ms measured from the midpoint of the puff application and during the following 5.5 s. Two measures of charge transfer were made. The first was measured for the first 500 ms and the second for 6 s from the onset of the current (this included the initial peak current). Subtraction of the charge transferred during the initial peak (first 500 ms) from that of the 6s response provides a measure of the charge transferred by the second current.

For the comparison of charge transferred during damage and in response to ATP the charge transfer was measured between the onset and the point at which the currents recovered to baseline in both cases.

Determination of the I-V relationship

In order to resolve the ATP-activated currents, Deiters' cell currents recorded at various voltages in the absence of ATP application were subtracted from those

recorded when ATP was applied. The peak of the ATP-activated current was plotted as a function of the applied voltage.

2.9 Sample numbers and statistical analysis

Experiments were performed on at least three cochlear cultures from three different animals. The experiments were conducted on at least two different days. N-numbers are indicated in the figure legends. All data are presented as mean ± S.E.M. Statistical analysis was carried out using Student's *t*-tests, unless otherwise stated.

3. The mechanism of the damage-induced Ca^{2+}-wave formation

Damage of various kinds has been shown to elicit changes in intracellular Ca^{2+} in HC epithelia (Hirose et al., 1999; Gale et al., 2004; Matsui et al., 2004; Piazza et al., 2007). Both Gale et al. (2004) and Piazza et al. (2007) described the formation of an intercellular Ca^{2+} wave triggered by damage to a single HC in cochlear explants using a microelectrode or oscillating probe. The intercellular Ca^{2+} wave was shown to propagate in an extracellular ATP-dependent fashion requiring the release of Ca^{2+} from intracellular IP_3-sensitive stores. These studies focused on the propagation of the Ca^{2+} wave outwards from the OHC region into the outer sulcus (OS) region of cochlear explants. In this chapter it was investigated whether the Ca^{2+} wave induced by damage to the HC epithelium also propagates into other regions of cochlear explants – namely the HC region itself and inwards to the inner sulcus (IS region). In this study a larger damage stimulus was used to investigate the mechanisms underlying the Ca^{2+} wave propagation induced by HC damage. Specifically, the source of Ca^{2+} necessary to constitute the damage-induced Ca^{2+} wave and the role of P2 receptor activation were determined for the distinct cochlear regions. In addition the involvement of gap junctions in the propagation of the damage-induced Ca^{2+} wave was assessed.

3.1 Damage elicits the propagation of an intercellular Ca^{2+} wave

To examine whether the Ca^{2+} wave propagates into the distinct cochlear regions, a cluster of cells were damaged in the HC region using a microneedle (Fig 3.1A, C). Intracellular changes in $[Ca^{2+}]$ were monitored using the ratiometric Ca^{2+} indicator Fura-2. Selected ΔR images from a time series data set reveal the propagation of the Ca^{2+} wave (Fig 3.1B, movie 1). In agreement with previous reports (Gale et al., 2004; Piazza et al., 2007) damage triggered the rise in intracellular Ca^{2+} in cells immediate to the lesion site. This rise subsequently travelled as an intercellular wave of cytoplasmic Ca^{2+} to further distances into the OS region comprised of Hensen and Claudius-like cells (Fig 3.1B). In addition, it was observed that the Ca^{2+} wave also propagated in the IS and HC region (Fig 3.1B). ΔRs changes in the IS and HC region

were smaller than those in the OS region. Detailed examination of the Ca^{2+} wave propagating in the HC region revealed two temporally distinct components – in effect two waves. The first wave spread faster with a velocity of 40.7 ± 5.4 μm/s (n = 11) and appeared to occur in a subset of cells in the HC region. The second slower wave seemed to involve all cells and travelled with a velocity of 13.7 ± 0.5 μm/s (n = 16), similar to that described for the OS region (Gale et al., 2004). The faster Ca^{2+} wave was not observed in the OS or IS region. The decline of intracellular Ca^{2+} to baseline levels was faster in the HC and IS region than in the OS region and occurred within 90 s following the insult. In contrast, Ca^{2+} levels in the OS region did not fully recover during the time course of the recording (150 s).

In order to quantify the propagation of the intercellular Ca^{2+} wave ΔRs were determined in 20 x 20 μm ROIs placed at various distances from the lesion site (see Fig 3.2A, C, E and chapter 2.5.2). Fig 3.2B shows ΔRs as a function of time for the ROIs displayed in Fig 3.2A. The graph depicts that the Ca^{2+} wave propagates to distances up to at least 154 – 168 μm from the lesion site and that the wave reaches the furthest ROI with a delay. The Ca^{2+} waves in the HC and IS region propagated to distances up to 120 – 140 and 140 – 160 μm from the lesion site, respectively. The Ca^{2+} waves were characterised by a decrease in peak Ca^{2+} changes as a function of distance. The magnitude of the Ca^{2+} changes in the HC and IS region were similar whereas those in the OS region were several magnitudes higher.

3.2 The source of Ca^{2+} required for damage-induced Ca^{2+} wave signals

Various mechanisms can result in the elevation of intracellular Ca^{2+} levels. Two major mechanisms are the release of Ca^{2+} from intracellular stores via generation of IP_3 or influx of extracellular Ca^{2+} facilitated by the opening of various types of Ca^{2+} channels in the plasma membrane. These Ca^{2+} sources were tested for their potential to mediate the damage-induced rise in intracellular Ca^{2+} levels. In this subset of experiments half of the Ca^{2+} wave was imaged in order to maximise the extent of Ca^{2+} wave propagation along the HC rows. Averages of the first 15 ΔR images from the time of the insult are compared in the presence of Ca^{2+} (Fig 3.3A, movie 2) and in

0 Ca^{2+} conditions (Fig 3.3B, movie 3). Switching to 0 Ca^{2+} significantly reduced baseline Ca^{2+} levels (R_0) in the HC region but not in the OS or IS region (Table 2.3, 2.5). In the OS region Ca^{2+} wave propagation was unaffected by 0 Ca^{2+} (Fig 3.3A, B). ΔRs expressed as a function of time shown at 154-182 μm confirmed that the extent of the Ca^{2+} wave propagation was not dependent on extracellular Ca^{2+} (Fig 3.4A). In contrast, when U73122, a PLC inhibitor was used to prevent release from IP_3-sensitive intracellular stores, Ca^{2+} wave propagation in the OS region was blocked (Fig 3.3C, Fig 3.4B, movie 4). A small rise in intracellular Ca^{2+} was observed at sites close to the lesion. When U73122 treatment was combined with 0 Ca^{2+} conditions the Ca^{2+} wave in the OS region was completely abolished (Fig 3.3D, movie 5). The damage-induced peak Ca^{2+} changes expressed as a function of the distance from the lesion site are shown in Fig 3.4D. The graph reiterates that in the OS region release of Ca^{2+} from IP_3-sensitive intracellular stores was the key mechanism mediating Ca^{2+} wave propagation.

Propagation of the damage-induced Ca^{2+} wave into the IS region was not reduced in 0 Ca^{2+} or by inhibition of PLC with U73122 (Fig 3.3A-C, Fig 3.5A, B). Assessing the damage-induced peak Ca^{2+} changes gave further evidence (Fig 3.5D, Table 3.1). Application of U73122 in 0 Ca^{2+} was sufficient to significantly decrease the propagation of the Ca^{2+} wave at 100 – 120 and 140 – 160 μm but not at 60 – 80 μm from the lesion site into the IS region (Fig 3.5C, D, Table 3.1).

In order to examine the propagation of the Ca^{2+} wave along the HC rows ΔR images were cropped to only show this region (Fig 3.6A-D). As described earlier, in this region Ca^{2+} wave spread was characterised by two distinct waves. The fast Ca^{2+} wave was observed to spread at least 280 μm from the lesion site (Fig 3.6A). The slower Ca^{2+} wave did not reach such distances. 20 x 20 μm ROIs placed along the HC region (see Fig 3.8A) were used to determine the peak Ca^{2+} changes. Along the length of the HC region peak Ca^{2+} changes decreased considerably at distances > ~180 μm at which the propagation was only facilitated by the fast Ca^{2+} wave (Fig 3.6, arrow; Fig 3.8B). The peak Ca^{2+} changes associated with the fast Ca^{2+} component were maintained at a small but consistent level at distances from ~ 180 up to at least 260 μm (Fig 3.8B). In 0 Ca^{2+} the fast Ca^{2+} wave was abolished (Fig 3.6B). The

Table 3.1: Overview of statistical significances for OS and IS regions between cultures damaged in control, 0 Ca^{2+}, U73122 and U73122 in 0 Ca^{2+}.

		Control		0 Ca^{2+}		U73122	
		ROI	significance	ROI	significance	ROI	significance
OS region	**Control**						
	0 Ca^{2+}	42 – 154 210	n.s.d. P < 0.05				
	U73122	all	P < 0.05	all	P < 0.05		
	0 Ca^{2+} + U73122	all	P < 0.05	all	P < 0.05	42, 70, 210 154	P < 0.05 n.s.d.
IS region	**Control**						
	0 Ca^{2+}	all	n.s.d.				
	U73122	all	n.s.d.	70, 110 150	ANOVA: n.s.d. P < 0.05		
	0 Ca^{2+} + U73122	70 110, 150	n.s.d. P < 0.05	70, 110 150	ANOVA: n.s.d. P < 0.05	70, 110 150	ANOVA: n.s.d. n.s.d.

Table 3.2: Overview of statistical significances for the HC region between cultures damaged in control, 0 Ca^{2+}, U73122 and U73122 in 0 Ca^{2+}.

		Control		0 Ca^{2+}		U73122	
		ROI	significance	ROI	significance	ROI	significance
HC region	**Control**						
	0 Ca^{2+}	all	$P < 0.05$				
	U73122	60, 100-180 40, 80, 200-260	$P < 0.05$ $P < 0.05$ n.s.d. n.s.d.	40-220 240-260	$P < 0.05$ n.s.d.		
	0 Ca^{2+} + U73122	all	$P < 0.05$	40-220 240-260	$P < 0.05$ n.s.d.	all	$P < 0.05$

damage-induced rise in intracellular Ca^{2+} was attenuated at 90 – 110 μm and abolished at 190 – 210 μm from the lesion site (Fig 3.7A, B). The peak Ca^{2+} change was significantly reduced in 0 Ca^{2+} at all distances measured. The PLC inhibitor U73122 reduced the magnitude of the slow Ca^{2+} wave but not the fast wave (Fig 3.6C). U73122 significantly decreased the peak Ca^{2+} levels at distances between 100 and 180 μm from the lesion site (Fig 3.7C, D). In 0 Ca^{2+} and the presence of U73122, propagation of the Ca^{2+} wave was limited to up to ~ 100 μm in the HC region (Fig 3.6C, Fig 3.8 B). Table 3.2 presents the statistical significances for the various conditions tested.

3.3 The Ca^{2+}wave spreads in an ATP dependent manner and is sensitive to the gap junction inhibitor CBX

The damage-induced Ca^{2+} wave in the OS region was modulated by the release of extracellular ATP (Gale et al., 2004). In some systems, gap junctions are thought to mediate Ca^{2+} wave propagation (Sanderson et al., 1990; Venance et al., 1997). Here, it was investigated whether extracellular ATP and gap junctions contribute to the propagation of the damage-induced Ca^{2+} wave into the distinct regions of the cochlear explant.

3.3.1 The effect of apyrase

In order to determine a role for extracellular ATP in mediating damage-induced rises in intracellular Ca^{2+}, cochlear explants were exposed to the ATP-hydrolysing enzyme apyrase (40 U/ml). Apyrase reduced the propagation of the Ca^{2+} wave into the OS region (Fig 3.9B, Fig 3.10A). In the presence of apyrase damage-induced peak Ca^{2+} changes were significantly decreased in all ROIs in the distinct cochlear regions (Fig 3.9A, B; Fig 3.10A, D; Fig 3.11A, D; Fig 3.12A, D).

3.3.2 The effect of CBX

To examine whether gap junctions participate in the formation of the damage-induced Ca^{2+} wave, CBX (75 μM) – an inhibitor of gap junctions – was used. CBX reduced the spread of the damage-induced Ca^{2+} wave into the OS region (Fig 3.9C). A

significant reduction in peak Ca^{2+} was observed at 98-126 and 154-182 µm from the lesion site (Fig 3.10B, E). In the IS region CBX affected Ca^{2+} wave propagation to a lesser degree (Fig 3.9C). A significant decrease in peak Ca^{2+} was only observed at 100-120 µm from the lesion site (Fig 3.10B, E). In the HC region CBX reduced the spread of the Ca^{2+} wave (Fig 3.9C). In close proximity to the lesion site the peak Ca^{2+} changes were not modulated by CBX whereas at further distances of 80-100 and 120-140 µm they were significantly reduced by 23 and 30 % respectively (Fig 3.12B, E). However, it is worth noting that CBX increased R_0 values. To summarise CBX attenuates the damage-induced Ca^{2+} wave in the distinct cochlear regions.

3.3.1 The effect of the combined treatment of apyrase and CBX

To investigate whether extracellular ATP and gap junctions act in parallel to facilitate the generation of the damage-induced Ca^{2+} wave, apyrase and CBX application was combined. Propagation of the damage-induced Ca^{2+} wave into the OS region in the presence of apyrase and CBX was attenuated to a greater extent than observed with either treatment alone (Fig 3.9D). Combining CBX and apyrase significantly reduced the peak Ca^{2+} levels at 98-126 and 154-182 µm from the lesion site compared to apyrase alone (Fig 3.10C, D). In contrast, in the IS and HC region combined treatment did not impose an additional effect to that of apyrase alone (Fig 3.9D; Fig 3.11C, D; Fig 3.12C, E).

3.4 Purinergic mechanism of Ca^{2+} wave formation

3.4.1 Exogenous application of ATP elicits a Ca^{2+} wave

The experiments in the previous sections and those by Gale et al. (2004) suggest that ATP is a mediator of the damage-induced Ca^{2+} wave. In order to investigate the presence of P2 receptors, ATP was locally puff-applied for 10 s in close proximity to the HC region of cochlear explants (Fig 3.13A). Peak changes in intracellular Ca^{2+} were measured in ROIs as indicated in Fig 3.2A, C and E and used to analyse the response of cells in the different cochlear regions. Cells in all regions showed a dose dependent increase in Ca^{2+} (Fig 3.13). Cells recovered to baseline within ~ 60 s following exogenous application of 1 µM ATP. At higher concentrations recovery

was slowed. In the OS region 100 μM ATP resulted in sustained elevation of Ca^{2+} (Fig 3.13B).

3.4.2 Ca^{2+} wave formation stimulated by other nucleotides

P2Y receptor subtypes are not only activated by ATP but also by other nucleotides and this knowledge can be used to establish a P2Y receptor expression profile. Here, UTP, UDP and ADP were investigated for their ability to elevate intracellular Ca^{2+} in the distinct cochlear regions. AMP was used to test whether conversion of ATP to adenosine that acts on P1 receptors contributed to the rise in intracellular Ca^{2+}. The nucleotides (100 μM) were puff-applied locally and analysis was carried out as described for application of ATP. The graph in Fig 3.14A depicts ΔRs as a function of time triggered by application of UTP (10 s), UDP (20 s), ADP (20 s) and AMP (20 s) in the OS region. UTP elicited a rise in intracellular Ca^{2+} in the OS region that had not fully recovered to baseline levels 150 s after application. ADP and UDP were both sufficient to trigger an increase in Ca^{2+} levels; however the magnitude was less than that induced by UTP (Fig 3.14A, B). AMP did not cause global changes in intracellular Ca^{2+} levels. However, in 3/5 experiments a few single OS cells responded with a rise in Ca^{2+} during the later phase of the time course (data not shown). The maximum Ca^{2+}changes triggered by the various nucleotides are summarised in Fig 3.14B. OS cells were characterised by P2Y receptors that are most sensitive to UTP followed by the rank order ATP >> UDP > ADP to trigger an increase in intracellular Ca^{2+}.

In the IS region, the rank was UTP > ATP >> ADP > UDP (Fig 3.15A, B). UDP was the least potent P2 receptor agonist in the IS region. AMP was not sufficient to induce changes in intracellular Ca^{2+} levels at any time in the IS region. Ca^{2+} responses to all nucleotides returned to baseline within 150 s (Fig 3.15A).

In the HC region ATP and UTP were similarly potent. The rank order of potency was ATP ≅ UTP > ADP ≅ UDP (Fig 3.16). Again, AMP did not induce a rise in intracellular Ca^{2+} at any time in the HC region. The Ca^{2+} responses to UTP, ADP and UDP recovered to baseline levels within 150 s (Fig 3.16A).

3.5 Damage-induced Ca^{2+} wave propagation is sensitive to P2 receptor antagonists

Previous sections of this chapter showed that the ATP-degrading enzyme apyrase significantly decreased the propagation of the damage-induced Ca^{2+} wave. Moreover, purinergic agonists triggered Ca^{2+} changes in distinct cochlear regions. Here, it was investigated whether the broad spectrum P2 receptor antagonists PPADS and suramin affected the damage-induced Ca^{2+} wave. When used at 10 μM, suramin did not decrease the damage-induced peak Ca^{2+} changes in any of the cochlear regions (data not shown). However, 100 μM suramin reduced the propagation of the Ca^{2+} wave into the OS, IS and HC region (Fig 3.17A, B). Peak Ca^{2+} changes were significantly reduced by suramin in the OS region at 98-126 and 154-182 μm, but not close to the lesion site (42-70 μm, Fig 3.18A, B) and at all distances in the IS region (Fig 3.19A, B). In the HC region propagation of the slow Ca^{2+} wave appeared to be restricted whereas the fast Ca^{2+} wave was still observed in the presence of suramin (Fig 3.17B). Peak Ca^{2+} levels were only significantly affected by suramin at 120-140 μm but not at distances closer to the lesion site (Fig 3.20A, B).

PPADS, another P2 receptor antagonist was not sufficient to reduce the propagation of the damage-induced Ca^{2+} wave when used at a concentration of 10 μM. In contrast, 150 μM PPADS significantly restricted the propagation of the intercellular Ca^{2+} wave into the distinct regions of the cochlear explant (Fig 3.17C, D). Quantification revealed that PPADS significantly decreased the peak Ca^{2+} changes at all distances into the OS, IS and along the HC region (Fig 3.18C, D – 3.20C, D, respectively). As demonstrated for suramin, the fast Ca^{2+} wave was not abolished in the presence of PPADS (Fig 3.17D).

3.6 Discussion

Characterisation of the Ca^{2+} wave propagation

Damaging a cluster of cells in the HC region with a microneedle triggered a rise in intracellular Ca^{2+} in the cells surrounding the lesion site. The increase in intracellular Ca^{2+} propagated to neighbouring cells as an intercellular Ca^{2+} wave that travelled into all regions of the organ. Propagation properties of the Ca^{2+} wave in the OS region were described previously (Gale et al., 2004; Piazza et al., 2007) and confirmed here. However, propagation of the Ca^{2+} wave in the HC region was markedly different in that it was formed by two waves. A faster wave reached distances of at least 280 μm and required entry of Ca^{2+} from outside the cell. It was followed by a slower wave that spread over distances of ~180 μm and was mediated by release of Ca^{2+} from IP_3-sensitive stores. Zero Ca^{2+} conditions or U73122 allowed the isolation of two waves in the HC region and might suggest that different cell types i.e. HCs and Deiters' cells form the distinct waves.

The velocity and the source of Ca^{2+} that constituted the slower wave in the HC region were similar to that reported previously for the OS region (Gale et al., 2004). In the IS region, the Ca^{2+} wave travelled with a similar velocity to that observed for the OS and the slow wave along the HC region. However, only the combined inhibition of IP_3 production in 0 Ca^{2+} moderately reduced the spread of the Ca^{2+} wave in the IS region. The epithelium in this region is relatively thick and tightly packed. It is therefore possible that the inhibitor as well as the chelator did not reach the target region and that residual Ca^{2+} was trapped between the cells. Assuming that there was good access for the solutions, then the simplest explanation is that the Ca^{2+} wave in the IS region depends upon a third mechanism. A wave was still observed in the HC region when 0 Ca^{2+} and U73122 were combined and perhaps this also depends on a third unknown mechanism. A variety of other mediators are reported in the literature to induce local Ca^{2+} changes. These include NAADP that releases Ca^{2+} from lysosomal compartments, cyclic ADP ribose (cADPR) acting on ryanodine-sensitive stores as well as sphingosine-1 phosphate (S1P) (Berridge et al., 2003). Ryanodine receptors are documented to be expressed in the cochlea and could therefore account for the third mechanism (Lioudyno et al., 2004; Grant et al., 2006; Morton-Jones et al., 2006).

Recovery of the damage-induced Ca^{2+} wave in the distinct regions

The kinetics of recovery of intracellular Ca^{2+} was also different in the distinct cochlear regions. In the OS region, prolonged Ca^{2+} increases were observed compared with those in the IS or HC regions; the latter exhibited similar recovery kinetics. The mechanisms that trigger elevated intracellular Ca^{2+} levels and those that result in their removal determine the recovery kinetics. In the OS region the signals mediating the release of Ca^{2+} from intracellular stores might be maintained over an extended period compared to that in the HC and IS region; thus resulting in prolonged elevated Ca^{2+} levels. However, these results could also reflect the engagement of different Ca^{2+} removal mechanisms in the OS and IS/HC region. The Ca^{2+} homeostasis of a cell can be re-established via various mechanisms that include uptake into mitochondria or the endoplasmic reticulum (Rizzuto et al., 1998; Boitier et al., 1999). Also, the PMCA or the Na^{+}-Ca^{2+} exchanger can facilitate extrusion of Ca^{2+} and thus accomplish return to baseline Ca^{2+} levels (Ishida and Paul, 2005; Ficarella et al., 2007). In IHCs it has been shown that the PMCA, mitochondria and the endoplasmic reticulum are involved in re-establishment of Ca^{2+} levels following depolarization-induced Ca^{2+} changes (Kennedy, 2002). The mechanisms that act in the various cochlear support cell types are currently unknown.

In addition to the mechanisms discussed above, the activation of distinct signalling cascades might also modulate the recovery rate. Recently, it has been demonstrated that PKC activation mediates an increased removal rate of Ca^{2+} through a mechanism that modulates both the PMCA4 and the SERCA pump (Usachev et al., 2006). Although there is no evidence for the expression of PMCA4 in the mammalian cochlea similar mechanisms could act at other PMCA subtypes (Dumont et al., 2001). It is possible that, as the signalling cascades activated by damage can vary in the distinct cochlear regions (see chapter 4) these may consequently alter the rates of cytoplasmic Ca^{2+} removal.

Ca^{2+} wave propagation in an ATP dependent manner

The propagation of the damage-induced Ca^{2+} wave into the distinct regions of the cochlea was mediated by the release of extracellular ATP. Data presented here confirm the results of Gale et al. (2004) for the OS region. In both HCs and Deiters'

cells exogenous application of ATP has been reported to trigger increases in intracellular Ca^{2+}. HCs increased Ca^{2+} levels in an IP_3 dependent fashion and removal of extracellular Ca^{2+} resulted in an increased Ca^{2+} response (Mammano et al., 1999). This phenomenon showing elevated intracellular Ca^{2+} levels in 0 Ca^{2+} was not documented during damage-induced signalling in the whole organ preparation in this thesis. ATP-induced elevations of intracellular Ca^{2+} in Deiters' cells have also been proposed to require intracellular Ca^{2+} stores (Dulon et al., 1993; Lagostena and Mammano, 2001). Both reports describe that ATP induces Ca^{2+} changes in 0 Ca^{2+} but the levels were not quantified. Therefore, it is not possible to estimate any possible contribution of extracellular Ca^{2+} in their work. Hensen cells are reported to respond with a biphasic rise of intracellular Ca^{2+} composed of a faster and slower component when exposed to exogenous ATP (Lagostena et al., 2001). The faster component was similar to that observed here dependent on extracellular Ca^{2+}, whereas the second more slowly developing rise in intracellular Ca^{2+} resulted from the opening of IP_3-sensitive stores, again similar to that shown here (Lagostena et al., 2001). The faster rise coincided temporally with an initial fast inward current, suggesting a role for P2X receptors. Here, the absence of the fast damage-induced Ca^{2+} wave along the HC region in 0 Ca^{2+} suggests that it is mediated through activation of P2X receptors whereas the slower IP_3-dependent wave, inhibited by U73122, was triggered through P2Y receptor activation.

Interpretation of Ca^{2+} wave formation on the basis of the purinergic agonist profile

A P2 receptor activation profile was established for the distinct cochlear regions using various purinergic agonists. The distinct cochlear regions were characterised by increased sensitivity to UTP and ATP over their dinucleotides. This profile suggests that the damage-induced Ca^{2+} wave was predominantly carried by UTP-sensitive P2 receptors that are also characterised by sensitivity to ATP. The receptors that meet these conditions are $P2Y_2$, $P2Y_4$ and $P2Y_{11}$ receptors (Nicholas et al., 1996; White et al., 2003; Wildman et al., 2003). Based on their sensitivities to UDP and ADP, the UDP sensitive receptor $P2Y_6$ and ADP sensitive receptors might play a minor role in the formation of the damage-induced Ca^{2+} wave. However, it cannot be excluded that Ca^{2+} changes elicited by ADP and UDP result from contamination with ATP or UTP, respectively. The profiles do not exclude activation of P2X receptors which are likely

contribute to the Ca^{2+} wave in the HC and IS region as the combination of U73122 with 0 Ca^{2+} reduced the damage-induced rise in intracellular Ca^{2+}. In contrast, only IP_3-sensitive stores mediated Ca^{2+} wave propagation in the OS region; thus indicating that P2Y receptors are activated exclusively.

Some differences were observed in the rank orders for the individual regions. In the OS region, cells were most sensitive to UTP followed by the rank order ATP >> UDP > ADP. By contrast, in the IS region cells were least sensitive to UDP suggesting that the involvement $P2Y_6$ receptors is negligible in this region. In the HC region ATP and UTP elicited equivalent changes in intracellular Ca^{2+}.

In summary, all cochlear regions are characterised by a dominance of UTP-sensitive P2 receptors suggesting that the propagation of the damage-induced slow Ca^{2+} wave might be facilitated in the different regions by the same receptor subtype. In addition, P2X receptor activation is implicated to occur in the HC and possibly to some extent in the IS region.

P2 receptor classification – based on the action of PPADS and suramin

The P2 receptor antagonists PPADS and suramin reduced Ca^{2+} wave propagation in the distinct regions of cochlear explants, providing further support that ATP acts on P2 receptors to trigger and propagate the damage-induced Ca^{2+} wave. PPADS and suramin both decreased the spread of the slow wave but did not affect the fast Ca^{2+} wave along the HC region. Moreover, the HC region was less sensitive to suramin compared to the OS or IS region which suggests the involvement of different P2 receptor subtypes. As described previously, based on the agonist profiles UTP-sensitive P2 receptors are likely the main carrier of the damage-induced slow Ca^{2+} wave into the distinct cochlear regions. $P2Y_2$ and $P2Y_{11}$ but not $P2Y_4$ receptors are sensitive to suramin (Communi et al., 1999; van der Weyden et al., 2000; Wildman et al., 2003). Thus, combining agonist properties with suramin sensitivity $P2Y_2$ and $P2Y_{11}$ receptor subtypes are potential mediators of the damage-induced Ca^{2+} wave into the OS and IS regions. In contrast, a reduced action of suramin in the HC region suggests that $P2Y_2$ and/or $P2Y_{11}$ receptors are less involved than in the OS and IS region.

PPADS is not a potent antagonist at either $P2Y_2$, $P2Y_4$ or $P2Y_{11}$ receptors (Communi et al., 1999; van der Weyden et al., 2000; Wildman et al., 2003). Thus a different PPADS-sensitive P2Y receptor is likely to be involved in mediating the damage-induced Ca^{2+} wave. $P2Y_1$ and $P2Y_6$ are sensitive to PPADS and could therefore play a role in the OS and HC region (King and Townsend-Nicholson, 2003). In contrast, only $P2Y_1$ but not $P2Y_6$ according to the agonist profile of the IS region might participate in the formation of the Ca^{2+} wave in this region. Data are only available for the human $P2Y_{11}$ receptor and therefore the profile of a rat $P2Y_{11}$-like receptor could differ to that of the human analogue. $P2Y_4$ cannot be excluded as a candidate as suramin and PPADS are not active at this receptor subtype, and both antagonists were only sufficient to reduce, but not abolish the slow Ca^{2+} wave.

The fast wave's requirement for extracellular Ca^{2+} suggests involvement of ion channels, possibly P2X receptors. However, both suramin and PPADS are documented to inhibit various P2X receptors at concentrations lower than those used here (King and Townsend-Nicholson, 2003) (Rassendren et al., 1997; Chessell et al., 1998; King and Townsend-Nicholson, 2003). The receptor that is less sensitive to both PPADS and suramin is the $P2X_4$ receptor (Jones et al., 2000). Therefore, the only likely P2X receptor candidate in mediating the damage-induced fast Ca^{2+} wave is $P2X_4$.

Extrapolating the nature of P2 receptor subtypes that mediated the damage-induced Ca^{2+} wave from the data obtained with PPADS and suramin is challenging. Pharmacological profiles for the various P2 receptors were determined in heterologous expression systems and therefore the pharmacology might differ for native tissues. In addition, coexpression of P2Y receptor subtypes and heteromer formation of P2X receptors are likely to occur in a native tissue such as the cochlea and this can alter pharmacological profiles (Le et al., 1998; Liu et al., 2001; Gallagher and Salter, 2003).

Fast Ca^{2+} wave propagation – other possible mechanisms

The fast Ca^{2+} wave could potentially also be formed through the action of other mechanisms. Assuming that the fast Ca^{2+} wave occurs in Deiters' cells ATP-induced depolarisation could be transmitted via gap junctions to neighbouring cells. This could mediate depolarisation-induced activation of voltage-gated Ca^{2+} channels and Ca^{2+} influx. Voltage-gated Ca^{2+} channels have been extensively characterised in HCs (Platzer et al., 2000; Brandt et al., 2005), but only one report suggests their expression during early postnatal development in Deiters' cells (Hafidi and Dulon, 2004).

Another possibility is that HCs are the mediators of the fast Ca^{2+} wave and this could be accomplished through mechano-transduction in response to needle, and thus reticular lamina and fluid movement. However, if this were the case, a simultaneous response rather than a wave would be expected to occur and thus it is unlikely that this mechanism can account for the generation of the fast Ca^{2+} wave. HCs are not coupled by gap junctions. Therefore, it can be excluded that this pathway mediates the fast damage-induced Ca^{2+} wave between HCs.

Considering aspects of *in vivo* setting

In the guinea pig, it has been demonstrated that ATP levels are increased in the endolymph following exposure to noise (Munoz et al., 2001). Thus, the damage-induced Ca^{2+} waves described in this chapter are likely to also arise *in vivo*.

Reviewing these data in the context of *in vivo* settings modulation of the Ca^{2+} wave might occur for the following reason. Apical and baso-lateral sites of cochlear cells are exposed to endolymph and perilymph, respectively. Both Ca^{2+} and K^+ – constituents that differ in these extracellular fluids have been demonstrated to modulate P2X and P2Y receptor responses, respectively (Ding and Sachs, 1999, 2000; Kanjhan et al., 2003; Pitt et al., 2005). The experimental medium used, is most similar to perilymph. Therefore, if ATP were released into endolymph containing high K^+ and low Ca^{2+} it is likely that a reduced fast Ca^{2+} wave might occur due to the lower Ca^{2+} concentration and thus reduced Ca^{2+} influx. However, in hair cells the IP_3-mediated intracellular Ca^{2+} changes were shown to be increased (Mammano et al., 1999). In addition, the P2Y mediated response that can be modulated by increased

K^+ might increase in this environment enriched in K^+ (Pitt et al., 2005). Thus, *in vivo* the ratio of the two mechanisms involved in the formation of the Ca^{2+} waves might be altered and consequently, downstream events might also be affected. The ion concentrations of the experimental setting described in this chapter more closely represent those of the perilymph. Thus, if ATP were released to the perilymphatic space, the Ca^{2+} waves triggered are likely similar to those described here.

To summarise, UTP sensitive $P2Y_2$, $P2Y_4$ and $P2Y_{11}$ receptors are the main candidates for mediation of the damage-induced slow Ca^{2+} wave, but other PPADS sensitive receptors such as $P2Y_1$ or $P2Y_6$ cannot be completely excluded. The only P2X receptor likely to mediate the fast Ca^{2+} wave is the $P2X_4$ receptor subtype based on its insensitivity to PPADS and suramin. Although, other Ca^{2+} permeable ion channels might mediate the fast Ca^{2+} wave and cannot therefore be excluded.

The role of gap junctions

The involvement of gap junctions in mediating Ca^{2+} wave propagation is dependent on the cell or organ type investigated with some reports demonstrating a role whereas in other cases agents that uncouple gap junctions had no effect (Sanderson et al., 1990; Venance et al., 1997; Newman, 2001; Sung et al., 2003). Expression and functional coupling of connexins has been demonstrated in the organ of Corti (Forge et al., 2003; Jagger and Forge, 2006). In this chapter, the gap junction inhibitor CBX reduced Ca^{2+} wave propagation in the OS and HC region. In contrast, Ca^{2+} wave spread in the IS region was reduced to a much lesser extent. This suggests that gap junctions might participate in the propagation of the Ca^{2+} wave into the OS region and along the HC region. IP_3 induced Ca^{2+} wave propagation between OS cells has been suggested to require gap junctions (Beltramello et al., 2005; Zhang et al., 2005).

Besides functioning as gap junctions, connexins can also form hemichannels and their opening has been implicated in the release of extracellular ATP (Stout et al., 2002; Pearson et al., 2005). In the mammalian cochlea ATP release has been demonstrated following mechanical stimulation that was sensitive to CBX (Zhao et al., 2005). Thus ATP release through hemichannels might mediate the damage-induced Ca^{2+} wave propagation described in this chapter. However, CBX was recently found to inhibit

$P2X_7$ receptors (Suadicani et al., 2006) and voltage-gated Ca^{2+} channels (Vessey et al., 2004). On the basis of the data presented here, $P2X_7$ receptors were thought not to be involved in the propagation of the damage-induced Ca^{2+} wave based on the antagonist profile and are therefore unlikely the target of CBX. In contrast, inhibition of voltage-gated Ca^{2+} channels by CBX cannot be excluded.

In the OS region, the combined application of apyrase and CBX resulted in an additional decrease in the Ca^{2+} wave compared to apyrase alone, suggesting that these mechanisms act synergistically. In contrast, the combined treatment with apyrase and CBX did not differ from exposure to apyrase alone in the HC region. This indicates that the underlying mechanisms might be the same. Both apyrase and CBX might interfere with the presence of extracellular ATP – apyrase hydrolysing ATP and CBX inhibiting ATP release.

Previous work has focussed on damage-induced Ca^{2+} signalling events in the OS region of the mammalian cochlea (Gale et al., 2004; Piazza et al., 2007). This chapter extended these studies by investigating the properties of the damage-induced Ca^{2+} wave spread in the HC and IS regions. The mechanisms underlying the formation and propagation of the damage-induced Ca^{2+} wave were found to be different in the distinct cochlear regions. However, a key mediator for the damage-induced Ca^{2+} wave in the entire cochlear explant was ATP. Propagation of the Ca^{2+} wave was also likely modulated by connexins. In the following chapter of this thesis one of the downstream signalling targets of the damage-induced Ca^{2+} wave will be investigated.

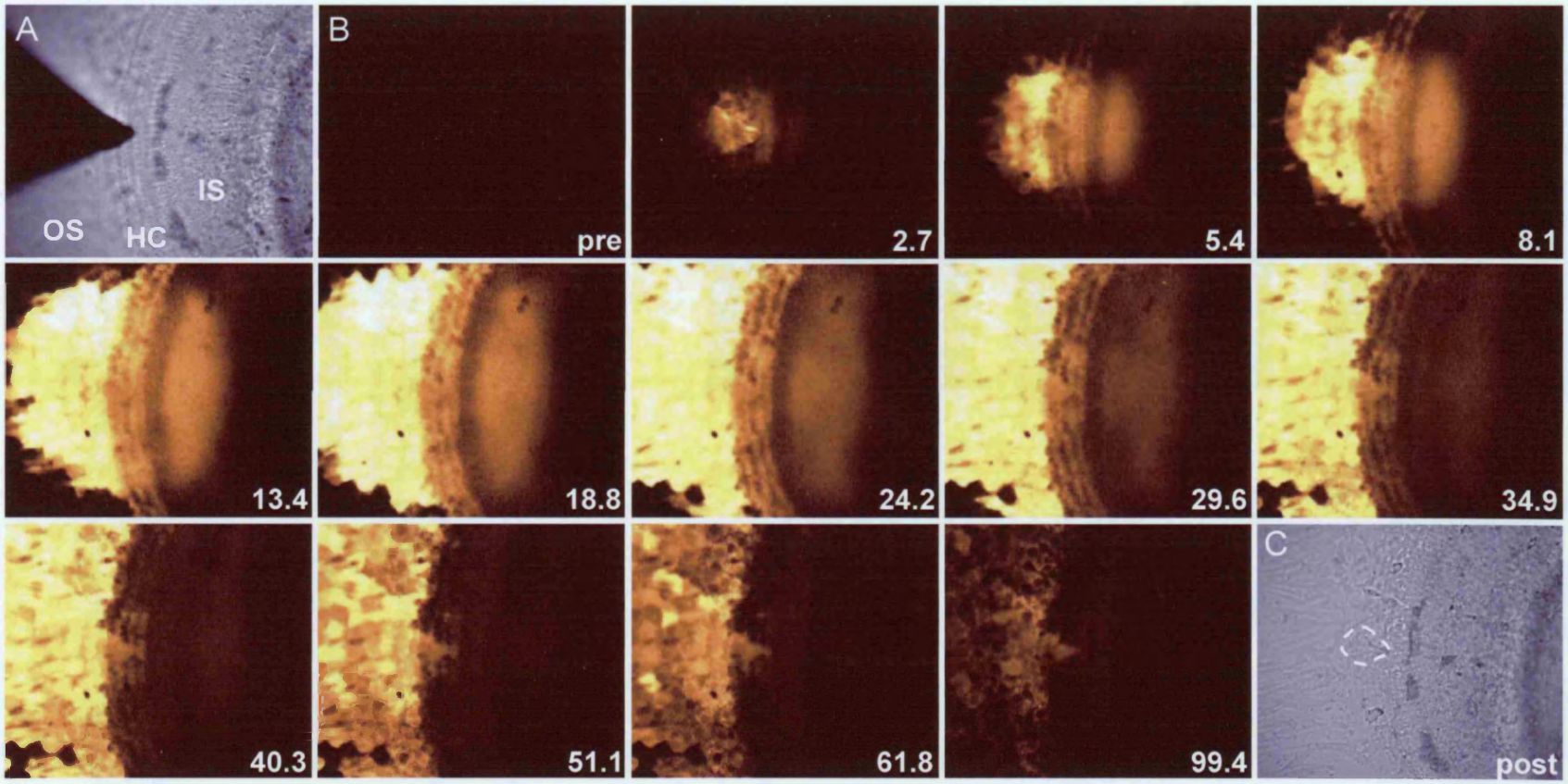

Fig 3.1 Time-series of a damage-induced Ca^{2+} wave.

A) Brightfield image of a cochlear culture focused at the level of the stereocilial hair bundles depicting the microneedle that was used to damage the HC epithelium. The cochlear culture is comprised of HC, IS and OS.

B) Series of ΔR images showing the propagation of a damage-induced Ca^{2+} wave.

C) Brightfield image of the same cochlear culture following damage.

The dotted line indicates the lesion site.

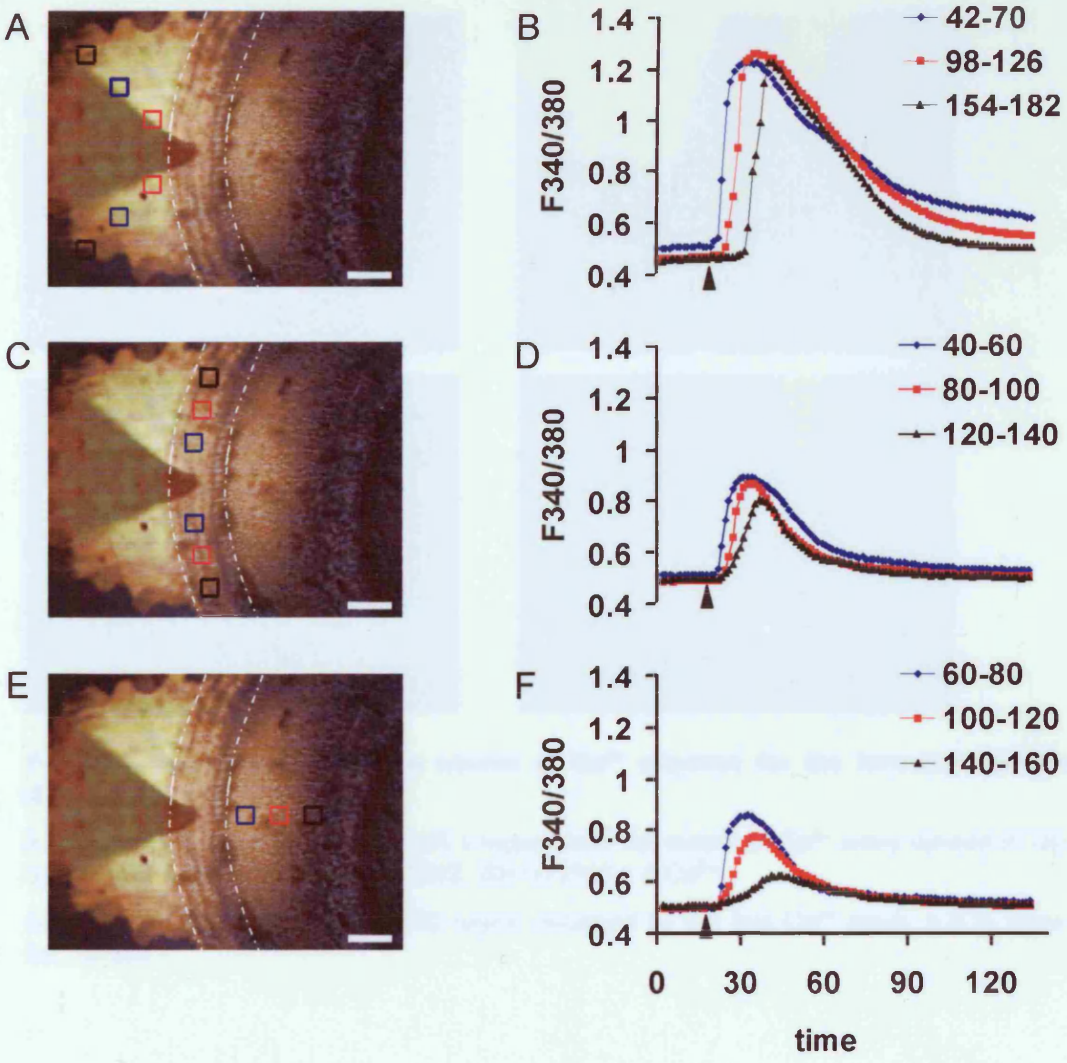

Fig 3.2 Properties of the damage-induced Ca^{2+} wave in the distinct regions of cochlear explants.

A, C, E) Averages of 10 consecutive baseline subtracted ΔR images starting at the time of damage merged with the corresponding brightfield image before the onset of the experiment. The white lines outline the HC region.

ROIs were placed at the following distances from the lesion site:

A) 42-70, 98-126 and 154-182 µm in the OS region;

C) 40-60, 80-100, 120-140 µm in the HC region and

E) 60-80, 100-120, 140-160 µm in the IS region.

B, D, F) The graphs depict the ΔRs as a function of time for the regions of interest in the **(B)** OS region, **(D)** HC region and **(F)** IS region. The arrow head marks the time of damage. For the OS and HC region the ΔR were averaged for the two ROIs placed at the same distance from the lesion site.

Scale bars 50 µm

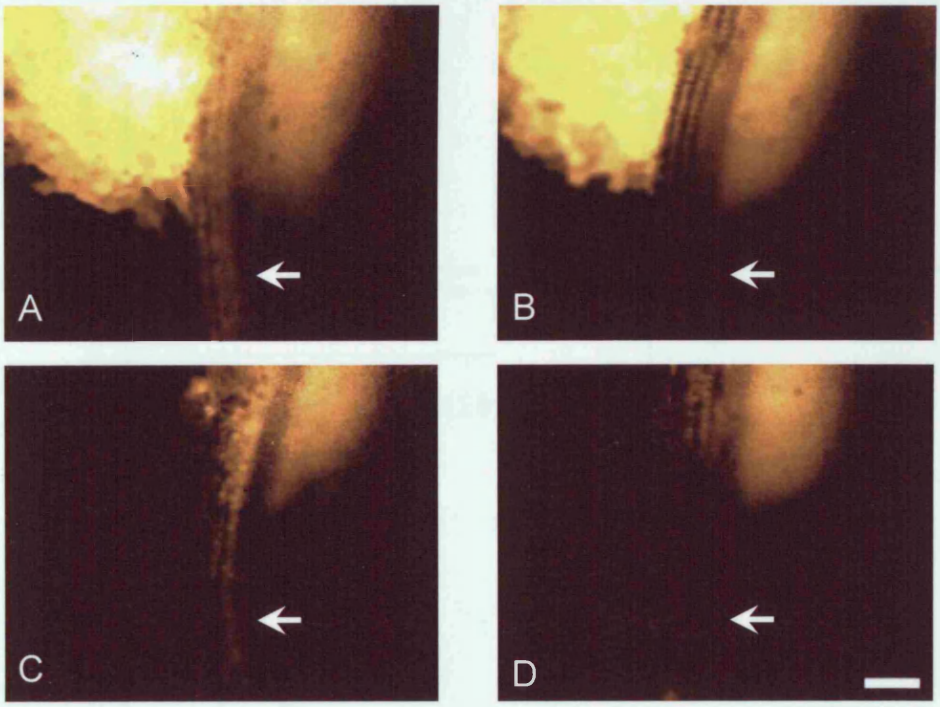

Fig 3.3 Characterisation of the source of Ca^{2+} required for the formation of the damage-induced Ca^{2+} wave.

A-D) Time averages (15 frames) ΔR images show the extent of Ca^{2+} wave spread in **(A)** control, **(B)** 0 Ca^{2+}, **(C)** 10 μM U73122, **(D)** U73122 + 0 Ca^{2+}.

Arrows point on the area of the HC region occupied by the fast Ca^{2+} wave. n ≥ 3; scale bar, 50 μm.

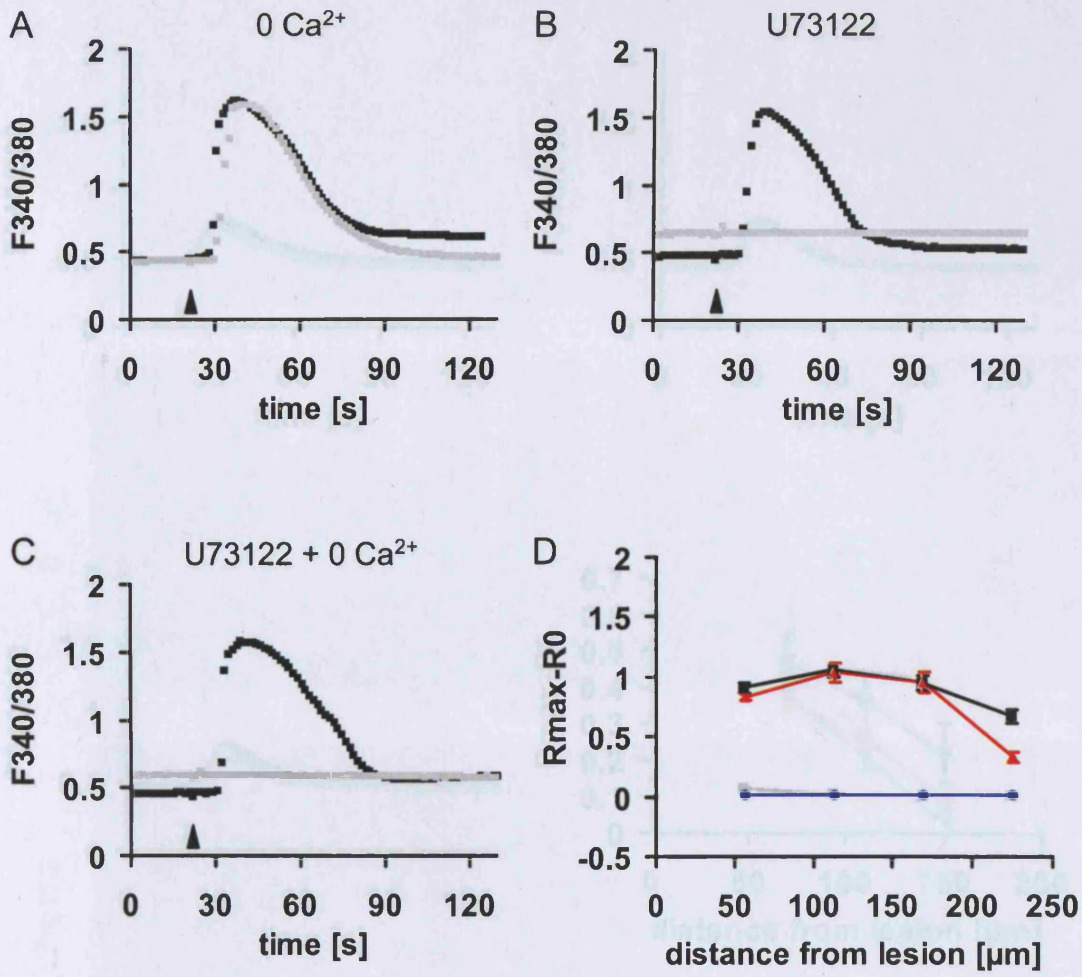

Fig 3.4 The propagation of the damage-induced Ca^{2+} wave in the OS region.

A-C) In the OS region: control (black) and treated (grey) ΔRs as a function of time at 154-182 µm from the lesion site showing in **(A)** 0 Ca^{2+}, **(B)** U73122 and **(C)** U73122 + 0 Ca^{2+}. Arrowheads indicate the time of damage.

D) Peak Ca^{2+} changes as a function of distance from the lesion site for control (black), 0 Ca^{2+} (red), U73122 (grey), U73122 + 0 Ca^{2+} (blue).

Mean ± S.E.M., n = 16 (control), n = 4 (0 Ca^{2+}), n = 6 (U73122), n = 5 (U73122 + 0 Ca^{2+}).

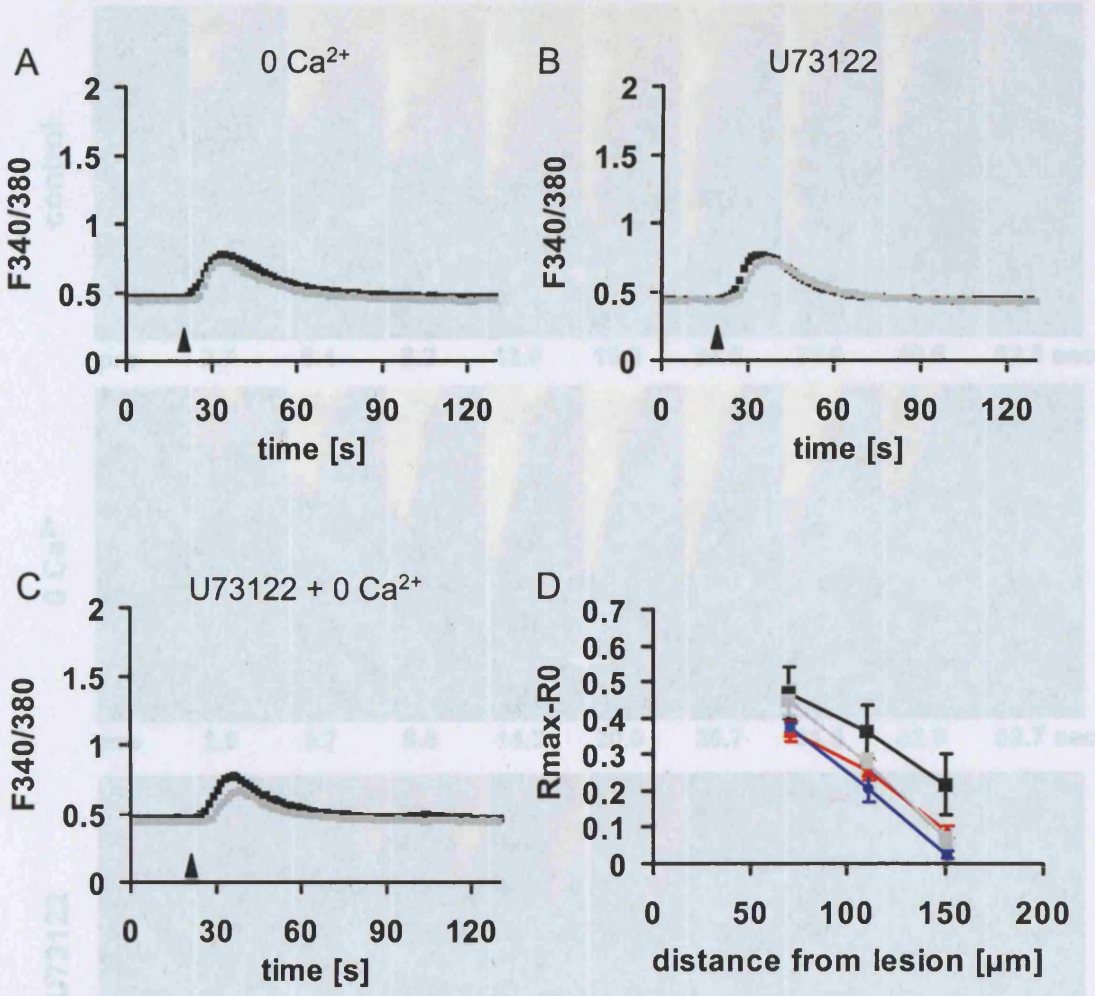

Fig 3.5 The propagation of the damage-induced Ca^{2+} wave in the IS region.

(A-C) In the IS region: control (black) and treated (grey) ΔRs as a function of time at 100-120 µm from the lesion site showing in **(A)** 0 Ca^{2+}, **(B)** U73122 and **(C)** U73122 + 0 Ca^{2+}. Arrowheads indicate the time of damage.

D) Peak Ca^{2+} changes as a function of distance from the lesion site for control (black), 0 Ca^{2+} (red), U73122 (grey), U73122 + 0 Ca^{2+} (blue).

Mean ± S.E.M., n = 16 (control), n = 4 (0 Ca^{2+}) , n = 6 (U73122), n = 5 (U73122 + 0 Ca^{2+}).

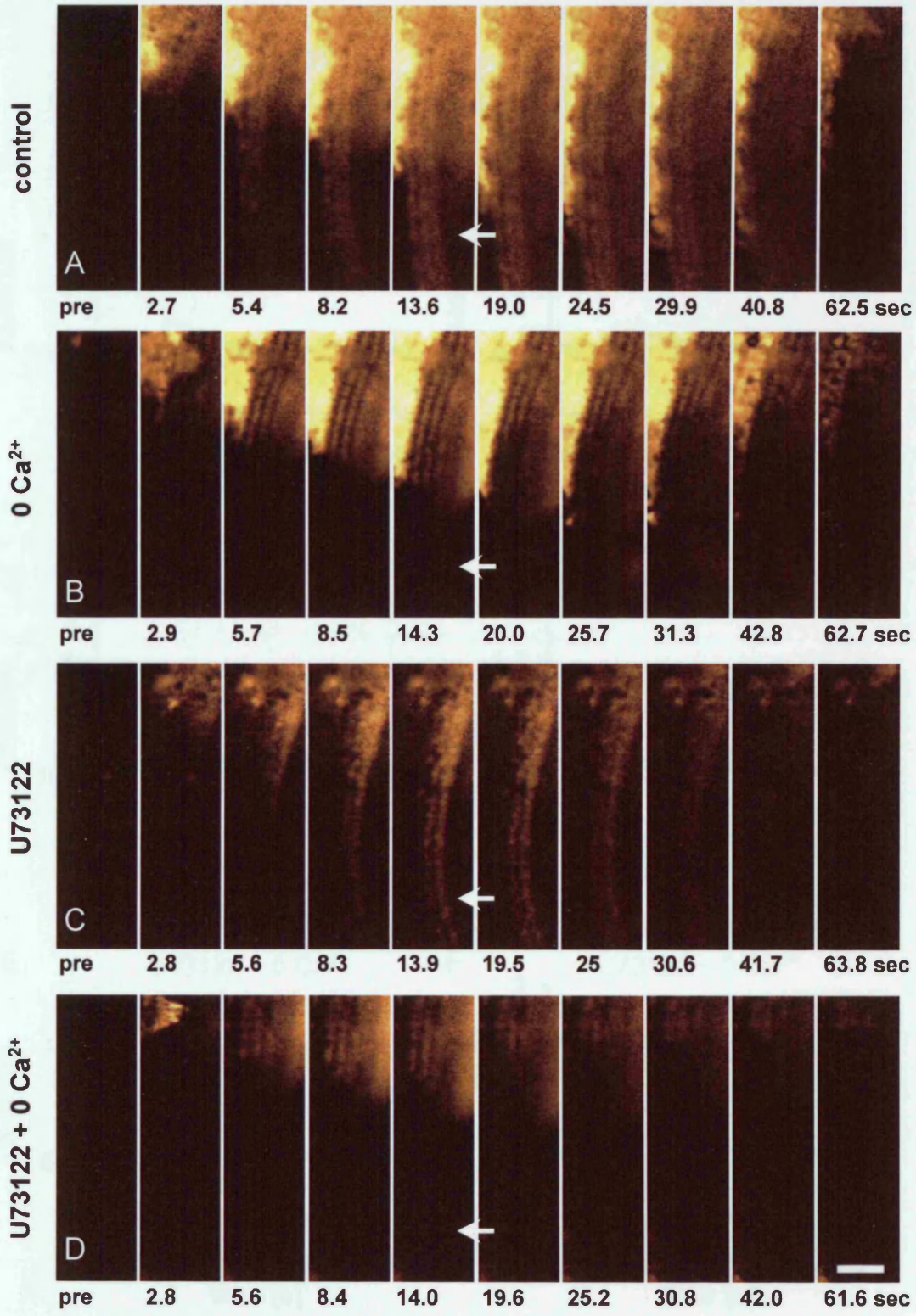

Fig 3.6 Damage-induced Ca^{2+} wave propagation in the HC region.

A-D) Time series of ΔR images showing the damage-induced Ca^{2+} wave propagation along the HC region in **(A)** control, **(B)** 0 Ca^{2+}, **(C)** U73122 and **(D)** U73122 + 0 Ca^{2+}.

Arrows indicate the region of the fast Ca^{2+} wave. $n \geq 3$; scale bar, 50 μm.

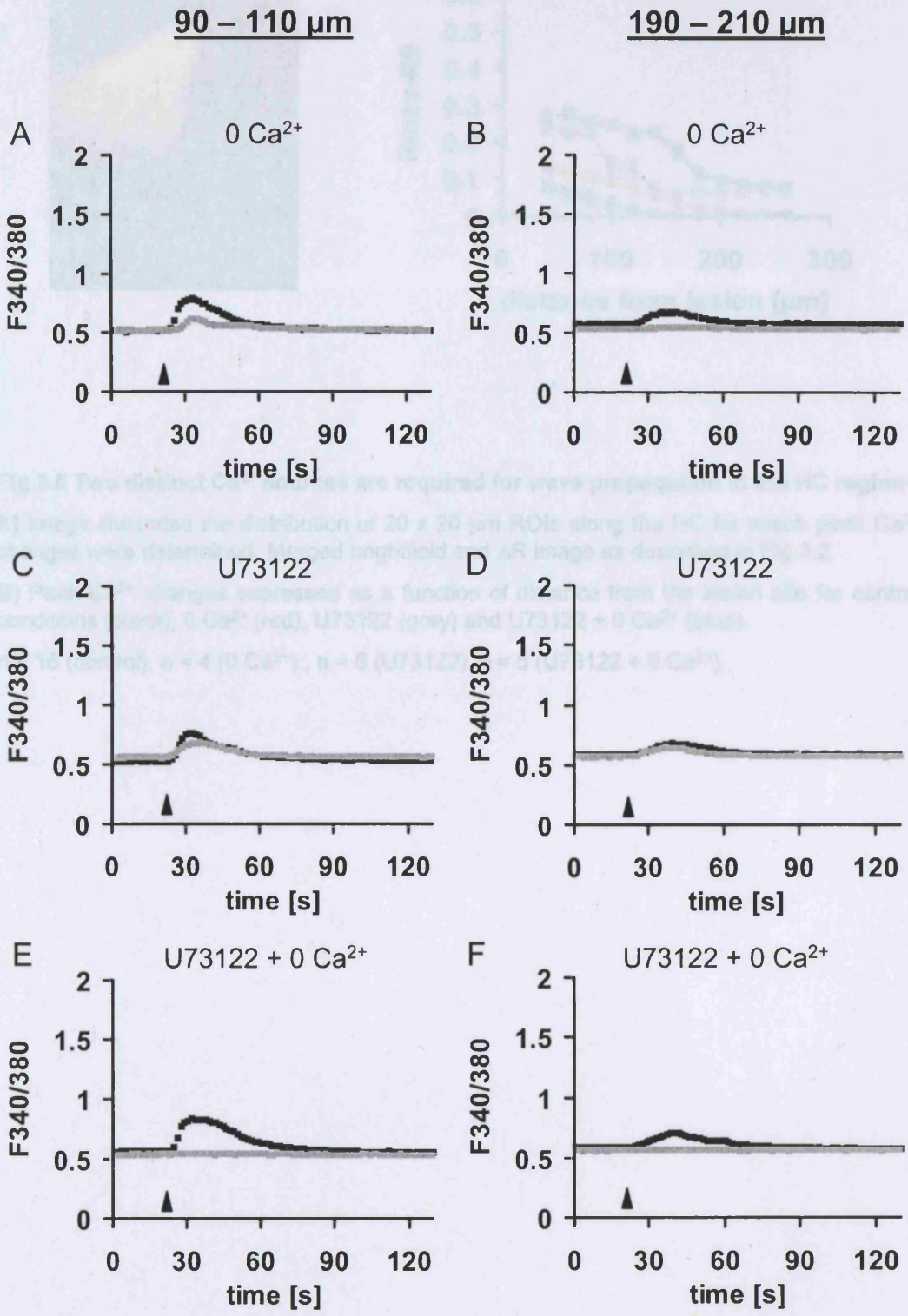

Fig 3.7 Kinetics of two distinct Ca^{2+} waves in the HC region.

(A-F) In the HC region control (black) and treated (grey) ΔRs as a function of time at **(A, C, E)** 90-110 and **(B, D, F)** 190-210 µm from the lesion site in **(A, B)** 0 Ca^{2+}, **(C, D)** U73122 **(E, F)** U73122 + 0 Ca^{2+}.

Arrowheads indicate the time of damage. n = 16 (control), n = 4 (0 Ca^{2+}) , n = 6 (U73122), n = 5 (U73122 + 0 Ca^{2+}).

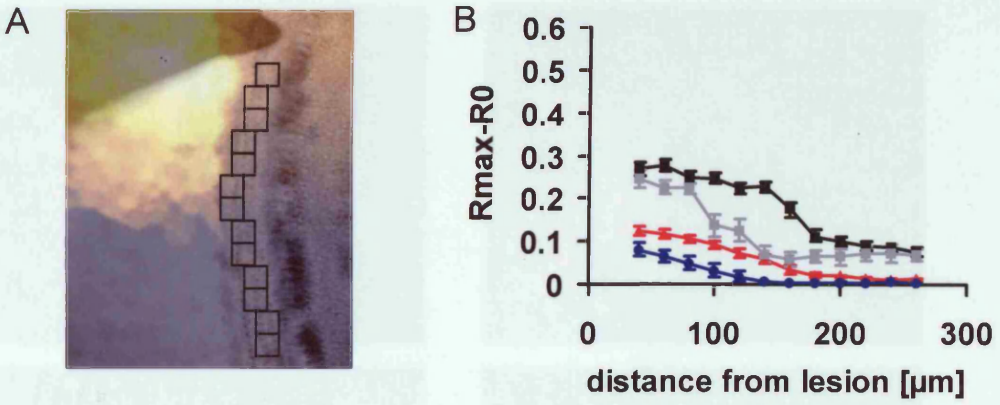

Fig 3.8 Two distinct Ca^{2+} sources are required for wave propagation in the HC region.

A) Image illustrates the distribution of 20 x 20 µm ROIs along the HC for which peak Ca^{2+} changes were determined. Merged brightfield and ΔR image as described in Fig 3.2.

B) Peak Ca^{2+} changes expressed as a function of distance from the lesion site for control conditions (black), 0 Ca^{2+} (red), U73122 (grey) and U73122 + 0 Ca^{2+} (blue).

n = 16 (control), n = 4 (0 Ca^{2+}) , n = 6 (U73122), n = 5 (U73122 + 0 Ca^{2+}).

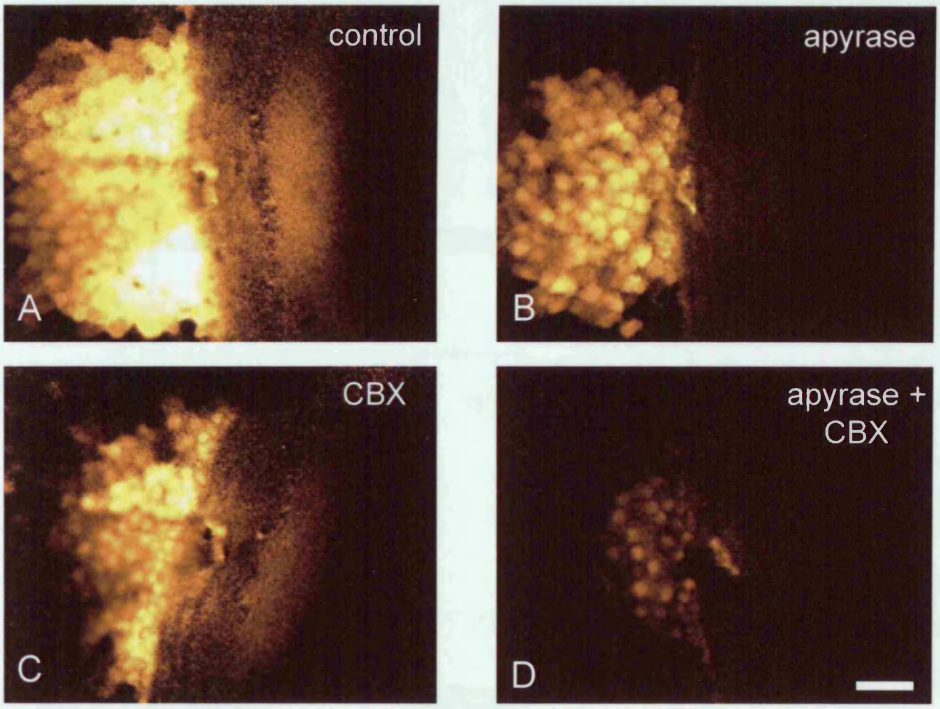

Fig 3.9 The damage-induced Ca^{2+} wave is modulated by extracellular ATP and require gap junctions.

A-D) Time R images (15 frames from damage start) in **(A)** control, **(B)** 40 U/ml apyrase, **(C)** 75 µM CBX and **(D)** apyrase combined with CBX.

Scale bar, 50 µm.

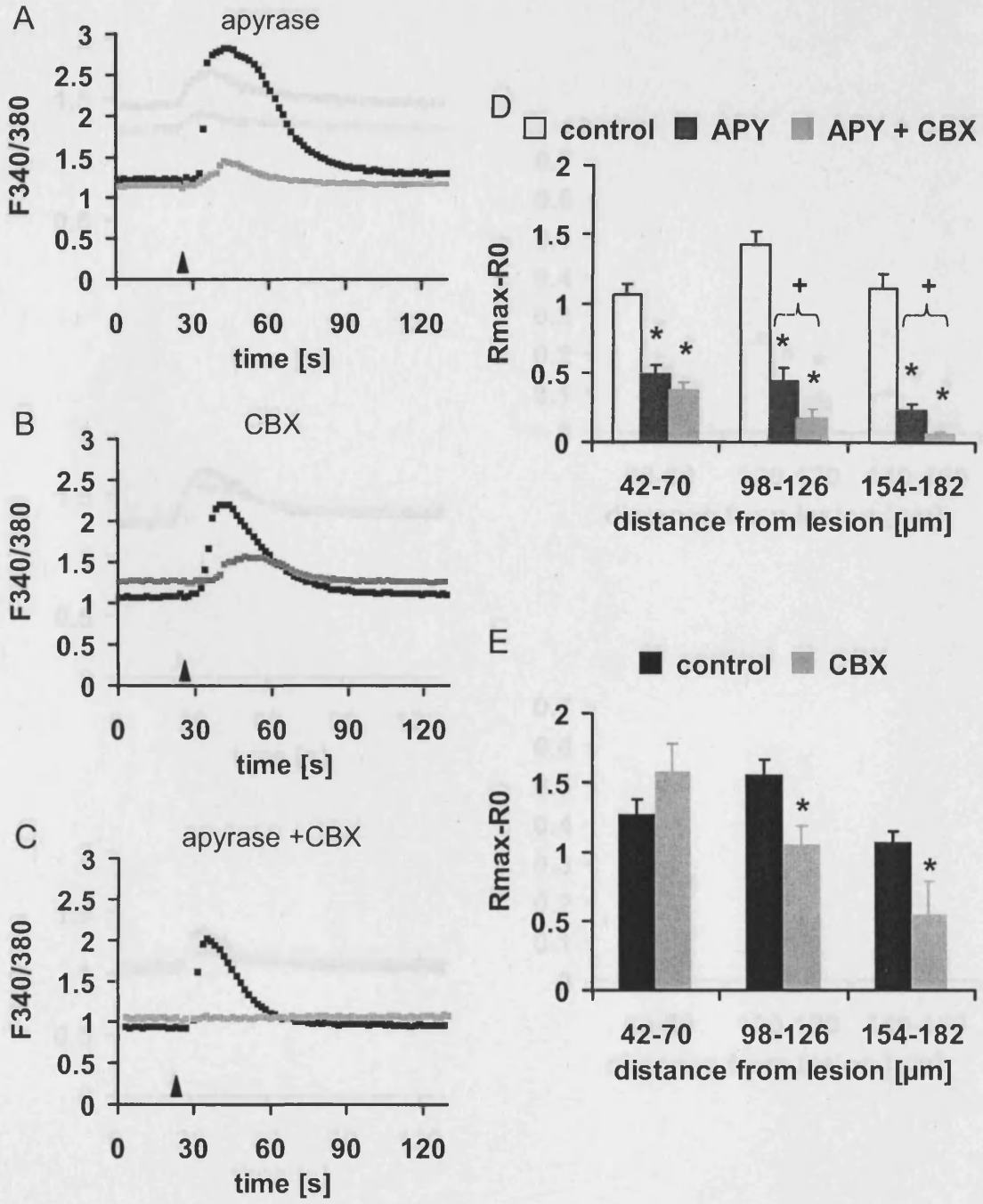

Fig 3.10 Ca^{2+} wave propagation is sensitive to apyrase and CBX in the OS region.

A-C) Control (black) and treated (grey) ΔRs as a function of time at 154-182 µm from the lesion site for explants exposed to **(A)** 40 U/ml apyrase, **(B)** 75 µM CBX and **(C)** apyrase and CBX combined. Arrowheads indicate the time of damage.

D, E) Peak Ca^{2+} changes as a function of distance from the lesion site in the OS region for **(D)** apyrase (APY) and combined with CBX and **(E)** CBX alone.

Mean ± S.E.M., n = 19 (control/CBX), n = 11 (CBX), n = 21 (control/apyrase), n = 9 (apyrase), n = 11 (apyrase + CBX), * indicates $P < 0.05$ between treated and control, + indicates $P < 0.05$ between apyrase and apyrase + CBX, ANOVA + Student's *t*-test.

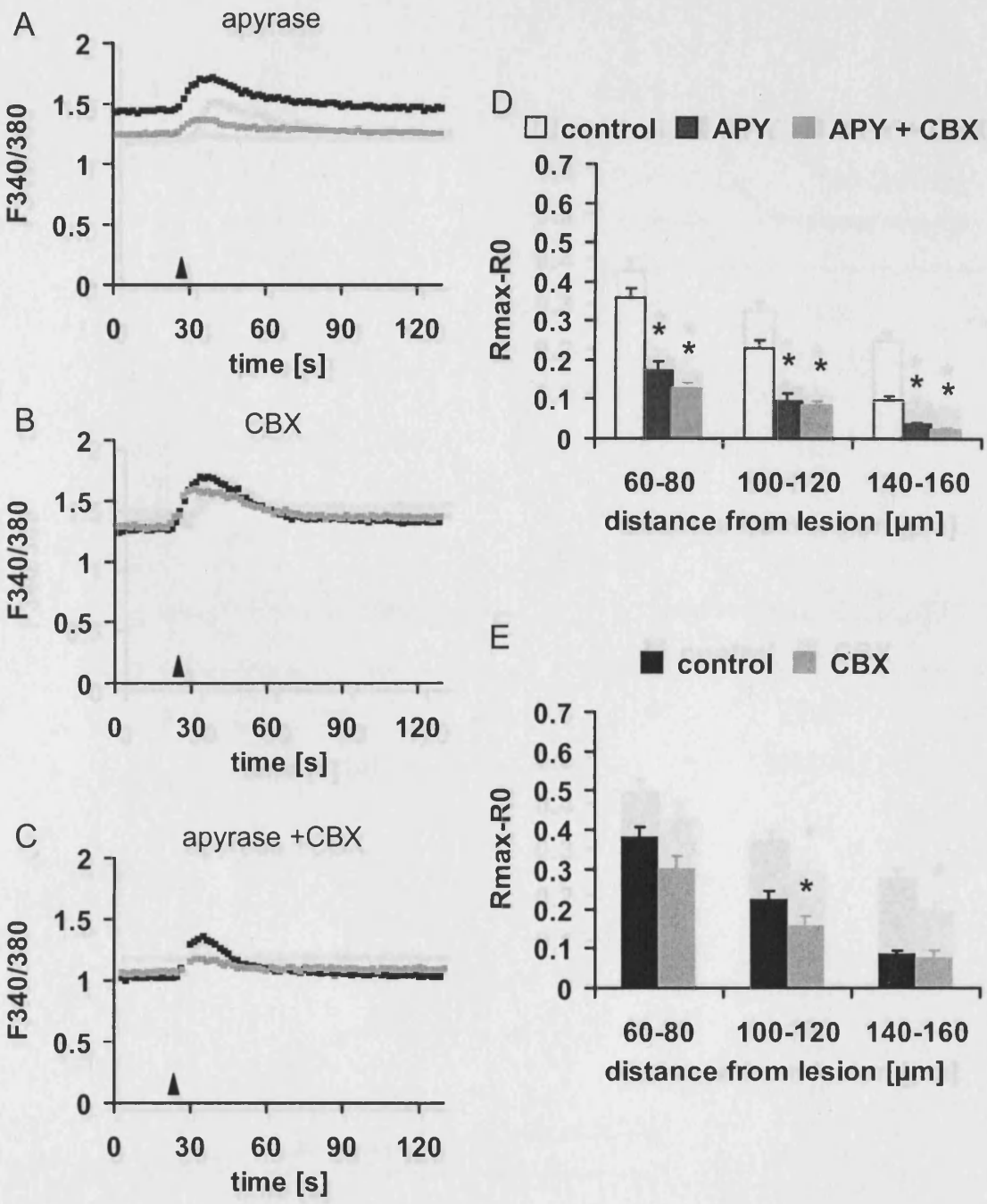

Fig 3.11 Apyrase and CBX modulate the damage-induced Ca^{2+} wave in the IS region.

A-C) Control (black) and treated (grey) ΔRs as a function of time at 100-120 µm from the lesion site for explants exposed to **(A)** 40 U/ml apyrase, **(B)** 75 µM carbenoxonlone (CBX) and **(C)** apyrase and CBX combined. Arrowheads indicate the time of damage.

D, E) Peak Ca^{2+} changes as a function of distance from the lesion site in the IS region for **(D)** apyrase (APY) and combined with CBX and **(E)** CBX alone.

Mean ± S.E.M., n = 19 (control/CBX), n = 11 (CBX), n = 21 (control/apyrase), n = 9 (apyrase), n = 11 (apyrase + CBX), * indicates $P < 0.05$ between treated and control, ANOVA + Student's *t*-test.

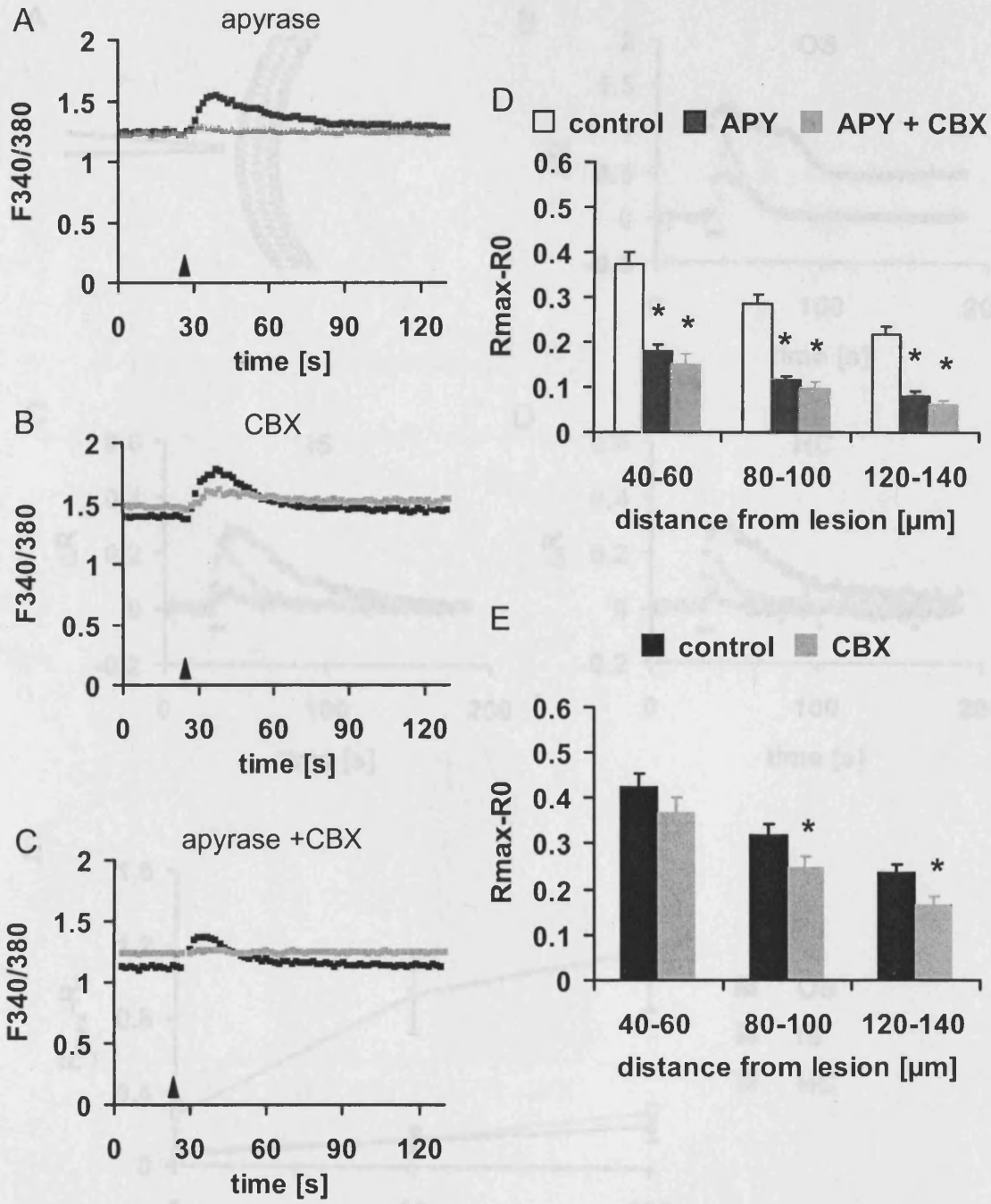

Fig 3.12 Apyrase and CBX modulate the Ca^{2+} wave in the HC region.

A-C) Control (black) and treated (grey) ΔRs as a function of time at 120-140 µm from the lesion site for explants exposed to **(A)** 40 U/ml apyrase (APY), **(B)** 75 µM carbenoxonlone (CBX) and **(C)** apyrase and CBX combined. Arrowheads indicate the time of damage.

D, E) Peak Ca^{2+} changes as a function of distance from the lesion site in the HC region for **(D)** apyrase and combined with CBX and **(E)** CBX alone.

Mean ± S.E.M., n = 19 (control/carbnexolone), n = 11 (CBX), n = 21 (control/apyrase), n = 9 (apyrase), n = 11 (apyrase + CBX), * indicates $P < 0.05$ between treated and control, ANOVA + Student's *t*-test.

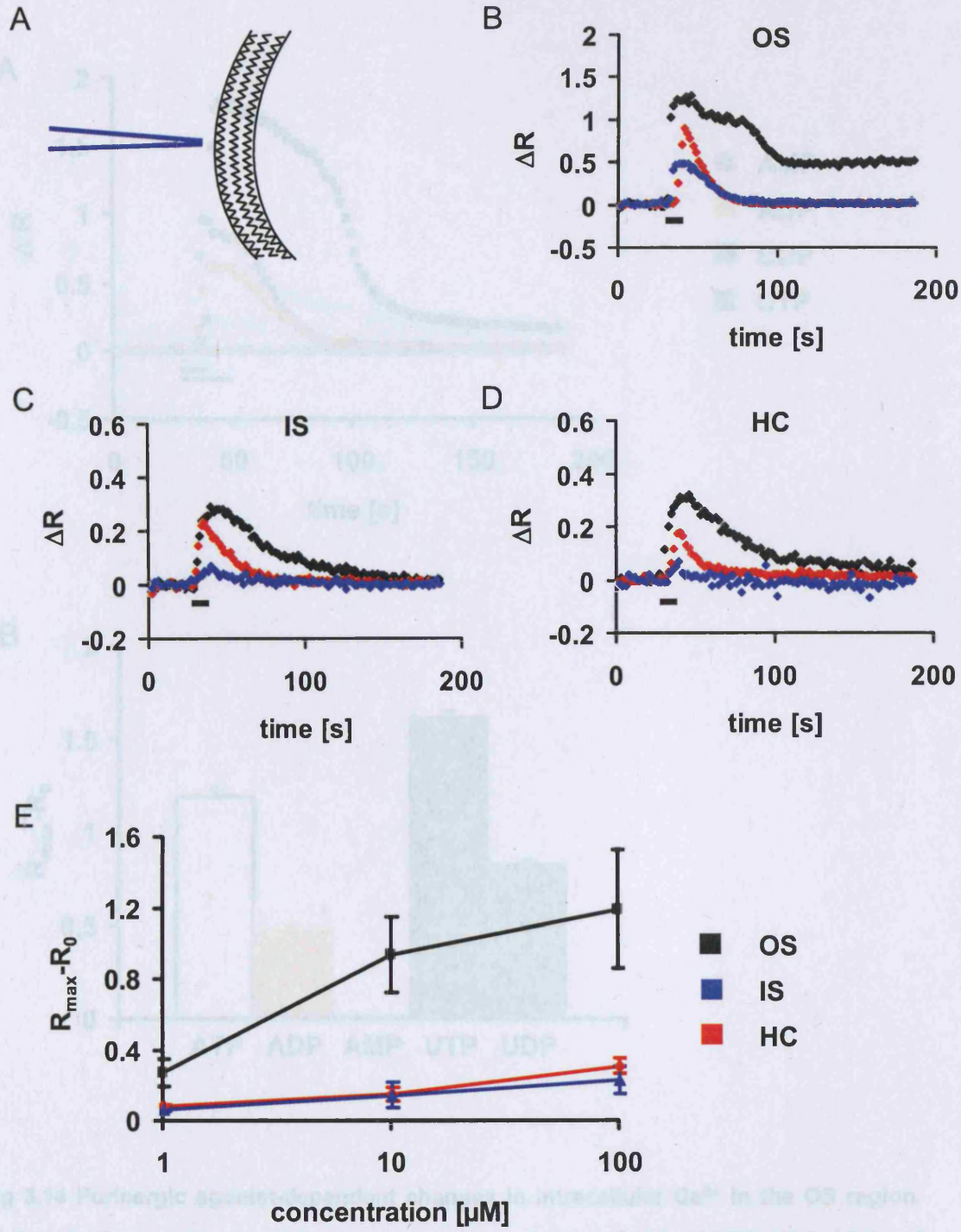

Fig 3.13 Ca^{2+} changes triggered by exogenous application of ATP

A) Schematic diagram illustrating puff application protocol.

B-D) ΔRs as a function of time in response to 1 (blue), 10 (red) and 100 µM ATP (black) in the **(B)** OS, **(C)** IS and **(D)** HC region. The solid black bar indicates duration of application.

E) Peak Ca^{2+} changes for 1, 10 and 100 µM ATP for the distinct regions of cochlear explants.

n ≥ 3 for each concentration.

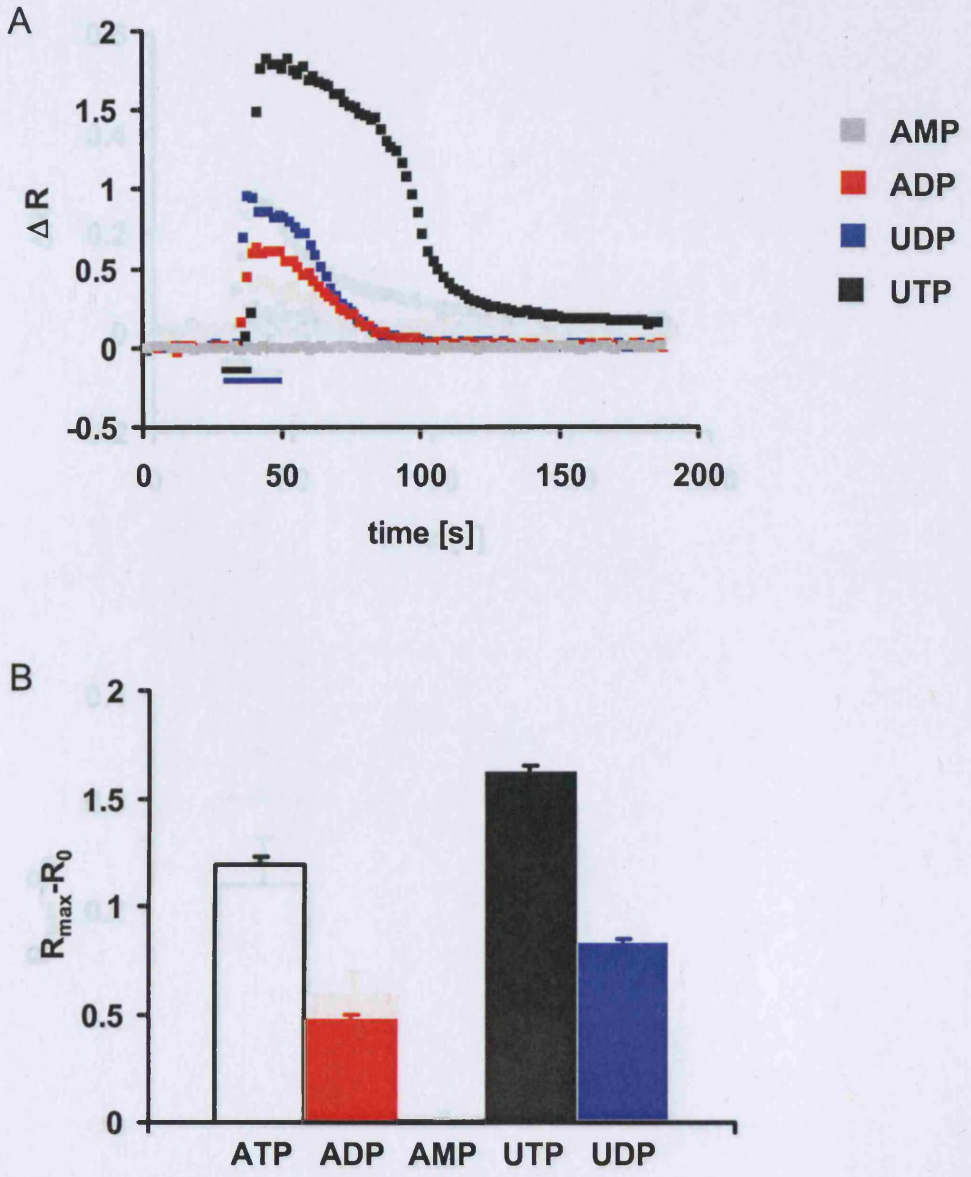

Fig 3.14 Purinergic agonist-dependent changes in intracellular Ca^{2+} in the OS region.

A) Fura-2 ΔRs as a function of time in response to application of 100 µM UTP, UDP, ADP and AMP in the OS region. Black (10 s) and blue bar (20 s) indicate the duration for UTP and for UDP, ADP and AMP applications, respectively.

B) Peak Ca^{2+} changes induced by 100 µM ATP, ADP, AMP, UTP and UDP.

Mean ± S.E.M., n ≥ 3

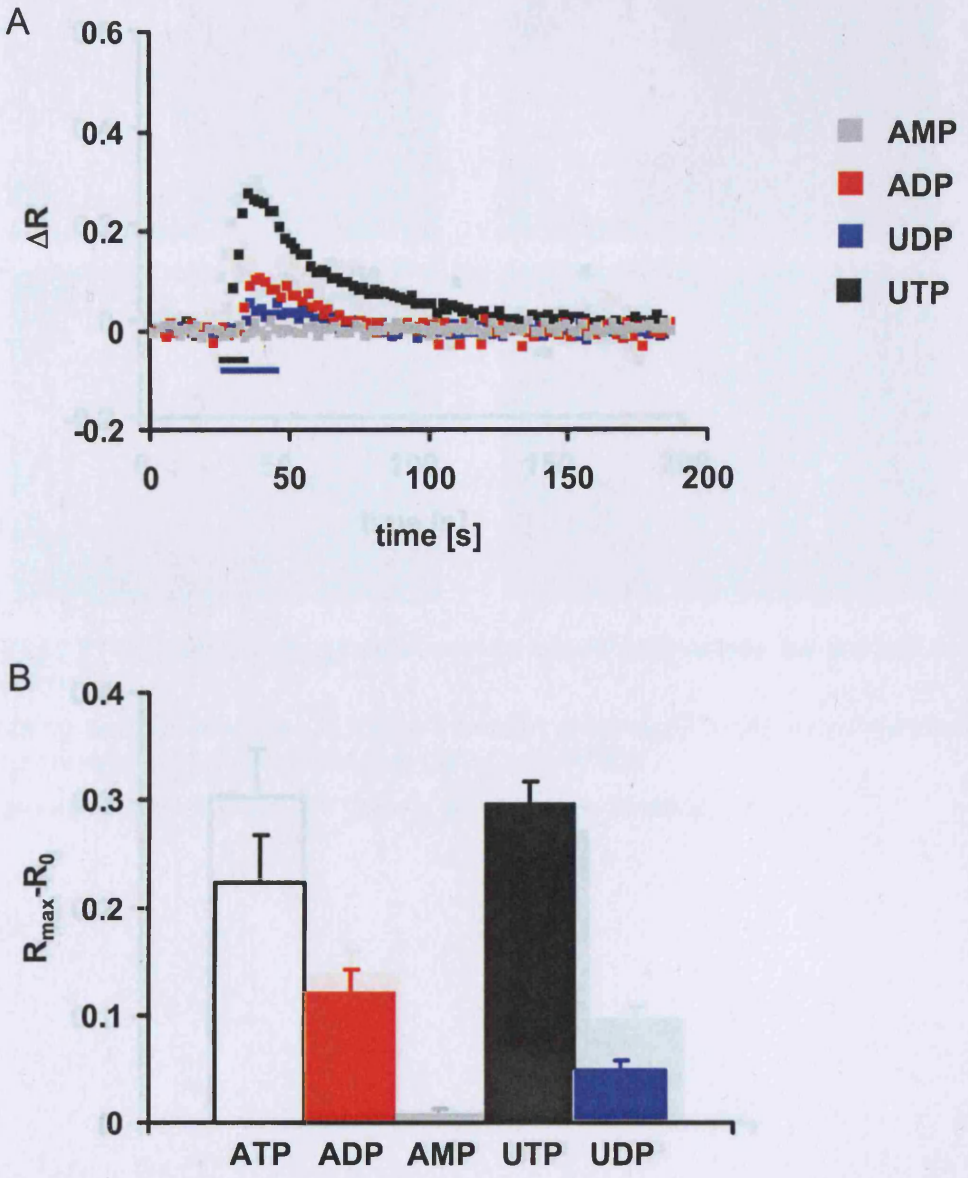

Fig 3.15 Purinergic agonist-dependent changes in intracellular Ca^{2+} in the IS region.

A) Fura-2 ΔRs as a function of time in response to application of 100 μM UTP, UDP, ADP and AMP in the IS region. Black (10 s) and blue (20 s) bars indicate the duration for UTP and for UDP, ADP and AMP applications, respectively.

B) Peak Ca^{2+} changes induced by 100 μM ATP, ADP, AMP, UTP and UDP.

Mean ± S.E.M, n ≥ 3

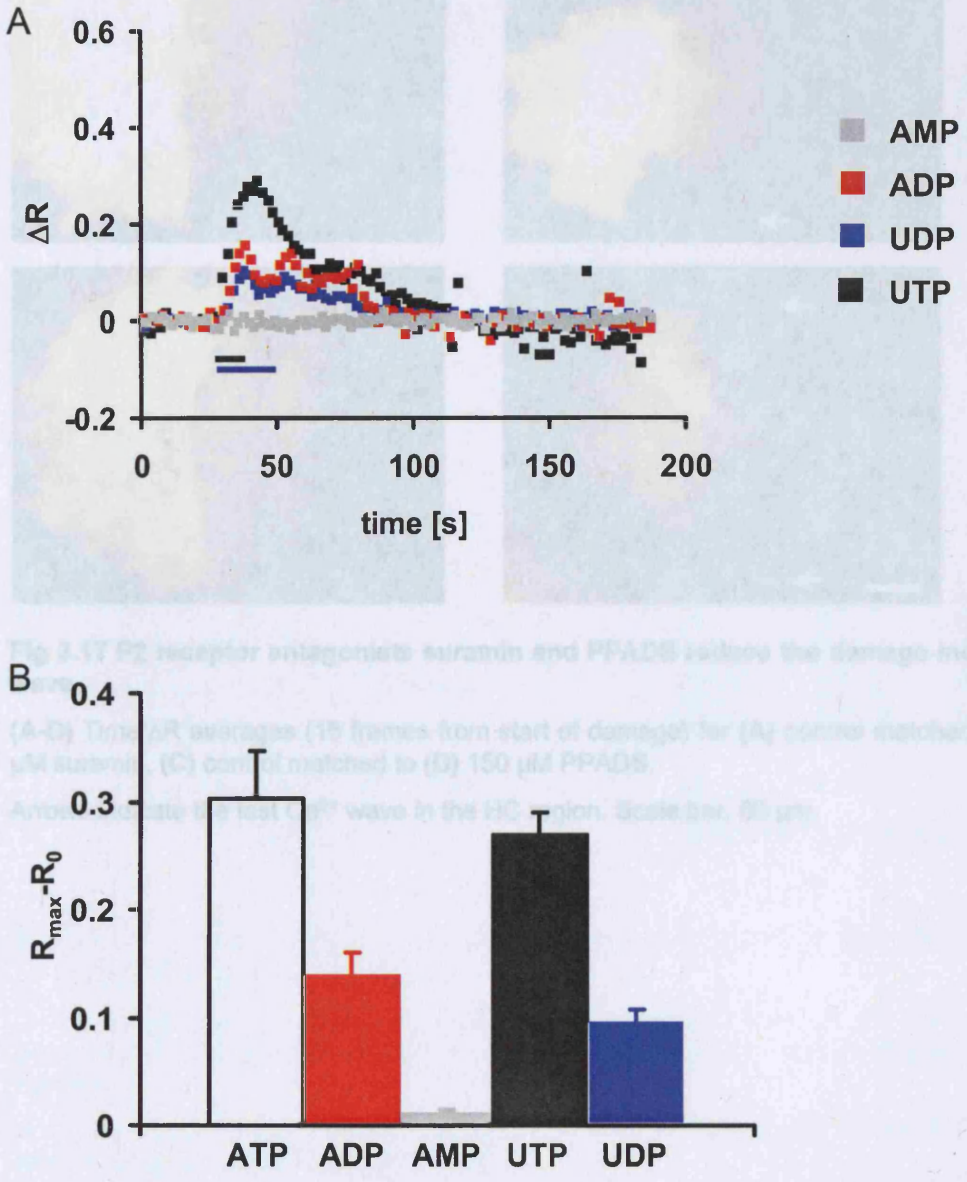

Fig 3.16 Purinergic agonist-dependent changes in intracellular Ca^{2+} in the HC region. **A)** Fura-2 ΔRs as a function of time in response to application of 100 μM UTP, UDP, ADP and AMP to the HC region. The black (10 s) and the blue (20 s) bars indicate the duration for UTP and for UDP, ADP and AMP applications, respectively.

B) Peak Ca^{2+} changes induced by 100 μM ATP, ADP, AMP, UTP and UDP.

Mean ± S.E.M, n ≥ 3

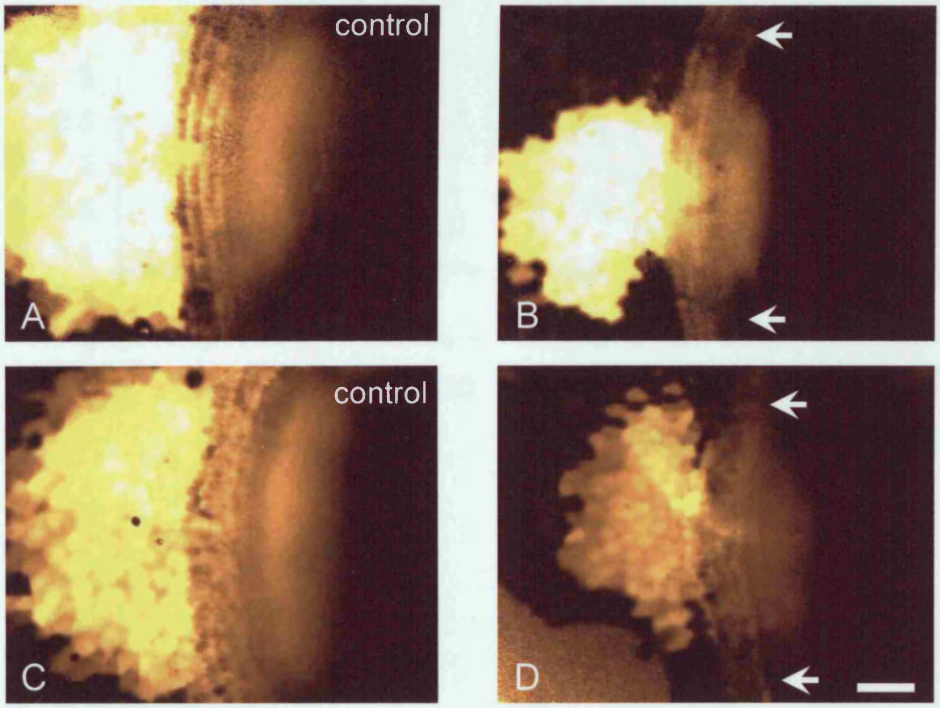

Fig 3.17 P2 receptor antagonists suramin and PPADS reduce the damage-induced Ca^{2+} wave.

(A-D) Time/ΔR averages (15 frames from start of damage) for **(A)** control matched to **(B)** 100 μM suramin, **(C)** control matched to **(D)** 150 μM PPADS.

Arrows indicate the fast Ca^{2+} wave in the HC region. Scale bar, 50 μm.

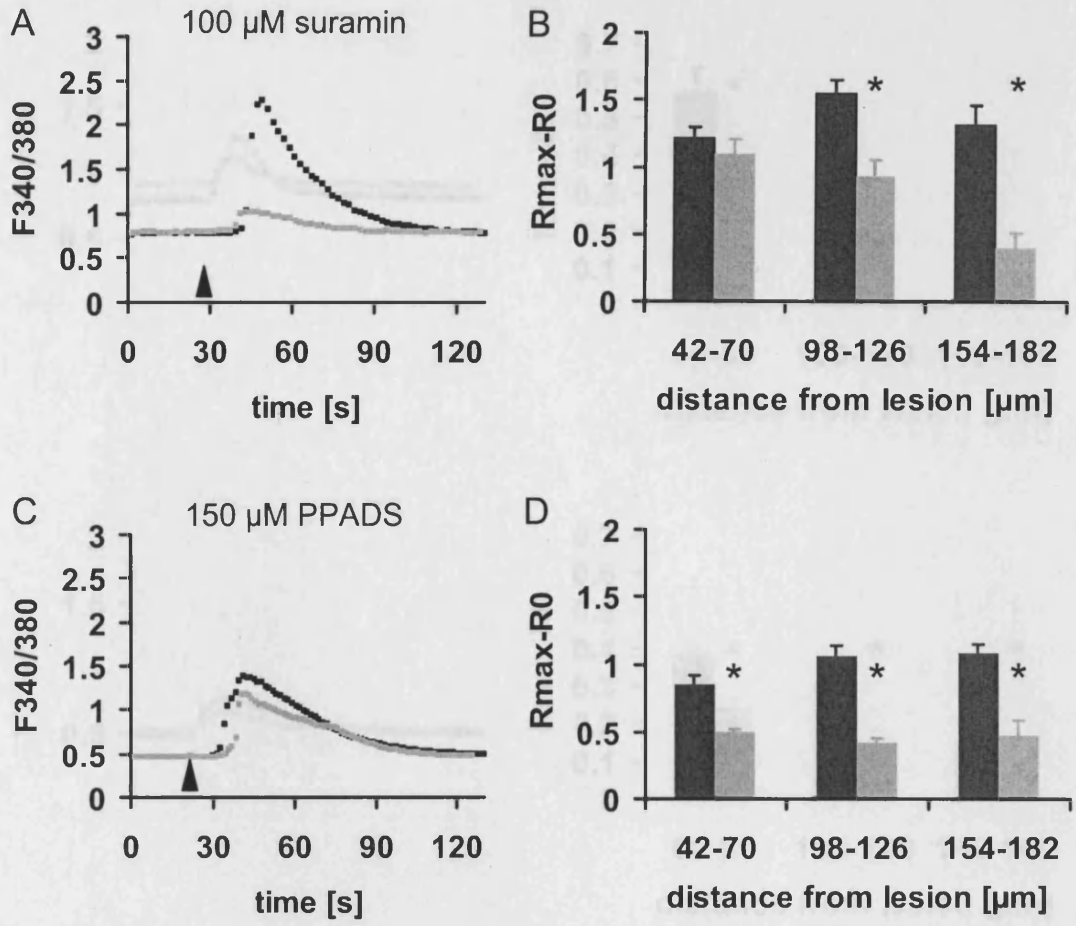

Fig 3.18 The effect of P2 receptor antagonists suramin and PPADS on the damage-induced Ca^{2+} wave in the OS region.

A, C) Control (black) and treated (grey) ΔRs as a function of time at 154-182 µm from the lesion site for **(A)** suramin and **(C)** PPADS exposed explants. Arrows indicate the time of damage.

B, D) Peak Ca^{2+} changes at various distances from the lesion site for control (black) and treated (grey) for **(B)** suramin and **(D)** PPADS.

Mean ± S.E.M., n = 11 (suramin), n = 5 (PPADS), n = 7 (control/PPADS), $^{*}P < 0.05$, Student's *t*-test.

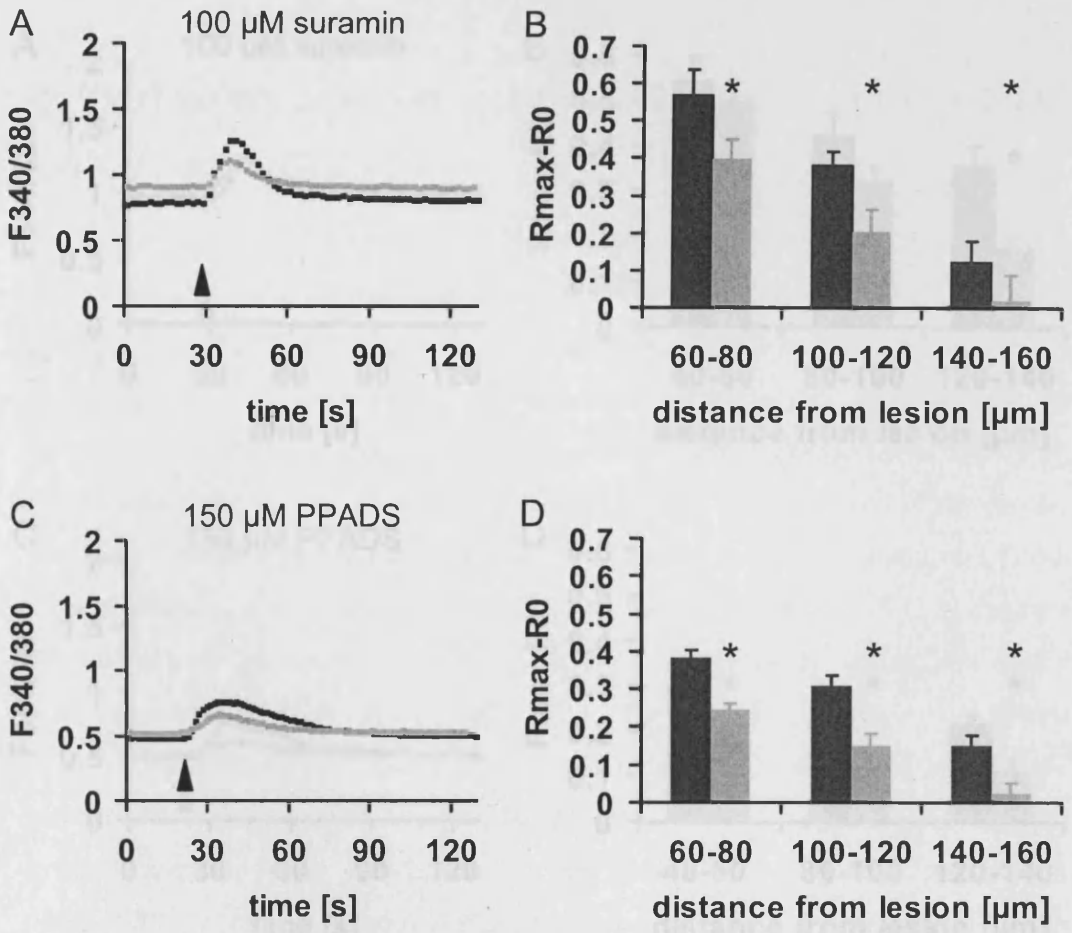

Fig 3.19 P2 receptor antagonists suramin and PPADS reduce the propagation of the damage-induced Ca^{2+} wave into the IS region.

(A, C) Control (black) and treated (grey) ΔRs as a function of time at 100-120 µm from the lesion site for **(A)** suramin and **(C)** PPADS exposed explants. Arrows indicate the time of damage.

B, D) Peak Ca^{2+} changes at various distances from the lesion site for control (black) and treated (grey) for **(B)** suramin and **(D)** PPADS.

Mean ± S.E.M, n = 11 (suramin), n = 5 (PPADS), n = 7 (control/PPADS), $^{*}P < 0.05$, Student's *t*-test.

.

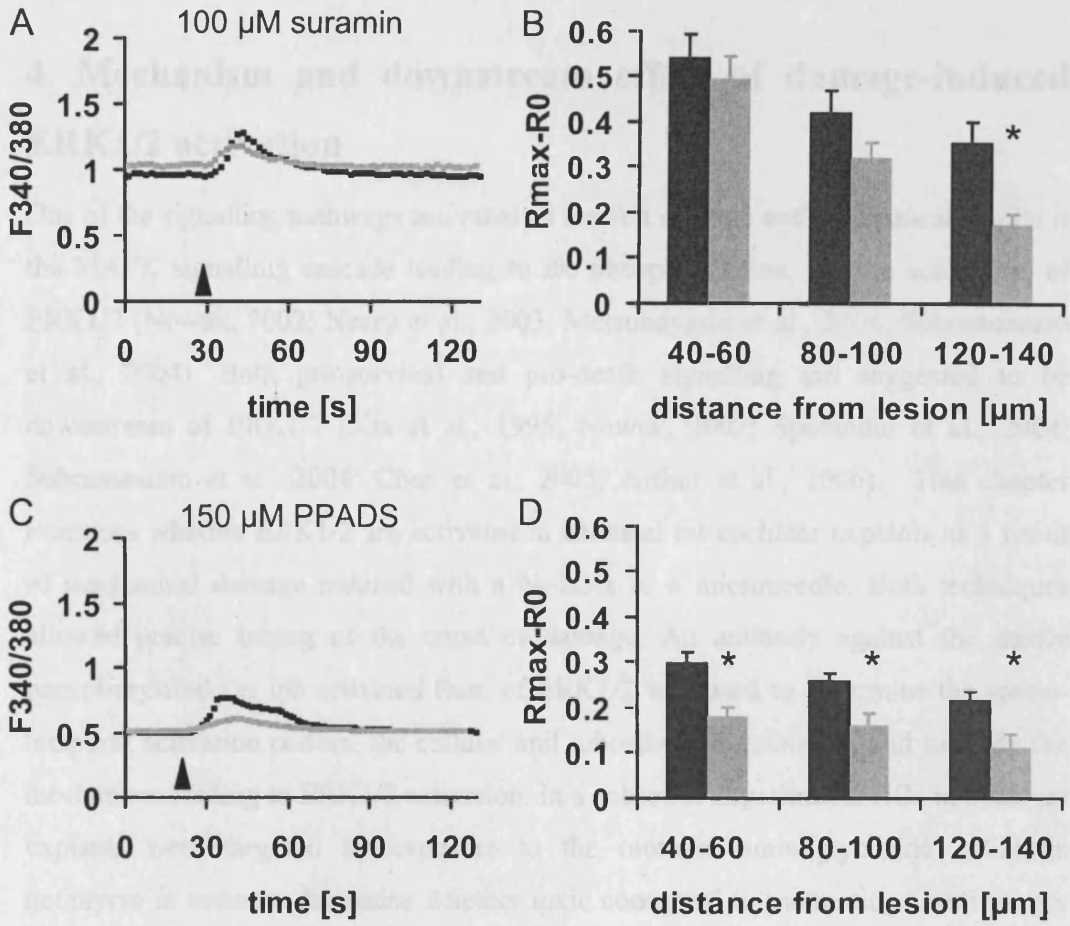

Fig 3.20 The effect of P2 receptor antagonists suramin and PPADS on the damage-induced Ca^{2+} wave in the HC region.

(A, C) Control (black) and treated (grey) ΔRs as a function of time at 120-140 µm from the lesion site for suramin **(A)** and **(C)** PPADS exposed explants. Arrows indicate the time of damage.

B, D) Peak Ca^{2+} changes at various distances from the lesion site for control (black) and treated (grey) for **(B)** suramin and **(D)** PPADS.

Mean ± S.E.M, n = 11 (suramin), n = 5 (PPADS), n = 7 (control/PPADS), *P < 0.05, Student's *t*-test.

4. Mechanism and downstream effect of damage-induced ERK1/2 activation

One of the signalling pathways activated as a result of toxic and mechanical insults is the MAPK signalling cascade leading to the phosphorylation, i.e. the activation, of ERK1/2 (Nowak, 2002; Neary et al., 2003; Matsubayashi et al., 2004; Subramaniam et al., 2004). Both pro-survival and pro-death signalling are suggested to be downstream of ERK1/2 (Xia et al., 1995; Nowak, 2002; Sperandio et al., 2004; Subramaniam et al., 2004; Chen et al., 2005; Arthur et al., 2006). This chapter examines whether ERK1/2 are activated in neonatal rat cochlear explants as a result of mechanical damage induced with a N_2-laser or a microneedle. Both techniques allowed precise timing of the onset of damage. An antibody against the dually phosphorylated i.e. the activated form of ERK1/2 was used to determine the spatio-temporal activation pattern, the cellular and subcellular distribution, and to study the mechanism leading to ERK1/2 activation. In a subset of experiments HCs in cochlear explants were targeted by exposure to the ototoxic aminoglycoside antibiotic neomycin in order to determine whether toxic compared to traumatic stimuli trigger the activation of ERK1/2. Subsequently, this model was used to study the role of ERK1/2 during aminoglycoside toxicity.

4.1 Mechanical damage induces ERK1/2 activation

4.1.1 Spatio-temporal aspects of N_2-laser induced ERK1/2 activation

To investigate whether signalling via the ERK1/2 pathway occurs as a consequence of damage to the mammalian cochlea, the HC epithelium of neonatal cochlear explants was damaged using a N_2-laser. A typical lesion site at 1 min post damage is displayed in Fig 4.1.1A where the actin-rich stereocilia of hair bundles are displaced or absent. Fig 4.1.1B is a representative image of the cochlear HC epithelium at 1 min post damage showing sporadic activation of ERK1/2 in a small number of cells in the epithelium. The pattern was not particularly coordinated with the lesion site. On the contrary, at 10 min post damage (Fig 4.1.2C) strong ERK1/2 activation was observed around the lesion site. The spatial pattern was non-uniform with activation predominantly along the HC rows (Fig 4.1.2C). Within 30 min the spread of ERK1/2

activation had retracted to cells in close proximity to the lesion site (Fig 4.1.1D) and signals returned to baseline levels 60 min post damage (Fig 4.1.1E).

The distance that activated ERK1/2 spread along the sensory region of the cochlear turn was quantified by performing a linescan analysis. Specifically, lines were placed separately along the OHC and IHC regions (Fig 4.1.1F). Both regions are comprised of sensory HCs and their non-sensory support cells (see 1.1). Fig 4.1.1G shows the spread of activated ERK1/2 as a function of time after damage. In the OHC region, ERK1/2 were first observed to be activated 2 min after damage at which point the signal had already spread 27 ± 12 μm (n = 9) from the lesion site. Over the following minutes the spread of activated ERK1/2 increased reaching a peak at 10 min post damage of 130 ± 19 μm (n = 5). The spread then declined resulting in ERK1/2 being activated only in cells lining the lesion site 30 min post damage (17 ± 7 μm, n = 4, Fig 4.1.1D, G) and by 60 min post damage ERK1/2 activation returned to baseline levels (1 ± 1 μm, n = 4, Fig 4.1.1E, G). The timecourse of ERK1/2 activation in the IHC region was similar to that in the OHC region with it first being observed at 2 min post damage (47 ± 13 μm, n = 9). In contrast to the OHC region the maximum spread of 92 ± 10 μm (n = 21) was detected at 5 min post damage after which the spread of ERK1/2 activation decreased to only cells in immediate proximity to the lesion site (22 ± 13 μm at 30 min post damage, n = 4, Fig 4.1.1D, G). At 60 min post damage ERK1/2 activation also returned to baseline in the IHC region.

4.1.2 Cellular and subcellular localisation of ERK1/2

The spatial pattern of ERK1/2 activation shown in Fig 4.1.1C suggested a cell-type specific activation. 3-D reconstructions (Fig 4.1.2A, B, movie 6) and orthogonal x-z projections of confocal z-stack images (Fig 4.1.2C-E) confirmed that ERK1/2 were activated in a cell-specific manner. ERK1/2 activation was observed in cell bodies and phalangeal processes of Deiters' cells (Fig 4.1.2A, E) that line the baso-lateral sites of OHCs (Fig 4.1.2A, E; see introduction Fig 1.1). Activated ERK1/2 was not detected in OHCs. Similarly, phalangeal cells also exhibited ERK1/2 activation (Fig 4.1.2B, E). Again, IHCs situated in the "cups" of phalangeal cells did not exhibit ERK1/2 activation. A few pillar cells (Fig 4.1.2A, B) activated ERK1/2 as a result of damage. In contrast to the spread of ERK1/2 activation along the rows of Deiters' and

phalangeal cells the activation in pillar cells remained restricted to the proximity of the lesion site.

The subcellular distribution of ERK1/2 is crucial for it to initiate specific cellular programs. The orthogonal projection of activated ERK1/2 counterstained with the nuclear marker DAPI (Fig 4.1.2C-E) revealed that in Deiters' cells it was localised to the nucleus and cytoplasm of Deiters' cells.

4.1.3 ERK1/2 activation occurs in a classical manner via the activation of c-RAF and MEK1/2

The 'textbook' mechanism of ERK1/2 activation occurs following stimulation of cell surface receptors that initiate the activation cascade via MAPKKKs such as RAFs that subsequently phosphorylate MEK1/2. MEK1/2 then dually phosphorylates and activates ERK1/2. Here, it was determined whether damage-induced activation of ERK1/2 was also mediated through the classical activation cascade using a cell-permeant inhibitor that targets cRAF1 (Lackey et al., 2000) and U0126 which inhibits MEK1/2 (Favata et al., 1998). The application of the cRAF1 inhibitor elicited an increase in basal levels of ERK1/2 activation in the cytoplasm both of HCs and of support cells in undamaged areas. In support cells nuclear localisation of activated ERK1/2 was also observed (Fig 4.1.3B, b). In the presence of the c-RAF1 inhibitor the damage-induced increase in activated ERK1/2 appeared to be restricted to only a few support cells lining the lesion site (Fig 4.1.3A, B).

Application of the MEK1/2 inhibitor U0126 abolished basal and damage-induced activation of ERK1/2 (Fig 4.1.3C). To confirm that a lesion was introduced to the sensory epithelium the corresponding image labelled for actin rich stereocilial hair bundles is shown in Fig 4.1.3D and displays a typical lesion site at 5 min post damage. Taken together, these data show that the damage-induced activation of ERK1/2 occurred via the classical Raf and MEK1/2 dependent activation cascade.

4.1.4 ERK1/2 activation depends on the release of extracellular ATP and is sensitive to CBX

Recently and in the previous chapter, it was shown that HC damage triggers the formation of a Ca^{2+}-wave in cochlear explants that depends on the release of extracellular ATP (Gale et al., 2004). The release of extracellular ATP and its subsequent action on P2 receptors have been suggested to elicit stretch-induced activation of ERK1/2 in astrocytes (Neary et al., 2003). Therefore it was tested here whether extracellular ATP released as a result of HC damage activates ERK1/2 in cochlear explants. In order to investigate this potential mechanism explants were pre-incubated for 30 min and then maintained in the ATP degrading enzyme apyrase (40 U/ml). The spread of activated ERK1/2 was determined using line scan analysis along the OHC and IHC rows as described earlier. Apyrase significantly reduced the damage-induced spread of ERK1/2 along the Deiters' cells in the OHC region from 148 ± 18 μm (n = 9; Fig 4.1.4A) to 58 ± 7 μm (n = 4) 5 min after damage (Fig 4.1.4B, E). Along the phalangeal cells in the IHC region apyrase also decreased the spread of activated ERK1/2, however this was not statistically significant (97.1 ± 9 μm, n = 9 to 69.6 ± 2.1 μm, n = 4, P = 0.074, Fig 4.1.4B, E). Although apyrase reduced the magnitude of activated ERK1/2 spread it did not completely abolish ERK1/2 activation. One potential reason could be an inefficiency of the enzyme to eliminate an excess of released ATP. However, it could also suggest the involvement of an ATP-independent mechanism. To reemphasise, activated ERK1/2 spread preferentially along Deiters' and phalangeal cells, the cells that are known to possess extensive gap junctional plaques and to efficiently couple to one another (Forge et al., 2003; Jagger and Forge, 2006). To investigate whether a signal that passes through gap junctions mediates the damage-induced spread of ERK1/2 activation CBX (75 μM) – a gap junction blocker – was used. CBX significantly reduced the spread of activated ERK1/2 both along Deiters' (23 ± 7 μm, n = 4) and phalangeal cells (19.3 ± 10.9 μm, n = 4; Fig 4.1.4C, E) suggesting a role for gap junctions in mediating spread of the signal activity of ERK1/2. When apyrase and CBX were applied together ERK1/2 activation was almost completely abolished (Fig 4.1.4D). In a few cases it was observed that ERK1/2 was activated and spread along Hensen cells (Fig 4.1.4D). Comparing ERK1/2 spread in explants damaged in the presence of apyrase to those treated with apyrase and CBX revealed a significant effect for both

the IHC and the OHC region (Fig 4.1.4E). The statistical significance of the spread in explants that were exposed to CBX alone compared to those that were additionally treated with apyrase was statistically different only for the OHC region ($P < 0.05$, whereas for IHC $P = 0.27$).

4.1.5 Purinergic activation of ERK1/2

4.1.5.1 Activation of ERK1/2 by local application of ATP

Reduction of ERK1/2 spread in the presence of apyrase suggests that extracellular ATP is a mediator of damage-induced activation of ERK1/2. If ATP is essential to facilitate the damage-induced activation of ERK1/2 exogenous application of ATP should be sufficient to induce ERK1/2 activation. ATP was locally applied to cochlear explants using a micropipette. Exogenous ATP resulted in the activation of ERK1/2 in a concentration-dependent manner. 1 μM ATP applied for 10 s was not sufficient to induce ERK1/2 activation (Fig 4.1.5A). However, as observed in chapter 3, 1 μM ATP for 10 s was able to activate P2 receptors and trigger increases in intracellular Ca^{2+}. Application of 10 μM ATP (10 s) elicited ERK1/2 activation local to the puff site (Fig 4.1.5B). In contrast, 100 μM ATP (Fig 4.1.5C) applied for 10 s resulted in a strong cell-specific non-uniform activation of ERK1/2 along the length of the cochlea. Orthogonal projections of confocal z-stack images reveal ERK1/2 activation in Deiters' and inner phalangeal cells but not in HCs (Fig 4.1.5c). In Claudius-like cells ERK1/2 activation was minimal. The cellular distribution and spread of activated ERK1/2 in response to 100 μM ATP was very similar to that observed following damage.

4.1.5.2 Profiling P2Y-receptor responses with UTP, UDP and ADP

Only a few specific pharmacological antagonists are available in order to distinguish between different receptor subtypes. However, agonists such as UTP, UDP and ADP are widely used to differentiate between various P2Y receptor subtypes (see section 1.3). Therefore application of different purinergic agonists was used to profile receptor expression. Local application of 100 μM UTP for 10 s elicited the activation of ERK1/2 in Deiters' cells but not in pillar, phalangeal or HCs (Fig 4.1.5D, d). The activation of ERK1/2 occurred along the length of Deiters' cell rows. The intensity

levels of ERK1/2 activation for UTP were lower compared to ATP in pairs matched for laser and acquisition settings Fig 4.1.5C, D). UDP (Fig 4.1.5E) and 100 μM ADP (Fig 4.1.5F) applied for 20 s each were not sufficient to activate ERK1/2, although these agonists were shown to trigger a rise in intracellular Ca^{2+} levels but to a lesser degree than ATP or UTP (see chapter 3.5.2). Taken together, only ATP and UTP are potent to induce ERK1/2 activation.

4.1.6 ERK1/2 spread is insensitive to the P2 receptor antagonist PPADS and suramin

The reduction of damage-induced ERK1/2 spread in response to the degradation of ATP by apyrase suggests an ATP-dependent mechanism. Moreover, exogenous application of ATP and UTP were sufficient to mimic the damage-induced ERK1/2 activation pattern thus suggesting that P2 receptors are the likely mediators of ERK1/2 activation. To investigate the involvement of P2 receptors in the activation of ERK1/2, two common P2 receptor antagonists PPADS (150 μM) and suramin (100 μM) were used. Treatment with PPADS (Fig 4.1.6A, B, E) or suramin (Fig 4.1.6C, D, E) did not result in decreased spread of activated ERK1/2 at 5 min post laser damage. The cellular localisation and the subcellular distribution of activated ERK1/2 in the cytoplasm and nuclei were also not affected by the presence of PPADS (Fig 4.16b) or suramin (Fig 4.1.6d) compared to their corresponding controls (Fig 4.16a, c, respectively).

4.1.7 ERK1/2 activation is dependent on the presence of extracellular Ca^{2+}

As shown earlier the damage-induced activation of ERK1/2 and the generation of the Ca^{2+}-wave similarly require the release of extracellular ATP. In addition, in many cell types ERK1/2 activation occurs in a Ca^{2+}-dependent manner (Neary et al., 2003; Kupzig et al., 2005) leading to the question of whether changes in cytoplasmic Ca^{2+} levels are necessary for ERK1/2 activation. In chapter 3, describing the formation of the damage-induced Ca^{2+}-wave it was observed that two distinct waves characterised by their velocity and origin of Ca^{2+} travel along the HC region. The faster wave was facilitated by the entry of extracellular Ca^{2+} suggesting the requirement for ion channels; potentially a P2X receptor dependent mechanism. Here, it was tested

whether removal of extracellular Ca^{2+} also affects activation of ERK1/2. In 0 Ca^{2+} ERK1/2 were activated; however the spread along the Deiters' cells was significantly reduced at 10 min post damage from 94.3 ± 19.9 μm in controls to 44.2 ± 10.5 μm in 0 Ca^{2+} (Fig 4.1.7A-C) but not at 5 min post damage (P = 0.14, Fig 4.1.7C). Although the levels of activated ERK1/2 were not quantified, the apparent intensity of the staining in pairs matched for laser excitation strength was consistently reduced in 0 Ca^{2+} (Fig 4.1.7A, B). The cellular and subcellular distribution of activated ERK1/2 as seen in orthogonal projections of z-stack images in 0 Ca^{2+} was similar to controls. Next, it was assessed whether global Ca^{2+} changes are critical to induce ERK1/2 activation following pre-incubation of cochlear cultures for 90 min in the membrane-permeable Ca^{2+}-chelator BAPTA-AM (10 μM). During these experiments the formation of the Ca^{2+} wave in response to damage was monitored and the explants were then processed to study ERK1/2 activation. In order to measure the extent of the Ca^{2+} wave a lower magnification objective lens (20 x) was required. The N_2 laser could not be used with this lens and so the HC epithelium was damaged with a microneedle (as described previously). The pattern of activated ERK1/2 spread and its cellular and subcellular localisation were similar in response to damage induced with a microneedle to that observed when the HC epithelium was ablated with a N_2 laser (Fig 4.1.7D compare to A, d). In the presence of BAPTA the spread of activated ERK1/2 was not significantly reduced at 5 or 10 min post damage (Fig 4.1.7D-F). Furthermore, BAPTA did not affect the cellular or subcellular distribution of activated ERK1/2. Ca^{2+} imaging experiments confirmed that BAPTA-AM was sufficient to chelate a significant amount of the rise in Ca^{2+}, decreasing the peak changes in intracellular Ca^{2+} to 26.5 ± 3.3 % of control levels at 70-90 μm and to 21.5 ± 3.2 % at 110-130 μm (Fig 4.1.7G) and was at least if not more potent than removal of extracellular Ca^{2+} (Fig 4.1.7 G).

4.2 The activation and role of ERK1/2 during neomycin-induced hair cell death

4.2.1 Characterisation of neomycin-induced hair cell death

Aminoglycoside antibiotics are known to be ototoxic both *in vivo* and *in vitro* (Forge and Schacht, 2000; Wang et al., 2003a). Recent reports have indicated that they enter

HCs via the mechano-transduction channel and therefore specifically target these cochlear cells (Gale et al., 2001; Marcotti et al., 2005). In order to determine whether ERK1/2 activation is a common damage signalling event in the rat cochlea the aminoglycoside antibiotic neomycin was used to induce HC death specifically. Basal and middle turn cochlear explants were exposed to 1 mM neomycin for 8 or 24 hrs. First, it was confirmed that HCs are damaged after 8 hrs of neomycin treatment using i) the DNA intercalating agent DAPI to assess nuclear morphology and ii) fluorescent phalloidin to monitor the integrity of actin-rich hair bundles. A significant number of IHC nuclei were observed to show signs of condensed chromatin after 8 hrs of neomycin exposure (Fig 4.2.1B). IHCs with pyknotic nuclei characteristically had missing or damaged hair bundles (Fig 4.2.1A). At this time point OHCs mostly appeared healthy as assessed by the integrity of their nuclei and hair bundles. After 24 hrs exposure to neomycin only pyknotic nuclei lined the length of the IHC row which was also marked by the absence of hair bundles. OHC nuclei show different degrees of chromatin condensation and disordered organisation (Fig 4.2.1H). Again the hair bundles of OHCs marked by pyknotic nuclei were either lost or damaged and dysmorphic (Fig 4.2.1G). It is known that HCs in the base of the cochlea are more sensitive to ototoxic stress than those further apical. The same trend was observed during these experiments between basal and middle turn cochlear explants for both IHCs and OHCs (Fig 4.2.2).

4.2.2 Characterisation of neomycin-induced ERK1/2 activation

ERK1/2 activation during exposure of cochlear explants to neomycin was assessed using immunocytochemistry as described earlier. ERK1/2 activation followed the pattern of cell damage as indicated by the presence of pyknotic nuclei. The formation of pyknotic IHC nuclei after 8 hrs of neomycin exposure coincided with ERK1/2 activation in phalangeal and border cells (Fig 4.21C, D, f'-f''). On rare occasions, ERK1/2 activation could be observed in HCs. Activated ERK1/2 was observed in both clusters and single cells and in almost all cases the cells were adjacent to pyknotic nuclei. On occasion, single Deiters' cells as indicated by its phalangeal process in Fig 4.2.1C&D exhibited ERK1/2 activation although the OHC nuclei in those regions appeared healthy. However, after 24 hrs exposure to neomycin when pyknotic OHC nuclei were present clusters of cells labelling for activated ERK1/2

were frequently observed in the OHC region (Fig 4.2.1I, J). Again, the cells that activated ERK1/2 were support cells – the Deiters' cells and they surrounded pyknotic HC nuclei. At this time point although pyknotic IHC nuclei were present ERK1/2 activation was observed less frequently compared to that in the OHC region. Along the OHC rows the labelling intensity for activated ERK1/2 varied between distinct clusters of cells.

4.2.3 The effect of U0126 on neomycin-induced hair cell death

Here, the role of ERK1/2 during neomycin-induced HC death was examined using the MEK1/2 inhibitor U0126. Cochlear explants were exposed to neomycin alone or in the presence of U0126 (10 μM) or its inactive analogue U0124 (10 μM). As expected, the activation of ERK1/2 was abolished by U0126 but not by U0124 treated neomycin-exposed cochlear explants. To quantify the effect of U0126 the number of pyknotic HC nuclei of DAPI stained explants were determined. After 8 hrs of neomycin in the presence of U0126 the number of pyknotic IHC nuclei was significantly decreased compared to neomycin treatment alone (Fig 4.2.3). Along a 100 μm segment of a cochlear coil on average 11 IHCs were present in control explants (Fig 4.2.6). After 8 hrs of neomycin there were 4.9 ± 1.2 pyknotic IHC nuclei/100 μm and when U0126 was included in the media the number was reduced to 1.0 ± 0.4/100 μm (Fig 4.2.6A). The inactive analogue U0124 during exposure to neomycin resulted in similar numbers of pyknotic IHC nuclei (4.0 ± 1.6/100 μm) as in neomycin only treated explants (Fig 4.2.6A). The number of pyknotic OHC nuclei was relatively low at 8 hrs and so no differences were observed for the various test conditions (Fig 4.2.3, Fig 4.2.8A). Along a 100 μm section of the cochlear coil on average 40 OHCs are arranged in the three rows. After 24 hrs of neomycin only pyknotic nuclei lined the IHC row (Fig 4.2.4). When U0126 was applied IHC pyknotic nuclei were observed at this time point, showing that the protective effect of U0126 was only temporary (Fig 4.2.4). Fewer pyknotic OHC nuclei were present at 24 hrs when neomycin exposed explants were treated with U0126. Neomycin induced 21.9 ± 5.8 OHC nuclei/100 μm to undergo nuclear condensation whereas in the presence of U0126 only 11.9 ± 5.8 pyknotic OHC nuclei/100 μm were observed (Fig 4.2.8A). However, this reduction was not statistically significant ($P = 0.26$, $n = 4$). As basal levels of activated ERK1/2 most likely play a pivotal role during

normal HC physiology it was tested whether the application of U0126 to control explants for 24 hrs affects cochlear HC integrity. The number of IHCs per 100 µm was not significantly changed. However, in explants treated with U0126 only 35.4 ± 1.2 OHCs/100 µm were observed in comparison to normally occurring 40.2 ± 0.9 OHCs/100 µm across the three rows of OHCs. This effect was significant ($P < 0.03$). To summarise, MEK1/2 inhibition during neomycin induced ototoxicity delays HC death. However, long-term inhibition of MEK1/2 in the absence of a toxic stimulus results in HC death.

4.2.4 The effect of U0126 on hair cells transiently exposed to neomycin

Inhibition of ERK1/2 activation delayed IHC death following 8 hr exposure to neomycin. Subsequently it was tested whether U0126 is sufficient to rescue HCs that are exposed only transiently to neomycin. Therefore, explants were treated with neomycin for 8 hrs and allowed to recover for another 16 hrs. In experiments where U0126 or U0124 were tested the inhibitor treatment was continued throughout the recovery phase. Following this application paradigm there were 6.4 ± 0.6 pyknotic IHC nuclei/100 µm in neomycin-treated explants (Fig 4.25, Fig 4.2.6A). The presence of U0126 or U0124 during neomycin exposure did not affect the numbers of pyknotic IHC nuclei resulting in 6.0 ± 0.6 and 5.5 ± 0.5 pyknotic IHC nuclei/100 µm respectively (Fig 4.2.5, Fig 4.2.6A). In the OHC region very few pyknotic nuclei were observed when explants were treated with neomycin for 8 hrs and recovered for an additional 16 hrs (Fig 4.2.5, Fig 4.2.8A). Transient exposure to neomycin for 8 hrs followed by a 16 hr recovery phase resulted in similar numbers of pyknotic IHC and OHC nuclei compared to those explants that had received neomycin for 8 hrs only when assessed (Fig 4.2.6A, Fig 4.2.8A). However, the number of remaining nuclei could potentially be changed as a result of removal or lysis of cells and this has to be considered too. In order to assess any such effect the total number of IHCs i.e. the sum of pyknotic and remaining healthy-appearing nuclei, was determined and compared between the various drug application paradigms assuming that the number of IHCs at the start of the experiment was similar. The total number of IHC nuclei was significantly reduced in explants transiently treated with neomycin and allowed to recover compared to those exposed to only 8 hrs or 24 hrs of neomycin (Fig 4.2.6B). Explants additionally treated with U0126 or U0124 for 8 hrs and allowed to

recover for 16 hrs showed a similar reduction in the total number of IHC nuclei to those treated with neomycin only (compare Fig 4.2.7 and Fig 4.2.6B). Moreover, in some cochlear explants the structure of condensed chromatin appeared differently shaped and less rounded following the transient exposure paradigm compared to those pyknotic nuclei in explants treated with neomycin for 8 or 24 hrs (Fig 4.2.3 – Fig 4.2.5). The total number of OHC nuclei did not differ significantly between the various exposure lengths for neomycin including those additionally treated with U0126 or U0124 (Fig 4.2.8B, Fig 4.2.9). The difference between total OHC nuclei in control explants to the various neomycin treated conditions results from estimating the number of remaining OHCs. Taken together these data suggest that inhibition of ERK1/2 activation during a transient period of neomycin exposure was not sufficient to rescue IHCs.

4.3 Discussion

Spatio-temporal aspects of ERK1/2 activation

ERK1/2 are activated in a range of cell types and organs and are thought to exert various effects during traumatic and toxic stimuli, including wound repair, induction of cell death or conversely cell survival (Xia et al., 1995; Nowak, 2002; Matsubayashi et al., 2004; Sperandio et al., 2004). However, the activation of ERK1/2 resulting from damage has not been directly studied in the cochlea. Therefore, in this chapter the following were examined i) whether ERK1/2 are activated, ii) the activation mechanisms and iii) the possible role of ERK1/2 activation.

An N_2-laser damage technique was applied to allow precise timing of the damage onset. This also enables determination of the temporal-spatial characteristics of ERK1/2 activation. The results of this study demonstrate that laser damage induced the transient and specific activation of ERK1/2 in a subset of support cells but not in HCs. The signal spread non-uniformly from the lesion site with maximum spread occurring 10 min after damage. A number of studies have shown that ERK1/2 are activated in several cell types resulting from different damage stimuli (Neary et al., 2003; Matsubayashi et al., 2004; Yang et al., 2004b). As shown here the activation of ERK1/2 can spread quite a distance from the site of damage to cells in non-damaged areas and is in agreement with data by Matsubayashi et al. (2004). Two waves of ERK1/2 activation were described by Matsubayashi et al. (2004): the first wave was activated rapidly and transiently reducing to only cells in close proximity of the lesion site by 30 min after damage. The second wave commenced 60 min post damage and was sustained for at least 4 hrs. In this chapter, activation was measured only up to 60 min. During this time period a transient wave similar to that described by Matsubayashi et al. (2004) was detected.

The duration of ERK1/2 activation can determine the subsequent cellular processes. In PC12 pheochromocytoma cells transient activation of ERK1/2 by EGF results in proliferation whereas sustained activation by NGF or overexpression of the EGF receptor induces neurite outgrowth indicative for differentiation of these cells (Cowley et al., 1994; Traverse et al., 1994). On the contrary, fibroblasts that experience transient ERK1/2 signals maintain their differentiated nature. However, in

fibroblasts stimuli that cause sustained activation lead to their transformation and tumour formation (Cowley et al., 1994; Mansour et al., 1994). The downstream effects of transient versus sustained ERK1/2 activation are context dependent and consequently it is not appropriate to extrapolate the fate of support cells that exhibit damage-induced ERK1/2 activation.

The function and downstream targets of activated ERK1/2 are also dependent on the cellular and subcellular localisation. A particularly interesting aspect of the data presented here is that in a complex organ like the cochlea damage activated ERK1/2 in a cell specific manner. Only a subset of cochlear support cells including Deiters', phalangeal, border and in some cases pillar cells are triggered to activate ERK1/2 but not the sensory HCs or Claudius-like cells. The majority of research on damage-induced ERK1/2 activation has been carried out using preparations of cellular mono-layers consisting only of a homogenous population of cells or by Western blot analysis. Neither technique allows the detection of cell type specific activation. In the retina – another multicellular organ - light-induced overstimulation elicited the activation of ERK1/2 in sensory cells, surrounding Mueller cells but only in a subpopulation of neuronal cells (Liu et al., 1998). The data presented here together with those by Liu et al. (1998) clearly indicate that damage-induced signalling leading to ERK1/2 activation can occur in a cell type specific manner. Therefore, in order to understand not only the function of ERK1/2 but other signalling pathways activated during pathological conditions it is a necessity to determine the cell specific site of activity and action.

The subcellular distribution of activated ERK1/2 can potentially also point towards a function of damage-induced ERK1/2. Here, activated ERK1/2 were observed in the cytoplasm and the nucleus, suggesting that ERK1/2 could have separate functions in these cellular compartments. On the other hand the activation of downstream events in both the nucleus and cytoplasm at the same time might be necessary for a concerted response following damage. Activated ERK1/2 in the cytoplasm targets molecules such as myosin light chain kinase, m-calpain or vinexin that are involved in migration or cytoskeletal remodelling (Klemke et al., 1997; Nguyen et al., 1999; Glading et al., 2004; Mitsushima et al., 2004). Activated ERK1/2 have also been shown to modulate gap junction function (Brandes et al., 2002) and to activate PLA_2

which produces arachidonic acid (Lin et al., 1993; van Rossum et al., 2001). In the nucleus activated ERK1/2 can phosphorylate transcription factors such as Elk-1 that lead to the expression of immediate early genes such as c-fos, egr-1 and junB (Hodge et al., 1998).

Activation via the classical RAF-Mek pathway

In this study it was investigated whether damage-induced ERK1/2 activation occurs through the activation of cRaf and MEK1/2 using the c-Raf1 inhibitor I and U0126 respectively. Residual damage-induced ERK1/2 activation was observed in the presence of the inhibitor for c-RAF1 whereas it was completely abolished when MEK1/2 were inhibited. Thus the classically activated signalling cascade to ERK1/2 through c-RAF1 and MEK1/2 activation is engaged following damage (Raman et al., 2007). However, inhibition of c-RAF1 did increase basal levels of ERK1/2 in both HCs and support cells in undamaged areas of the explants indicating that ERK1/2 activation can be triggered in HCs depending on the stimulating conditions. The mechanism by which ERK1/2 was activated when c-RAF was inhibited is unknown.

Damage-induced release of extracellular ATP triggers ERK1/2 activation

The present data show that damage-induced ERK1/2 activation in the cochlea was elicited by the release of extracellular ATP. P2 receptor mediated activation of ERK1/2 as a result of ATP released by damage has been shown for other cellular systems (Neary et al., 2003; Yang et al., 2004b). Both ionotropic and metabotropic P2 receptors are expressed in the cochlea (Jarlebark et al., 2000; Gale et al., 2004) see section 1.3). Following noise trauma endolymphatic ATP levels are increased (Munoz et al., 2001) and can subsequently act on P2 receptors that can potentially activate downstream signalling pathways such as ERK1/2 as shown here. Damage-induced ERK1/2 activation could be mimicked by exogenous application of ATP. However, only a relatively high dose of ATP (100 μM) for a short period (10 s) was sufficient to induce a similar activation pattern. UTP an agonist specific for $P2Y_{2,4,6,11}$ and $P2X_3$ receptors stimulated ERK1/2 activation in Deiters' cells, but not in inner phalangeal or border cells. Neither UDP active on $P2Y_6$ (Nicholas et al., 1996) nor ADP which activates $P2Y_1$ receptors was found to induce ERK1/2 activation in rat cochlear explants. Taken together these data suggest that $P2Y_1$ and $P2Y_6$ can be excluded as the receptors leading to ERK1/2 activation. The intensity of activated ERK1/2

labelling induced by UTP was lower compared to that by ATP. This suggests that ERK1/2 activation mediated by ATP involved two pathways – one that required UTP-sensitive P2Y receptors and a second, based on the insufficiency of ADP to trigger ERK1/2 activation, P2X receptor-mediated pathway. Potential candidates for triggering ERK1/2 activation are P2X and $P2Y_{2,4,11}$ receptors. The activation and spread of ERK1/2 was not affected by the P2 receptor antagonists PPADS and suramin. $P2Y_2$ and the human $P2Y_{11}$ receptors are sensitive to suramin, but not to PPADS (Communi et al., 1999; van der Weyden et al., 2000; Wildman et al., 2003). Thus, these receptors are unlikely the mediators of damage-induced ERK1/2 activation. $P2Y_4$ receptors are insensitive to both PPADS and suramin and cannot be excluded to stimulate ERK1/2 activation. The majority of P2X receptors are inhibited by at least one if not both of the antagonists at the concentrations used here, except for $P2X_4$ receptor which is less sensitive (Buell et al., 1996; Rassendren et al., 1997; Chessell et al., 1998; Jones et al., 2000; King and Townsend-Nicholson, 2003). Taken together, the likely candidates are $P2X_4$ and $P2Y_4$ receptor. However, the pharmacological data for the various P2 receptor subtypes were obtained from heterologous expression systems. The interaction between various native P2 receptors might alter their pharmacological profiles as it has been demonstrated by co-expression experiments (Liu et al., 2001; Gallagher and Salter, 2003; Greenwood et al., 2007). Thus the proposed interpretation of the antagonist data must be considered with caution.

Gap junctions – potential candidate mediating ERK1/2 spread

The potential role of gap junctions in mediating ERK1/2 spread was investigated using CBX – a known gap junction blocker and it was found that it was sufficient to reduce the spread of activated ERK1/2. This effect can potentially arise via two mechanisms: first, a signal such as IP_3, cAMP or cGMP could pass through gap junctions (Bevans et al., 1998; Ayad et al., 2006; Bedner et al., 2006) and mediate the activation of ERK1/2; or second, ATP could be released from cells via connexin hemichannels (Stout et al., 2002; Pearson et al., 2005). The permeability of gap junctions/hemichannel heavily depends on the connexin subtypes that form the channels. The permeability for the aforementioned potential mediators has not been determined for the heteromeric gap junctional pores formed by connexin 26 and 30 that are expressed in the cochlea. IP_3 has been suggested to pass through the

connexins that form gap junctions in the cochlea (Beltramello et al., 2005). ERK1/2 activation was abolished in the presence of both CBX and apyrase. Thus two separate pathways may contribute to the activation of ERK1/2. In contrast, CBX was demonstrated to reduce the damage-induced Ca^{2+} wave but not exert a synergistic effect when applied together with apyrase. Taken together, this comparative examination of the actions of apyrase and CBX suggests that the CBX-sensitive mechanism mediating ERK1/2 spread occurs independently of Ca^{2+}.

Recently, CBX was reported to exert inhibitory effects on $P2X_7$ receptors and voltage-gated Ca^{2+} channels (Vessey et al., 2004; Suadicani et al., 2006). If these channels or connexin hemichannels were activated following damage they would allow influx of Ca^{2+} and this should be reflected in changes of intracellular Ca^{2+} levels. However, CBX did not exert an additional effect to that by apyrase on reducing damage-induced Ca^{2+} levels. Thus, the CBX-sensitive mechanism that results in ERK1/2 activation is unlikely occurring through the action of any of these channels and therefore gap junctions are the likely mediators of ERK1/2 spread.

Ca^{2+}-dependent and independent mechanisms leading to ERK1/2 activation

The removal of extracellular Ca^{2+} also reduced the spread of ERK1/2 activation suggesting a role of Ca^{2+} in activating the ERK1/2 cascade. However, buffering of intracellular Ca^{2+} levels with BAPTA did not affect ERK1/2 activation or its spread. These data are further evidence that two components result in the activation of ERK1/2 – one dependent on the presence of extracellular Ca^{2+} and the other independent of cytoplasmic Ca^{2+}. The reduction of the fast Ca^{2+} wave as shown in chapter 3 together with the decreased spread of activated ERK1/2 as well as the dependency on extracellular ATP are indicative of P2X receptor mediated activation of ERK1/2. Moreover, activation of ERK1/2 by UTP which only facilitates the activation of P2Y receptors resulted in decreased labelling intensity compared to that induced by ATP (matched for acquisition settings). This effect was similar to that observed when cochlear explants were damaged in 0 Ca^{2+} compared to their controls in the presence of extracellular Ca^{2+}, respectively, supporting the notion that P2X and P2Y receptors facilitate the damage-induced activation of ERK1/2. However, other mechanisms such as the opening of voltage-gated Ca^{2+}-channels (Hur et al., 2001) or

store-operated Ca^{2+} entry could also operate and result in the activation of ERK1/2. Entry of extracellular Ca^{2+} caused the rise of the fast damage-induced Ca^{2+} wave that did not depend on the release of Ca^{2+} from intracellular stores (see chapter 3). Hence the role of store-operated Ca^{2+} entry in the activation of ERK1/2 can be excluded. The entry of Ca^{2+} through could account for the inability of BAPTA to reduce ERK1/2 spread. The opening of ion channels could result in the rapid formation of Ca^{2+} microdomains that enable ERK1/2 activation. Although BAPTA is a fast Ca^{2+} buffer it is still unable to buffer and counteract the rapid formation of high Ca^{2+}-microdomains very close to ion channels (Naraghi and Neher, 1997). This suggests that the Ca^{2+} dependent cascade leading to ERK1/2 activation requires a rapid local elevation rather than global changes in cellular Ca^{2+}. However, another explanation is that both the activation of ERK1/2 and the deactivation of the MAPK cascade have been shown to be dependent on Ca^{2+} (Farnsworth et al., 1995; Cook et al., 1997; Lockyer et al., 2001; Neary et al., 2003; Paul et al., 2003; Schmitt et al., 2004; Kupzig et al., 2005). Hence in the present experiments, BAPTA could affect both pathways and therefore a reduced deactivation rate could counteract reduced activation of ERK1/2.

The Ca^{2+}-independent component of ERK1/2 activation likely occurred in a P2Y-mediated manner that could potentially recruit a Ca^{2+}-independent PKC, choline-specific PLC or other G-proteins (Jo et al., 1997; Neary et al., 1999; Neary et al., 2003; Nicole et al., 2005).

ERK1/2 inhibition delays inner hair cell death

ERK1/2 were originally thought to function as survival kinases (Xia et al., 1995; Arthur et al., 2006). More recent evidence suggests that cell type dependent ERK1/2 activation can induce apoptosis (Nowak, 2002; Sperandio et al., 2004; Subramaniam et al., 2004; Chen et al., 2005). Data presented in this report demonstrated that ERK1/2 were activated in support cells during neomycin-induced otoxicity. Together with the results following mechanical damage these data indicate that this activation is a common mechanism to signal damage in the rat cochlea. Moreover, inhibiting MEK1/2 and thus ERK1/2 activation delayed neomycin-induced HC death. A critical observation was that ERK1/2 were not activated in dying HCs but in their

surrounding support cells which survive. This indicates that the death of HCs was caused by intercellular interaction with their surrounding support cells. These data are in contrast to previous reports that presented ERK1/2 dependent cell death of the cells in which activation occurred. In those reports, the effect of MEK1/2 inhibition was studied in a homogenous population of cells, whereas in this thesis it was probed in a multicellular organ. This indicates that it is critical to understand signalling in the context of multicellular organs to assess effects exerted by intercellular communication.

Inhibition of MEK1/2 activation can however only temporarily protect HCs from neomycin-induced ototoxicity. Moreover, inhibition of ERK1/2 activation over a period of 24 hrs resulted in OHC death even without any ototoxic stimuli. This is in agreement with Battaglia et al. (2003) reporting that U0126 itself applied over a period of 48 hrs elicited an increase in OHC death compared to controls. This indicates that basal levels of activated ERK1/2 act as a factor crucial for OHC survival. Therefore, over longer periods observed in this thesis, the protective effect of MEK1/2 inhibition in support cells observed following 8 hrs of neomycin might be counteracted by the absence of activated ERK1/2 in HCs that acts as a survival factor. Another possible explanation is the activation of other signalling pathways that result in the execution of cell death when MEK1/2 are inhibited. Those signalling mechanisms would overcome the protective effect exerted by inhibition of MEK1/2. It is even likely that the two possible mechansisms described above act together to counteract the protective effect and to cause HC death over prolonged periods of neomycin exposure.

Transient exposure to neomycin followed by a recovery phase

Data presented in this chapter demonstrate that continued inhibition of ERK1/2 during exposure of cochlear explants to an 8 hr pulse of neomycin followed by a 16 hr recovery phase cannot protect HCs. Again ERK1/2 might function as a survival signal in HCs, which might be crucial for the HCs in order to regain a functional status. This raises the question whether inhibition of ERK1/2 activation during transient application of neomycin followed by a recovery phase during which the MEK1/2 inhibitor is omitted could rescue HCs?

During 8 hrs of neomycin followed by 16 hrs recovery a similar number of pyknotic IHC nuclei were observed compared to explants that were treated with neomycin for 8 hrs only. However, the total number of nuclei (comprised of pyknotic and healthy appearing nuclei) was significantly reduced in explants treated with neomycin for 8 hrs and allowed to recover for 16 hrs when compared to those following 8 or 24 hrs of neomycin exposure. These data might suggest that the removal of the ototoxic stimulus might induce signalling cascades that result in secondary traumatic injury. It has been shown that ROS are generated in astrocytes during hypoxic events and that another boost of ROS production occurs in the period of reoxygenation. The latter was suggested to cause secondary injury observed during reoxygenation (Abramov et al., 2007). In addition, following removal of neomycin a mechanism could be triggered that accelerates the elimination of cellular corpses. This hypothesis is supported by the less rounded and misshapen structure of pyknotic nuclei compared to those seen after 24 hrs of neomycin. The accelerated removal of dead cell bodies could be established through an increase in support cell activity to remove cells or a signal could be released that attracts macrophages.

ERK1/2 activation in support cells influences hair cell death – a potential mechanism

In this chapter it was shown that during neomycin-induced ototoxicity ERK1/2 were specifically activated in support cells that surround pyknotic HC nuclei. Inhibition of the upstream kinases of ERK1/2 – MEK1/2 delays HC death. Unless HC survival results from inhibiting basal levels of ERK1/2, which were not detected with the chosen method, a convincing explanation has to be found. The simplest interpretation is that support cells exert an effect on HCs which consequently promotes HC death. Support cells could influence HC death potentially via two mechanisms – one involving migration and wound repair and the other the release of a soluble factor by support cells that triggers the subsequent HC death. Migration has been shown to occur in an ERK1/2 dependent manner (Klemke et al., 1997; Nguyen et al., 1999). More importantly a recent report suggests that activated ERK1/2 are crucial for wound repair resulting in the closure of the scrape-wounded area in MDCK cell monolayers (Matsubayashi et al., 2004). Apoptotic cells can be cleared by 'non-professional phagocytes' that are the cells neighbouring the dying cells and cochlear support cells have been suggested to fulfil this function (Forge and Li, 2000; Parnaik

et al., 2000; Abrashkin et al., 2006). Thus, if the support cells can sense the impaired integrity of HCs, they could be triggered to instigate a wound repair program that then as a result of structural rearrangements in the cochlea imposed by support cells promotes HC death.

Another mechanism could rely on ERK1/2 inducing the formation of free radicals such superoxide (O_2^-) or nitric oxide (NO). Both free radicals have been suggested to be employed by microglia to execute cell death (Chao et al., 1992; Marin-Teva et al., 2004). Similarly, support cells could produce free radicals and promote HC death. Moreover, the formation of free radicals is thought to be involved in the death executing cascade during noise-damage and aminoglycoside ototoxicity (Hirose et al., 1997; Hirose et al., 1999; Ohinata et al., 2003). Therefore O_2^- and NO are suitable candidates for a mechanism that involves support cells in triggering HC death. The NADPH oxidase one of the enzymes that produces O_2^- has been reported to be activated following binding of arachidonic acid. PLA_2 can liberate arachidonic acids from lipids in cellular membranes following the activation by ERK1/2. NO production is also documented to be downstream of ERK1/2 activation (Joy et al., 2006). However, NO production is not associated with HC death during noise-exposure as implicated by studies using inhibitors (Ohinata et al., 2003). However, these studies investigated a late time point following acoustic overstimulation. As shown here ERK1/2 promotes HC death during the early phase of neomycin exposure but prolonged ERK1/2 inhibition can result in HC death. Similarly, NO could play a role during the early phase that was not detected as a consequence of the chosen late time point (Ohinata et al., 2003). The MEK1/2 inhibitor U0126 has also been shown to act on MKK5 – the kinase that phosphorylates ERK5 (Mody et al., 2003). At the present it can not be excluded that ERK5 participates in the signalling cascade leading to neomycin-induced HC death and further investigations are required to eliminate this possibility.

Does damage-induced ERK1/2 play a role in support cells?

It is an interesting aspect that ERK1/2 activation in support cells promotes the death of a different cell type. However, it raises the question whether ERK1/2 exerts an effect on the cell in which it is actually activated. The downstream targets of ERK1/2 activation are diverse and include survival signalling (Xia et al., 1995; Arthur et al.,

2006) as well as proliferation (Cowley et al., 1994; Mansour et al., 1994). Proliferation in avian utricular sheet cultures is reduced when ERK1/2 activation is inhibited (Witte et al., 2001). Recombinant human glial growth factor-2 triggered cells in mammalian utricular sheet cultures to proliferate and this process was also partially dependent on the activation of ERK1/2 (Montcouquiol and Corwin, 2001). In avian HC epithelia the support cells are the progenitors that generate new HCs (Warchol and Corwin, 1996) after ototoxic insults. The specific activation of ERK1/2 in support cells poses the question whether ERK1/2 are a proliferative signal in the non-proliferating mammalian cochlea? Simultaneously occurring inhibitory signalling events could lead to abrogation of the proliferative signalling cascade which is initiated by ERK1/2. Further research will clarify the function of ERK1/2 and determine its potential role as a proliferative signal in the mammalian cochlea.

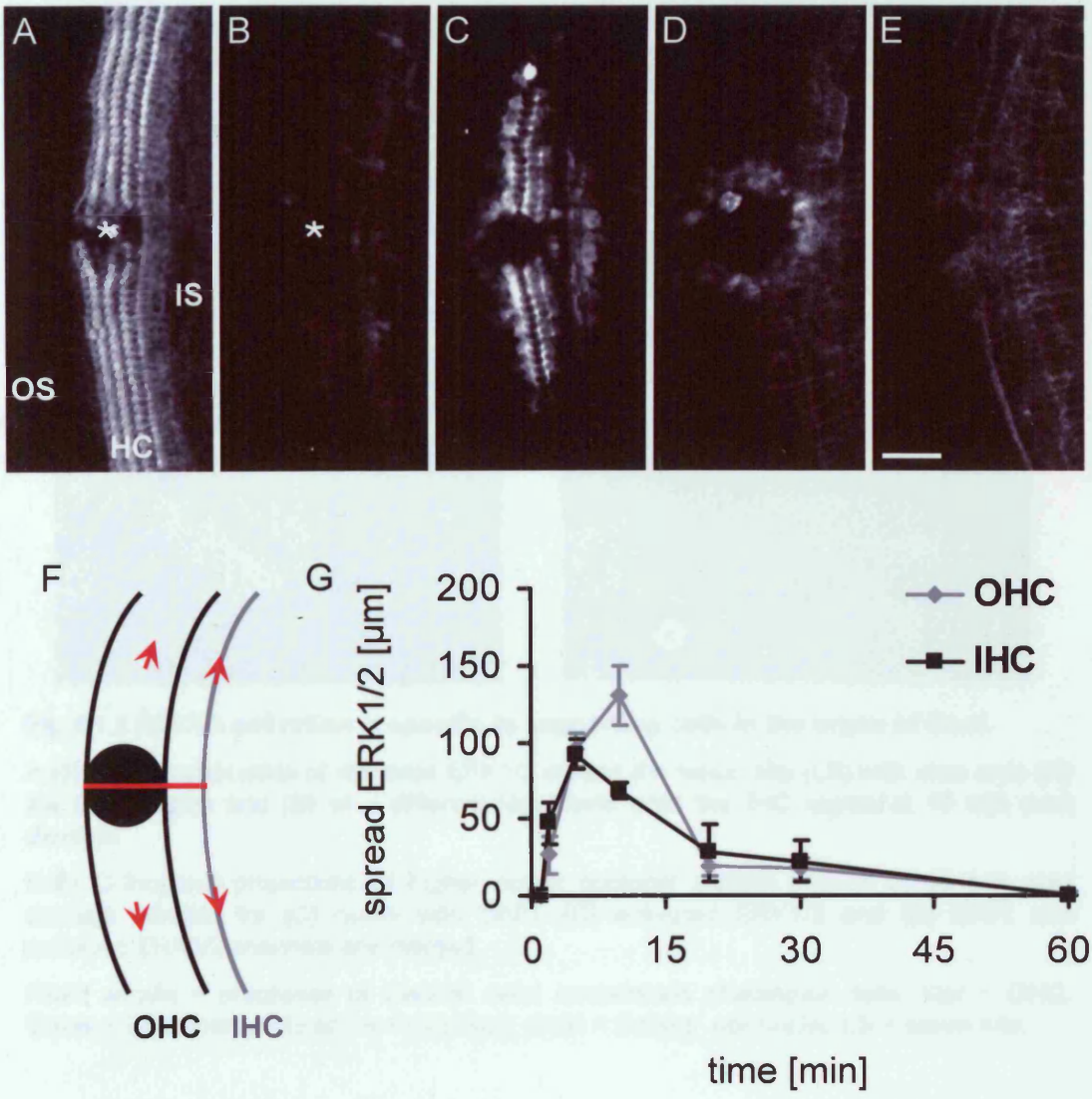

Fig 4.1.1 Spatio-temporal characteristics of damage-induced ERK1/2 activation in the organ of Corti.

A) Average of confocal z-stack images of a phalloidin-stained explant depicts hair bundles of the three OHC and IHC rows. The integrity of the HC rows is disturbed by the lesion site (star) which is a typical lesion induced with a N_2-laser at 1 min post damage.

B-E) Averages of confocal z-stack images immuno-stained for activated ERK1/2 at **B)** 1 min (corresponding image to A), **C)** 10 min **D)** 30 min and **E)** 60 min post damage.

F) The lines in cartoon indicate the OHC and IHC regions that were subjected to a line scan analysis. ERK1/2 spread was determined longitudinally (arrows) to both sides from the lesion site (filled black circle) and averaged for each region. Red line represents the middle of the lesion site.

G) The graph depicts the spread of activated ERK1/2 as a function of time post damage. Mean ± S.E.M, n ≥ 4 scale bar, 50 µm

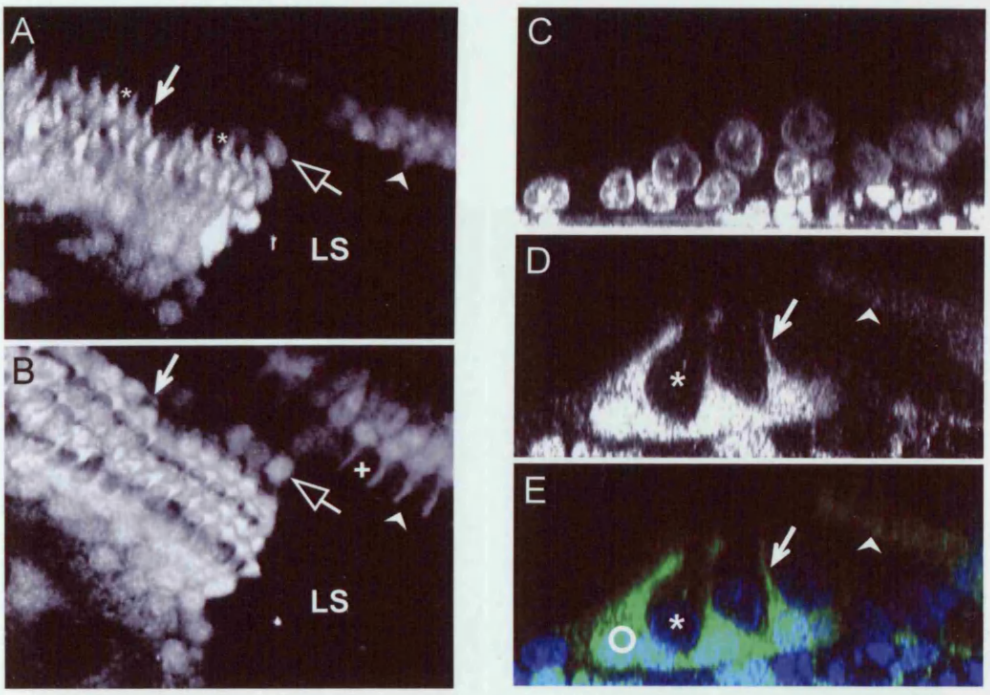

Fig 4.1.2 ERK1/2 activation is specific to supporting cells in the organ of Corti.

A-B) 3-D reconstruction of activated ERK1/2 around the lesion site (LS) with view onto **(A)** the OHC region and **(B)** at a different focal level onto the IHC region at 10 min post damage.

C-E) Orthogonal projections of higher power confocal z-stack images at 10 min post damage labelled for **(C)** nuclei with DAPI, **(D)** activated ERK1/2 and **(E)** DAPI and activated ERK1/2 channels are merged.

Filled arrows = processes of Deiters' cells; arrowheads phalangeal cells. star = OHC; Cross = IHC; open white arrow = pillar cell; circle = Deiters' cell nuclei; LS = lesion site.

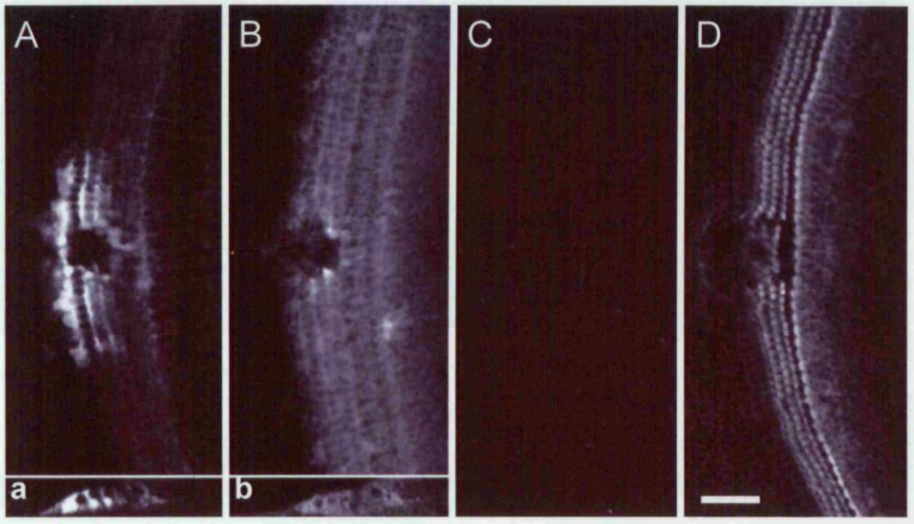

Fig 4.1.3 Damage-induced activation of ERK1/2 occurs via a c-RAF and MEK1/2-dependent mechanism.

A-C) Averages of confocal z-stack images of activated ERK1/2 at 5 min post damage in **(A)** control, explants exposed to **(B)** RAF1 inhibititor I or **(C)** MEK1/2 inhibitior U0126

a, b) Orthogonal x-z projection of activated ERK1/2 in **(a)** control and **(b)** presence of RAF1 inhibitor I.

D) Average of confocal z-stack images labelled with fluorescent phalloidin (corresponding image to **C**)

n = 3; scale bar, 50 µm

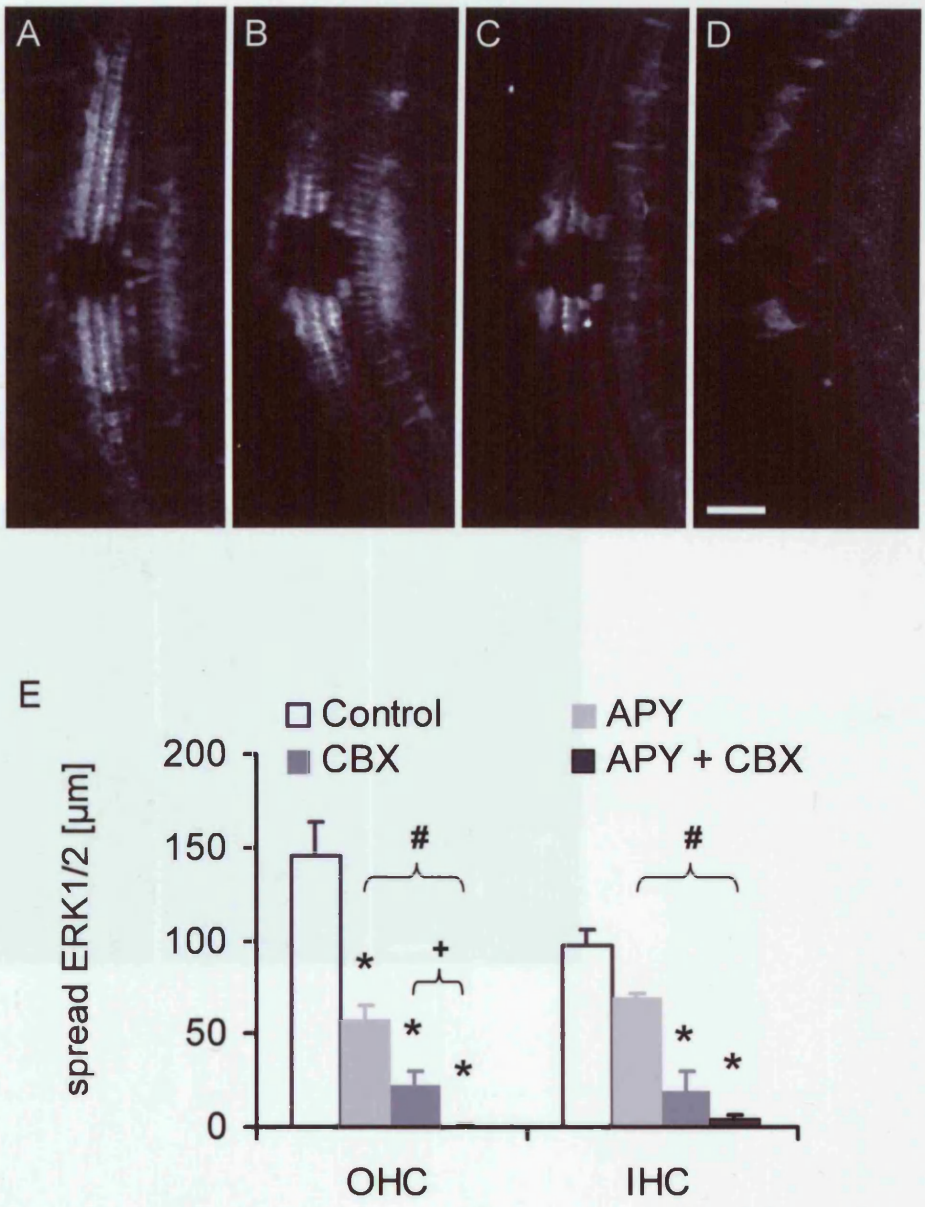

Fig 4.1.4 ERK1/2 activation is dependent on the release of extracellular ATP and sensitive to CBX.

A-D) Averages of z-stack images immuno-stained for activated ERK1/2 at 5 min post laser damage in **(A)** control , in the presence of **(B)** 40 U/ml apyrase (APY), **(C)** 75 µM CBX or **(D)** APY and CBX applied together.

E) ERK1/2 spread measured using a line scan analysis for the conditions in A-D.

Mean ± S.E.M, * indicates $P < 0.05$ between treated and control, # indicates $P < 0.05$ between APY and APY + CBX; + indicates $P < 0.05$ between CBX and APY + CBX , n = 9 (control), n = 5 (APY), n = 4 (CBX), n = 4 (APY + CBX), Student's *t*-test; Scale bar, 50 µm

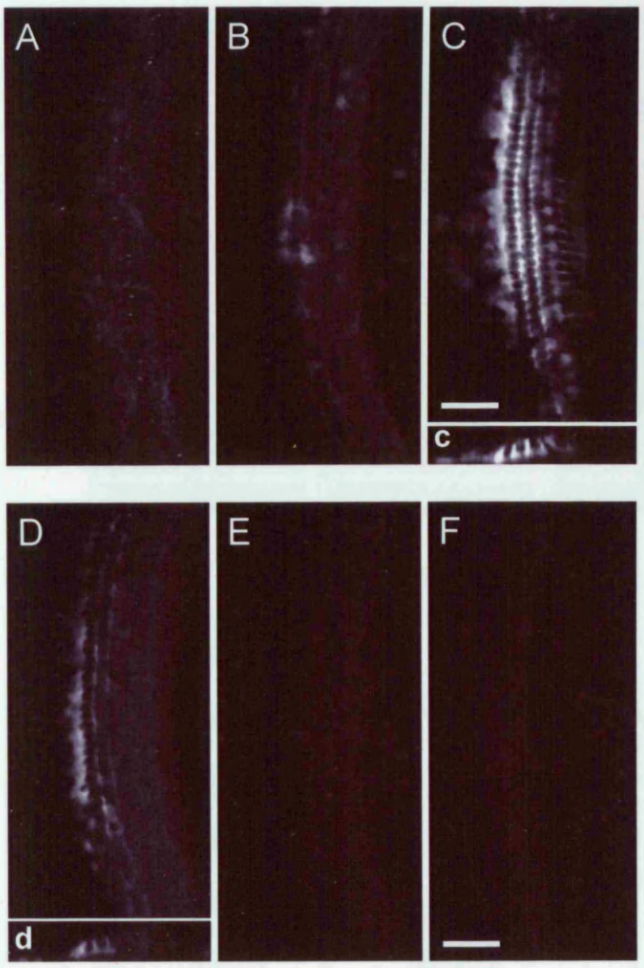

Fig 4.1.5 Purinergic activation of ERK1/2.

A-F) Averages of z-stack images immuno-labelled for activated ERK1/2 at 5 min post exposure to exogenous puff application of **(A)** 1 µM (10 s), **(B)** 10 µM (10 s), **(C)** 100 µM ATP (10 s), **(D)** 100 µM UTP (10 s), **(E)** 100 µM UDP (20 s) and **(F)** 100 µM ADP (20 s).

c, d) x-z projection of confocal z-stack images of activated ERK1/2 corresponding to **(C)** and **(D)**.

n ≥ 3, scale bar, 50 µm.

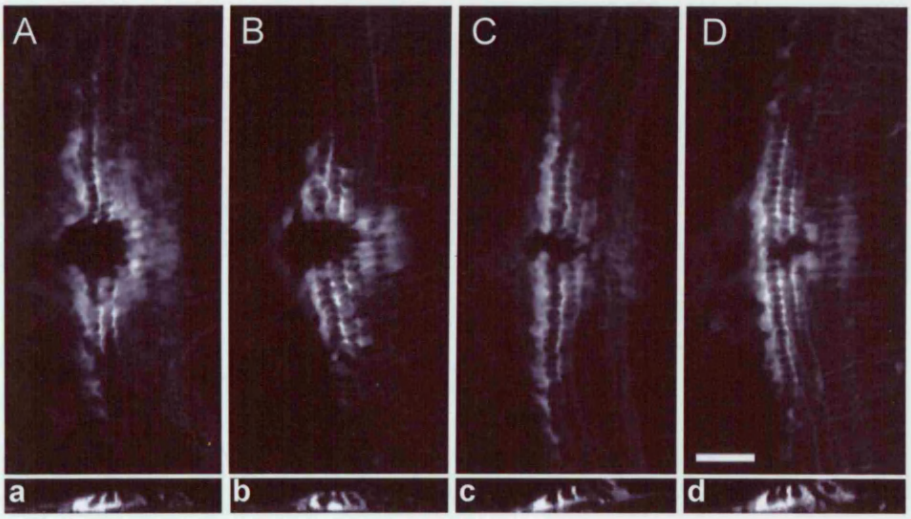

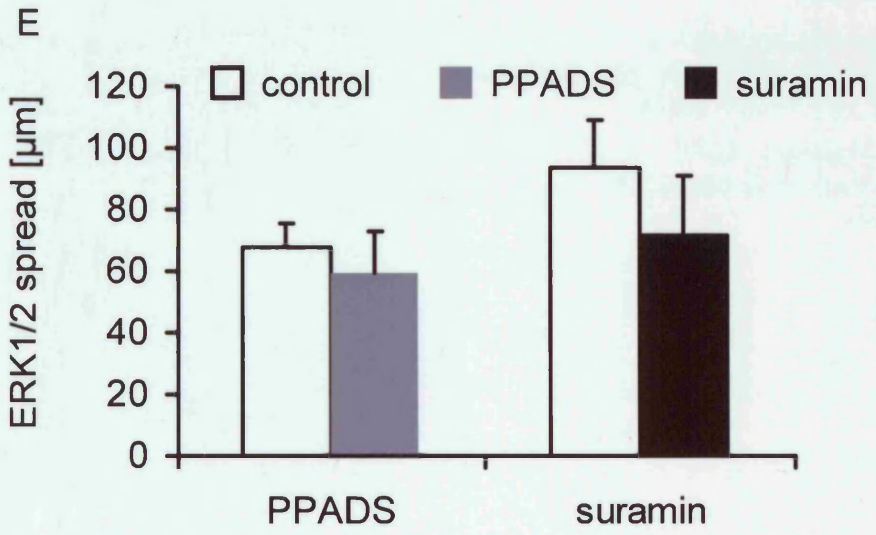

Fig 4.1.6 Damage-induced ERK1/2 activation is insensitive to the P2 receptor antagonists PPADS and suramin.

A-D) Averages of confocal z-stack images labelled for activated ERK1/2 at 5 min post laser damage in **(A, C)** matched control for **(B)** 150 µM PPADS and **(D)** 100 µM suramin exposed explants respectively.

a-d) Orthogonal x-z projections of activated ERK1/2 corresponding to **(A-D)**

E) Spread of activated ERK1/2 for conditions in **(A-D)**.

Mean ± S.E.M.; n ≥ 3; P > 0.05; Student's *t*-test; scale bar, 50 µm.

Fig 4.1.7 ERK1/2 activation partially depends on influx of extracellular Ca^{2+}.

A, B, D, E) Averages of z-stack images immuno-labelled for activated ERK1/2 at 10 min post laser damage in **(A, D)** matched control to **(B)** in 0 Ca^{2+} and **(E)** BAPTA.

a, b, d, e) x-z projections of activated ERK1/2 corresponding to **(A, B, D, E)**.

C, F) Spread of activated ERK1/2 at 5 and 10 min post laser damage for **(C)** 0 Ca^{2+} and **(F)** BAPTA-AM.

G) Damage-induced peak Ca^{2+} changes at various distances from the lesion site in 0 Ca^{2+} and presence of BAPTA-AM expressed as percentage of control changes. Damage was introduced with a microneedle.

$n \leq 7$ (control/0 Ca^{2+}), $n \leq 12$ (control/BAPTA-AM); * indicates $P < 0.05$; Student's *t*-test; scale bar, 50 µm.

ERK1/2 activation

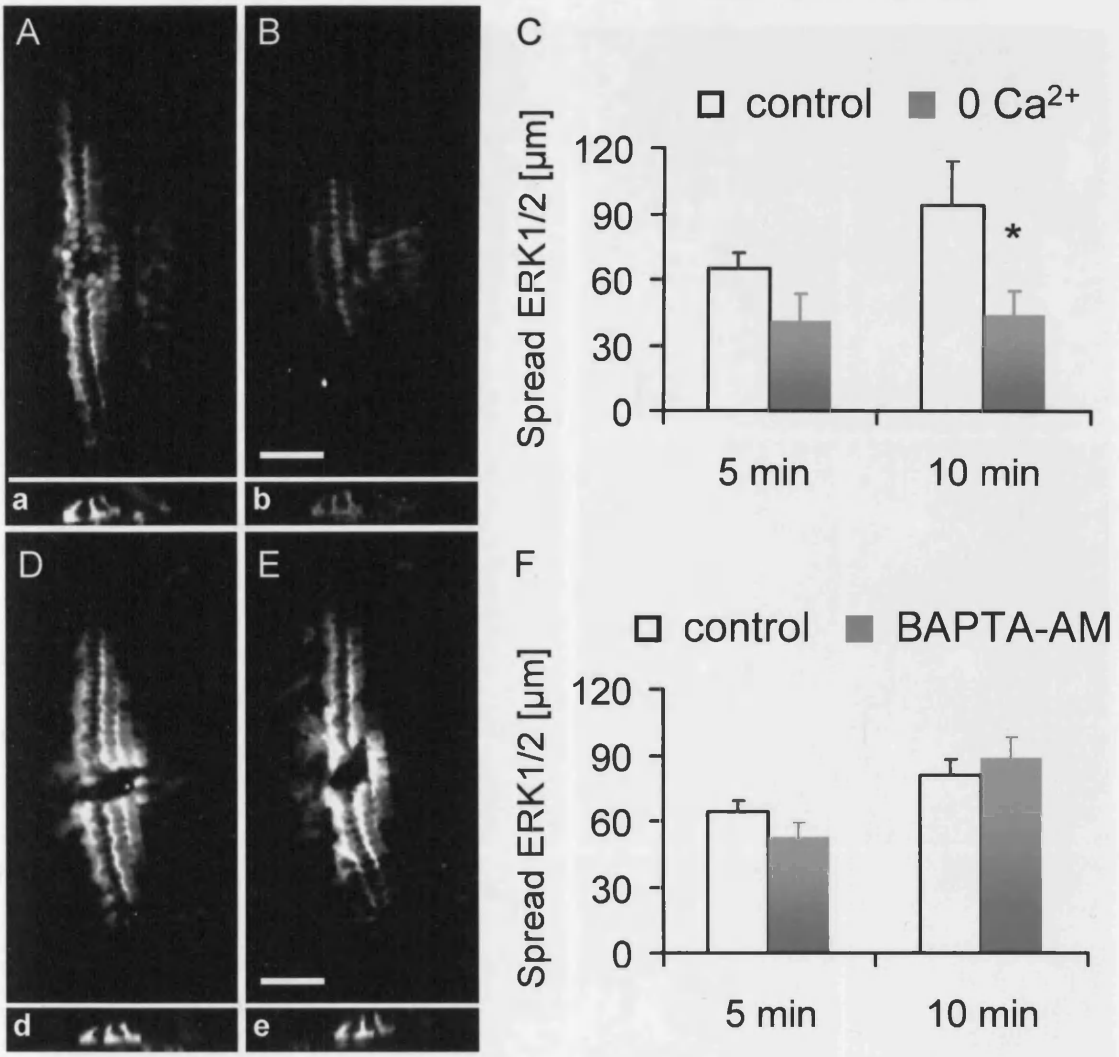

Ca^{2+} imaging

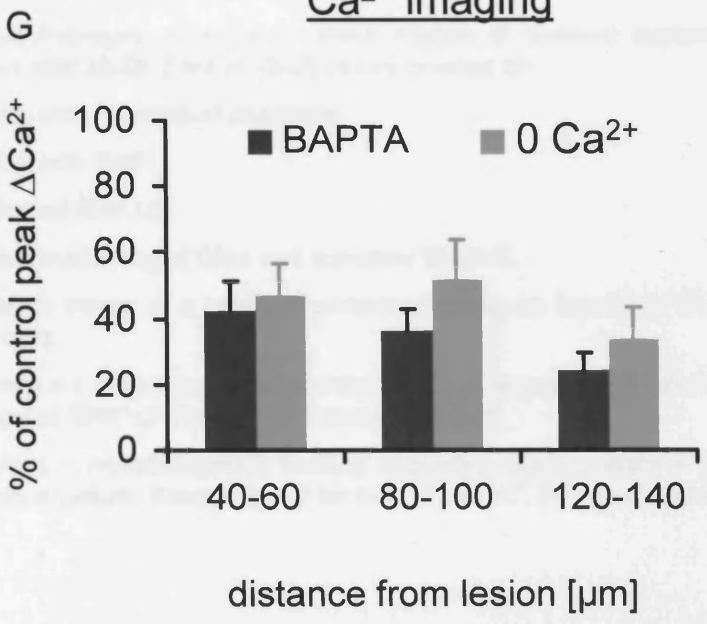

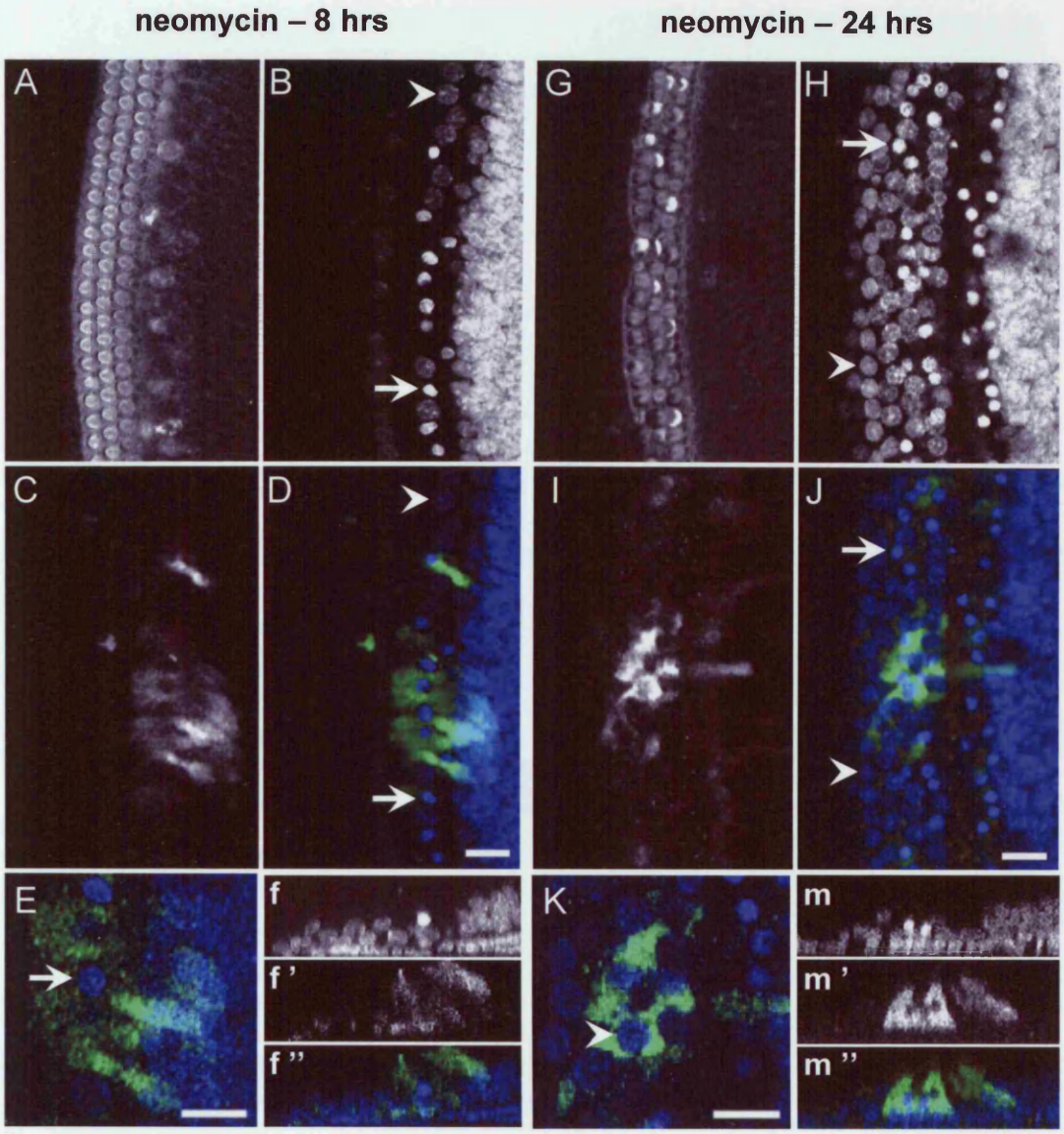

Fig 4.2.1 Neomycin-induced activation of ERK1/2

A-D, G-J) Averages of confocal z-stack images of cochlear explants treated with 1 mM neomycin after **(A-D)** 8 hrs or **(G-J)** 24 hrs labelled for:

A, G) actin with fluorescent phalloidin.

B, H) DNA with DAPI

C, I) activated ERK1/2.

D, J) Double-labelling of DNA and activated ERK1/2.

E, K) Single image of a confocal z-stack showing an extract of D or J respectively at a higher zoom.

f-f'', m-m'') x-z projection corresponding to **(D, J,** respectively) labelled for **(f, m)** DAPI, **(f', m')** activated ERK1/2 and **(f'', m'')** double-labelled.

Arrowheads = morphologically healthy appearing nuclei; arrow = nuclei with condensed chromatin structure. Scale bar in J for A-J, f-f', m-m'', 20 µm; E and K, 10 µm

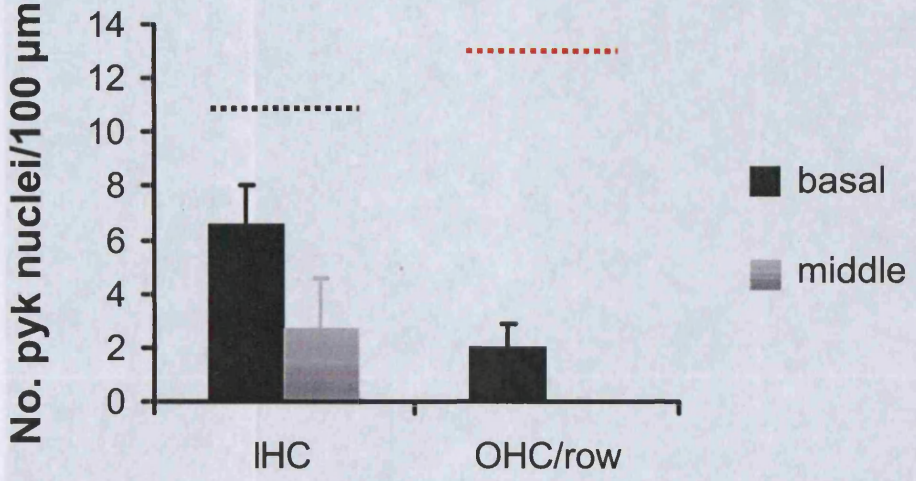

Fig 4.2.2 Tonotopical gradient of neomycin-induced hair cell death after 8 hrs.

Comparison of the number of pyknotic IHC and OHC nuclei/100 µm present in basal and middle turn cochlear explants after exposure to neomycin for 8 hrs.

The black and red dotted lines indicate the number of IHC and OHC nuclei per 100 µm per cochlear turn, respectively. Note that the number of OHCs is given for one row only.

Mean ± S.E.M, n = 7 (basal IHC & OHC), n = 5 (middle IHC & OHC)

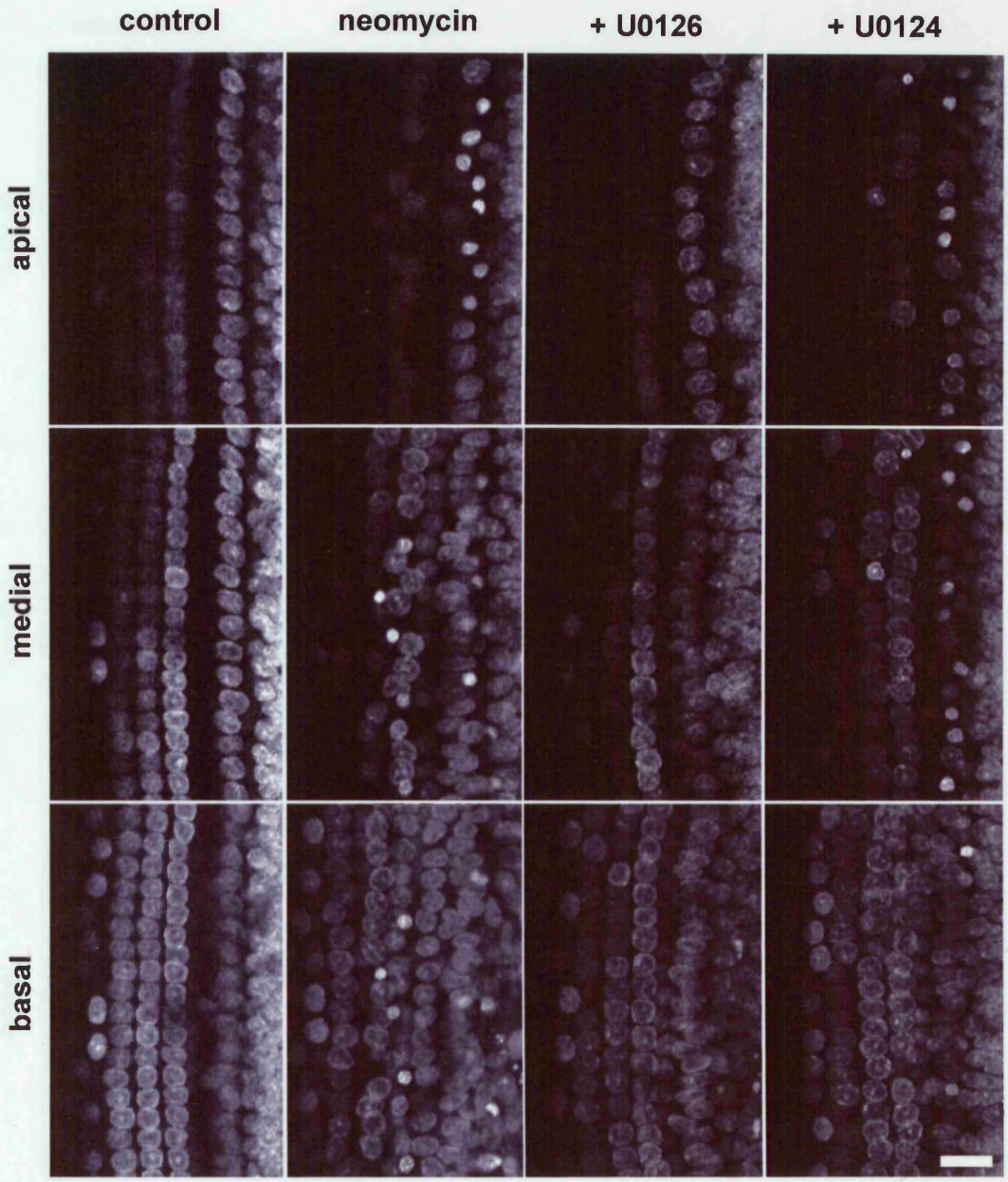

Fig 4.2.3 Inhibition of neomycin-induced ERK1/2 activation reduces hair cell death at 8 hours.

Averages of 5 z-stack images (z-slice: 0.86) labelled for DNA with DAPI at three different consecutive planes starting at the apical surface of IHCs and progressing towards the basal end of the 3rd row of OHCs.

The average in plane **(i)** shows nuclei in IHC region; plane **(ii)** includes IHC + OHC, whereas plane **(iii)** focuses on the lower level of OHCs.

Panels from the left to the right show: **(column 1)** control, a cochlear explant treated with **(column 2)** neomycin for 8 hours, **(column 3)** 10 μM U0126 or **(column 4)** its inactive analogue U0124 (10 μM) in addition to neomycin.

$n \geq 11$. Scale bar, 20 μm

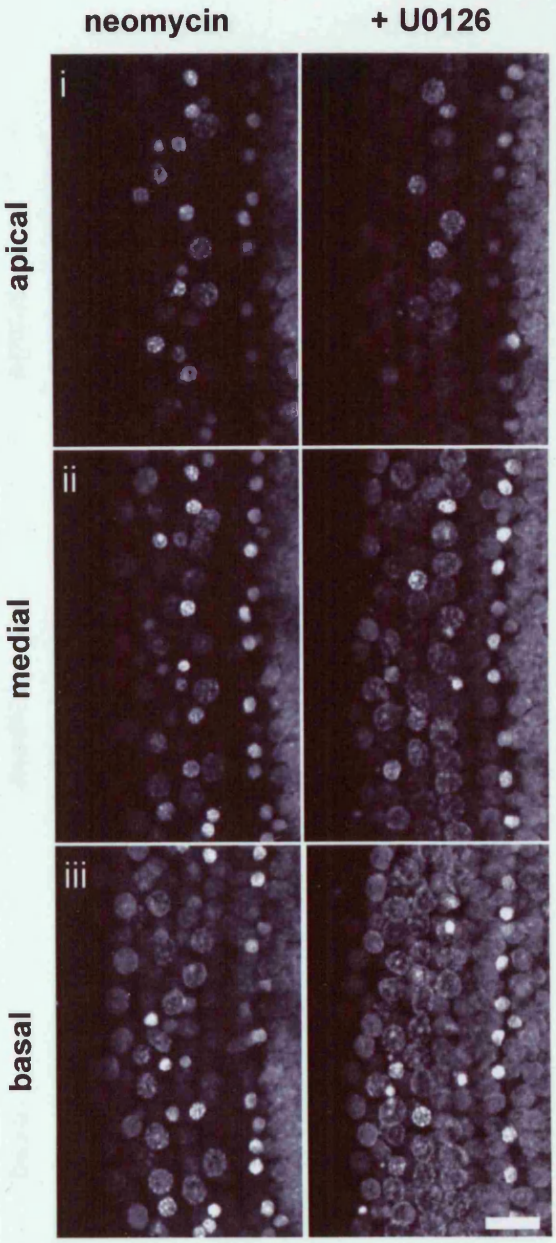

Fig 4.2.4 Inhibition of neomycin-induced ERK1/2 activation is not sufficient to protect hair cells from death at 24 hours.

Averages of 5 z-stack images (z-slice: 0.86) labelled for DNA with DAPI at three different consecutive planes starting at the apical surface of the IHC and lowering towards the basal end of the 3rd row of OHC.

The average shows nuclei in the plane of **(i)** IHCs, **(ii)** IHCs + OHCs, **(iii)** lower level of OHCs.

(column 1) 1mM neomycin and **(column 2)** additionally treated with 10 μM U0126 for 24 hours.

Scale bar, 20 μm

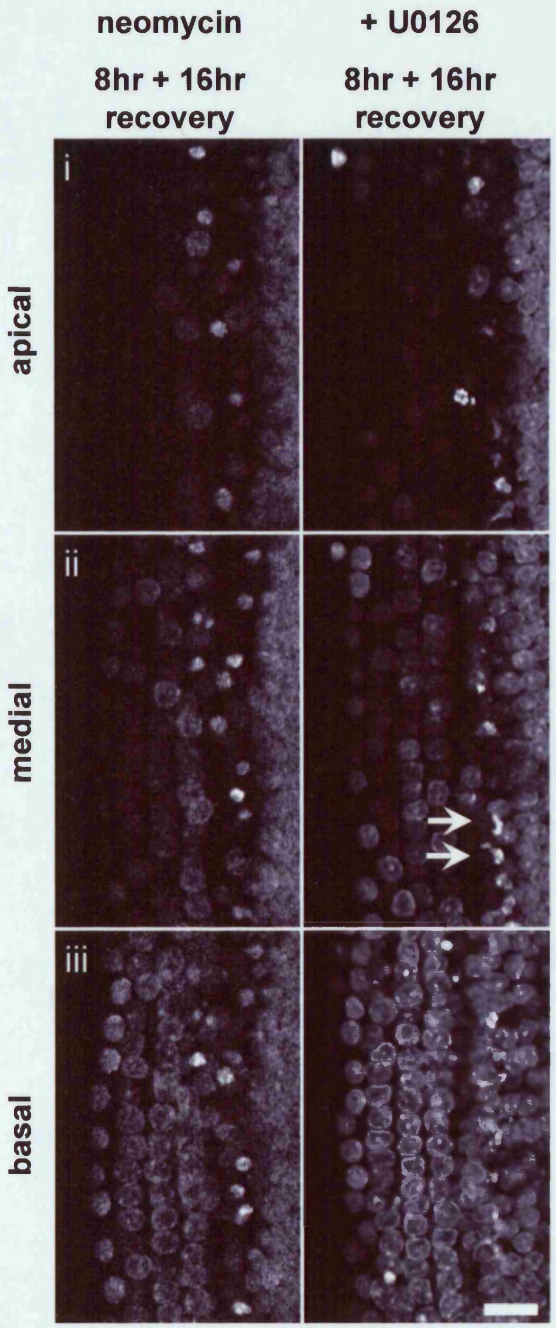

Fig 4.2.5 ERK1/2 inhibition during and following transient exposure to neomycin is not effective to protect IHCs from death.

Averages of 5 z-stack (z-slice: 0.86) images labelled for DNA with DAPI at three consecutive planes starting at the apical surface of the IHC and lowering towards basal aspects of 3rd row OHCs.

The averages show nuclei in the plane of **(i)** IHCs, **(ii)** IHCs + OHCs and (iii) lower aspects of 3rd row OHCs.

(column 1) neomycin for 8 hrs followed by a 16 hour recovery phase or **(column 2)** additionally treated with 10 μM U0126 throughout the 24 hrs.

Arrows point on irregular structures of some nuclei in the IHC region. Scale bar, 20 μm.

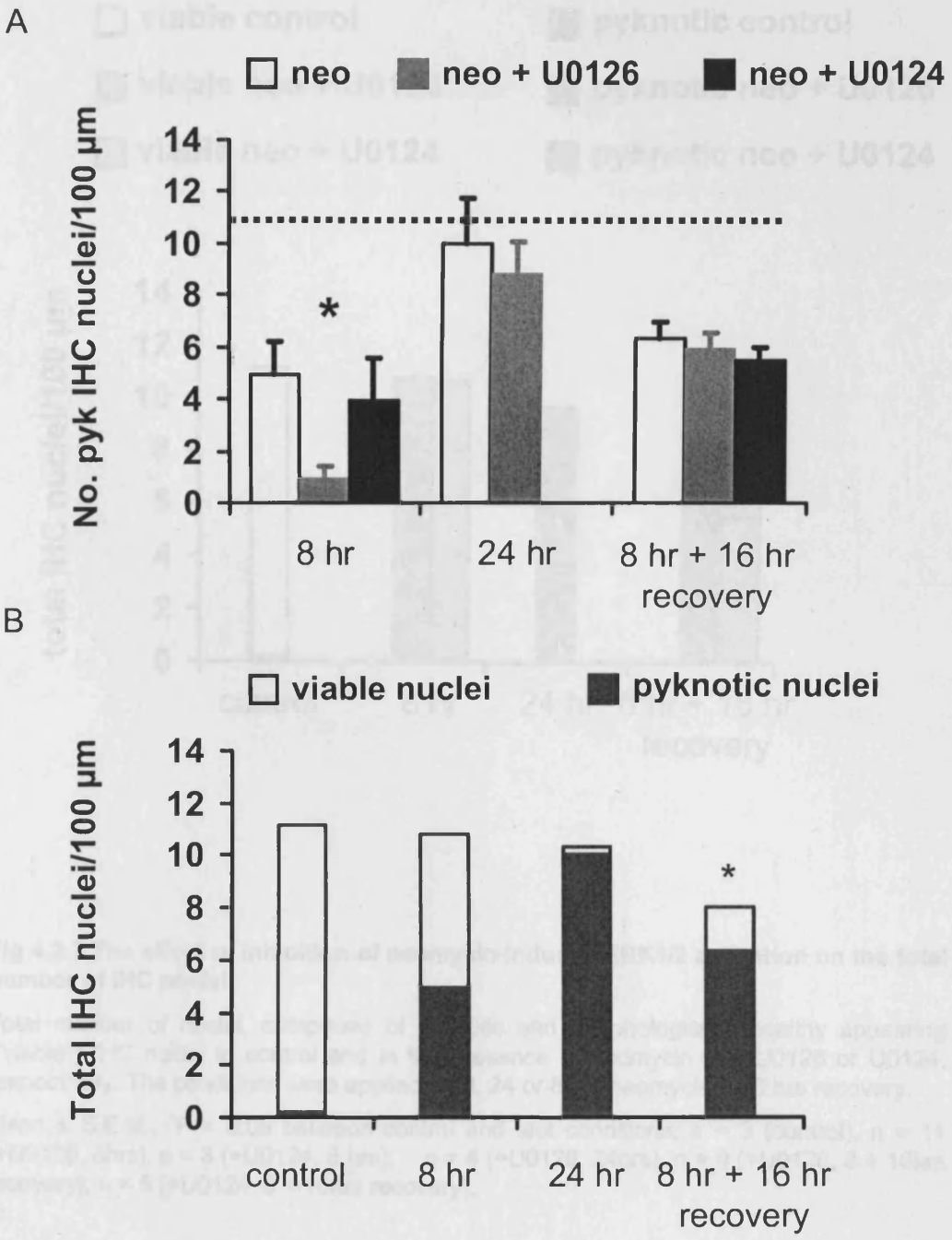

Fig 4.2.6 The effect of ERK1/2 inhibition on the viability of cochlear IHCs exposed to neomycin.

A) Comparison of the number of pyknotic IHC nuclei/100 µm in cochlear explants exposed to neomycin or in the additional presence of U0126 or U0124. Explants were exposed to the aforementioned conditions for 8, 24 or 8 hrs plus a 16 hr recovery phase (quantification paradigm see 2.7.5). The dotted line indicates the number of IHC nuclei present along 100 µm of the cochlear turn.

B) Total number of IHC nuclei comprised of pyknotic and healthy nuclei present along 100 µm in control cochlear turns and those exposed to neomycin for 8, 24 or 8 plus 16 hrs recovery.

Mean ± S.E.M., $^{*}P < 0.05$, n = 3 (control), n = 12 (neomycin 8 hrs), n = 11 (+U0126, 8hrs), n = 3 (+U0124, 8 hrs), n = 4 (neomycin, +U0126, 24hrs), n = 9 (neomycin, +U0126, 8 + 16hrs recovery), n = 5 (+U0124, 8 + 16hrs recovery).

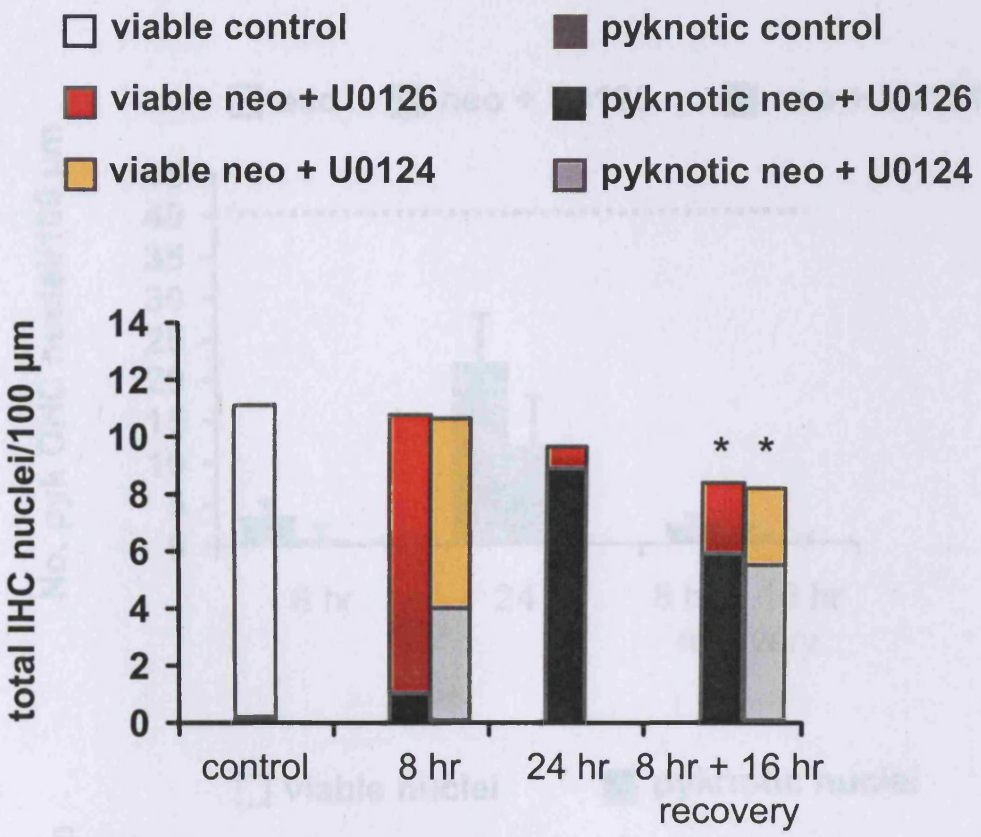

Fig 4.2.7 The effect of inhibition of neomycin-induced ERK1/2 activation on the total number of IHC nuclei.

Total number of nuclei, comprised of pyknotic and morphologically healthy appearing ("viable") IHC nuclei in control and in the presence of neomycin and U0126 or U0124, respectively. The conditions were applied for 8, 24 or 8 hrs neomycin + 16 hrs recovery.

Mean ± S.E.M., *P < 0.05 between control and test conditions, n = 3 (control), n = 11 (+U0126, 8hrs), n = 3 (+U0124, 8 hrs), n = 4 (+U0126, 24hrs), n = 9 (+U0126, 8 + 16hrs recovery), n = 5 (+U0124, 8 + 16hrs recovery).

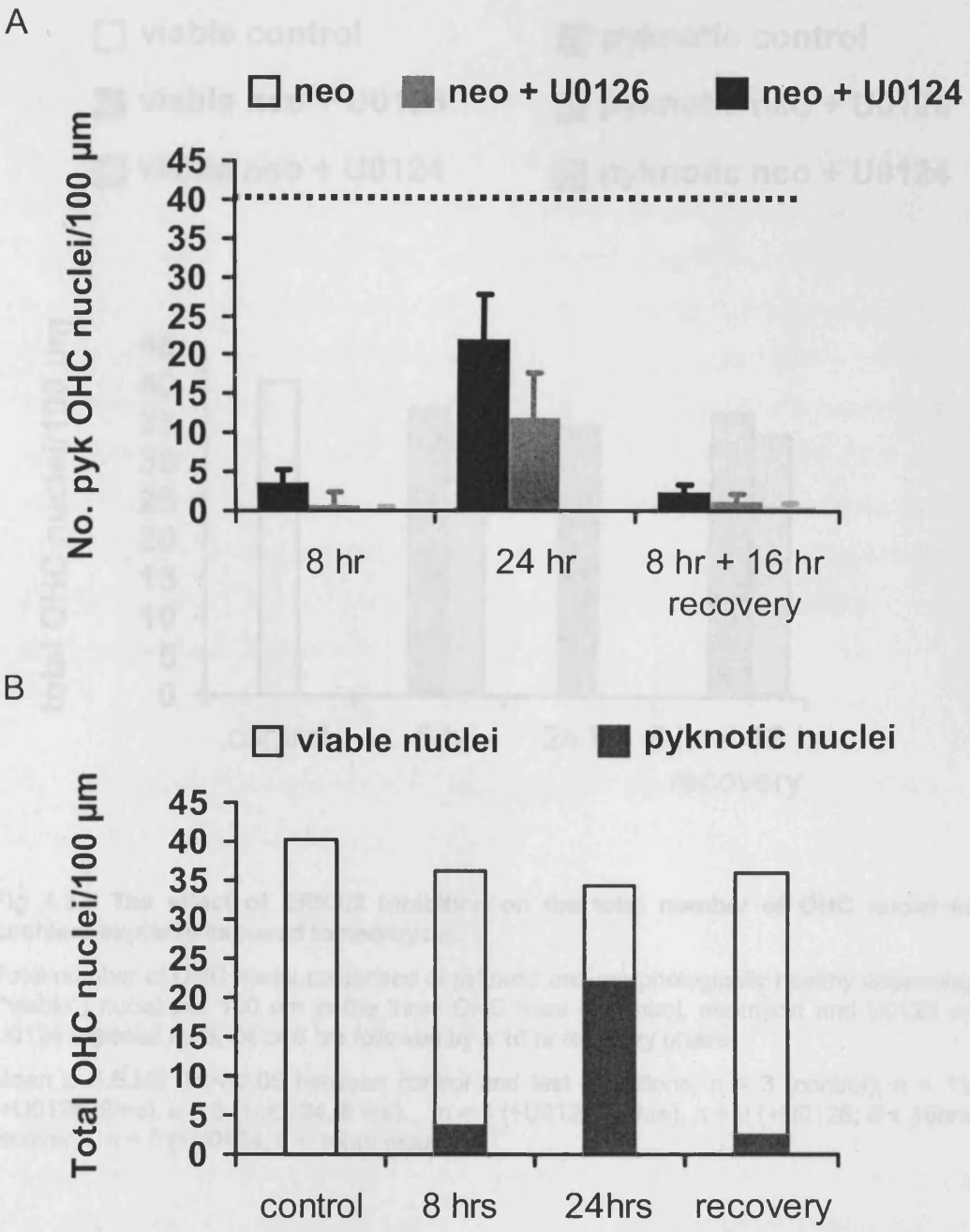

Fig 4.2.8 The effect of ERK1/2 inhibition on the formation of pyknotic nuclei in cochlear explants exposed to neomycin.

A) Comparison of the number of pyknotic OHC nuclei in cochlear explants exposed to neomycin or additionally to U0126 or U0124 for 8, 24 or 8 hrs followed by a 16 hr recovery phase. The dotted line indicates the number of OHC nuclei present in the three rows along 100 µm of the cochlear turn.

B) Total number of OHC nuclei comprised of pyknotic and morphologically healthy appearing ("viable") nuclei in control and exposed to neomycin for 8, 24 and 8 hrs followed by a recovery phase.

Mean ± S.E.M., $P > 0.05$, n = 3 (control), n = 12 (neomycin 8 hrs), n = 11 (+U0126, 8hrs), n = 3 (+U0124, 8 hrs), n = 4 (neomycin, +U0126, 24hrs), n = 9 (neomycin, +U0126, 8 + 16hrs recovery), n = 5 (+U0124, 8 + 16hrs recovery).

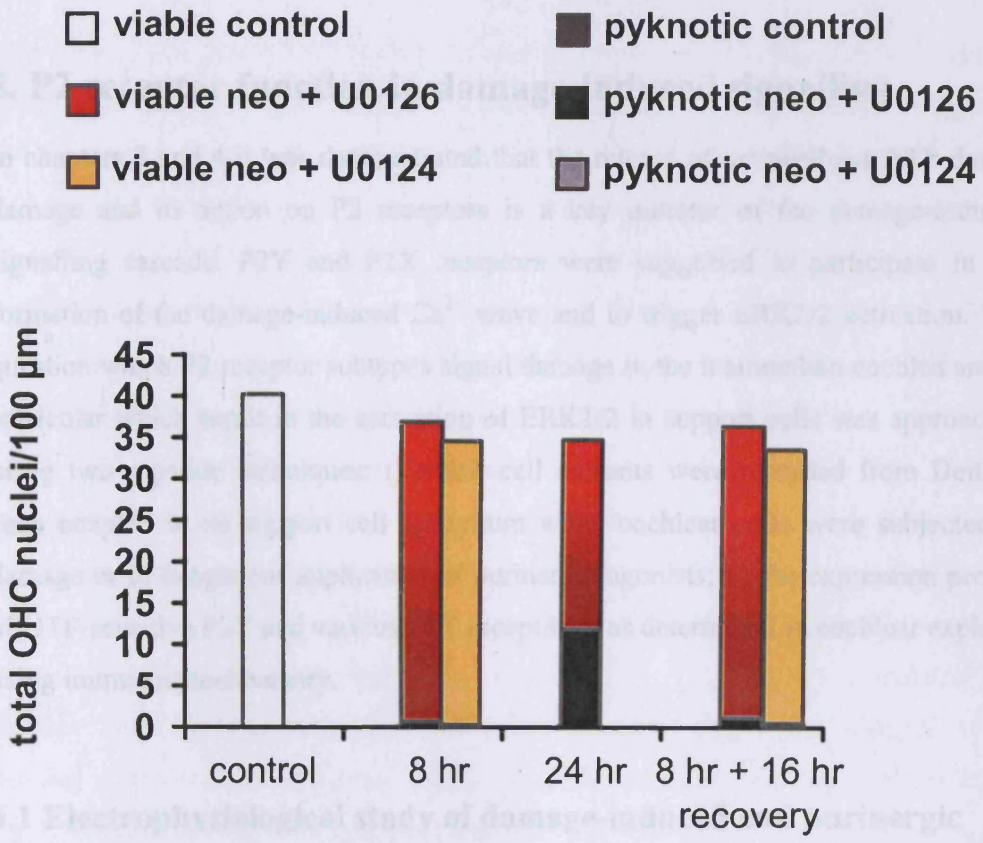

Fig 4.2.9 The effect of ERK1/2 inhibition on the total number of OHC nuclei in cochlear explants exposed to neomycin.

Total number of OHC nuclei comprised of pyknotic and morphologically healthy appearing ("viable") nuclei per 100 µm in the three OHC rows in control, neomycin and U0126 or U0124 exposed for 8, 24 or 8 hrs followed by a 16 hr recovery phase.

Mean ± S.E.M., $^{*}P < 0.05$ between control and test conditions, n = 3 (control), n = 11 (+U0126, 8hrs), n = 3 (+U0124, 8 hrs), n = 4 (+U0126, 24hrs), n = 9 (+U0126, 8 + 16hrs recovery), n = 5 (+U0124, 8 + 16hrs recovery).

5. P2 receptor function in damage-induced signalling

In chapters 3 and 4 it was demonstrated that the release of extracellular ATP during damage and its action on P2 receptors is a key initiator of the damage-induced signalling cascade. P2Y and P2X receptors were suggested to participate in the formation of the damage-induced Ca^{2+} wave and to trigger ERK1/2 activation. The question which P2 receptor subtypes signal damage in the mammalian cochlea and in particular which result in the activation of ERK1/2 in support cells was approached using two separate techniques: i) whole-cell currents were recorded from Deiters' cells coupled to its support cell syncytium when cochlear coils were subjected to damage or to exogenous application of purinergic agonists; ii) the expression profile of UTP-sensitive P2Y and various P2X receptors was determined in cochlear explants using immunocytochemistry.

5.1 Electrophysiological study of damage-induced and purinergic events in Deiters' cells

5.1.1 Characterisation of the damage-induced currents

Damaging the mammalian cochlea induced the propagation of an intercellular wave of increased cytoplasmic Ca^{2+} triggered by the release of extracellular ATP (chapter 3.1). To investigate whether damage elicits whole cell currents patch clamp recordings were made from Deiters' cells maintained in their cellular network or support cell syncytium (Fig 5.1.1A right panel). Deiters' cells were voltage-clamped at -90 mV and a microneedle, placed five cells from the patched Deiters' cell was used to induce damage to the HC region (Fig 5.1.1A, left panel). A baseline (~20 min) was recorded before the "first lesion" was induced followed by a 30 min interval and a second lesion at the same site. Recordings from Deiters' cells were characterised by spontaneously occurring inward currents as illustrated by the trace that represents 5 min of recording (Fig 5.1.1B). Damage activated an inward current in Deiters' cells located approximately 50 μm from the lesion site. The magnitude of the inward current was greater than the majority of spontaneously occurring current oscillations (Fig 5.1.1B upper panel). Moreover, a prolonged ion flux was observed in contrast to the shorter spontaneous inward currents. The rise time of the inward

current was not determined as the damage protocol was not automated. Therefore marking of the event was not very accurate, so that it was not possible to determine the exact starting point. Following the initial rise an increase in the noise in the trace was observed suggesting an increase in the number of openings and closings of ion channels (Fig 5.1.1B lower panel). The current recovered to baseline within 16.2 ± 4.6 s following the first lesion (n = 3, Table 5.1). During the recovery phase smaller single events that most likely arise from spontaneous oscillations add to a prolongation of the damage-induced signal (Fig 5.1.1B lower panel).

The peak current and the integral of the whole cell current, the charge transferred across the plasma membrane, were measured in order to quantify the magnitude of damage-induced currents in Deiters' cells. The magnitude of the damage-induced current is a function of the membrane resistance R_m (Fig 5.1.2A). Assuming that Deiters' cells have approximately the same resistance, R_m is an estimate of the number of cells in the syncytium and thus actually represents the syncytial resistance R_{Sync}. The lower R_{Sync} the higher was the observed peak current measured in Deiters' cells. The total charge transferred following damage was similarly dependent on R_{Sync}. These data suggest that the current is a property of the syncytium. A rise in intracellular Ca^{2+} has been suggested to modulate gap junctional connectivity and lead to their closure (Dakin et al., 2005). Damage triggers the formation of an intercellular Ca^{2+} wave of increased cytoplasmic Ca^{2+} (chapter 3.1). In order to test whether damage affects R_{Sync} over longer periods R_{Sync} was determined using a 10 mV voltage-step protocol. There was no significant difference between R_{Sync} measured before and 2 – 3 min after damage (pre: 192 ± 36 MΩ; post: 180 ± 29 MΩ; n = 8; P = 0.27).

Two consecutive lesions separated by an interval of 30 min were made in the same region of the HC epithelium. The damage stimuli differed in their intensity with the second being stronger (chapter 2.3.2). Both damage stimuli were sufficient to elicit inward currents in Deiters' cells (Fig 5.1.2B, Table 5.1.). The peak current induced by the first lesion was -324.8 ± 155.2 pA and the second lesion reached -622.4 ± 179.6 pA (n = 3). Similarly the charge transferred across the plasma membrane was increased to 8.5 ± 2.8 μC compared to -2.1 ± 0.7 μC following the

Table 5.1 Comparison of currents resulting from two consecutive lesions (n = 3)

Mean	Lesion 1	Lesion 2	P value
R_{Sync} [MΩ]	122.8 ± 45.5	119.3 ± 42.9	0.32
Peak current [pA]	-324.8 ± 155.2	-622.4 ± 179.6	0.15
Charge [nC]	-2.1 ± 0.7	-8.5 ± 2.8	0.13
$\Delta t_{current}$ [s]	19.0 ± 4.4	30.7 ± 6.9	0.20
$\Delta t_{peak\text{-}baseline}$ [s]	16.2 ± 4.6	25.6 ± 6.2	0.29

first lesion (Fig 5.1.2C, Table 5.1.1). The differences were however not statistically significant. These data indicate that Deiters' cells maintain their capacity to respond to two consecutive damage stimuli.

5.1.2 The effect of P2 receptor antagonist PPADS

It is possible that P2 receptor activation during damage triggered the inward current. Therefore damage was induced in the presence of the broad spectrum P2 receptor antagonist PPADS (150 μM). PPADS abolished the spontaneous inward currents suggesting that these events occur in a P2 receptor dependent manner. In contrast the damage-induced inward current persisted in the presence of PPADS (Fig 5.1.1C). The magnitude of the peak current and the total charge transferred as a result of damage were determined in order to assess the effect of PPADS. As shown it is critical for the comparison of these damage-induced currents that R_{Sync} is taken into account. Note that R_{Sync} in the PPADS group was greater than that of the control (Table 5.2). This was not a result of PPADS application because the R_{Sync} measured prior to the exposure to PPADS was 281.2 ± 55.4 MΩ. In order to compensate for the difference in R_{Sync} it was assumed that the current-R_{sync} relationship is linear (see Fig 5.1.2A). Thus the peak current and the charge transferred were normalised to the conductance G_{Sync} ($G_{sync} = \frac{1}{R_{sync}}$). The data are summarised in Table 5.2 and Fig 5.1.3. The damage-induced I_{norm} in the presence of PPADS was decreased to a minor degree but it was not statistically significant from control data. Similarly, the normalised total

Table 5.2: Comparison of damage-induced currents

Mean	Control	PPADS	P value
R_{sync} [MΩ]	122.8 ± 45.5	281.2 ± 55.4	0.09
Peak $current_{norm}$ [arb. units]	-54.2 ± 5.6	-34.9 ± 11.3	0.2
$Charge_{norm}$ [arb. units]	-796.4 ± 168.2	-439.1 ± 157.7	0.098
$\Delta t_{current}$ [s]	30.7 ± 6.9	48.2 ± 4.6	0.10
$\Delta t_{peak\text{-}baseline}$ [s]	25.6 ± 6.2	45.4 ± 5.2	0.07

charge transferred was also reduced when exposed to PPADS compared to controls. The given P-value of 0.097 indicates that this effect was not statistically significant with a sample number of three.

5.1.3 Characterisation of whole-cell Deiters' currents elicited by purinergic agonists

In order to explore whether P2 receptors are the likely mediators of the damage-induced currents the response was compared to that induced by various agonists. Deiters' cells were exposed to brief local puff applications of purinergic agonists to the apical surface of cochlear turns. P2X receptor mediated currents arise instantaneously whereas metabotropic P2Y receptors require intermediate steps to initiate the opening of ion channels and thus the response is delayed. Exogenous puff application of ATP (100 μM) for 10 ms elicited an immediate inward current I_{fast}, which reached its peak within approximately 100-150 ms (Fig 5.1.4B). A second inward current I_{slow} developed during the decay phase of I_{fast}. The charge transferred during the second response was larger compared to I_{fast}. Moreover, I_{slow} appeared to be comprised of smaller events that resulted in a fluctuating noisy response (Fig 5.1.4B). I_{slow} was abolished when gap junctional coupling was inhibited by octanol (1 mM, Fig 5.1.4B) strongly suggesting that the current was a property of the syncytium.

Exogenous application of 100 μM UTP for 10 ms was not sufficient to mediate I_{fast} in Deiters' cells (Fig 5.1.4B). However, a current with similar kinetics to I_{slow} was observed. ADP and UDP did not trigger ion flux (Fig 5.1.4B).

The data in Fig 5.1.5A and B reiterate that only ATP elicits a rapid current. The mean charge transferred during I_{fast} was -0.039 ± 0.023 nC whereas that of I_{slow} was -1.383 ± 0.186 nC. The peak of I_{slow} measured in response to ATP was -428.5 ± 105.3 pA and thus greater than that observed with UTP (-262.2 ± 138.3 pA). Similarly, the total charge transfer elicited by ATP was larger than that triggered by UTP (-1.383 ± 186.0 nC, -0.651 ± 0.375 nC; respectively).

5.1.4 Characterisation of ATP-induced whole-cell currents

In order to record from single Deiters' cells the syncytium was uncoupled using octanol (1 mM). Fig 5.16A and B show a comparison of the response to ATP before and after uncoupling of the syncytium. I_{slow} was no longer observed after exposure to octanol whereas I_{fast} remained. The peak I_{slow} was reduced from -633.5 ± 170.7 pA to -104.6 ± 66.9 pA in the presence of octanol. The charge transferred across the membrane during I_{slow} was also decreased when cochlear coils were exposed to octanol (-1.913 ± 0.563 nC to -0.071 ± 0.029 nC). In a few cases cells were found to be uncoupled under control conditions. These cells exhibited the same phenotype as those recorded from in the presence of 1 mM octanol. Spontaneously uncoupled cells were subjected to repetitive application of ATP (10 ms) during voltage-commands ranging from -100 mV to +60 mV stepping in 40 mV increments. Representative current traces are displayed in Fig 5.1.6C. The current-voltage (I-V) relationship revealed an inwardly rectified current (Fig 5.1.6C, D). The I-V curve represents an average of currents obtained from three voltage-clamped Deiters' cells (2 animals). A number of other Deiters' cells (n = 3) also showed inward rectification of the ATP-induced current; however the magnitude of the current was smaller and was thus not included in the average. As the second current was dependent on the gap junctional connectivity it was not possible to determine the current-voltage relationship. The UTP-induced current was similarly dependent on functional gap junction coupling.

Table 5.3: Comparison of I_{damage} and I_{ATP}

Mean	Damage L1	ATP I_{slow}	P value
R_{sync} [MΩ]	230.7 ± 83.0	119.1 ± 23.9	0.27
Peak current [pA]	-111.5 ± 37.4	-428.5 ± 105.3	0.047
Charge [nC]	-0.88 ± 0.31	-1.29 ± 0.14	0.29
$\Delta t_{current}$ [s]	21.3 ± 1.8	8.6 ± 0.55	0.002
Δt_{Islow}[s]	-	8.3 ± 0.62	-

Fig 5.1.7 displays that the peak current reduced as a function of increased R_{sync}. Thus the current-voltage relationship of the UTP-induced current could also not be assessed.

5.1.5 Comparison of damage-induced and purinergic currents

Damage elicited one current (I_{damage}) in comparison to the biphasic current induced by exogenous application of ATP (100 μM). I_{slow} and I_{damage} share the following features: i) dependency on R_{sync} and ii) current fluctuations. In contrast, I_{damage} occurs over a time course of 21.3 ± 1.8 s whereas the ATP-induced total ion flux was considerably shorter (8.6 ± 0.55 s), although the total charge transferred by the ATP-mediated I_{slow} was larger than that of I_{damage} (Table 5.3). However, this effect was not statistically significant. The peak of I_{slow} was significantly greater than that of I_{damage} (Table 5.3).

5.2 P2 receptor expression

The activation profile of ERK1/2 and the induction of currents by ATP and UTP but not by UDP or ADP, suggest a specific role for the $P2Y_2$, $P2Y_4$, $P2Y_{11}$ and P2X receptor subtypes. The expression pattern of various P2X receptor subtypes has been determined in cryosections using immunocytochemistry (Housley et al., 1999; Jarlebark et al., 2000; Nikolic et al., 2001; Jarlebark et al., 2002; Nikolic et al., 2003; Szucs et al., 2004). Knowledge about the cell type specific expression of P2Y receptors in the cochlea is more limited. Moreover, protein expression profiles may change in culture models compared to *in vivo*. Thus, the expression pattern of various P2Y and P2X receptors were studied in cochlear cultures.

5.2.1 P2Y receptor expression in neonatal rat cochlear explants

UTP-induced ERK1/2 activation together with the insufficiency of ADP and UDP implicate a role for the $P2Y_2$, $P2Y_4$ and $P2Y_{11}$ receptor subtypes. Thus, in this section the expression pattern of these subtypes was determined in cochlear explants. Single confocal z-stack images are displayed at two levels to show the expression of the examined P2 receptors. The $P2Y_2$ receptor was expressed in Deiters' cell bodies and their processes as well as in Hensen and outgrowing Claudius-like cells (Fig 5.2.1C-E). $P2Y_2$ did not appear to be present in HCs. Additionally punctate staining was observed along the region of the IHCs (Fig 5.2.1C). Double-labelling with synaptophysin suggests that this punctate pattern represents nerve boutons that are already synapsed with IHCs at this time in development (Fig 5.2.1C inset). The specificity of the labelling was tested using the peptide against which the antibody was raised. The antibody was pre-incubated for 30 min with the peptide. Fig 5.2.1A is a representative averaged image for $P2Y_2$ receptor expression that shows extensive punctate labelling in the region of the IHCs. Moreover, the OHC region was characterised by structurally defined labelling of Deiters' cells. In contrast, pre-incubation with the peptide abolished the labelling in the OHC region and reduced the punctate pattern (Fig 5.2.1B). The expression pattern of $P2Y_4$ was different to that of $P2Y_2$. $P2Y_4$ was strongly expressed in HCs (Fig 5.2.1I-L). The labelling of Deiters', pillar, Hensen and IS cells was observed but to a lesser extent than in HCs. In Deiters' cells the $P2Y_4$ receptor localised to the plasma membrane whereas in the other cell types the labelling was additionally observed in the cytoplasm and in nuclei of HCs. The cellular differences of $P2Y_4$ receptor expression are most likely not due to reduced accessibility of the antibody to Deiters' cells. At least 3rd row Deiters' cells would be expected to label similarly to OHCs as these should be exposed to the antibody to a similar extent as the OHCs. Pre-incubation with the control peptide abolished the $P2Y_4$ receptor labelling suggesting that the expression pattern obtained was specific (Fig 5.2.1G, H).

Assessment of the $P2Y_{11}$ receptor subtype revealed a different expression pattern (Fig 5.2.2). Labelling was observed at the plasma membrane of HCs. Diffuse labelling was also found in the cytoplasm of HCs, pillar and Hensen cells. In the Deiters' cell region it was difficult to distinguish whether the labelling is attributable

to dendrites/nerve fibres or Deiters' cells. The pattern as seen at the level of Deiters' cell nuclei in Fig 5.2.2B is quite irregular and the labelling does not outline the cell borders of all Deiters' cells. Averages of five confocal z-stack images of $P2Y_{11}$ receptor labelling at the apical aspects of Deiters' and HCs revealed a specific pattern (Fig 5.2.2E, F). The 1st row of OHCs is displayed and was characterised by strong staining of discrete triangular structures that aligned and represented a row of Deiters' cell processes (Fig 5.2.2E). Neighbouring labelling of 1st row OHCs and intercalated outer pillar cell processes was also observed. Fig 5.2.2F shows that inner pillar and IHCs were also characterised by $P2Y_{11}$ receptor labelling at their apical aspects. Pre-incubation with the peptide against which the anti $P2Y_{11}$ antibody was raised against abolished the labelling (Fig 5.2.2G, H).

In summary, $P2Y_2$, $P2Y_4$ and $P2Y_{11}$ receptors were expressed in distinct patterns in rat cochlear explants. In Deiters' cells, all three receptors were expressed with $P2Y_{11}$ being localised to the top of Deiters' cell processes.

5.2.2 P2X receptor expression in neonatal rat cochlear explants

The ionotropic $P2X_2$ receptor was strongly expressed in Deiters' cells but not in HCs or neurons (Fig 5.2.3A-F). In Deiters' cells its expression was polarised with stronger staining at the top of their phalangeal processes compared to the other regions of the cell (Fig 5.2.3A-F). Outer pillar, Hensen and Claudius-like cells also expressed $P2X_2$ receptors. Pre-absorption of the $P2X_2$ antibody to the peptide it was raised against abolished the labelling (Fig 5.2.3A, B).

$P2X_3$ receptor expression was characterised by punctate labelling that was localised to HCs. Moreover, Deiters' cells showed labelling, as indicated by the regular pattern at the level of Deiters' cell bodies (Fig 5.2.3J). The Deiters' cell phalangeal processes are outlined at the level of HCs as displayed in Fig 5.2.3I. This supports the interpretation that $P2X_3$ receptors are expressed in Deiters' cells. However, the x-z projection does not give a clear image and rather suggests neuronal expression of $P2X_3$ receptors (Fig 5.2.3K, L). Neuronal expression is supported by the outline of a neuronal fibre in the IHC region and one that crosses the pillar cell region to the OHC region (Fig 5.2.3I, J). Furthermore, the average of 20 images in Fig 5.2.3G also

suggests neuronal expression of the $P2X_3$ receptor. Punctate staining was also observed in Hensen, Claudius-like and cells beneath the basement membrane. When the antibody was pre-adsorbed to its specific peptide the immuno-reactivity and the labelling were abolished (Fig 5.2.3H).

Punctate labelling was observed for $P2X_4$ receptors in OHCs, Deiters', Hensen and pillar cells as illustrated in the orthogonal x-z projections (Fig 5.2.4F, G). Some immuno-reactivity was also observed around the IHCs and in cells underneath the basement membrane. Furthermore, an average of five images at the level of the Hensen and Claudius-like cells revealed strong expression in structures that resemble macrophages (Fig 5.2.4B). $P2X_4$-labelling of neural projections was variable. In the example shown neural projections were immuno-negative, but in a different explant $P2X_4$ receptors were present in neurons. The immuno-labelling of the cochlear explants was eliminated when the $P2X_4$ antibody was pre-incubated with its specific peptide (Fig 5.2.4C). In summary, the $P2X_2$ receptors were strongly expressed in support cells including Deiters', outer pillar, Hensen and Claudius-like cells. $P2X_3$ and $P2X_4$ were also observed in Deiters' cells but these receptors were additionally expressed in HCs and other cell types.

5.3 Discussion

This chapter investigated P2 receptor expression in Deiters' cells assessed using immunocytochemical localisation studies and voltage-clamp recordings in the context of damage-induced signalling. Immunocytochemical localisation revealed that $P2X_2$, $P2X_3$, $P2X_4$, $P2Y_2$, $P2Y_4$ and $P2Y_{11}$ receptors are expressed in cochlear explants. $P2Y_2$ and $P2X_2$ receptor subtypes were expressed in Deiters' cells and other support cells but not in HCs. Thus these receptors represent likely candidates that trigger ERK1/2 activation in Deiters' cells. Mechanical damage elicited ion flux in Deiters' cells. The magnitude of the resultant current was inversely proportional to R_{sync} and thus was dependent on gap junctional connectivity. This current was challenged with the P2 receptor antagonist PPADS and compared to currents elicited by P2 receptor agonists. The P2 receptor antagonist PPADS was not effective at reducing the damage-induced current. The agonists ATP and UTP activated currents whereas ADP and UDP did not. ATP evoked a biphasic response – comprised of I_{fast} and I_{slow} and the latter was found to require functional gap junctions. UTP application mimicked the slowly developing ion flux implying that P2Y receptors are the mediators. The magnitude was also dependent on the R_{sync} similarly to that of the current evoked by damage leading to the hypothesis that the underlying mechanisms are identical.

Immunocytochemical analysis of P2Y receptor expression

The expression pattern of P2Y receptor subtypes $P2Y_2$, $P2Y_4$ and $P2Y_{11}$ was determined. $P2Y_2$ was detected in Deiters', Hensen and outgrowing Claudius-like cells, but not in sensory HCs. Gale et al. (2004) reported the presence of $P2Y_2$ receptors in Hensen and Claudius-like cells which is in agreement with the data presented here. However, Gale et al. (2004) also observed labelling of stereocilial bundles of IHCs and a different study detected localisation of $P2Y_2$ in the apical aspects of OHC bodies(Szucs et al., 2004). These studies are in contrast to the observation of this report demonstrating that HCs did not label positively for $P2Y_2$. Species and age differences might explain the opposing results. The model used in this study and by Gale et al. (2004) only varies by the lengths of time the cochlear explant was maintained in culture. A potential extra day in culture as in the model of

Gale et al. could change the expression pattern and cause the observed localisation of $P2Y_2$ to stereocilial bundles of IHCs.

$P2Y_4$ receptor expression was observed in HCs and to a lesser degree in Deiters', pillar, Hensen, Claudius and IS cells. There is little knowledge about $P2Y_4$ receptor expression in the cochlea. The expression of $P2Y_4$ mRNA was detected in cochleae of P2 rats by RT-PCR (Gale et al., 2004). Moreover, an immunohistochemical study suggested that $P2Y_4$ receptors are present in Deiters' cells but not in HCs (Parker et al., 2003). The localisation of $P2Y_4$ in Deiters' cells is in agreement with the data presented here. In contrast to the study by Parker et al. (2003), HCs expressed $P2Y_4$ receptors. There are a number of reasons that could explain the differences: i) species ii) developmental stage, iii) dissection and maintenance in vitro for 24 hrs could alter gene expression.

$P2Y_{11}$ receptor expression was observed at the apical aspects of HC bodies and in Deiters' and pillar cells phalangeal processes. A possible explanation is that $P2Y_{11}$ receptors co-localise to the region of the basal body. However, this was not tested. Labelling was also observed in the basal region of Deiters' cells, but it was difficult to determine whether the pattern was resulting from expression in Deiters' cells or neurons. The expression of $P2Y_{11}$ receptors has not been investigated in auditory or vestibular HC epithelia. The peptide used to raise the anti-$P2Y_{11}$ antibody was subjected to a Blast search and revealed only similarity to $P2Y_{11}$ clones from various species and thus suggests specificity of the antibody. However, Western Blot analysis carried out by the supplier of the antibody (Alomone Labs, data sheet, Lot #: AN-01) gave rise to several protein bands. Hence, the expression profile presented here has to be taken with caution.

P2X receptor expression

The expression patterns of $P2X_2$, $P2X_3$ and $P2X_4$ were investigated in rat cochlear explants. $P2X_2$ receptors were localised in Deiters', outer pillar, Hensen and Claudius-like cells. Previously, the expression of $P2X_2$ has been reported for the support cell subtypes mentioned above with the exception of the outer pillar cell. However those reports in contrast to the data presented here detected $P2X_2$ receptor

immunoreactivity also in stereocilial hair bundles of outer and in some species inner HCs (Housley et al., 1999; Jarlebark et al., 2000; Jarlebark et al., 2002). There are a number of reasons that could explain the differences: i) developmental stage, ii) in vitro alteration in gene expression, iii) different antibodies used.

HCs, Hensen and Claudius-like cells express $P2X_3$ receptors. Moreover, the labelling pattern also suggests expression in neuronal fibres and Deiters' cells. At this age immunohistochemical data using cryosections revealed $P2X_3$ receptor expression in HCs and spiral ganglion neurons, but not in support cells of mouse cochleae. The differences in the expression might be related to the species or to the different antibodies used in the two studies (Huang et al., 2005).

$P2X_4$ was widely expressed in cochlear explants. Cells include hair, Deiters', Hensen, pillar, Claudius-like cells and also those beneath the basement membrane. Previous studies have shown that $P2X_4$ mRNA was present in postnatal day 1 to 16 rat cochleae (Brandle et al., 1999). Published immunohistochemical data are scarce and focused on spiral ganglion neurons and isolated outer HCs. Both cell types expressed the $P2X_4$ receptors (Xiang et al., 1999; Szucs et al., 2004). Here, the expression of $P2X_4$ receptors in neuronal fibres was variable. $P2X_4$ expression was characterised predominantly by punctate labelling. In olfactory bulb neurons $P2X_4$ receptors localised to early endosomes and continuous receptor trafficking was described (Bobanovic et al., 2002).

$P2X_4$ receptor expression was also observed in cells with dendritic processes that most likely resemble macrophages. There is some evidence that macrophages and microglia express $P2X_4$ receptors (Bowler et al., 2003)

P2 receptor expression in the light of ERK activation

Damage-induced ERK1/2 activation was observed in a subset of non-sensory support cells, Deiters' and phalangeal cells. In contrast, HCs did not respond to damage with ERK1/2 activation. The P2 receptor expression profiles that most closely resemble the ERK1/2 activation pattern are those of the $P2X_2$ and the $P2Y_2$ receptors. Data presented here show that both receptors are expressed in Deiters' cells but not in HCs

and are thus potential candidates for triggering the activation of ERK1/2 in Deiters' cells. However, it can not be excluded that other P2 receptors that are expressed in both Deiters' and HCs stimulate the activation of ERK1/2. The same P2 receptor subtype could recruit different downstream signalling molecules depending on the cell type resulting in diverse signalling events. $P2X_7$ receptors which were not examined here are known to be expressed in postnatal and adult Deiters' and IHCs. This P2 receptor is only present during the first days after birth in OHCs (Nikolic et al., 2003). In $P2X_7$ transfected cells it has been shown that activation of the receptor leads to the activation of ERK1/2 (Amstrup and Novak, 2003; Gendron et al., 2003). However, PPADS, which is an effective blocker of $P2X_7$ receptors failed to reduce ERK1/2 spread; thus $P2X_7$ receptors can likely be excluded. The absence of $P2X_1$ receptor expression in Deiters' cells (Nikolic et al., 2001) excludes that these receptors mediate ERK1/2 activation. To summarise, based on the selective expression of $P2X_2$ and $P2Y_2$ receptors in Deiters' cells, these are the likely candidates to initiate signalling towards ERK1/2 during inner ear damage.

P2 receptor expression and Ca-signalling

Propagation of the damage-induced Ca^{2+} wave into the distinct regions of the cochlea required different sources of Ca^{2+}. In the OS region the Ca^{2+} rise was established solely through release of Ca^{2+} from intracellular IP_3 sensitive stores suggesting P2Y receptors as the main regulators. $P2Y_2$, $P2Y_4$ and $P2Y_{11}$ receptors were expressed in Hensen and Claudius-like cells. Based on the agonist study UDP and ADP-sensitive receptors could contribute to the Ca^{2+} wave. The expression of those receptors remains to be determined. The redundancy of extracellular Ca^{2+} in the propagation of the damage-induced Ca^{2+} wave suggests that P2X receptors are not involved in the OS region. In contrast, $P2X_2$, $P2X_3$ and $P2X_4$ receptors were observed in Hensen and Claudius-like cells and could thus also facilitate the formation of the damage-induced Ca^{2+} wave. It is possible that during the damage-induce Ca^{2+} wave the levels of ATP released might not be sufficient to activate P2X receptors and thus to mediate influx of extracellular Ca^{2+}.

Two distinct Ca^{2+} waves propagated along the HC region. Influx of Ca^{2+} from the extracellular space facilitated the formation of the fast wave whereas IP_3 sensitive

Ca^{2+} stores were required to mediate the slow Ca^{2+} wave. HCs and Deiters' cells can contribute to the signal measured along the HC region. The receptor subtypes investigated were present in one or the other cell type if not in both. Thus it is not possible to extrapolate their specific contribution to the wave propagation. Again, ADP and UDP were able to elicit a Ca^{2+} response. Therefore, ADP- and UDP-sensitive P2Y receptors which were not investigated here might contribute to a minor extent. ADP has also been demonstrated to activate $P2X_3$ receptors or its heteromer $P2X_{2\text{-}3/3}$ (Greenwood et al., 2007). Both $P2X_2$ and $P2X_3$ receptors are expressed in the HC region and thus could be the mediators of the ADP-induced rise in intracellular Ca^{2+}. However it is not known whether the specific $P2X_{2\text{-}3}$ splice variant is present in hair or Deiters' cells in cochlear explants.

Propagation of the damage-induced Ca^{2+} wave into the IS region required both extracellular Ca^{2+} and release from intracellular stores. However, it is possible that a third mechanism acts in this region to facilitate the Ca^{2+} wave. The only P2Y receptor clearly expressed in the IS region was $P2Y_4$. As UTP was the most potent agonist to elicit an intracellular rise in Ca^{2+} it is likely that $P2Y_4$ is the predominant candidate to evoke the IP_3 dependent Ca^{2+} wave formation. As ADP was able to elicit Ca^{2+} changes ADP-sensitive P2Y receptors might play a minor role. $P2X_2$, $P2X_3$ and $P2X_4$ receptor subtypes were not observed in this region. Thus other P2X receptors might mediate the influx of extracellular Ca^{2+}.

Damage-induced currents

Mechanical damage of cochlear cells elicited an inward current in a Deiters' cell located five cells (~50 μm) from the site of damage. During the damage protocol Deiters' cells were maintained in their support cell syncytium. The magnitude of the peak current was inversely proportional to R_{sync}, which is inversely proportional to the number of cells in the syncytium. Therefore, the magnitude of I_{damage} is proportional to the number of cells in the syncytium. Cell death of keratinocytes or nociceptive neurons elicited an inward current in surrounding nociceptors. The current induced by a dying nociceptor was inhibited by TNP-ATP – a P2X receptor antagonist (Cook and McCleskey, 2002). In this report the application of the P2

receptor antagonist PPADS did not significantly reduce the peak current. There was a reduction in the total charge transferred across the Deiters' cell membrane during the damage-induced response, but again this was not statistically significant. Only a subset of P2 receptors are sensitive to PPADS (King and Townsend-Nicholson, 2003) and therefore a variety of antagonists are required to clarify whether ATP is a mediator of the damage-induced current. Of course, cell damage is likely to also result in the release of other molecules such as glutamate which could result in inward currents at negative holding potentials (Glowatzki et al., 2006).

Gap junctional coupling has been suggested to be modulated by elevated intracellular Ca^{2+} (Dakin et al., 2005). However mechanical damage of the HC epithelium that results in increased intracellular Ca^{2+} (see chapter 3) did not affect R_{Sync} when assessed 2-3 min after damage. Ca^{2+} levels return to baseline typically within 1.5 min following damage in the HC region. The Ca^{2+} concentrations achieved might not be sufficient to uncouple gap junctions. Moreover, Dakin et al. (2005) demonstrated that gap junction uncoupling was dependent on the mechanism that resulted in elevated intracellular Ca^{2+}. Agonist-induced Ca^{2+} rises triggered by histamine or bradykinin were not sufficient to dissociate gap junctions. In contrast, store-operated Ca^{2+} entry was able to mediate gap junctional uncoupling. This might suggest that the pathway required to uncouple gap junctions is not activated in response to the mechanical stimulus used in this study.

Nucleotide-induced currents

Whole-cell currents were recorded from Deiters' cells in a support cell syncytium exposed to exogenous application of various P2 receptor agonists in order to investigate whether such currents mimic the damage-induced current. Here the features of P2 receptor activated currents are discussed and in the following subsection the currents are compared to those elicited by damage.

Local pressure application of ATP elicited two temporally separate inward currents – I_{fast} and I_{slow} and the latter requiring a functional syncytium. The current-voltage relationship of the first component reveals an inward rectification. This is in agreement with previous reports for ATP-induced currents in Deiters' cells (Chen et

al., 2000; Lagostena and Mammano, 2001). $P2X_2$ receptor and splice variants specific to the cochlea have been reported to inwardly rectify (Zhou and Hume, 1998; Chen et al., 2000). In addition $P2X_{1/5}$ receptors exhibit inward rectification to a minor degree (Haines et al., 1999) but not $P2X_4$ receptors (Khakh et al., 1999b). Published data on the P2X receptor subtype dependent rectification assessed in heterologous expression systems are quite scarce. Moreover in a native tissue several P2X receptors are expressed simultaneously and are likely to form heteromers which might render their properties. Thus in agreement with the immunohistochemical data the likely receptor expressed in Deiters' cells that infers rectification is a $P2X_2$-like receptor. The current-voltage relationship of the second component was not determined as clamping the voltage of the syncytium was not possible.

Due to the slow decay of I_{slow} the total charge transferred was considerably larger compared to that of I_{fast}. A similar biphasic current in response to ATP has been described in Hensen cells of adult guinea pigs (Lagostena et al., 2001). In contrast in Deiters' cells from adult guinea pigs only a monophasic current that was identical to I_{fast} was observed (Lagostena and Mammano, 2001). Results presented here show that UTP but not ADP or UDP was sufficient to elicit I_{slow}. The data indicate that I_{slow} is mediated through the activation of one of the UTP sensitive $P2Y_2$, $P2Y_4$ or $P2Y_{11}$ receptors. Moreover, as I_{fast} was not observed with UTP this suggests that $P2X_3$ receptors are absent from the apical aspect of Deiters' cell. These data are in agreement with an IP_3 dependent mechanism that was described for Hensen cells (Lagostena et al., 2001). The nature of that current was a Ca^{2+}-induced Cl^- conductance. Thus the ionic current observed in Deiters' cells in this thesis might be mediated by the same mechanism. However, unless octanol – a gap junction inhibitor affects the suggested channels, the absence of the slow current in the presence of octanol has to be explained. Deiters' cells that uncoupled without the addition of gap junction inhibitors were also characterised by the absence of I_{slow}; thus suggesting that octanol does not exert a direct effect on the channel that mediates I_{slow}. The data suggest that I_{slow} does not originate from Deiters' cells. Lagostena and Mammano (2001) reported a biphasic response to ATP in Hensen cells that was composed of a fast P2X-mediated and a slower Ca^{2+}-activated Cl^- conductance. Thus I_{slow} observed in Deiters' cells likely originates from nearby Hensen cells. In addition it cannot be

excluded that other support cell types or cells in the IS region also contribute to the generation of I_{slow}. However, data are not available for other support cell types.

Comparison of I_{ATP} and I_{damage}

Exogenous application of ATP resulted in a biphasic current that consisted of I_{fast}, a P2X-mediated current, and I_{slow} which was mediated by P2Y receptor activation. Damage elicited a current that was similar to the second component I_{slow} in that it was dependent on the activity of the support cell syncytium. Thus it is likely that these currents result from the activation of the same receptor – a UTP-sensitive P2Y receptor. I_{fast} – the P2X-like current was not obvious as a component of the damage-induced current.

One possibility is that the damage stimulus used would result in more gradual release of ATP than the stepped pulse of ATP application. Therefore, the onset of P2X receptor activation might be delayed and thus coincide with that of P2Y receptors. Therefore, this might result in the masking of I_{fast} by I_{slow}. A smaller I_{fast} component could also have been missed due to the spontaneous current activity in recordings from Deiters' cells in a syncytium. Both I_{slow} and the spontaneous activity were reduced when R_{sync} was high. Therefore, it might be expected that I_{fast} would be observed at high R_{sync}'s due to its continued presence as shown when treated with octanol (see section 5.1.4). This was however not observed, which indicates that P2X receptor activation does not occur in Deiters' cells during damage of the cochlea.

Damage-induced currents typically lasted longer than those triggered by exogenous ATP application. This likely represents a prolonged presence of ATP during the damage stimulus compared to the 10 ms bolus of ATP.

Damage-induced Ca^{2+}-waves and ERK1/2 activation in the light of damage-induced currents

The aim of this study was to elucidate whether damage induces P2X and P2Y-mediated currents for comparison with data on damage-induced Ca^{2+} wave formation and ERK1/2 activation. The data presented here favour a model that can

Table 5.4 Comparison of features of I_{damage} and ERK1/2 activation

	I_{damage}	ERK1/2 activation
PPADS sensitivity	No	No
P2Y-mediated (UTP)	Yes	Yes
Gap junctions	Yes	Yes

exclude P2X receptors (see previous section) in the facilitation of damage-induced signalling. However, exclusion of P2X receptors results in a conundrum with respect to the mechanism of the fast Ca^{2+} wave that requires influx of extracellular Ca^{2+} and the partial activation of ERK1/2. I_{damage} shares properties with the P2Y-mediated ATP-induced I_{slow} arguing that it does not involve the entry of extracellular Ca^{2+}, unless the current results in voltage changes in neighbouring cells that enable the opening of voltage-gated Ca^{2+} channels over quite some distance. However, there is only one report suggesting that voltage-gated Ca^{2+} channels are expressed in Deiters' cells (Hafidi and Dulon, 2004). It is possible that the entry of extracellular Ca^{2+} is not associated with Deiters' cells but actually occurs in HCs. Furthermore, ATP released during damage could provoke HCs to release a molecule that triggers ERK1/2 activation in surrounding cells.

Table 5.4 summarises the features of I_{damage} and ERK1/2 activation. I_{damage} and damage-induced ERK1/2 are both characterised by their i) P2Y-mediated activation based on their activation by UTP, ii) insensitivity to the P2 receptor antagonist PPADS and iii) requirement for functional gap junctions (Table 5.4). It could be speculated that the mechanism underlying those events are the same. However, gap junction mediated ERK1/2 spread occurred independently of intracellular Ca^{2+}, whereas the damage-induced current is likely a Ca^{2+}-activated Cl^- current; thus indicating that both events require gap junctions but are likely occurring independently of each other.

In contrast to the activation of ERK1/2 and the generation of damage-induced currents, the formation of the damage-induced Ca^{2+} wave was significantly reduced in the presence of PPADS. This indicates different underlying mechanisms. The

remainder of the Ca^{2+} wave was predominantly the fast Ca^{2+} wave (see section 3.5 and 3.6) that was proposed earlier to partially mediate ERK1/2 activation.

Spontaneous oscillations

Spontaneous oscillations of inward currents were observed when Deiters' cells maintained in their support cell syncytium were held at -90 mV. These currents were sensitive to PPADS suggesting that they result from the action of extracellular ATP or a nucleotide analogue on P2 receptors. This is the first observation of such ATP-induced spontaneous oscillations in Deiters' cells. Megakaryocytes exhibit spontaneous current oscillations. The frequency of these spontaneous oscillations is reduced in megakaryocytes harvested from both $P2X_1^{-/-}$ and $P2Y_1^{-/-}$ mice (Tolhurst et al., 2005). Similarly, these receptors could be employed by cochlear Deiters' cells to facilitate the spontaneous events.

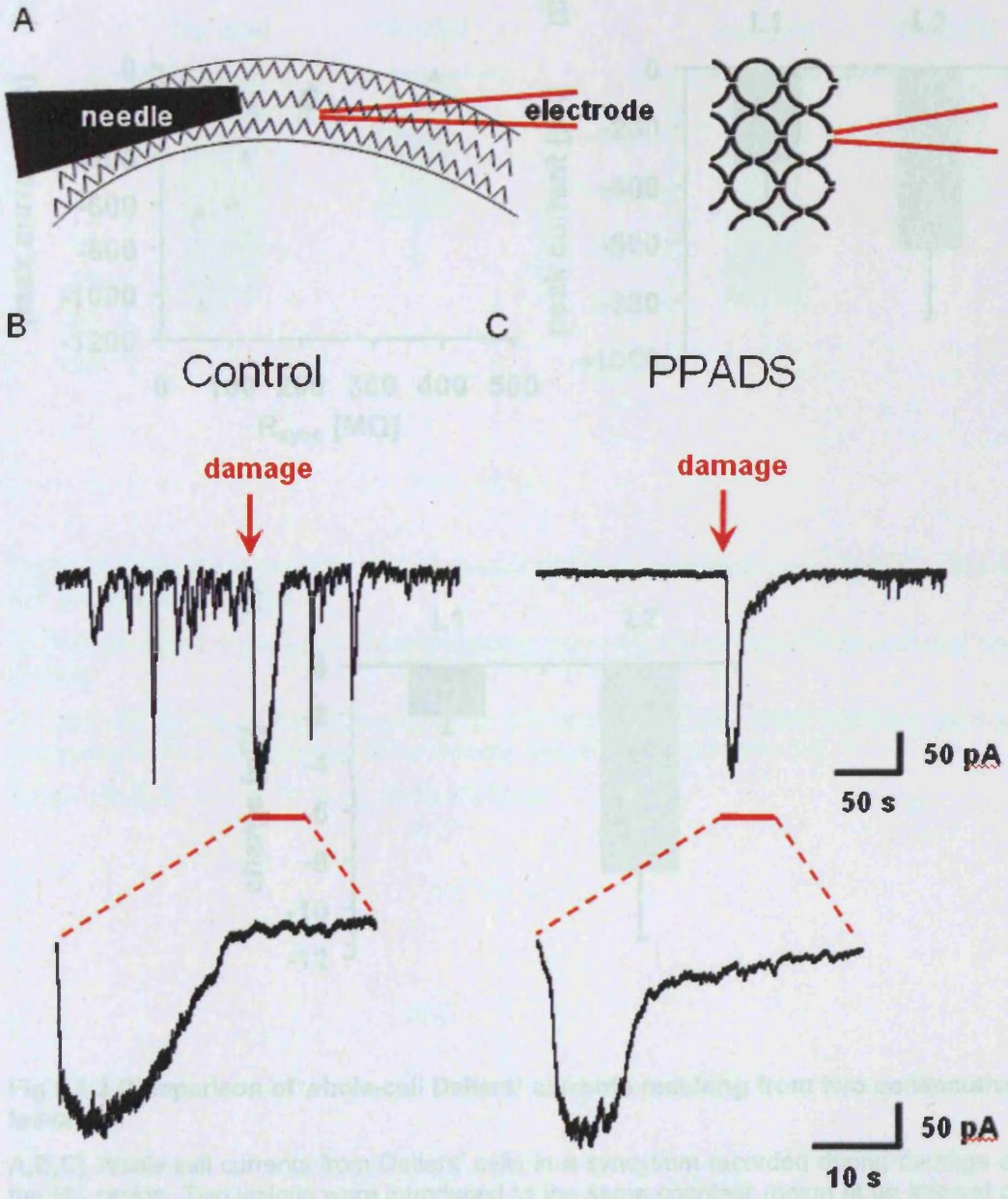

Fig 5.1.1 Damage-induced ionic currents in Deiters' cells.

A) Experimental layout,

Left panel: Damage to the HC region was induced using a microneedle. The patched Deiters' cell was situated 5 cells from the lesion site along the cochlear length.

Right panel: currents were recorded from a voltage-clamped Deiters' cell in a syncytium of support cells held at -90 mV.

B, C) Current traces of two Deiters' cells in a syncytium subjected to damage in **(B)** control (R_{sync} = 209 MΩ) and **(C)** 150 µM PPADS (R_{sync} = 254 MΩ).

Upper panel a 5 min trace that includes spontaneous inward currents and one damage. The arrow marks the time of damage.

Lower panel: higher temporal resolution of the damage-induced current.

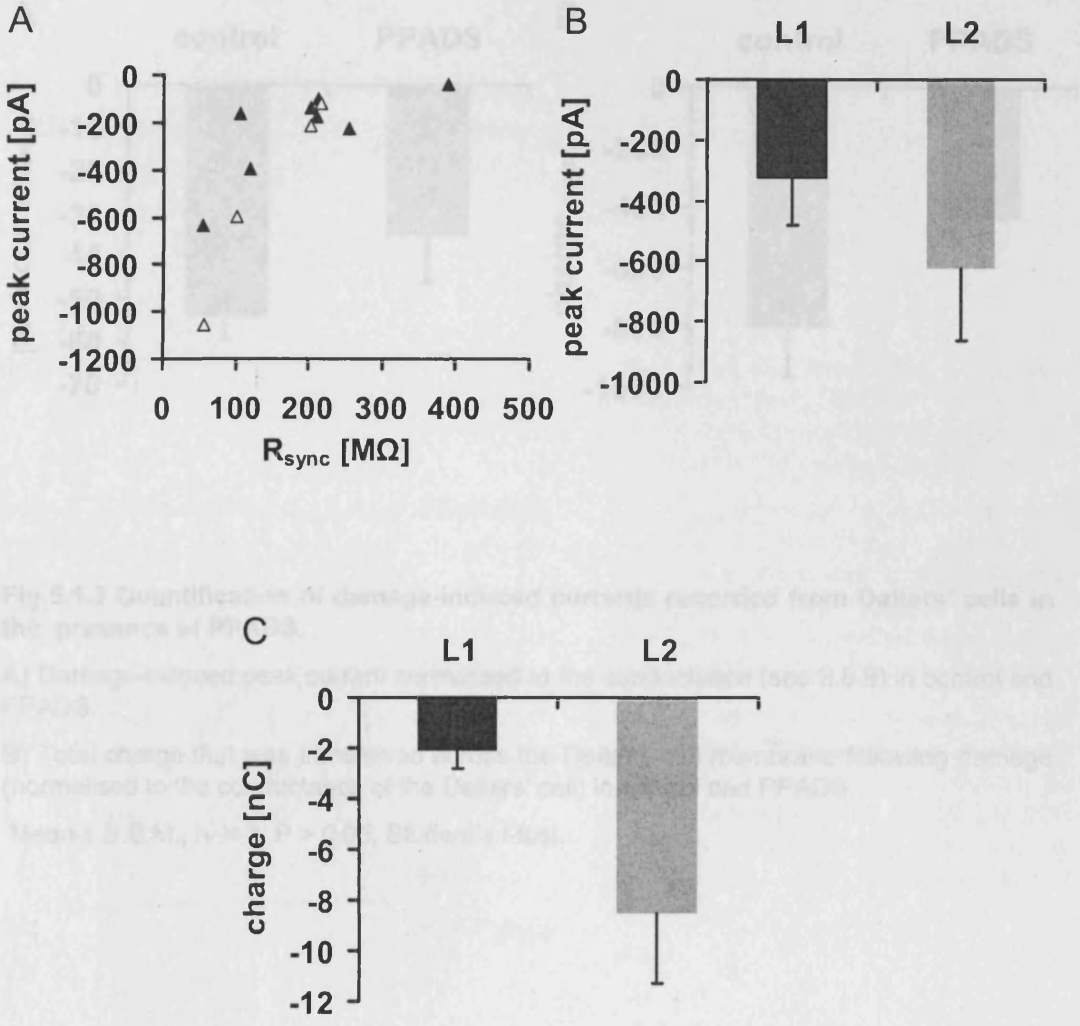

Fig 5.1.2 Comparison of whole-cell Deiters' currents resulting from two consecutive lesions.

A,B,C) Whole-cell currents from Deiters' cells in a syncytium recorded during damage of the HC region. Two lesions were introduced to the same cochlear region at an interval of 30 min.

A) Peak current of lesion 1 (closed triangle) and 2 (open triangle) as a function of R_{sync}.

B) Damage-induced peak current following lesion 1 (L1) and 2 (L2).

C) Total charge transferred following lesion 1 (L1) and 2 (L2).

Mean ± S.E.M., n = 12 for A, n = 3 for B, C

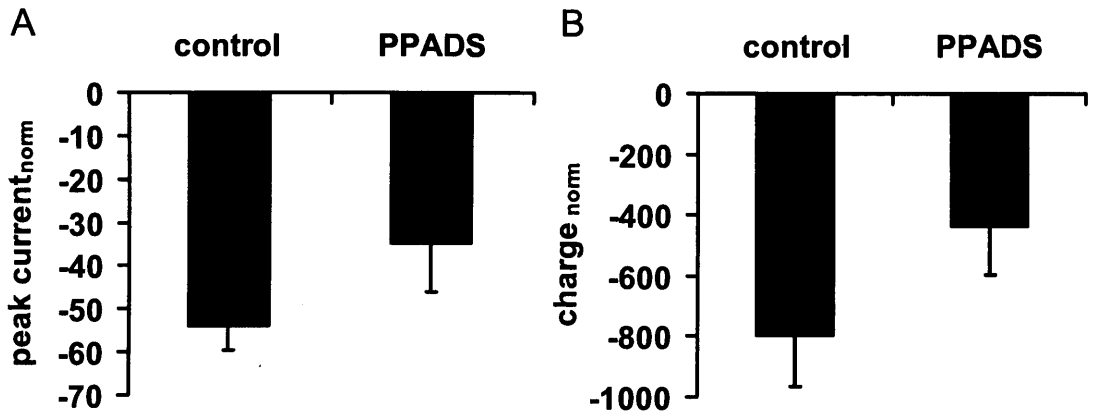

Fig 5.1.3 Quantification of damage-induced currents recorded from Deiters' cells in the presence of PPADS.

A) Damage-induced peak current normalised to the conductance (see 2.8.6) in control and PPADS.

B) Total charge that was transferred across the Deiters' cell membrane following damage (normalised to the conductance of the Deiters' cell) in control and PPADS.

Mean ± S.E.M., n = 3, P > 0.05, Student's *t*-test.

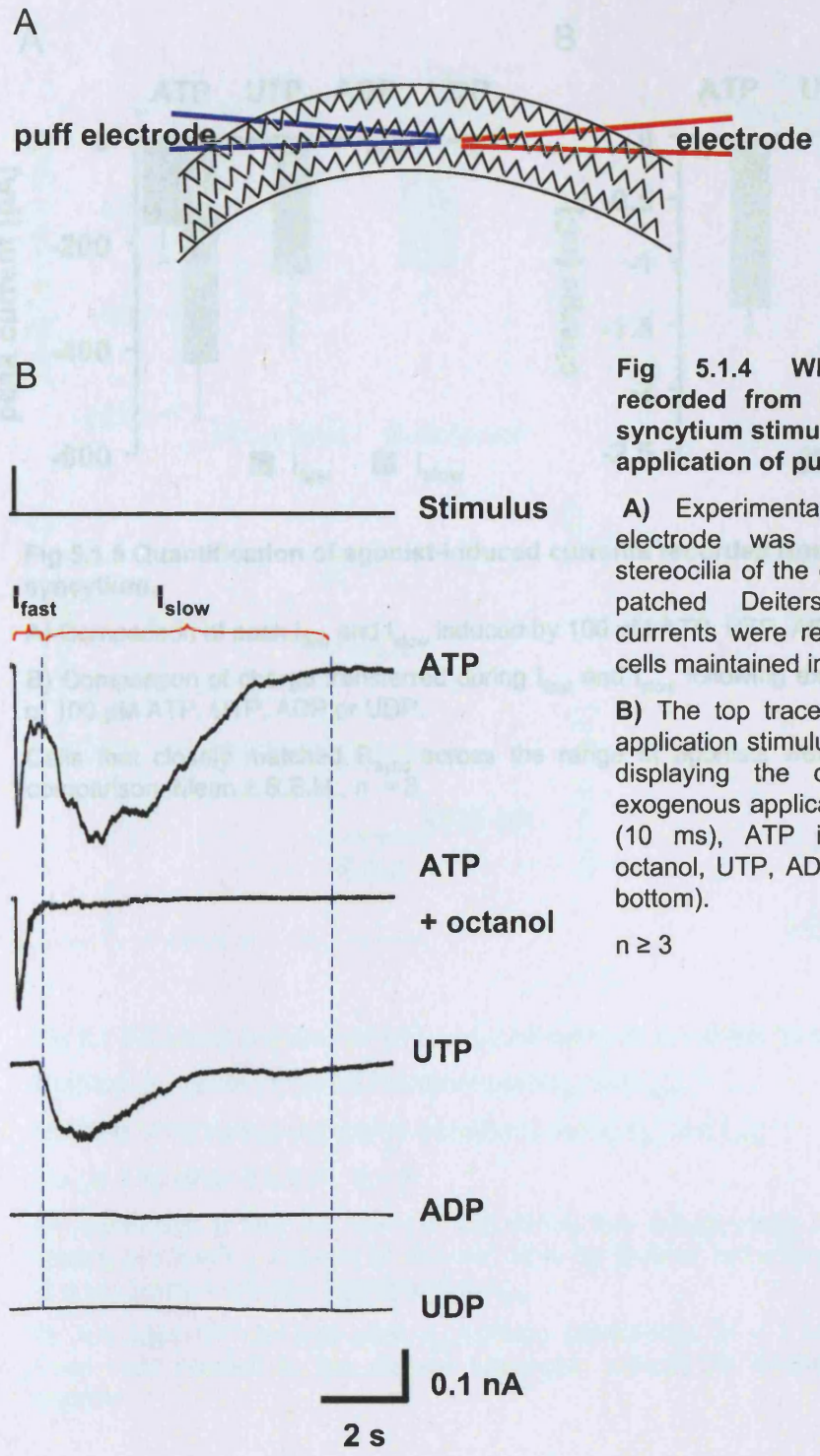

Fig 5.1.4 Whole-cell currents recorded from Deiters' cells in a syncytium stimulated by exogenous application of purinergic agonists.

A) Experimental layout: The puff electrode was placed above the stereocilia of the cell neighbouring the patched Deiters' cell. Whole-cell currrents were recorded from Deiters cells maintained in the syncytium.

B) The top trace represents the puff application stimulus followed by traces displaying the currents elicited by exogenous application of 100 µM ATP (10 ms), ATP in the presence of octanol, UTP, ADP, UDP (from top to bottom).

$n \geq 3$

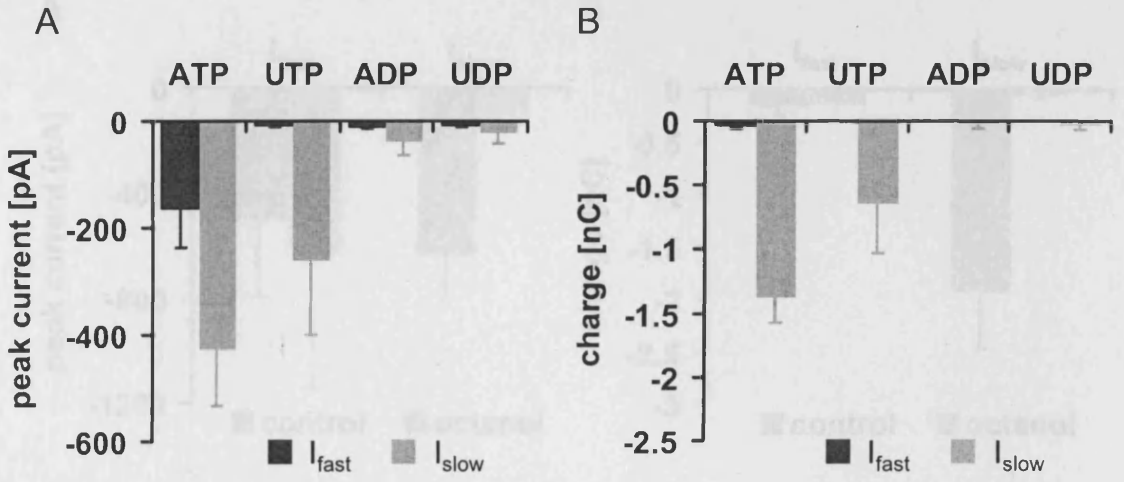

Fig 5.1.5 Quantification of agonist-induced currents recorded from Deiters' cells in a syncytium.

A) Comparison of peak I_{fast} and I_{slow} induced by 100 µM ATP, UTP, ADP or UDP.

B) Comparison of charge transferred during I_{fast} and I_{slow} following exogenous application of 100 µM ATP, UTP, ADP or UDP.

Cells that closely matched R_{sync} across the range of agonists were included into the comparison. Mean ± S.E.M., n = 3

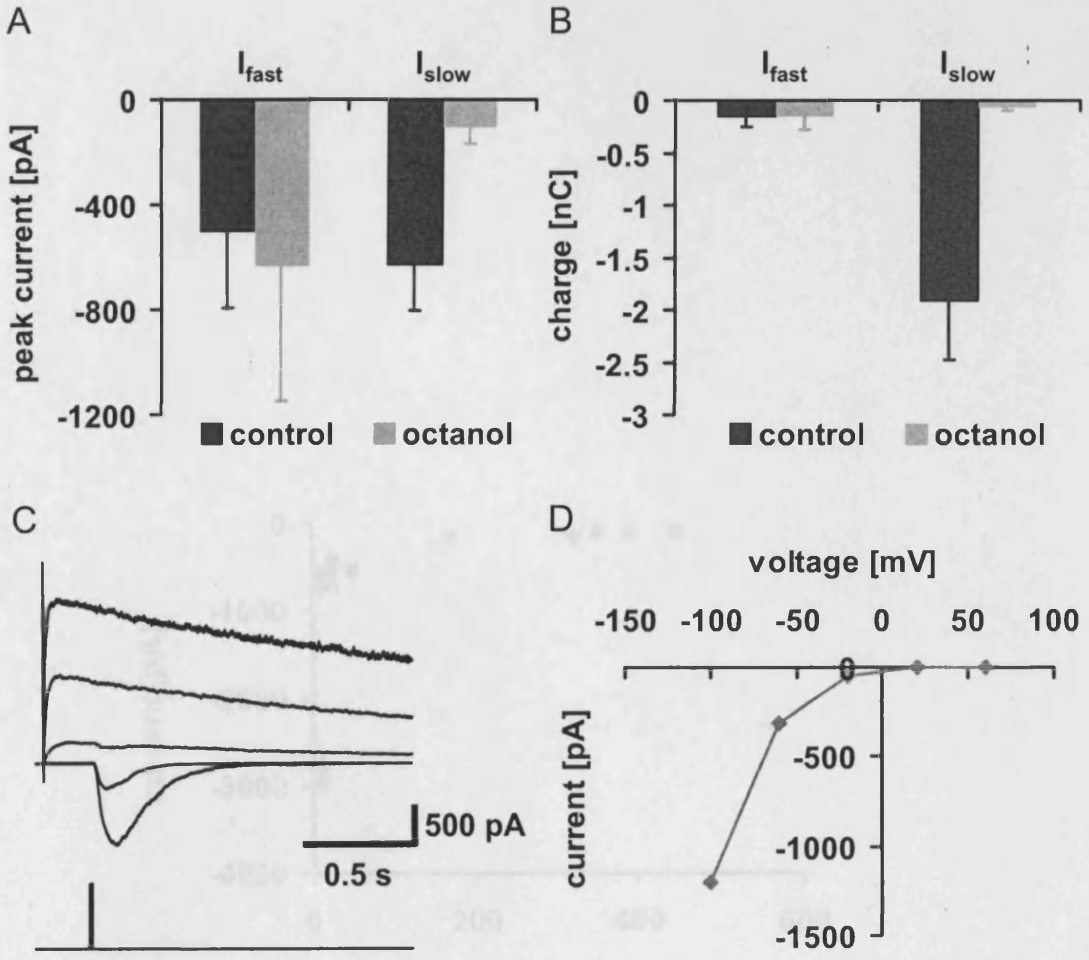

Fig 5.1.6 Characterisation of ATP-induced currents recorded from Deiters' cells.

A) Effect of octanol on the ATP-induced peak I_{fast} and I_{slow}.

B) Effect of octanol on the charge transferred during I_{fast} and I_{slow}.

For **(A & B)** Mean ± S.E.M., n = 3

C) Application of 100 µM ATP (10 ms) during five voltage-steps of 40 mV increments starting at a holding potential of -100 mV. Note the Deiters' cell uncoupled without addition of a gap junction inhibitor displayed only I_{fast}.

D) Averaged ATP-induced peak I_{fast}-voltage relationship. (n = 3 cells, 2 animals). The three cells included in the average uncoupled without the addition of a gap junction inhibitor.

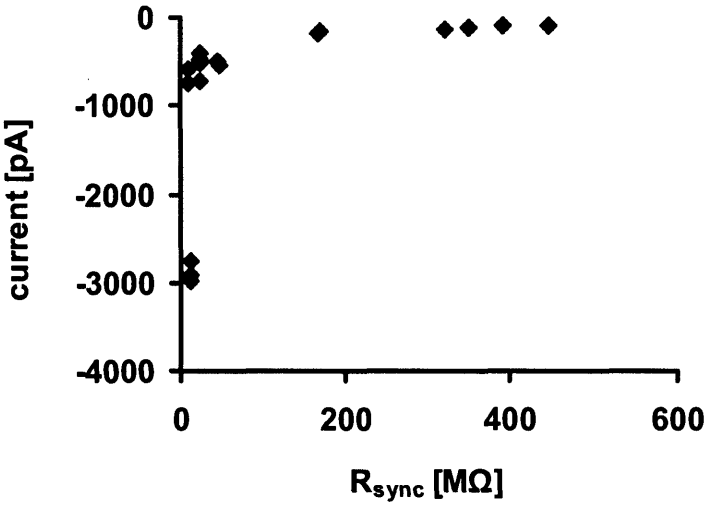

Fig 5.1.7 Dependency of UTP induced peak current on R_{sync}.

Peak current induced by exogenous application of UTP (100 µM) as a function of R_{sync}.

Fig 5.2.1 Expression of $P2Y_2$ and $P2Y_4$ receptors in rat cochlear explants.

A-F, G-L) Immunocytochemical labelling of cochlear explants with an antibody against **(A-F)** $P2Y_2$ or **(G-L)** $P2Y_4$ receptors.

A, B, G, H) Average of 20 confocal z-stack images (optical slice: 1.43 µm) displaying **(A)** $P2Y_2$ and **(G)** $P2Y_4$ receptor labelling or **(B, H respectively)** following pre-incubation with their specific peptide antigens.

C, D, I, J) Higher magnification single confocal images at the plane of **(C, I)** OHCs or **(D, J)**1st and 2nd row Deiters' cell nuclei. Inset in **(C)** x-z projection focused on IHC triple-labelled for $P2Y_2$ (green), synaptophysin (red) and nuclei (blue).

E, F, K, L) Average of 5 consecutive x-z projections labelled for **(E, K)** the respective P2Y receptors and **(F, L)** double-labelled with DAPI (blue).

Arrowheads in **(A, C)** point on labelling in synaptic region – likely afferent boutons; arrow in **(E)** indicates a Deiters' cell process. Scale bars, 50 µm in **(B, H)** for **(A,B,G,H)**; 10 µm in **(D,L)** for **(C-F, I-L)**.

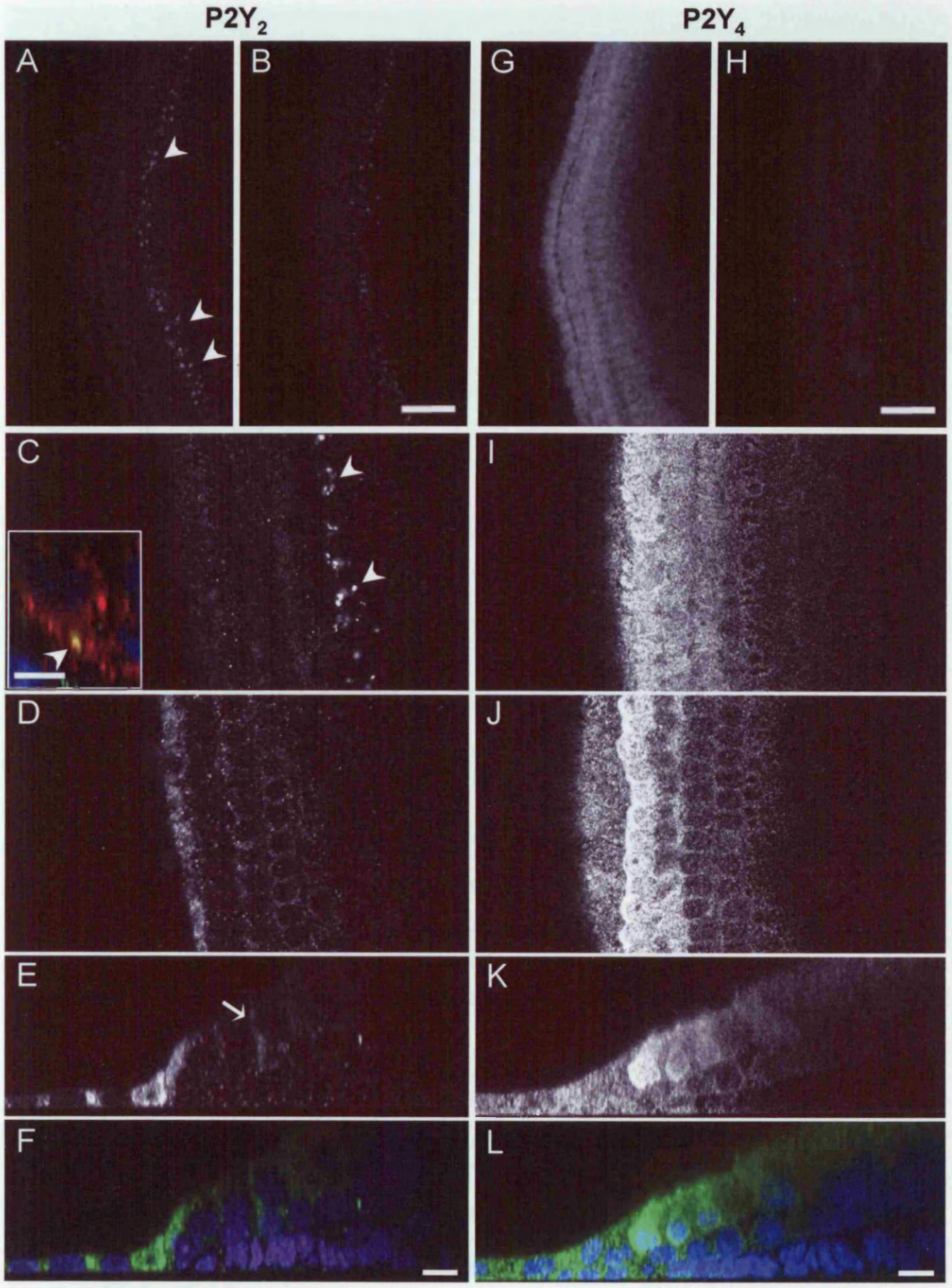
P2Y2
P2Y4
A
B
G
H
C
I
D
J
E
K
F
L

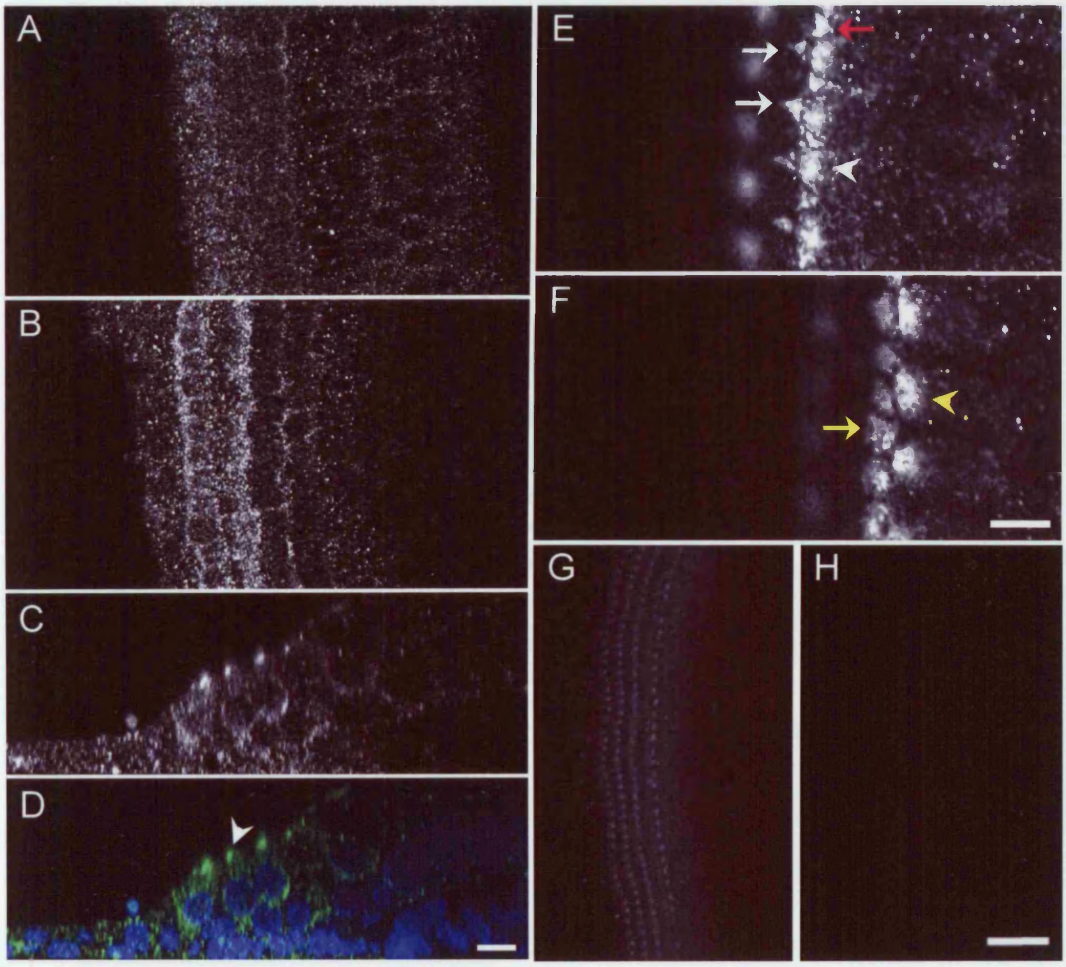

Fig 5.2.2 Expression of $P2Y_{11}$ receptors in rat cochlear explants.

A, B) Single confocal z-stack images of cochlear explants labeled with an antibody against $P2Y_{11}$ receptors at the plane of **(A)** OHC and **(B)** 1st and 2nd row Deiters' cell nuclei.

C, D) Average of 5 consecutive x-z projections of **(C)** $P2Y_{11}$ receptor expression and **(D)** double-labelled with DAPI (blue).

E, F) Higher resolution images of $P2Y_{11}$ at the plane of apical aspects of **(E)** 1st row OHCs and **(F)** IHCs.

G, H) Averages of 20 lower magnification confocal z-stack images (optical slice: 1.43 µm) of **(G)** $P2Y_{11}$ receptor labelling and **(H)** following pre-incubation with its specific peptide.

White arrowheads in **(D, E)** indicate apical aspects of OHCs, yellow arrowheads of IHCs **(F)**. White arrows indicate apical aspect of Deiters' cells **(E)**, pink arrow of outer pillar **(E)** and yellow arrow of inner piller cells **(F)** Scale bars, 10 µm in **(D)** for **(A-D)** & **(F)** for **(E,F)**; 50 µm in **(H)** for **(G+H)**.

Fig 5.2.3 Expression of $P2X_2$ and $P2X_3$ receptors in rat cochlear explants.

A-F, G-L) Immunocytochemical labelling of cochlear explants with an antibody against **(A-F)** $P2X_2$ or **(G-L)** $P2X_3$ receptors.

A, B, G, H) Average of 20 confocal z-stack images (optical slice 1.43 µm) displaying **(A)** $P2X_2$ and **(G)** $P2X_3$ receptor immuno-reactivity or **(B, H respectively)** when pre-incubated with their specific peptides

C-F, I-L) Single confocal images at higher magnification at the level of **(C, I)** OHCs or **(D, J)** 1st and 2nd row Deiters' cell nuclei.

E, F, K, L) x-z projections (average of 5) labelling **(E, K)** the respective P2X receptor and **(F, L)** double-labelled with DAPI (blue).

Arrow in **(E)** indicates Deiters' cell top. Arrowheads in **(G, I, J, L)** indicate potential neuronal fibres. Scale bars, 50 µm in **(B, H)** for **(A,B,G,H)**; 10 µm in **(F,L)** for **(C-F, I-L)**.

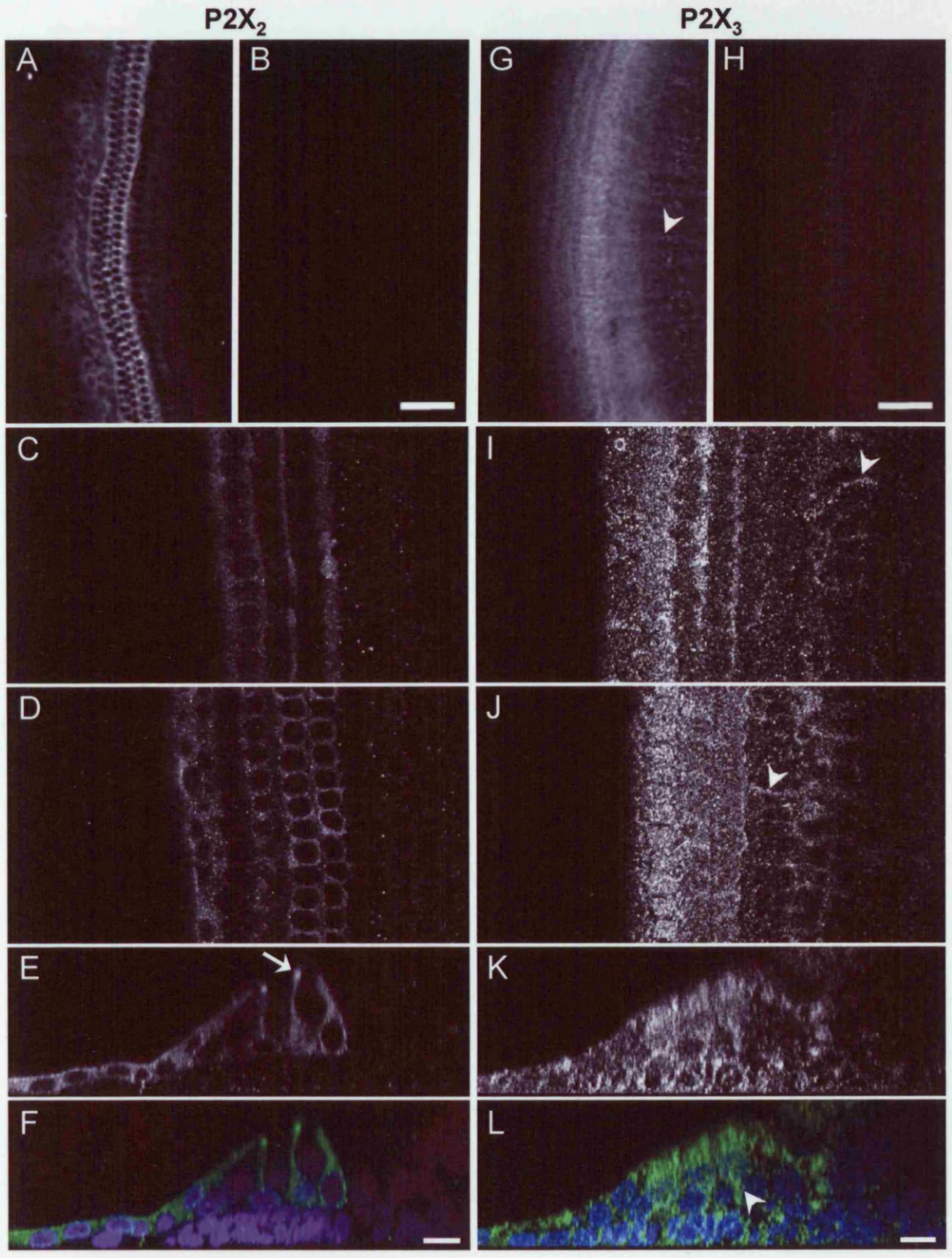
P2X2
P2X3
A
B
G
H
C
I
D
J
E
K
F
L

Fig 5.2.4 Expression of $P2X_4$ receptor and synaptophysin in rat cochlear explants.

A-G, H-K) Immunocytochemical labelling of cochlear explants with an antibody against **(A-G)** $P2X_4$ or **(H-K)** synaptophysin.

A, C) Average of 20 confocal z-stack images (optical slice: 1.43 µm) for **(A)** $P2X_4$ receptor immunoreactivity or **(C)** when pre-incubated with its specific peptide. **(B)** Average of 10 confocal z-stack images at the level of Hensen and Claudius-like cells labelling macrophages (arrow head).

D-G) Higher magnification single confocal images at the plane of **(D)** OHCs and **(E)** 1st and 2nd row Deiters' cell nuclei.

F, G) Average of 5 consecutive x-z projections of **(F)** $P2X_4$ receptors and **(G)** double-labelled with DAPI (blue).

H-K) Labelling of synaptophysin at similar planes as in (D-G).

Scale bars, 50 µm in **(C)**, for **(A-B)**; 10 µm in **(G, K)** for **(D-K)**.

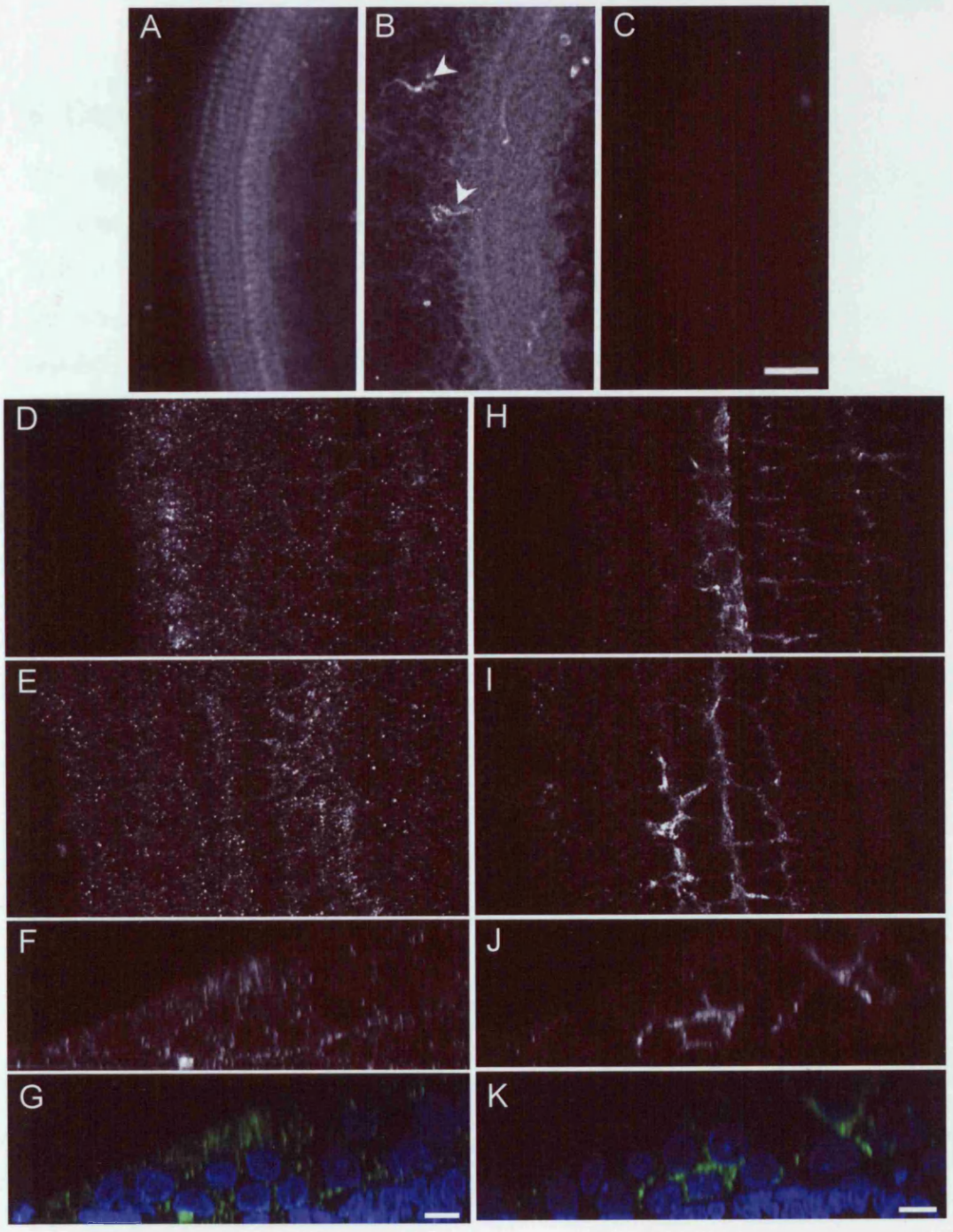
A
B
C
D
H
E
I
F
J
G
K

6. General Discussion

The experiments presented in this thesis address damage-induced signalling events in the neonatal rat cochlea. These events include: i) activation of ionic currents in Deiters' cells; ii) formation and propagation of intercellular Ca^{2+} waves into the distinct cochlear regions; iii) activation of ERK1/2 in Deiters' and phalangeal cells and iv) MEK1/2 dependent HC death that could involve the action of support cells. This general discussion will review the damage paradigms used and then attempt to establish a model of damage-induced signalling events in the mammalian cochlea.

Damage model

Acoustic overstimulation can either result in temporary or permanent threshold shifts depending on the magnitude of the sound stimulus. The most common cause of permanent threshold shifts is the death of sensory HCs (Nicotera et al., 2003; Wang et al., 2003a). Intense noise stimuli can result in the rupture of the HC epithelium (Wang et al., 2002b). In the present study the HC epithelium was mechanically damaged using a microneedle or an N_2-laser in order to investigate subsequent signalling pathways. The magnitude of damage induced using these *in vitro* techniques can be considered to represent the *in vivo* situation during the sorts of acoustic overstimulation leading to permanent threshold shifts and epithelial rupture. Thus, these damage models offer the opportunity to have precise timing enabling the study of signalling events that are short-lasting and are therefore unlikely to be detected *in vivo*. Moreover the interplay between different signalling cascades can be relatively easily assessed.

However, of course this model has limitations that might affect the signalling cascades. The apical and basal aspects of cochlear hair and support cells are exposed to distinct extracellular fluids – endolymph and perilymph, respectively. The ionic balance of these fluids is tightly regulated. The endolymph is characterised by high K^+ and low Ca^{2+} whereas the composition of the perilymph is similar to other extracellular fluids (high Na^+ and Ca^{2+} and low K^+). Using organotypic cochlear explants means that the apical aspects of cells are exposed to an extracellular fluid that is most similar to perilymph. P2 receptor responses, key elements of the

signalling cascades presented here, have been described to be modulated by high K^+ and Ca^{2+} (Ding and Sachs, 1999; Mammano et al., 1999; Ding and Sachs, 2000; Kanjhan et al., 2003; King and Townsend-Nicholson, 2003; Pitt et al., 2005). Thus depending on whether ATP acts at the apical or baso-lateral sites of cells the P2 receptor responses might be altered accordingly. It is worth noting that during excess damage *in vivo*, especially when the HC epithelium is ruptured the ionic gradient across the epithelium will not be maintained and P2 receptors in both apical and baso-lateral membranes of the cells are likely to experience similar conditions at the immediate site of damage.

Age of animal

The onset of hearing occurs in rats between P12 and P14 (Geal-Dor et al., 1993; Freeman et al., 1999). The early postnatal period up to the onset of hearing and even beyond is characterised by developmental restructuring of the cochlea and changes in various protein expression profiles. The key players – that enable damage-induced signalling, the propagation of a Ca^{2+} wave and activation of ERK1/2 are P2 receptors and gap junctions. The expression of both constituents of the damage-induced signalling cascade has been observed to be changed during the early postnatal period (Nikolic et al., 2003; Huang et al., 2005; Jagger and Forge, 2006). Although, the exact P2 receptors that mediate damage-signalling events in the rat cochlea are not known, it has to be considered that developmental changes of P2 receptor expression might alter the ability of the cells to induce the described signalling cascades.

The expression profile of connexins is also altered during postnatal development. At P0 coupling occurs between Deiters' cells. This is however not mediated by connexin 26 and 30, as these are not expressed at this stage. Protein expression of these connexins and thus heteromer formation is observed by P8 (Jagger and Forge, 2006). Gap junctions formed by different connexin subunits determine the nature of molecules that are enabled to pass.

Purinergic and damage-induced currents recorded from Deiters' cells

Application of ATP induced a biphasic current in Deiters' cells that were connected to their support cell syncytium: The current consisted of I_{fast}, a P2X receptor mediated

current, and I_{slow}, most likely a P2Y-mediated current. UTP activated I_{slow} but not I_{fast} suggesting; i) that functional $P2X_3$ receptors are not present at the apical aspects of Deiters' cells and ii) that I_{slow} is mediated by $P2Y_2$, $P2Y_4$ or $P2Y_{11}$ receptors. The magnitude of I_{slow} is dependent on the syncytial resistance and is therefore a property of the network of neighbouring cells. Taken together, data presented here and by Lagostena et al. (2001) indicate that I_{slow} is a P2Y receptor mediated Ca^{2+}-activated Cl^- current. I_{damage} was characterized by the absence of I_{fast} and by its dependency on R_{sync}, identical to UTP-induced I_{slow}. Thus I_{damage} is likely to be a P2Y receptor induced Ca^{2+} activated Cl^- current. The absence of I_{fast} indicates and absence of P2X receptor activation during damage. Unless I_{damage} resembles a current that is a merged response of I_{fast} and I_{slow}, a damage model has to be proposed that excludes P2X receptors.

Proposed model of damage-induced Ca^{2+} waves in the organ of Corti

Mechanical damage of the HC epithelium triggers the release of extracellular ATP which activates an intercellular Ca^{2+} wave that propagates into the distinct cochlear regions. The model in Fig 6.1 summarises specifically the mechanism resulting in Ca^{2+} wave propagation in the HC region where damage elicits two distinct intercellular Ca^{2+} waves. Different velocities, extent of spread and sources of Ca^{2+} distinguish the two intercellular Ca^{2+} waves. The slower Ca^{2+} wave depends upon IP_3-sensitive stores, whereas the faster wave requires extracellular Ca^{2+}. Combining analysis of Ca^{2+} signals activated by purinergic agonists with the observed restriction of the Ca^{2+} wave propagation in the presence of the P2 receptor antagonists suramin and PPADS implicates a role for $P2Y_{2,4}$ or $_{11}$ receptors. $P2Y_1$ and/or $P2Y_6$ receptors may also be involved, but to a lesser extent (see chapters 3.4 – 3.6). A requirement for extracellular Ca^{2+} to generate the faster Ca^{2+} wave suggests the involvement of ion channels and thus most likely of P2X receptors. However, in the presence of PPADS and suramin, which inhibit the majority of P2X receptors except for $P2X_4$, the faster Ca^{2+} wave was still observed. I_{damage} recorded from Deiters' cells resembles I_{slow} – the component of the ATP-activated current that is observed when UTP is applied. In contrast, an I_{fast}-like ATP-activated P2X current was not observed for I_{damage}. Taken together, the results of the patch-clamp and antagonist study indicate that P2X receptors are unlikely to be involved in damage-induced signalling and are thus not

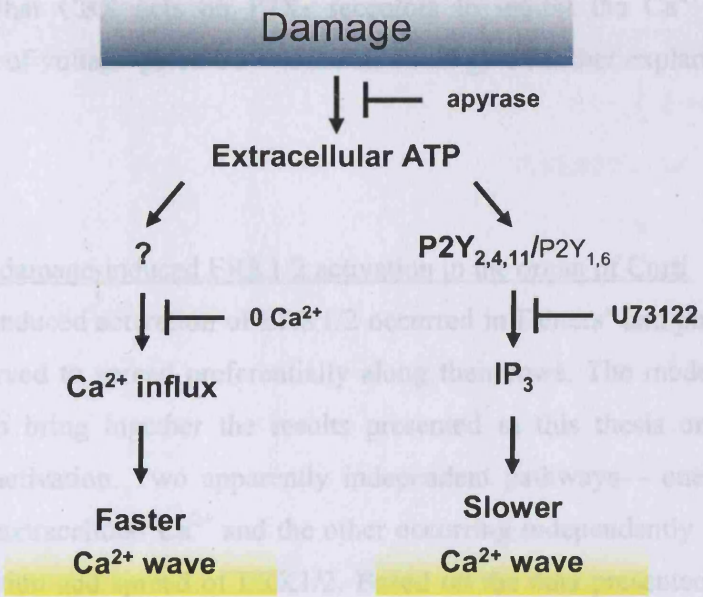

Fig 6.1 Model of damage-induced Ca^{2+} wave propagation in the HC region

Damage of the HC epithelium triggers the release of ATP that mediates the propagation of two Ca^{2+} waves. The question mark indicates a yet unknown mechanism that results in the formation of the faster Ca^{2+} wave.

the source for influx of extracellular Ca^{2+}. This raises the question to the nature of the mechanism that mediates the influx of extracellular Ca^{2+}.

Ca^{2+} wave propagation was also reduced in the presence of CBX. Assuming that CBX affects connexins this suggests an involvement of either functional hemichannels and/or gap junctions. The damage-induced Ca^{2+} wave was not further reduced when CBX treatment was combined with apyrase indicating that both substances act on the same underlying mechanism– that is the action of ATP. This hypothesis assumes that that apyrase is not 100 % efficient based on its i) enzymatic activity and ii) residual Ca^{2+} signals are recorded in the presence of apyrase. CBX might affect the release of ATP by connexin hemichannels, whereas apyrase degrades ATP. $P2X_7$ receptors and voltage-gated Ca^{2+} channels have also been described to be inhibited by CBX (Vessey et al., 2004; Suadicani et al., 2006). However, damage-induced $P2X_7$ receptor activation was excluded on the basis of the insensitivity of the fast Ca^{2+} wave, which requires Ca^{2+} entry, to PPADS. Thus, it is

unlikely that CBX acts on $P2X_7$ receptors to inhibit the Ca^{2+} wave. However, inhibition of voltage-gated Ca^{2+} channels could give another explanation of the effect of CBX.

Model of damage-induced ERK1/2 activation in the organ of Corti

Damage-induced activation of ERK1/2 occurred in Deiters' and phalangeal cells and was observed to spread preferentially along their rows. The model in Fig 6.2 is an attempt to bring together the results presented in this thesis on damage-induced ERK1/2 activation. Two apparently independent pathways – one that requires the influx of extracellular Ca^{2+} and the other occurring independently of Ca^{2+} – mediate the activation and spread of ERK1/2. Based on the data presented in this thesis the simplest explanation is that the Ca^{2+} dependent pathway is linked to the faster damage-induced Ca^{2+} wave mediated by influx of extracellular Ca^{2+}. The conclusion of a Ca^{2+}-independent pathway is based on interpretation of the effects of CBX and apyrase on both the damage-induced Ca^{2+} wave and the activation of ERK1/2. For ERK1/2 activation, CBX and apyrase were demonstrated to act synergistically to completely abolish its activation. In contrast, with respect to the damage-induced Ca^{2+} wave no synergistic action was observed. Taken together, these aspects suggest that CBX-sensitive ERK1/2 spread occurs independently of Ca^{2+}. CBX is a promiscuous drug that in addition to gap junctions also inhibits connexin hemichannels, $P2X_7$ receptors and voltage-gated Ca^{2+} channels (Vessey et al., 2004; Suadicani et al., 2006). All of these are effectively ion channels that allow Ca^{2+} influx. If CBX was active at these sites during damage a significant decrease in Ca^{2+} signals would be predicted. The latter was not observed and therefore an action of CBX at these channels can be ruled out. This leaves CBX activity at gap junctions as the most likely site for the Ca^{2+}-independent ERK activation signal.

In addition to the CBX-sensitive pathway the reduction of ERK1/2 spread in the presence of apyrase suggests that damage triggers the release of ATP that mediates the activation and spread of ERK1/2. Exogenous application of ATP and UTP

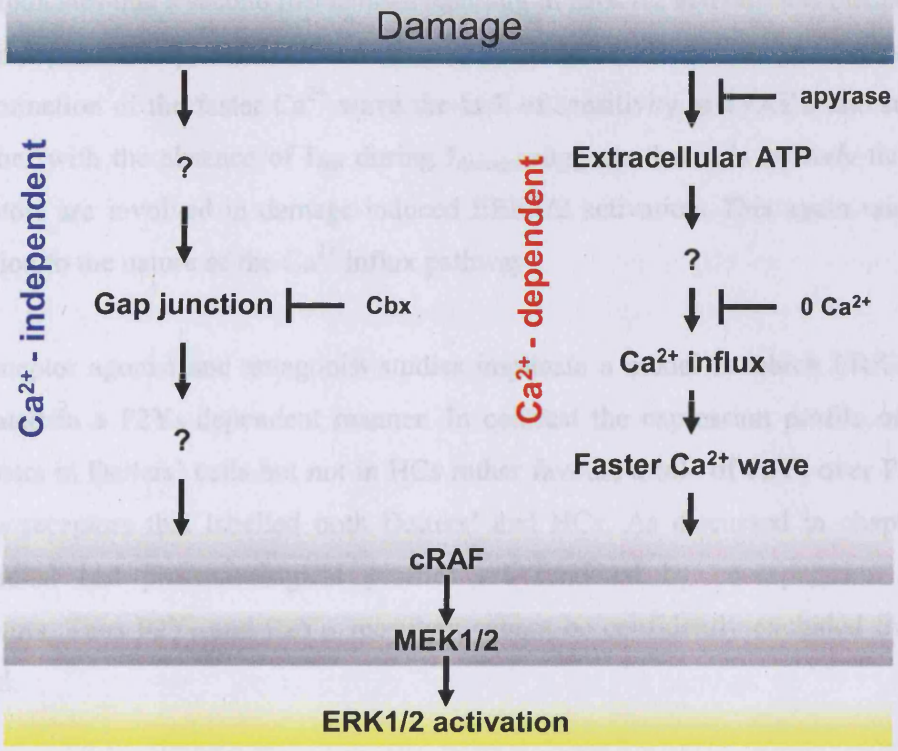

Fig 6.2 Model of the mechanism that results in damage-induced ERK1/2 activation

Two pathways mediate damage-induced ERK1/2 activation – one that requires extracellular Ca^{2+} (red) and the other occurring independently of Ca^{2+}. Question marks indicate yet unknown intermediate steps.

mimicked the damage-induced ERK1/2 activation pattern. First the focus will be turned to UTP – an agonist at $P2Y_2$, $P2Y_4$, $P2Y_{11}$, $P2X_3$ and its heteromer $P2X_{2/3}$ receptors (Nicholas et al., 1996; van der Weyden et al., 2000; Liu et al., 2001; White et al., 2003; Wildman et al., 2003). The absence of I_{fast} in response to UTP indicates that functional $P2X_3$ receptors are not present at apical aspects of Deiters' cells and therefore UTP-induced ERK1/2 activation is likely to be mediated by $P2Y_2$, $P2Y_4$ or $P2Y_{11}$. The lack of effect of suramin implicates a model in which ERK1/2 are activated in a $P2Y_4$ dependent manner.

The comparison of intensity levels of activated ERK1/2 induced by ATP to that induced by UTP suggest that ATP might activate an additional P2 receptor resulting in increased ERK1/2 activation compared to UTP. As ADP did not elicit ERK1/2 activation other ATP-sensitive, but UTP-insensitive P2Y receptors can be excluded.

This indicates that a second mechanism resulting in ERK1/2 activation is mediated by P2X receptors except for UTP-sensitive $P2X_3$ receptors. However, as discussed for the formation of the faster Ca^{2+} wave the lack of sensitivity to PPADS and suramin together with the absence of I_{fast} during I_{damage} suggests that it is *unlikely* that P2X receptors are involved in damage-induced ERK1/2 activation. This again raises the question to the nature of the Ca^{2+} influx pathway.

P2 receptor agonist and antagonist studies implicate a model in which ERK1/2 are activated in a $P2Y_4$ dependent manner. In contrast the expression profile of $P2Y_2$ receptors in Deiters' cells but not in HCs rather favours a role of $P2Y_2$ over $P2Y_4$ or $P2Y_{11}$ receptors that labelled both Deiters' and HCs. As discussed in chapter 4.3 functional and pharmacological profiles are rendered by co-expression of P2 receptors. Thus $P2Y_2$ and $P2Y_{11}$ receptors cannot be confidently excluded from the model.

ERK1/2 spread is proposed to be mediated via two mechanisms - one that requires the release of extracellular ATP and the subsequent influx of extracellular Ca^{2+} and the other occurring independently of Ca^{2+} but in a gap junction dependent manner. P2Y receptor activation is also suggested to activate ERK1/2. However, it is not possible to conclude from the data presented here, through which of the two described pathways P2Y receptors mediate ERK1/2 activation. It is also possible that P2Y receptor activation is a third mechanism in addition to the two discussed pathways. Similarly, if it is assumed that apyrase cannot eliminate an excess of released ATP the activation of P2 receptors could potentially also be upstream of the gap junction mediated ERK1/2 spread. Thus, P2Y receptors could be the initiators of a signal that passes through gap junctions to mediate ERK1/2 activation and spread. The suggestion is that this would be a Ca^{2+} independent process, which finds support in the lack effect of BAPTA-AM in reducing the spread of ERK1/2.

Inhibition of cRAF almost completely abolished and that of MEK1/2 prevented ERK1/2 activation (shown in section 4.3). These data indicate that all of the ERK1/2 activation pathways described resulted from the hierarchical activation of cRAF and MEK1/2.

When the aminoglycoside neomycin was used to specifically target HCs, ERK1/2 activation was also observed in Deiters' and phalangeal cells. In the majority of cases those Deiters' and phalangeal cells that activated ERK1/2 surrounded pyknotic HC nuclei. Combining ERK1/2 activation data from different models suggests that in the immature rat cochlea, the activation of ERK1/2 in support cells surrounding damaged HCs is a common damage signalling mechanism. Further to this: recent work in the laboratory has shown that in chick utricles a similar support cell specific activation pattern was observed (Bird, 2007). Given a similar cell type specific activation pattern of ERK1/2 activation during aminoglycoside-induced HC toxicity to that following mechanical damage it is very likely that the underlying mechanisms are also similar if not the same (see model in Fig 6.2).

ATP and P2 receptors – key signalling elements during HC damage

The data presented here advance the understanding of damage-induced signalling mechanisms in the mammalian cochlea. In particular, two further events activated by damage have been attributed to the release and action of extracellular ATP which consolidates evidence by various groups that ATP is a key signalling molecule during HC damage (Munoz et al., 1995; Munoz et al., 2001; Gale et al., 2004; Zhao et al., 2005). Moreover, different processes activated by ATP during damage have been demonstrated herein to be interlinked – the damage-induced fast Ca^{2+} wave and ERK1/2 activation and also most likely the damage-induced current and the slower Ca^{2+} wave. Linkage of the latter processes is based on combining data presented here with those of Lagostena et al. (2001) suggesting that the damage-induced current is a Cl^- current activated by IP_3 mediated release of Ca^{2+} from intracellular stores. This links the damage-induced slow Ca^{2+} wave and the damage-induced current.

This study not only extended data on P2 receptor expression profiles especially for $P2Y_{2,4,11}$ and $P2X_4$ receptors but also narrowed the number of potential candidates that mediate damage-induced ERK1/2 activation and Ca^{2+} wave formation. However, questions unable to be answered by this research were the nature of the mechanism that facilitates the fast Ca^{2+} wave by extracellular Ca^{2+} and how the subsequent

activation of ERK1/2 occurs. The conundrum to the mechanisms underlying will have to be tackled in the future.

The role of connexins/gap junctions in damage-induced signalling

In this thesis gap junctions were demonstrated to contribute to the damage-induced ERK1/2 activation (see damage model for ERK1/2 activation). The nature of the signal that passes through gap junctions to mediate ERK1/2 activation is not yet known, although likely candidates are IP_3, cAMP or cGMP (Bevans et al., 1998; Ayad et al., 2006; Bedner et al., 2006). Gap junctions also allowed the coupling of ion fluxes between cells in the support cell syncytium. Taken together these data strengthen a role for gap junctions to signal an impaired cochlear integrity to neighbouring cells.

Connexin hemichannels have been suggested to release ATP (Stout et al., 2002; Pearson et al., 2005; Zhao et al., 2005). In contrast to their effects on ERK1/2 activation, CBX and apyrase did not act synergistically to reduce the Ca^{2+} wave propagation in the HC region. However, CBX alone was effective to decrease the Ca^{2+} wave formation suggesting that both apyrase and CBX act on the same underlying mechanism which is the action of ATP. Thus CBX might exert its effect on connexin hemichannels. However, voltage-gated Ca^{2+} channels cannot be excluded.

Cell specific damage responses

A critical observation is the cell type specificity of the Ca^{2+} wave. Two distinct Ca^{2+} waves were observed along the HC region. An explanation for the observation is that they originate from different cell types in the HC region i.e. HCs and Deiters' cells. Another cell type specific pattern was seen with the damage-induced activation of ERK1/2 in Deiters' and phalangeal cells. The majority of recent studies aiming at understanding signalling pathways involved in HC death revealed activation or specific expression in HCs (Pirvola et al., 2000; Matsui et al., 2004) or used techniques, such as Western blotting, that do not distinguish cell type specific responses. Here, it was shown that clusters of support cells surrounding pyknotic HC

nuclei but not HCs themselves activate ERK1/2, implicating a specific function in these cells during damage.

MEK1/2 dependent HC death mediated by support cells

In an attempt to understand the role that ERK1/2 activation might play MEK1/2 were inhibited during aminoglycoside-induced HC toxicity. MEK1/2 inhibition resulted in the reduction of HC death. The implication of these data is that activation of ERK1/2 in support cells can promote HC death, implying that support cells play an active role in HC death (see model 6.3).

In chapter 4.3 two potential mechanisms were put forward. Firstly, ERK1/2 might cause the release of a molecule that stimulates HC death and secondly, ERK1/2 might activate a wound repair program that triggers support cells to engulf HCs. There is some evidence in the literature that suggests that this can occur (Forge and Li, 2000; Gale et al., 2002; Abrashkin et al., 2006) and recent data from this lab has confirmed this in chick utricular epithelium (Bird, 2007). At least two modes of ERK1/2 activation were described in chapter 4. It is possible that more than one mechanism is engaged in order to assure the execution of damaged HCs in case of failure of one of these pathways.

However, MEK1/2 inhibition only protected HCs temporarily. In agreement with data by Battaglia et al. (2003) inhibition of MEK1/2 over extended periods was observed to mediate HC death without any toxic insult. It is likely that ERK1/2 act as survival signals in HCs in this case. Thus the protective effect resulting from inhibition of support cell actions could have been counteracted by a missing pro-survival signal in HCs. A cell specific knock down approach would be required to determine whether this signalling pathway is a major pathway for promoting HC death. This knowledge would indicate whether this cascade is of potential therapeutic value. A greater understanding of the signals activated both upstream and downstream could reveal potential therapeutic strategies for the future.

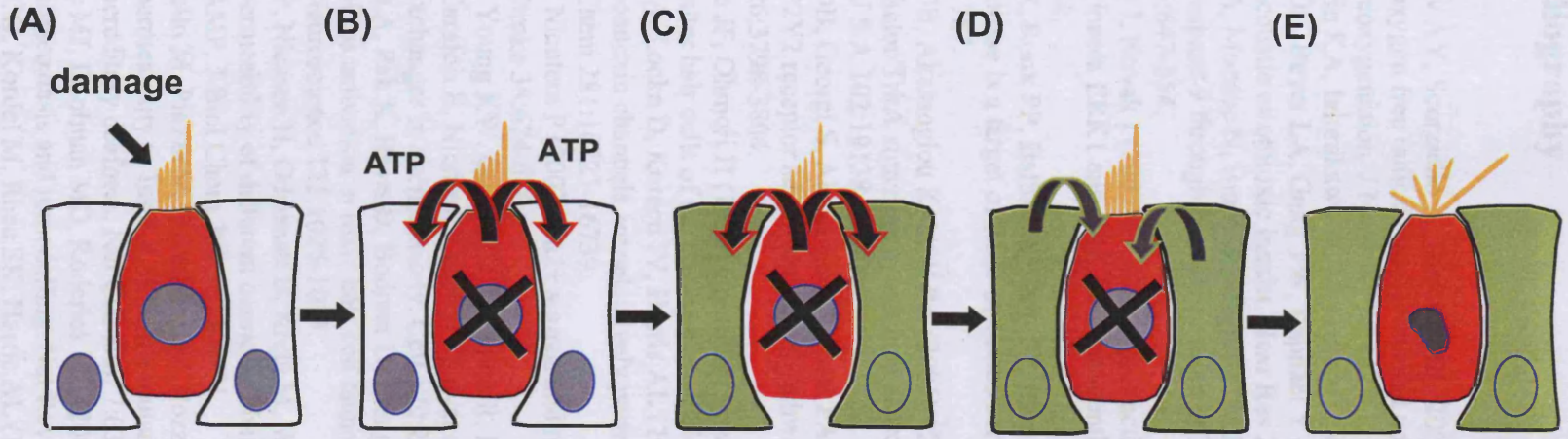

Fig 6.3 Model of HC-support cell interaction in response to damage

(A) Damage to HCs triggers them to **(B)** signal their impaired integrity (cross on top of nuclei) to their neighbouring support cells, likely through release of ATP.

(C) Support cells respond with activation of ERK1/2 that then **(D)** triggers the support cells to exert an effect on HCs (release of a death inducing molecule or migration).

(E) Subsequently HCs die.

7. Bibliography

Abramov AY, Scorziello A, Duchen MR (2007) Three distinct mechanisms generate oxygen free radicals in neurons and contribute to cell death during anoxia and reoxygenation. J Neurosci 27:1129-1138.

Abrashkin KA, Izumikawa M, Miyazawa T, Wang CH, Crumling MA, Swiderski DL, Beyer LA, Gong TW, Raphael Y (2006) The fate of outer hair cells after acoustic or ototoxic insults. Hear Res 218:20-29.

Allan LA, Morrice N, Brady S, Magee G, Pathak S, Clarke PR (2003) Inhibition of caspase-9 through phosphorylation at Thr 125 by ERK MAPK. Nat Cell Biol 5:647-654.

Amstrup J, Novak I (2003) P2X7 receptor activates extracellular signal-regulated kinases ERK1 and ERK2 independently of Ca2+ influx. Biochem J 374:51-61.

Anjum R, Roux PP, Ballif BA, Gygi SP, Blenis J (2005) The tumor suppressor DAP kinase is a target of RSK-mediated survival signaling. Curr Biol 15:1762-1767.

Arthur DB, Akassoglou K, Insel PA (2005) P2Y2 receptor activates nerve growth factor/TrkA signaling to enhance neuronal differentiation. Proc Natl Acad Sci U S A 102:19138-19143.

Arthur DB, Georgi S, Akassoglou K, Insel PA (2006) Inhibition of apoptosis by P2Y2 receptor activation: novel pathways for neuronal survival. J Neurosci 26:3798-3804.

Ashmore JF, Ohmori H (1990) Control of intracellular calcium by ATP in isolated outer hair cells of the guinea-pig cochlea. J Physiol 428:109-131.

Ayad WA, Locke D, Koreen IV, Harris AL (2006) Heteromeric, but not homomeric, connexin channels are selectively permeable to inositol phosphates. J Biol Chem 281:16727-16739.

Bano D, Nicotera P (2007) Ca2+ signals and neuronal death in brain ischemia. Stroke 38:674-676.

Bano D, Young KW, Guerin CJ, Lefeuvre R, Rothwell NJ, Naldini L, Rizzuto R, Carafoli E, Nicotera P (2005) Cleavage of the plasma membrane Na+/Ca2+ exchanger in excitotoxicity. Cell 120:275-285.

Battaglia A, Pak K, Brors D, Bodmer D, Frangos JA, Ryan AF (2003) Involvement of ras activation in toxic hair cell damage of the mammalian cochlea. Neuroscience 122:1025-1035.

Bedner P, Niessen H, Odermatt B, Kretz M, Willecke K, Harz H (2006) Selective permeability of different connexin channels to the second messenger cyclic AMP. J Biol Chem 281:6673-6681.

Beltramello M, Piazza V, Bukauskas FF, Pozzan T, Mammano F (2005) Impaired permeability to Ins(1,4,5)P3 in a mutant connexin underlies recessive hereditary deafness. Nat Cell Biol 7:63-69.

Berridge MJ, Bootman MD, Roderick HL (2003) Calcium signalling: dynamics, homeostasis and remodelling. Nat Rev Mol Cell Biol 4:517-529.

Bevans CG, Kordel M, Rhee SK, Harris AL (1998) Isoform composition of connexin channels determines selectivity among second messengers and uncharged molecules. J Biol Chem 273:2808-2816.

Bianchi BR, Lynch KJ, Touma E, Niforatos W, Burgard EC, Alexander KM, Park HS, Yu H, Metzger R, Kowaluk E, Jarvis MF, van Biesen T (1999) Pharmacological characterization of recombinant human and rat P2X receptor subtypes. Eur J Pharmacol 376:127-138.

Bird JE (2007) Epithelial wound repair in avian hair cell epithelia. PhD thesis.

Bobanovic LK, Royle SJ, Murrell-Lagnado RD (2002) P2X receptor trafficking in neurons is subunit specific. J Neurosci 22:4814-4824.

Boettger T, Hubner CA, Maier H, Rust MB, Beck FX, Jentsch TJ (2002) Deafness and renal tubular acidosis in mice lacking the K-Cl co-transporter Kcc4. Nature 416:874-878.

Boitier E, Rea R, Duchen MR (1999) Mitochondria exert a negative feedback on the propagation of intracellular Ca2+ waves in rat cortical astrocytes. J Cell Biol 145:795-808.

Bonni A, Brunet A, West AE, Datta SR, Takasu MA, Greenberg ME (1999) Cell survival promoted by the Ras-MAPK signaling pathway by transcription-dependent and -independent mechanisms. Science 286:1358-1362.

Bowler JW, Bailey RJ, North RA, Surprenant A (2003) P2X4, P2Y1 and P2Y2 receptors on rat alveolar macrophages. Br J Pharmacol 140:567-575.

Brandes RP, Popp R, Ott G, Bredenkotter D, Wallner C, Busse R, Fleming I (2002) The extracellular regulated kinases (ERK) 1/2 mediate cannabinoid-induced inhibition of gap junctional communication in endothelial cells. Br J Pharmacol 136:709-716.

Brandle U, Zenner HP, Ruppersberg JP (1999) Gene expression of P2X-receptors in the developing inner ear of the rat. Neurosci Lett 273:105-108.

Brandle U, Spielmanns P, Osteroth R, Sim J, Surprenant A, Buell G, Ruppersberg JP, Plinkert PK, Zenner HP, Glowatzki E (1997) Desensitization of the P2X(2) receptor controlled by alternative splicing. FEBS Lett 404:294-298.

Brandt A, Khimich D, Moser T (2005) Few CaV1.3 channels regulate the exocytosis of a synaptic vesicle at the hair cell ribbon synapse. J Neurosci 25:11577-11585.

Braun S, Hanselmann C, Gassmann MG, auf dem Keller U, Born-Berclaz C, Chan K, Kan YW, Werner S (2002) Nrf2 transcription factor, a novel target of keratinocyte growth factor action which regulates gene expression and inflammation in the healing skin wound. Mol Cell Biol 22:5492-5505.

Buell G, Lewis C, Collo G, North RA, Surprenant A (1996) An antagonist-insensitive P2X receptor expressed in epithelia and brain. Embo J 15:55-62.

Chan K, Han XD, Kan YW (2001) An important function of Nrf2 in combating oxidative stress: detoxification of acetaminophen. Proc Natl Acad Sci U S A 98:4611-4616.

Chao CC, Hu S, Molitor TW, Shaskan EG, Peterson PK (1992) Activated microglia mediate neuronal cell injury via a nitric oxide mechanism. J Immunol 149:2736-2741.

Chardin S, Romand R (1995) Regeneration and mammalian auditory hair cells. Science 267:707-711.

Charles AC, Merrill JE, Dirksen ER, Sanderson MJ (1991) Intercellular signaling in glial cells: calcium waves and oscillations in response to mechanical stimulation and glutamate. Neuron 6:983-992.

Chen C, Bobbin RP (1998) P2X receptors in cochlear Deiters' cells. Br J Pharmacol 124:337-344.

Chen C, Parker MS, Barnes AP, Deininger P, Bobbin RP (2000) Functional expression of three P2X(2) receptor splice variants from guinea pig cochlea. J Neurophysiol 83:1502-1509.

Chen CH, Wang WJ, Kuo JC, Tsai HC, Lin JR, Chang ZF, Chen RH (2005) Bidirectional signals transduced by DAPK-ERK interaction promote the apoptotic effect of DAPK. Embo J 24:294-304.

Cheng AG, Cunningham LL, Rubel EW (2003) Hair cell death in the avian basilar papilla: characterization of the in vitro model and caspase activation. J Assoc Res Otolaryngol 4:91-105.

Chessell IP, Michel AD, Humphrey PP (1998) Effects of antagonists at the human recombinant P2X7 receptor. Br J Pharmacol 124:1314-1320.

Churchill GC, Okada Y, Thomas JM, Genazzani AA, Patel S, Galione A (2002) NAADP mobilizes Ca(2+) from reserve granules, lysosome-related organelles, in sea urchin eggs. Cell 111:703-708.

Communi D, Robaye B, Boeynaems JM (1999) Pharmacological characterization of the human P2Y11 receptor. Br J Pharmacol 128:1199-1206.

Cook SJ, McCormick F (1993) Inhibition by cAMP of Ras-dependent activation of Raf. Science 262:1069-1072.

Cook SJ, Beltman J, Cadwallader KA, McMahon M, McCormick F (1997) Regulation of mitogen-activated protein kinase phosphatase-1 expression by extracellular signal-related kinase-dependent and Ca2+-dependent signal pathways in Rat-1 cells. J Biol Chem 272:13309-13319.

Cook SP, McCleskey EW (2002) Cell damage excites nociceptors through release of cytosolic ATP. Pain 95:41-47.

Corbit KC, Soh JW, Yoshida K, Eves EM, Weinstein IB, Rosner MR (2000) Different protein kinase C isoforms determine growth factor specificity in neuronal cells. Mol Cell Biol 20:5392-5403.

Corwin JT, Cotanche DA (1988) Regeneration of sensory hair cells after acoustic trauma. Science 240:1772-1774.

Cowley S, Paterson H, Kemp P, Marshall CJ (1994) Activation of MAP kinase kinase is necessary and sufficient for PC12 differentiation and for transformation of NIH 3T3 cells. Cell 77:841-852.

Cunningham LL, Cheng AG, Rubel EW (2002) Caspase activation in hair cells of the mouse utricle exposed to neomycin. J Neurosci 22:8532-8540.

Cunningham LL, Matsui JI, Warchol ME, Rubel EW (2004) Overexpression of Bcl-2 prevents neomycin-induced hair cell death and caspase-9 activation in the adult mouse utricle in vitro. J Neurobiol 60:89-100.

Dakin K, Zhao Y, Li WH (2005) LAMP, a new imaging assay of gap junctional communication unveils that Ca2+ influx inhibits cell coupling. Nat Methods 2:55-62.

Dehne N, Rauen U, de Groot H, Lautermann J (2002) Involvement of the mitochondrial permeability transition in gentamicin ototoxicity. Hear Res 169:47-55.

Dhillon AS, Hagan S, Rath O, Kolch W (2007) MAP kinase signalling pathways in cancer. Oncogene 26:3279-3290.

Ding D, Stracher A, Salvi RJ (2002) Leupeptin protects cochlear and vestibular hair cells from gentamicin ototoxicity. Hear Res 164:115-126.

Ding S, Sachs F (1999) Ion permeation and block of P2X(2) purinoceptors: single channel recordings. J Membr Biol 172:215-223.

Ding S, Sachs F (2000) Inactivation of P2X2 purinoceptors by divalent cations. J Physiol 522 Pt 2:199-214.

Dulon D, Moataz R, Mollard P (1993) Characterization of Ca2+ signals generated by extracellular nucleotides in supporting cells of the organ of Corti. Cell Calcium 14:245-254.

Dumont RA, Lins U, Filoteo AG, Penniston JT, Kachar B, Gillespie PG (2001) Plasma membrane Ca2+-ATPase isoform 2a is the PMCA of hair bundles. J Neurosci 21:5066-5078.

Evans RJ, Lewis C, Virginio C, Lundstrom K, Buell G, Surprenant A, North RA (1996) Ionic permeability of, and divalent cation effects on, two ATP-gated cation channels (P2X receptors) expressed in mammalian cells. J Physiol 497 (Pt 2):413-422.

Farnsworth CL, Freshney NW, Rosen LB, Ghosh A, Greenberg ME, Feig LA (1995) Calcium activation of Ras mediated by neuronal exchange factor Ras-GRF. Nature 376:524-527.

Favata MF, Horiuchi KY, Manos EJ, Daulerio AJ, Stradley DA, Feeser WS, Van Dyk DE, Pitts WJ, Earl RA, Hobbs F, Copeland RA, Magolda RL, Scherle PA, Trzaskos JM (1998) Identification of a novel inhibitor of mitogen-activated protein kinase kinase. J Biol Chem 273:18623-18632.

Ficarella R, Di Leva F, Bortolozzi M, Ortolano S, Donaudy F, Petrillo M, Melchionda S, Lelli A, Domi T, Fedrizzi L, Lim D, Shull GE, Gasparini P, Brini M, Mammano F, Carafoli E (2007) A functional study of plasma-membrane calcium-pump isoform 2 mutants causing digenic deafness. Proc Natl Acad Sci U S A 104:1516-1521.

Forge A (1985) Outer hair cell loss and supporting cell expansion following chronic gentamicin treatment. Hear Res 19:171-182.

Forge A, Schacht J (2000) Aminoglycoside antibiotics. Audiol Neurootol 5:3-22.

Forge A, Li L (2000) Apoptotic death of hair cells in mammalian vestibular sensory epithelia. Hear Res 139:97-115.

Forge A, Li L, Nevill G (1998) Hair cell recovery in the vestibular sensory epithelia of mature guinea pigs. J Comp Neurol 397:69-88.

Forge A, Li L, Corwin JT, Nevill G (1993) Ultrastructural evidence for hair cell regeneration in the mammalian inner ear. Science 259:1616-1619.

Forge A, Becker D, Casalotti S, Edwards J, Marziano N, Nevill G (2003) Gap junctions in the inner ear: comparison of distribution patterns in different vertebrates and assessement of connexin composition in mammals. J Comp Neurol 467:207-231.

Freeman S, Geal-Dor M, Sohmer H (1999) Development of inner ear (cochlear and vestibular) function in the fetus-neonate. J Basic Clin Physiol Pharmacol 10:173-189.

Gale JE, Meyers JR, Periasamy A, Corwin JT (2002) Survival of bundleless hair cells and subsequent bundle replacement in the bullfrog's saccule. J Neurobiol 50:81-92.

Gale JE, Piazza V, Ciubotaru CD, Mammano F (2004) A mechanism for sensing noise damage in the inner ear. Curr Biol 14:526-529.

Gale JE, Marcotti W, Kennedy HJ, Kros CJ, Richardson GP (2001) FM1-43 dye behaves as a permeant blocker of the hair-cell mechanotransducer channel. J Neurosci 21:7013-7025.

Gallagher CJ, Salter MW (2003) Differential properties of astrocyte calcium waves mediated by P2Y1 and P2Y2 receptors. J Neurosci 23:6728-6739.

Gardai SJ, Whitlock BB, Xiao YQ, Bratton DB, Henson PM (2004) Oxidants inhibit ERK/MAPK and prevent its ability to delay neutrophil apoptosis downstream of mitochondrial changes and at the level of XIAP. J Biol Chem 279:44695-44703.

Garetz SL, Altschuler RA, Schacht J (1994) Attenuation of gentamicin ototoxicity by glutathione in the guinea pig in vivo. Hear Res 77:81-87.

Geal-Dor M, Freeman S, Li G, Sohmer H (1993) Development of hearing in neonatal rats: air and bone conducted ABR thresholds. Hear Res 69:236-242.

Gendron FP, Neary JT, Theiss PM, Sun GY, Gonzalez FA, Weisman GA (2003) Mechanisms of P2X7 receptor-mediated ERK1/2 phosphorylation in human astrocytoma cells. Am J Physiol Cell Physiol 284:C571-581.

Glading A, Bodnar RJ, Reynolds IJ, Shiraha H, Satish L, Potter DA, Blair HC, Wells A (2004) Epidermal growth factor activates m-calpain (calpain II), at least in part, by extracellular signal-regulated kinase-mediated phosphorylation. Mol Cell Biol 24:2499-2512.

Glowatzki E, Cheng N, Hiel H, Yi E, Tanaka K, Ellis-Davies GC, Rothstein JD, Bergles DE (2006) The glutamate-aspartate transporter GLAST mediates glutamate uptake at inner hair cell afferent synapses in the mammalian cochlea. J Neurosci 26:7659-7664.

Goldsmith ZG, Dhanasekaran DN (2007) G protein regulation of MAPK networks. Oncogene 26:3122-3142.

Grant L, Slapnick S, Kennedy H, Hackney C (2006) Ryanodine receptor localisation in the mammalian cochlea: an ultrastructural study. Hear Res 219:101-109.

Greenwood D, Jagger DJ, Huang LC, Hoya N, Thorne PR, Wildman SS, King BF, Pak K, Ryan AF, Housley GD (2007) P2X receptor signaling inhibits BDNF-mediated spiral ganglion neuron development in the neonatal rat cochlea. Development 134:1407-1417.

Hackney CM, Mahendrasingam S, Penn A, Fettiplace R (2005) The concentrations of calcium buffering proteins in mammalian cochlear hair cells. J Neurosci 25:7867-7875.

Hafidi A, Dulon D (2004) Developmental expression of Ca(v)1.3 (alpha1d) calcium channels in the mouse inner ear. Brain Res Dev Brain Res 150:167-175.

Haines WR, Torres GE, Voigt MM, Egan TM (1999) Properties of the novel ATP-gated ionotropic receptor composed of the P2X(1) and P2X(5) isoforms. Mol Pharmacol 56:720-727.

Han W, Shi X, Nuttall AL (2006) AIF and endoG translocation in noise exposure induced hair cell death. Hear Res 211:85-95.

Hansen M, Boitano S, Dirksen ER, Sanderson MJ (1993) Intercellular calcium signaling induced by extracellular adenosine 5'-triphosphate and mechanical stimulation in airway epithelial cells. J Cell Sci 106 (Pt 4):995-1004.

Hansen M, Boitano S, Dirksen ER, Sanderson MJ (1995) A role for phospholipase C activity but not ryanodine receptors in the initiation and propagation of intercellular calcium waves. J Cell Sci 108 (Pt 7):2583-2590.

Hara MR, Snyder SH (2007) Cell signaling and neuronal death. Annu Rev Pharmacol Toxicol 47:117-141.

Harrisingh MC, Perez-Nadales E, Parkinson DB, Malcolm DS, Mudge AW, Lloyd AC (2004) The Ras/Raf/ERK signalling pathway drives Schwann cell dedifferentiation. Embo J 23:3061-3071.

Hashino E, Shero M (1995) Endocytosis of aminoglycoside antibiotics in sensory hair cells. Brain Res 704:135-140.

Hashino E, Shero M, Salvi RJ (1997) Lysosomal targeting and accumulation of aminoglycoside antibiotics in sensory hair cells. Brain Res 777:75-85.

Hirose K, Hockenbery DM, Rubel EW (1997) Reactive oxygen species in chick hair cells after gentamicin exposure in vitro. Hear Res 104:1-14.

Hirose K, Westrum LE, Stone JS, Zirpel L, Rubel EW (1999) Dynamic studies of ototoxicity in mature avian auditory epithelium. Ann N Y Acad Sci 884:389-409.

Hodge C, Liao J, Stofega M, Guan K, Carter-Su C, Schwartz J (1998) Growth hormone stimulates phosphorylation and activation of elk-1 and expression of c-fos, egr-1, and junB through activation of extracellular signal-regulated kinases 1 and 2. J Biol Chem 273:31327-31336.

Holley MC (1996) Outer Hair Cell Motility. In: The cochlea, pp 386-434. New York: Springer.

Housley GD, Marcotti W, Navaratnam D, Yamoah EN (2006) Hair cells--beyond the transducer. J Membr Biol 209:89-118.

Housley GD, Kanjhan R, Raybould NP, Greenwood D, Salih SG, Jarlebark L, Burton LD, Setz VC, Cannell MB, Soeller C, Christie DL, Usami S, Matsubara A, Yoshie H, Ryan AF, Thorne PR (1999) Expression of the P2X(2) receptor subunit of the ATP-gated ion channel in the cochlea: implications for sound transduction and auditory neurotransmission. J Neurosci 19:8377-8388.

Huang LC, Greenwood D, Thorne PR, Housley GD (2005) Developmental regulation of neuron-specific P2X3 receptor expression in the rat cochlea. J Comp Neurol 484:133-143.

Hur EM, Park TJ, Kim KT (2001) Coupling of L-type voltage-sensitive calcium channels to P2X(2) purinoceptors in PC-12 cells. Am J Physiol Cell Physiol 280:C1121-1129.

Ishida Y, Paul RJ (2005) Ca2+ clearance in smooth muscle: lessons from gene-altered mice. J Smooth Muscle Res 41:235-245.

Jagger DJ, Forge A (2006) Compartmentalized and signal-selective gap junctional coupling in the hearing cochlea. J Neurosci 26:1260-1268.

Jarlebark LE, Housley GD, Thorne PR (2000) Immunohistochemical localization of adenosine 5'-triphosphate-gated ion channel P2X(2) receptor subunits in adult and developing rat cochlea. J Comp Neurol 421:289-301.

Jarlebark LE, Housley GD, Raybould NP, Vlajkovic S, Thorne PR (2002) ATP-gated ion channels assembled from P2X2 receptor subunits in the mouse cochlea. Neuroreport 13:1979-1984.

Jiang H, Sha SH, Forge A, Schacht J (2006) Caspase-independent pathways of hair cell death induced by kanamycin in vivo. Cell Death Differ 13:20-30.

Jiang LH, Mackenzie AB, North RA, Surprenant A (2000) Brilliant blue G selectively blocks ATP-gated rat P2X(7) receptors. Mol Pharmacol 58:82-88.

Jo H, Sipos K, Go YM, Law R, Rong J, McDonald JM (1997) Differential effect of shear stress on extracellular signal-regulated kinase and N-terminal Jun kinase in endothelial cells. Gi2- and Gbeta/gamma-dependent signaling pathways. J Biol Chem 272:1395-1401.

Jones CA, Chessell IP, Simon J, Barnard EA, Miller KJ, Michel AD, Humphrey PP (2000) Functional characterization of the P2X(4) receptor orthologues. Br J Pharmacol 129:388-394.

Joy S, Siow RC, Rowlands DJ, Becker M, Wyatt AW, Aaronson PI, Coen CW, Kallo I, Jacob R, Mann GE (2006) The isoflavone Equol mediates rapid vascular

relaxation: Ca2+-independent activation of endothelial nitric-oxide synthase/Hsp90 involving ERK1/2 and Akt phosphorylation in human endothelial cells. J Biol Chem 281:27335-27345.

Kalinec GM, Fernandez-Zapico ME, Urrutia R, Esteban-Cruciani N, Chen S, Kalinec F (2005) Pivotal role of Harakiri in the induction and prevention of gentamicin-induced hearing loss. Proc Natl Acad Sci U S A 102:16019-16024.

Kanjhan R, Raybould NP, Jagger DJ, Greenwood D, Housley GD (2003) Allosteric modulation of native cochlear P2X receptors: insights from comparison with recombinant P2X2 receptors. Audiol Neurootol 8:115-128.

Kelley MW, Talreja DR, Corwin JT (1995) Replacement of hair cells after laser microbeam irradiation in cultured organs of corti from embryonic and neonatal mice. J Neurosci 15:3013-3026.

Kennedy HJ (2002) Intracellular calcium regulation in inner hair cells from neonatal mice. Cell Calcium 31:127-136.

Kennedy HJ, Meech RW (2002) Fast Ca2+ signals at mouse inner hair cell synapse: a role for Ca2+-induced Ca2+ release. J Physiol 539:15-23.

Khakh BS, Bao XR, Labarca C, Lester HA (1999a) Neuronal P2X transmitter-gated cation channels change their ion selectivity in seconds. Nat Neurosci 2:322-330.

Khakh BS, Proctor WR, Dunwiddie TV, Labarca C, Lester HA (1999b) Allosteric control of gating and kinetics at P2X(4) receptor channels. J Neurosci 19:7289-7299.

Kim GS, Hong JS, Kim SW, Koh JM, An CS, Choi JY, Cheng SL (2003) Leptin induces apoptosis via ERK/cPLA2/cytochrome c pathway in human bone marrow stromal cells. J Biol Chem 278:21920-21929.

King BF, Townsend-Nicholson A (2003) Nucleotide and Nucleoside Receptors. Tocris reviews 23.

King BF, Wildman SS, Ziganshina LE, Pintor J, Burnstock G (1997) Effects of extracellular pH on agonism and antagonism at a recombinant P2X2 receptor. Br J Pharmacol 121:1445-1453.

King BF, Townsend-Nicholson A, Wildman SS, Thomas T, Spyer KM, Burnstock G (2000) Coexpression of rat P2X2 and P2X6 subunits in Xenopus oocytes. J Neurosci 20:4871-4877.

Kirk DL, Yates GK (1998) ATP in endolymph enhances electrically-evoked oto-acoustic emissions from the guinea pig cochlea. Neurosci Lett 250:149-152.

Klemke RL, Cai S, Giannini AL, Gallagher PJ, de Lanerolle P, Cheresh DA (1997) Regulation of cell motility by mitogen-activated protein kinase. J Cell Biol 137:481-492.

Kupzig S, Walker SA, Cullen PJ (2005) The frequencies of calcium oscillations are optimized for efficient calcium-mediated activation of Ras and the ERK/MAPK cascade. Proc Natl Acad Sci U S A 102:7577-7582.

Lackey K, Cory M, Davis R, Frye SV, Harris PA, Hunter RN, Jung DK, McDonald OB, McNutt RW, Peel MR, Rutkowske RD, Veal JM, Wood ER (2000) The discovery of potent cRaf1 kinase inhibitors. Bioorg Med Chem Lett 10:223-226.

Lagostena L, Mammano F (2001) Intracellular calcium dynamics and membrane conductance changes evoked by Deiters' cell purinoceptor activation in the organ of Corti. Cell Calcium 29:191-198.

Lagostena L, Ashmore JF, Kachar B, Mammano F (2001) Purinergic control of intercellular communication between Hensen's cells of the guinea-pig cochlea. J Physiol 531:693-706.

Lavoie JN, L'Allemain G, Brunet A, Muller R, Pouyssegur J (1996) Cyclin D1 expression is regulated positively by the p42/p44MAPK and negatively by the p38/HOGMAPK pathway. J Biol Chem 271:20608-20616.

Le KT, Babinski K, Seguela P (1998) Central P2X4 and P2X6 channel subunits coassemble into a novel heteromeric ATP receptor. J Neurosci 18:7152-7159.

Le KT, Boue-Grabot E, Archambault V, Seguela P (1999) Functional and biochemical evidence for heteromeric ATP-gated channels composed of P2X1 and P2X5 subunits. J Biol Chem 274:15415-15419.

Leonova EV, Raphael Y (1997) Organization of cell junctions and cytoskeleton in the reticular lamina in normal and ototoxically damaged organ of Corti. Hear Res 113:14-28.

Levinthal DJ, Defranco DB (2005) Reversible oxidation of ERK-directed protein phosphatases drives oxidative toxicity in neurons. J Biol Chem 280:5875-5883.

Li DW, Liu JP, Mao YW, Xiang H, Wang J, Ma WY, Dong Z, Pike HM, Brown RE, Reed JC (2005) Calcium-activated RAF/MEK/ERK signaling pathway mediates p53-dependent apoptosis and is abrogated by alpha B-crystallin through inhibition of RAS activation. Mol Biol Cell 16:4437-4453.

Li L, Nevill G, Forge A (1995) Two modes of hair cell loss from the vestibular sensory epithelia of the guinea pig inner ear. J Comp Neurol 355:405-417.

Lin LL, Wartmann M, Lin AY, Knopf JL, Seth A, Davis RJ (1993) cPLA2 is phosphorylated and activated by MAP kinase. Cell 72:269-278.

Lioudyno M, Hiel H, Kong JH, Katz E, Waldman E, Parameshwaran-Iyer S, Glowatzki E, Fuchs PA (2004) A "synaptoplasmic cistern" mediates rapid inhibition of cochlear hair cells. J Neurosci 24:11160-11164.

Liu C, Peng M, Laties AM, Wen R (1998) Preconditioning with bright light evokes a protective response against light damage in the rat retina. J Neurosci 18:1337-1344.

Liu M, King BF, Dunn PM, Rong W, Townsend-Nicholson A, Burnstock G (2001) Coexpression of P2X(3) and P2X(2) receptor subunits in varying amounts generates heterogeneous populations of P2X receptors that evoke a spectrum of agonist responses comparable to that seen in sensory neurons. J Pharmacol Exp Ther 296:1043-1050.

Lockyer PJ, Kupzig S, Cullen PJ (2001) CAPRI regulates Ca(2+)-dependent inactivation of the Ras-MAPK pathway. Curr Biol 11:981-986.

Mammano F, Bortolozzi M, Ortolano S, Anselmi F (2007) Ca2+ signaling in the inner ear. Physiology (Bethesda) 22:131-144.

Mammano F, Frolenkov GI, Lagostena L, Belyantseva IA, Kurc M, Dodane V, Colavita A, Kachar B (1999) ATP-Induced Ca(2+) release in cochlear outer hair cells: localization of an inositol triphosphate-gated Ca(2+) store to the base of the sensory hair bundle. J Neurosci 19:6918-6929.

Mangiardi DA, McLaughlin-Williamson K, May KE, Messana EP, Mountain DC, Cotanche DA (2004) Progression of hair cell ejection and molecular markers of apoptosis in the avian cochlea following gentamicin treatment. J Comp Neurol 475:1-18.

Mansour SJ, Matten WT, Hermann AS, Candia JM, Rong S, Fukasawa K, Vande Woude GF, Ahn NG (1994) Transformation of mammalian cells by constitutively active MAP kinase kinase. Science 265:966-970.

Marcotti W, van Netten SM, Kros CJ (2005) The aminoglycoside antibiotic dihydrostreptomycin rapidly enters mouse outer hair cells through the mechano-electrical transducer channels. J Physiol 567:505-521.

Marin-Teva JL, Dusart I, Colin C, Gervais A, van Rooijen N, Mallat M (2004) Microglia promote the death of developing Purkinje cells. Neuron 41:535-547.

Marshall CJ (1995) Specificity of receptor tyrosine kinase signaling: transient versus sustained extracellular signal-regulated kinase activation. Cell 80:179-185.

Matsubayashi Y, Ebisuya M, Honjoh S, Nishida E (2004) ERK activation propagates in epithelial cell sheets and regulates their migration during wound healing. Curr Biol 14:731-735.

Matsui JI, Ogilvie JM, Warchol ME (2002) Inhibition of caspases prevents ototoxic and ongoing hair cell death. J Neurosci 22:1218-1227.

Matsui JI, Gale JE, Warchol ME (2004) Critical signaling events during the aminoglycoside-induced death of sensory hair cells in vitro. J Neurobiol 61:250-266.

Meyers JR, Corwin JT (2007) Shape change controls supporting cell proliferation in lesioned mammalian balance epithelium. J Neurosci 27:4313-4325.

Meyers JR, MacDonald RB, Duggan A, Lenzi D, Standaert DG, Corwin JT, Corey DP (2003) Lighting up the senses: FM1-43 loading of sensory cells through nonselective ion channels. J Neurosci 23:4054-4065.

Minami SB, Yamashita D, Schacht J, Miller JM (2004) Calcineurin activation contributes to noise-induced hearing loss. J Neurosci Res 78:383-392.

Mitsushima M, Suwa A, Amachi T, Ueda K, Kioka N (2004) Extracellular signal-regulated kinase activated by epidermal growth factor and cell adhesion interacts with and phosphorylates vinexin. J Biol Chem 279:34570-34577.

Mody N, Campbell DG, Morrice N, Peggie M, Cohen P (2003) An analysis of the phosphorylation and activation of extracellular-signal-regulated protein kinase 5 (ERK5) by mitogen-activated protein kinase kinase 5 (MKK5) in vitro. Biochem J 372:567-575.

Montcouquiol M, Corwin JT (2001) Intracellular signals that control cell proliferation in mammalian balance epithelia: key roles for phosphatidylinositol-3 kinase, mammalian target of rapamycin, and S6 kinases in preference to calcium, protein kinase C, and mitogen-activated protein kinase. J Neurosci 21:570-580.

Morton-Jones RT, Cannell MB, Jeyakumar LH, Fleischer S, Housley GD (2006) Differential expression of ryanodine receptors in the rat cochlea. Neuroscience 137:275-286.

Munoz DJ, Thorne PR, Housley GD, Billett TE (1995) Adenosine 5'-triphosphate (ATP) concentrations in the endolymph and perilymph of the guinea-pig cochlea. Hear Res 90:119-125.

Munoz DJ, Kendrick IS, Rassam M, Thorne PR (2001) Vesicular storage of adenosine triphosphate in the guinea-pig cochlear lateral wall and concentrations of ATP in the endolymph during sound exposure and hypoxia. Acta Otolaryngol 121:10-15.

Nakagawa T, Akaike N, Kimitsuki T, Komune S, Arima T (1990) ATP-induced current in isolated outer hair cells of guinea pig cochlea. J Neurophysiol 63:1068-1074.

Naraghi M, Neher E (1997) Linearized buffered Ca2+ diffusion in microdomains and its implications for calculation of [Ca2+] at the mouth of a calcium channel. J Neurosci 17:6961-6973.

Neary JT, Kang Y, Willoughby KA, Ellis EF (2003) Activation of extracellular signal-regulated kinase by stretch-induced injury in astrocytes involves extracellular ATP and P2 purinergic receptors. J Neurosci 23:2348-2356.

Neary JT, Kang Y, Bu Y, Yu E, Akong K, Peters CM (1999) Mitogenic signaling by ATP/P2Y purinergic receptors in astrocytes: involvement of a calcium-independent protein kinase C, extracellular signal-regulated protein kinase pathway distinct from the phosphatidylinositol-specific phospholipase C/calcium pathway. J Neurosci 19:4211-4220.

Newman EA (2001) Propagation of intercellular calcium waves in retinal astrocytes and Muller cells. J Neurosci 21:2215-2223.

Newman EA, Zahs KR (1997) Calcium waves in retinal glial cells. Science 275:844-847.

Nguyen DH, Catling AD, Webb DJ, Sankovic M, Walker LA, Somlyo AV, Weber MJ, Gonias SL (1999) Myosin light chain kinase functions downstream of Ras/ERK to promote migration of urokinase-type plasminogen activator-stimulated cells in an integrin-selective manner. J Cell Biol 146:149-164.

Nicholas RA, Lazarowski ER, Watt WC, Li Q, Boyer J, Harden TK (1996) Pharmacological and second messenger signalling selectivities of cloned P2Y receptors. J Auton Pharmacol 16:319-323.

Nicole O, Goldshmidt A, Hamill CE, Sorensen SD, Sastre A, Lyuboslavsky P, Hepler JR, McKeon RJ, Traynelis SF (2005) Activation of protease-activated receptor-1 triggers astrogliosis after brain injury. J Neurosci 25:4319-4329.

Nicotera TM, Hu BH, Henderson D (2003) The caspase pathway in noise-induced apoptosis of the chinchilla cochlea. J Assoc Res Otolaryngol 4:466-477.

Nikolic P, Housley GD, Thorne PR (2003) Expression of the P2X7 receptor subunit of the adenosine 5'-triphosphate-gated ion channel in the developing and adult rat cochlea. Audiol Neurootol 8:28-37.

Nikolic P, Housley GD, Luo L, Ryan AF, Thorne PR (2001) Transient expression of P2X(1) receptor subunits of ATP-gated ion channels in the developing rat cochlea. Brain Res Dev Brain Res 126:173-182.

Noshita N, Sugawara T, Fujimura M, Morita-Fujimura Y, Chan PH (2001) Manganese Superoxide Dismutase Affects Cytochrome c Release and Caspase-9 Activation After Transient Focal Cerebral Ischemia in Mice. J Cereb Blood Flow Metab 21:557-567.

Nowak G (2002) Protein kinase C-alpha and ERK1/2 mediate mitochondrial dysfunction, decreases in active Na+ transport, and cisplatin-induced apoptosis in renal cells. J Biol Chem 277:43377-43388.

Ohinata Y, Miller JM, Schacht J (2003) Protection from noise-induced lipid peroxidation and hair cell loss in the cochlea. Brain Res 966:265-273.

Pack AK, Slepecky NB (1995) Cytoskeletal and calcium-binding proteins in the mammalian organ of Corti: cell type-specific proteins displaying longitudinal and radial gradients. Hear Res 91:119-135.

Paemeleire K, Martin PE, Coleman SL, Fogarty KE, Carrington WA, Leybaert L, Tuft RA, Evans WH, Sanderson MJ (2000) Intercellular calcium waves in

HeLa cells expressing GFP-labeled connexin 43, 32, or 26. Mol Biol Cell 11:1815-1827.

Papaiahgari S, Kleeberger SR, Cho HY, Kalvakolanu DV, Reddy SP (2004) NADPH oxidase and ERK signaling regulates hyperoxia-induced Nrf2-ARE transcriptional response in pulmonary epithelial cells. J Biol Chem 279:42302-42312.

Parker MS, Onyenekwu NN, Bobbin RP (2003) Localization of the P2Y4 receptor in the guinea pig organ of Corti. J Am Acad Audiol 14:286-295.

Parnaik R, Raff MC, Scholes J (2000) Differences between the clearance of apoptotic cells by professional and non-professional phagocytes. Curr Biol 10:857-860.

Paul S, Nairn AC, Wang P, Lombroso PJ (2003) NMDA-mediated activation of the tyrosine phosphatase STEP regulates the duration of ERK signaling. Nat Neurosci 6:34-42.

Pearson RA, Dale N, Llaudet E, Mobbs P (2005) ATP released via gap junction hemichannels from the pigment epithelium regulates neural retinal progenitor proliferation. Neuron 46:731-744.

Pelegrin P, Surprenant A (2006) Pannexin-1 mediates large pore formation and interleukin-1beta release by the ATP-gated P2X7 receptor. Embo J 25:5071-5082.

Pessach I, Leto TL, Malech HL, Levy R (2001) Essential requirement of cytosolic phospholipase A(2) for stimulation of NADPH oxidase-associated diaphorase activity in granulocyte-like cells. J Biol Chem 276:33495-33503.

Piazza V, Ciubotaru CD, Gale JE, Mammano F (2007) Purinergic signalling and intercellular Ca2+ wave propagation in the organ of Corti. Cell Calcium 41:77-86.

Pickles JO (1988) An Introduction to the Physiology of Hearing, Second Edition: Academic Press, London.

Pickles JO, Comis SD, Osborne MP (1984) Cross-links between stereocilia in the guinea pig organ of Corti, and their possible relation to sensory transduction. Hear Res 15:103-112.

Pirvola U, Xing-Qun L, Virkkala J, Saarma M, Murakata C, Camoratto AM, Walton KM, Ylikoski J (2000) Rescue of hearing, auditory hair cells, and neurons by CEP-1347/KT7515, an inhibitor of c-Jun N-terminal kinase activation. J Neurosci 20:43-50.

Pitt SJ, Martinez-Pinna J, Barnard EA, Mahaut-Smith MP (2005) Potentiation of P2Y receptors by physiological elevations of extracellular K+ via a mechanism independent of Ca2+ influx. Mol Pharmacol 67:1705-1713.

Platzer J, Engel J, Schrott-Fischer A, Stephan K, Bova S, Chen H, Zheng H, Striessnig J (2000) Congenital deafness and sinoatrial node dysfunction in mice lacking class D L-type Ca2+ channels. Cell 102:89-97.

Previati M, Lanzoni I, Astolfi L, Fagioli F, Vecchiati G, Pagnoni A, Martini A, Capitani S (2007) Cisplatin cytotoxicity in organ of corti-derived immortalized cells. J Cell Biochem.

Providence KM, Higgins PJ (2004) PAI-1 expression is required for epithelial cell migration in two distinct phases of in vitro wound repair. J Cell Physiol 200:297-308.

Raman M, Chen W, Cobb MH (2007) Differential regulation and properties of MAPKs. Oncogene 26:3100-3112.

Raphael Y, Altschuler RA (1991) Scar formation after drug-induced cochlear insult. Hear Res 51:173-183.

Raphael Y, Altschuler RA (2003) Structure and innervation of the cochlea. Brain Res Bull 60:397-422.

Rassendren F, Buell GN, Virginio C, Collo G, North RA, Surprenant A (1997) The permeabilizing ATP receptor, P2X7. Cloning and expression of a human cDNA. J Biol Chem 272:5482-5486.

Raybould NP, Jagger DJ, Kanjhan R, Greenwood D, Laslo P, Hoya N, Soeller C, Cannell MB, Housley GD (2007) TRPC-like conductance mediates restoration of intracellular Ca2+ in cochlear outer hair cells in the guinea pig and rat. J Physiol 579:101-113.

reviewed in Housley GD, Marcotti W, Navaratnam D, Yamoah EN (2006) Hair cells--beyond the transducer. J Membr Biol 209:89-118.

reviewed in Raman M, Chen W, Cobb MH (2007) Differential regulation and properties of MAPKs. Oncogene 26:3100-3112.

Ricci AJ, Wu YC, Fettiplace R (1998) The endogenous calcium buffer and the time course of transducer adaptation in auditory hair cells. J Neurosci 18:8261-8277.

Richardson GP, Russell IJ (1991) Cochlear cultures as a model system for studying aminoglycoside induced ototoxicity. Hear Res 53:293-311.

Rizzuto R, Pinton P, Carrington W, Fay FS, Fogarty KE, Lifshitz LM, Tuft RA, Pozzan T (1998) Close contacts with the endoplasmic reticulum as determinants of mitochondrial Ca2+ responses. Science 280:1763-1766.

Rubel EW, Dew LA, Roberson DW (1995) Mammalian vestibular hair cell regeneration. Science 267:701-707.

Ryals BM, Rubel EW (1988) Hair cell regeneration after acoustic trauma in adult Coturnix quail. Science 240:1774-1776.

Sakaguchi N, Henzl MT, Thalmann I, Thalmann R, Schulte BA (1998) Oncomodulin is expressed exclusively by outer hair cells in the organ of Corti. J Histochem Cytochem 46:29-40.

Sanderson MJ, Charles AC, Dirksen ER (1990) Mechanical stimulation and intercellular communication increases intracellular Ca2+ in epithelial cells. Cell Regul 1:585-596.

Schmitt JM, Wayman GA, Nozaki N, Soderling TR (2004) Calcium activation of ERK mediated by calmodulin kinase I. J Biol Chem 279:24064-24072.

Schonwasser DC, Marais RM, Marshall CJ, Parker PJ (1998) Activation of the mitogen-activated protein kinase/extracellular signal-regulated kinase pathway by conventional, novel, and atypical protein kinase C isotypes. Mol Cell Biol 18:790-798.

Schwab BL, Guerini D, Didszun C, Bano D, Ferrando-May E, Fava E, Tam J, Xu D, Xanthoudakis S, Nicholson DW, Carafoli E, Nicotera P (2002) Cleavage of plasma membrane calcium pumps by caspases: a link between apoptosis and necrosis. Cell Death Differ 9:818-831.

Sha SH, Schacht J (1999) Stimulation of free radical formation by aminoglycoside antibiotics. Hear Res 128:112-118.

Shen J, Harada N, Nakazawa H, Yamashita T (2005) Involvement of the nitric oxide-cyclic GMP pathway and neuronal nitric oxide synthase in ATP-induced Ca2+ signalling in cochlear inner hair cells. Eur J Neurosci 21:2912-2922.

Shen J, Harada N, Nakazawa H, Kaneko T, Izumikawa M, Yamashita T (2006) Role of nitric oxide on ATP-induced Ca2+ signaling in outer hair cells of the guinea pig cochlea. Brain Res 1081:101-112.

So H, Kim H, Lee JH, Park C, Kim Y, Kim E, Kim JK, Yun KJ, Lee KM, Lee HY, Moon SK, Lim DJ, Park R (2007) Cisplatin Cytotoxicity of Auditory Cells Requires Secretions of Proinflammatory Cytokines via Activation of ERK and NF-kappaB. J Assoc Res Otolaryngol.

Soltoff SP, Avraham H, Avraham S, Cantley LC (1998) Activation of P2Y2 receptors by UTP and ATP stimulates mitogen-activated kinase activity through a pathway that involves related adhesion focal tyrosine kinase and protein kinase C. J Biol Chem 273:2653-2660.

Sperandio S, Poksay K, de Belle I, Lafuente MJ, Liu B, Nasir J, Bredesen DE (2004) Paraptosis: mediation by MAP kinases and inhibition by AIP-1/Alix. Cell Death Differ 11:1066-1075.

Stevens C, Lin Y, Sanchez C, Amin E, Copson E, White H, Durston V, Eccles S, Hupp T (2007) A germline mutation in the death domain of DAPK-1 inactivates ERK induced apoptosis. J Biol Chem.

Stork PJ, Schmitt JM (2002) Crosstalk between cAMP and MAP kinase signaling in the regulation of cell proliferation. Trends Cell Biol 12:258-266.

Stout CE, Costantin JL, Naus CC, Charles AC (2002) Intercellular calcium signaling in astrocytes via ATP release through connexin hemichannels. J Biol Chem 277:10482-10488.

Street VA, McKee-Johnson JW, Fonseca RC, Tempel BL, Noben-Trauth K (1998) Mutations in a plasma membrane Ca2+-ATPase gene cause deafness in deafwaddler mice. Nat Genet 19:390-394.

Suadicani SO, Brosnan CF, Scemes E (2006) P2X7 receptors mediate ATP release and amplification of astrocytic intercellular Ca2+ signaling. J Neurosci 26:1378-1385.

Subramaniam S, Zirrgiebel U, von Bohlen Und Halbach O, Strelau J, Laliberte C, Kaplan DR, Unsicker K (2004) ERK activation promotes neuronal degeneration predominantly through plasma membrane damage and independently of caspase-3. J Cell Biol 165:357-369.

Sueta T, Paki B, Everett AW, Robertson D (2003) Purinergic receptors in auditory neurotransmission. Hear Res 183:97-108.

Sugahara K, Rubel EW, Cunningham LL (2006) JNK signaling in neomycin-induced vestibular hair cell death. Hear Res 221:128-135.

Sung YJ, Sung Z, Ho CL, Lin MT, Wang JS, Yang SC, Chen YJ, Lin CH (2003) Intercellular calcium waves mediate preferential cell growth toward the wound edge in polarized hepatic cells. Exp Cell Res 287:209-218.

Surprenant A, Rassendren F, Kawashima E, North RA, Buell G (1996) The cytolytic P2Z receptor for extracellular ATP identified as a P2X receptor (P2X7). Science 272:735-738.

Szucs A, Szappanos H, Toth A, Farkas Z, Panyi G, Csernoch L, Sziklai I (2004) Differential expression of purinergic receptor subtypes in the outer hair cells of the guinea pig. Hear Res 196:2-7.

Tan Y, Wu C, De Veyra T, Greer PA (2006) Ubiquitous calpains promote both apoptosis and survival signals in response to different cell death stimuli. J Biol Chem 281:17689-17698.

Thorne PR, Munoz DJ, Housley GD (2004) Purinergic modulation of cochlear partition resistance and its effect on the endocochlear potential in the Guinea pig. J Assoc Res Otolaryngol 5:58-65.

Tolhurst G, Vial C, Leon C, Gachet C, Evans RJ, Mahaut-Smith MP (2005) Interplay between P2Y(1), P2Y(12), and P2X(1) receptors in the activation of megakaryocyte cation influx currents by ADP: evidence that the primary megakaryocyte represents a fully functional model of platelet P2 receptor signaling. Blood 106:1644-1651.

Traverse S, Seedorf K, Paterson H, Marshall CJ, Cohen P, Ullrich A (1994) EGF triggers neuronal differentiation of PC12 cells that overexpress the EGF receptor. Curr Biol 4:694-701.

Usachev YM, Marsh AJ, Johanns TM, Lemke MM, Thayer SA (2006) Activation of protein kinase C in sensory neurons accelerates Ca2+ uptake into the endoplasmic reticulum. J Neurosci 26:311-318.

van der Weyden L, Adams DJ, Luttrell BM, Conigrave AD, Morris MB (2000) Pharmacological characterisation of the P2Y11 receptor in stably transfected haematological cell lines. Mol Cell Biochem 213:75-81.

van Rossum GS, Klooster R, van den Bosch H, Verkleij AJ, Boonstra J (2001) Phosphorylation of p42/44(MAPK) by various signal transduction pathways activates cytosolic phospholipase A(2) to variable degrees. J Biol Chem 276:28976-28983.

Venance L, Stella N, Glowinski J, Giaume C (1997) Mechanism involved in initiation and propagation of receptor-induced intercellular calcium signaling in cultured rat astrocytes. J Neurosci 17:1981-1992.

Vessey JP, Lalonde MR, Mizan HA, Welch NC, Kelly ME, Barnes S (2004) Carbenoxolone inhibition of voltage-gated Ca channels and synaptic transmission in the retina. J Neurophysiol 92:1252-1256.

Virginio C, Robertson G, Surprenant A, North RA (1998) Trinitrophenyl-substituted nucleotides are potent antagonists selective for P2X1, P2X3, and heteromeric P2X2/3 receptors. Mol Pharmacol 53:969-973.

Vlajkovic SM, Thorne PR, Sevigny J, Robson SC, Housley GD (2002a) NTPDase1 and NTPDase2 immunolocalization in mouse cochlea: implications for regulation of p2 receptor signaling. J Histochem Cytochem 50:1435-1442.

Vlajkovic SM, Thorne PR, Sevigny J, Robson SC, Housley GD (2002b) Distribution of ectonucleoside triphosphate diphosphohydrolases 1 and 2 in rat cochlea. Hear Res 170:127-138.

von Kugelgen I (2006) Pharmacological profiles of cloned mammalian P2Y-receptor subtypes. Pharmacol Ther 110:415-432.

Vossler MR, Yao H, York RD, Pan MG, Rim CS, Stork PJ (1997) cAMP activates MAP kinase and Elk-1 through a B-Raf- and Rap1-dependent pathway. Cell 89:73-82.

Wang CX, Song JH, Song DK, Yong VW, Shuaib A, Hao C (2006a) Cyclin-dependent kinase-5 prevents neuronal apoptosis through ERK-mediated upregulation of Bcl-2. Cell Death Differ 13:1203-1212.

Wang HG, Pathan N, Ethell IM, Krajewski S, Yamaguchi Y, Shibasaki F, McKeon F, Bobo T, Franke TF, Reed JC (1999) Ca2+-induced apoptosis through calcineurin dephosphorylation of BAD. Science 284:339-343.

Wang J, Van De Water TR, Bonny C, de Ribaupierre F, Puel JL, Zine A (2003a) A peptide inhibitor of c-Jun N-terminal kinase protects against both

aminoglycoside and acoustic trauma-induced auditory hair cell death and hearing loss. J Neurosci 23:8596-8607.
Wang J, Ladrech S, Pujol R, Brabet P, Van De Water TR, Puel JL (2004) Caspase inhibitors, but not c-Jun NH2-terminal kinase inhibitor treatment, prevent cisplatin-induced hearing loss. Cancer Res 64:9217-9224.
Wang J, Ruel J, Ladrech S, Bonny C, TR VDW, Puel JL (2006b) Inhibition of the JNK-mediated mitochondrial cell death pathway restores auditory function in sound exposed animals. Mol Pharmacol.
Wang JC, Raybould NP, Luo L, Ryan AF, Cannell MB, Thorne PR, Housley GD (2003b) Noise induces up-regulation of P2X2 receptor subunit of ATP-gated ion channels in the rat cochlea. Neuroreport 14:817-823.
Wang WJ, Kuo JC, Yao CC, Chen RH (2002a) DAP-kinase induces apoptosis by suppressing integrin activity and disrupting matrix survival signals. J Cell Biol 159:169-179.
Wang X, Martindale JL, Holbrook NJ (2000) Requirement for ERK activation in cisplatin-induced apoptosis. J Biol Chem 275:39435-39443.
Wang Y, Hirose K, Liberman MC (2002b) Dynamics of noise-induced cellular injury and repair in the mouse cochlea. J Assoc Res Otolaryngol 3:248-268.
Wangemann P, Schacht J (1996) Homeostatic Mechanisms in the Cochlea. In: The cochlea, pp 130-185. New York: Springer.
Warchol ME, Corwin JT (1996) Regenerative proliferation in organ cultures of the avian cochlea: identification of the initial progenitors and determination of the latency of the proliferative response. J Neurosci 16:5466-5477.
Warchol ME, Lambert PR, Goldstein BJ, Forge A, Corwin JT (1993) Regenerative proliferation in inner ear sensory epithelia from adult guinea pigs and humans. Science 259:1619-1622.
Wei X, Zhao L, Liu J, Dodel RC, Farlow MR, Du Y (2005) Minocycline prevents gentamicin-induced ototoxicity by inhibiting p38 MAP kinase phosphorylation and caspase 3 activation. Neuroscience 131:513-521.
Werry TD, Sexton PM, Christopoulos A (2005) "Ins and outs" of seven-transmembrane receptor signalling to ERK. Trends Endocrinol Metab 16:26-33.
White PJ, Webb TE, Boarder MR (2003) Characterization of a Ca2+ response to both UTP and ATP at human P2Y11 receptors: evidence for agonist-specific signaling. Mol Pharmacol 63:1356-1363.
Wikstrom MA, Lawoko G, Heilbronn E (1998) Cholinergic modulation of extracellular ATP-induced cytoplasmic calcium concentrations in cochlear outer hair cells. J Physiol Paris 92:345-349.
Wildman SS, Unwin RJ, King BF (2003) Extended pharmacological profiles of rat P2Y2 and rat P2Y4 receptors and their sensitivity to extracellular H+ and Zn2+ ions. Br J Pharmacol 140:1177-1186.
Witte MC, Montcouquiol M, Corwin JT (2001) Regeneration in avian hair cell epithelia: identification of intracellular signals required for S-phase entry. Eur J Neurosci 14:829-838.
Xia Z, Dickens M, Raingeaud J, Davis RJ, Greenberg ME (1995) Opposing effects of ERK and JNK-p38 MAP kinases on apoptosis. Science 270:1326-1331.
Xiang Z, Bo X, Burnstock G (1999) P2X receptor immunoreactivity in the rat cochlea, vestibular ganglion and cochlear nucleus. Hear Res 128:190-196.

Yamamoto T, Ebisuya M, Ashida F, Okamoto K, Yonehara S, Nishida E (2006) Continuous ERK activation downregulates antiproliferative genes throughout G1 phase to allow cell-cycle progression. Curr Biol 16:1171-1182.

Yamasaki M, Masgrau R, Morgan AJ, Churchill GC, Patel S, Ashcroft SJ, Galione A (2004) Organelle selection determines agonist-specific Ca2+ signals in pancreatic acinar and beta cells. J Biol Chem 279:7234-7240.

Yamoah EN, Lumpkin EA, Dumont RA, Smith PJ, Hudspeth AJ, Gillespie PG (1998) Plasma membrane Ca2+-ATPase extrudes Ca2+ from hair cell stereocilia. J Neurosci 18:610-624.

Yang D, Thalmann I, Thalmann R, Simmons DD (2004a) Expression of alpha and beta parvalbumin is differentially regulated in the rat organ of corti during development. J Neurobiol 58:479-492.

Yang L, Cranson D, Trinkaus-Randall V (2004b) Cellular injury induces activation of MAPK via P2Y receptors. J Cell Biochem 91:938-950.

Yang L, Mao L, Tang Q, Samdani S, Liu Z, Wang JQ (2004c) A novel Ca2+-independent signaling pathway to extracellular signal-regulated protein kinase by coactivation of NMDA receptors and metabotropic glutamate receptor 5 in neurons. J Neurosci 24:10846-10857.

Yang PS, Alseikhan BA, Hiel H, Grant L, Mori MX, Yang W, Fuchs PA, Yue DT (2006) Switching of Ca2+-dependent inactivation of Ca(v)1.3 channels by calcium binding proteins of auditory hair cells. J Neurosci 26:10677-10689.

Ylikoski J, Xing-Qun L, Virkkala J, Pirvola U (2002) Blockade of c-Jun N-terminal kinase pathway attenuates gentamicin-induced cochlear and vestibular hair cell death. Hear Res 163:71-81.

Zhang Y, Tang W, Ahmad S, Sipp JA, Chen P, Lin X (2005) Gap junction-mediated intercellular biochemical coupling in cochlear supporting cells is required for normal cochlear functions. Proc Natl Acad Sci U S A 102:15201-15206.

Zhao HB, Yu N, Fleming CR (2005) Gap junctional hemichannel-mediated ATP release and hearing controls in the inner ear. Proc Natl Acad Sci U S A 102:18724-18729.

Zhou Z, Hume RI (1998) Two mechanisms for inward rectification of current flow through the purinoceptor P2X2 class of ATP-gated channels. J Physiol 507 (Pt 2):353-364.